THÈSE

IRSN
INSTITUT
DE RADIOPROTECTION
ET DE SÛRETÉ NUCLÉAIRE

Optimisation des programmes de surveillance de la contamination interne par l'étude des incertitudes liées à l'évaluation dosimétrique

Estelle Davesne

Rapport DRPH/SDI/2010-11
ISRN/IRSN-2010/135

Laboratoire d'Evaluation de la Dose Interne

UNIVERSITÉ PARIS XI
UFR SCIENTIFIQUE D'ORSAY

THÈSE

présentée en vue de l'obtention du

DOCTORAT DE L'UNIVERSITÉ PARIS XI

Spécialité : PHYSIQUE

Optimisation des programmes de surveillance de la contamination interne par l'étude des incertitudes liées à l'évaluation dosimétrique

par

Estelle DAVESNE

Directeur de thèse : Pr. François PAQUET

Soutenue le 14 septembre 2010 devant la commission d'examen

Pr. Eric SIMONI	Vice-doyen de la faculté des sciences de Paris XI	Président
Pr. Alan BIRCHALL	Directeur de recherche, Health Protection Agency	Rapporteur
Dr. Volodymyr BERKOVSKYY	Chargé de programmes de recherche à l'AIEA	Rapporteur
Dr. Philippe CASANOVA	Médecin, AREVA NC	Examinateur
M. Eric CHOJNACKI	Expert, IRSN	Examinateur
Pr. François PAQUET	Expert senior, IRSN	Directeur de thèse
Dr. Eric BLANCHARDON	Expert, IRSN,	Invité

Recherches effectuées au Laboratoire d'Evaluation de la Dose Interne de l'IRSN
IRSN/DRPH/SDI/LEDI, BP 17, 92262 Fontenay-aux-Roses Cedex

Acknowledgements - Remerciements

Je remercie la Direction de la Radioprotection de l'Homme, Monsieur Patrick GOURMELON et Madame Jocelyne AIGUEPERSE, pour m'avoir permis de réaliser ce travail de thèse à l'IRSN. Je souhaite également remercier Monsieur Jean-René JOURDAIN, Monsieur Jean-Michel DELIGNE, chefs successifs du Service de Dosimétrie Interne, ainsi que Madame Michèle AGARANDE, chef de service par intérim et Monsieur Didier FRANCK, chef du Laboratoire d'Evaluation de la Dose Interne, pour m'avoir accueillie et avoir mis à disposition les moyens de mener ce projet de thèse dans les meilleures conditions. Merci également pour la relecture de mes articles.

Je tiens à remercier tout particulièrement les membres du Comité Technique du Programme d'intérêt Commun entre AREVA et l'IRSN en Dosimétrie Interne pour leur soutien durant toute la durée de cette étude : Monsieur Alain ACKER et le Docteur Stéphane HENRY de la Direction Médicale d'AREVA, Madame Inès V. de LAGUERIE de la Direction des Technologies, de la Recherche et de l'Innovation d'AREVA, Madame Isabelle DUBLINEAU et Monsieur Fabrice PETITOT du Laboratoire de Radiotoxicologie de l'IRSN.

Je remercie également Monsieur Bernard BERTHIER pour m'avoir accueillie au sein de l'école doctorale Rayonnements et Environnement devenue l'école doctorale MIPEGE dirigée par Monsieur Xavier QUIDELLEUR secondé par Monsieur Bruno ESPAGNON.

Je tiens à remercier vivement Monsieur Eric SIMONI, vice-doyen de la faculté des sciences de l'Université Paris XI d'avoir accepté de prendre part au jury de cette thèse.

I really want to thank Dr Volodymyr BERKOVSKYY, radiation protection specialist at the International Atomic Energy Agency, and Pr Alan BIRCHALL, head of the Biomathematics group at the Health Protection Agency, for their review of this long manuscript and for having brought to this work their extensive knowledge of the radiological protection policy, of internal dosimetry and of uncertainty modelling and propagation. Thank you Alan for the very interesting discussions we had in Paris or in Didcot.

Je remercie chaleureusement le Dr Philippe CASANOVA, médecin chef du Service de Santé au Travail du centre AREVA NC de La Hague, pour son enthousiasme pour cette étude, pour m'avoir permis d'obtenir toutes les données qui ont permis à ce travail d'être concret.

Un grand merci à Monsieur Eric CHOJNACKI pour m'avoir aidé tout au long de ce travail à comprendre et à manipuler l'incertain, pour nos longues discussions téléphoniques et pour m'avoir permis d'aller aussi loin dans la propagation directe ou inverse des probabilités bayésiennes continues ou discrètes et des possibilités.

A Monsieur François PAQUET, un très grand merci pour avoir accepté d'être mon directeur de thèse, pour avoir apporté ses connaissances en radioprotection et sur la notion de dose efficace, pour avoir été l'œil extérieur sur toutes mes présentations et articles, pour les bons moments passés lors du congrès HEIR et pour les discussions sur mon avenir.

Comment remercier suffisamment Monsieur Eric BLANCHARDON, mon encadrant, qui a réussi à me supporter durant ces trois années, qui m'a donné ma chance lors d'un stage de Master 1 et m'a permis de faire cette thèse sur ce superbe sujet, qui m'a tout appris sur la dosimétrie interne, le calcul de dose, l'utilisation des modèles biocinétiques, la radioprotection, les programmes de surveillance, les incertitudes, mais également à être autonome et qui sait si bien améliorer ma prose. Merci de m'avoir encouragée lorsque je me décourageais, de m'avoir poussée aussi loin que possible. Merci également pour nos longues discussions sur le théâtre. Et merci de m'accepter comme collègue.

Je tiens à remercier tout particulièrement l'équipe du Secteur d'Analyse Médicale du centre AREVA NC de La Hague pour m'avoir donné tous les détails sur les mesures radiotoxicologiques et anthroporadiamétriques. Merci à Monsieur Philippe CORREZE, Madame Bernadette PELEAU, Monsieur Xavier LECHAFTOIS et Monsieur Jérôme MARIN. Merci également à Madame HENRION secrétaire médicale pour m'avoir tout expliqué des programmes de surveillance à La Hague.

Je remercie vivement Monsieur Serge BONHOMME, chargé de radioprotection pour m'avoir présenté la politique de radioprotection en place à La Hague et Monsieur Jean-Philippe REISS, responsable des Moyennes Activité à La Hague pour m'avoir permis de visiter l'atelier T4 et pour m'avoir fourni toutes les données qui m'étaient nécessaires.

Thank you very much to Dr Andrey MOLOKANOV, researcher of the FMBC in Moscow who worked temporarily in the LEDI, for the very interesting and passionate discussions we had about frequentist and bayesian probabilities and for having explained to me the classical method and for our quality comparison. I really want to thank Dr Matthew PUNCHER, researcher in the Biomathematics group of HPA, for the very interesting discussions in Didcot and to have given me the secrets of the WeLMoS

method. Thank you to Dr Guthrie MILLER, researcher at the Los Alamos National Laboratory, for our meetings in Santa-Fe and his comments on this work.

J'aimerais également remercier Monsieur Didier DUBOIS, directeur de recherche au CNRS, pour l'aide qu'il m'a apporté pour l'utilisation des réseaux bayésiens probabilistes et imprécis, et pour avoir apporté un regard d'informaticien des connaissances sur ce sujet.

I really want to thank Dr Mike BAILEY, researcher at HPA, for its help on the preparation of the article on the pulmonary absorption of plutonium. His knowledge about the HRTM improved a lot this work which would have been very different without his advice.

Un grand merci à Monsieur François GENSDARMES, chef du Laboratoire de Physique et de Métrologie des Aérosols de l'IRSN, pour son aide sur la compréhension des mesures granulométriques et pour nous avoir présenté les différents modèles existants permettant d'estimer la mise en suspension et le transport des aérosols.

Je tiens également à remercier mes professeurs d'anglais d'Inlingua Vélizy pour avoir relu et corrigé cette thèse. Merci à Messieurs Robert GASIOR et Vittorio CALLEA.

Merci également à Madame Bérangère CASSON d'ITT pour son aide lors de la programmation d'OPSCI avec IDL.

Je remercie très chaleureusement tous les membres du LEDI pour leur soutien, leurs questions, leur aide au cours de ces trois ans mais également pour leur bonne humeur, leur enthousiasme. J'ai vraiment eu un grand plaisir à travailler ici et à échanger avec vous tous. Merci également à Mesdames Juliette AMBROISE et Françoise GRIGNON pour leur aide pour la préparation des missions et de toutes les petites choses dont j'ai eu besoin. Merci à Mademoiselle Stéphanie LAMART, pour sa gentillesse, pour m'avoir aidé avec IDL et avec les démarches à l'université.

Résumé

En vue d'optimiser la protection des travailleurs vis-à-vis des rayonnements ionisants, la réglementation française impose des limites de dose et une démarche de réduction progressive de l'exposition, dans la continuité des recommandations de la Commission Internationale de Protection Radiologique. Afin de vérifier le respect des limites et contraintes de dose lorsqu'un risque de contamination interne existe, des programmes de surveillance sont mis en place par des mesures radiotoxicologiques périodiques. Cependant, des incertitudes dans l'interprétation dosimétrique de ces mesures sont introduites par leur variabilité propre et par la connaissance incomplète des conditions de contamination.

Ces incertitudes ont été prises en compte par des techniques statistiques classique, bayésienne et possibiliste. La méthodologie développée a été appliquée à l'évaluation de l'exposition potentielle lors de la fabrication du combustible nucléaire et dans les mines d'uranium, ainsi qu'à l'analyse du programme de surveillance des travailleurs des ateliers de purification du plutonium du site AREVA NC de La Hague.

A partir du seuil de décision du comptage nucléaire, la dose minimale détectable (DMD) par le programme avec un niveau de confiance donné peut être calculée à l'aide du logiciel « Optimisation des Programmes de Surveillance de la Contamination Interne » (OPSCI). Elle s'avère un support utile à l'optimisation des programmes de surveillance, en recherchant le meilleur compromis entre leur sensibilité et leur coût.

Mots-clés: radioprotection, dosimétrie interne, incertitudes, uranium, plutonium

Résumé de la thèse

1. Surveillance de la contamination interne

1.1. Exposition aux rayonnements ionisants

Les travailleurs de l'industrie nucléaire peuvent être exposés aux rayonnements ionisants durant les différentes opérations du cycle nucléaire. Après son extraction, le minerai d'uranium est converti en yellow cake puis enrichi afin de préparer le combustible. Après son utilisation, le combustible est retraité pour en extraire l'uranium (U) et le plutonium (Pu) qui sont ensuite recyclés notamment en combustible Mixed Oxide (MOX) pour le Pu.

1.2. Radioprotection

Pour quantifier l'exposition aux rayonnements ionisants, la Commission Internationale pour la Protection Radiologique (CIPR) définit la notion de dose (ICRP, 2007) :

- La dose absorbée $D_{T,R}$ est la quantité d'énergie cédée au tissu T par le rayonnement R et s'exprime en Gray (Gy), avec 1 Gy = 1 $J.kg^{-1}$.
- La dose équivalente pour un organe ou un tissu, H_T, prend en compte l'effet biologique relatif des différents types de rayonnement par l'intermédiaire d'un facteur de pondération w_R, dont la valeur est recommandée par la CIPR. Elle se calcule, en Sievert (Sv), par la formule :

$$H_T = \sum_R w_R D_{T,R}$$

- La dose efficace E est une grandeur de radioprotection se rapportant au risque global pour un individu de référence. Elle est calculée, en Sv, comme étant la somme des doses équivalentes reçues par les tissus les plus radiosensibles, pondérée par un facteur w_T déduit des études épidémiologiques et biologiques :

$$E = \sum_T w_T H_T$$

Le caractère prolongé de l'irradiation due à une contamination interne a conduit à définir le concept spécifique de dose engagée. Celle-ci est définie comme étant la somme des doses

équivalentes ou efficaces reçues pendant 50 ans après l'incorporation de radioactivité par un adulte ou jusqu'à l'âge de 70 ans pour un enfant.

Pour limiter l'exposition, un système de radioprotection a été développé par la CIPR (ICRP, 2007) et adopté par la réglementation française (Code du travail, 2008a):

Justification: Seules les opérations utiles et nécessaires impliquant une exposition doivent être réalisées; de plus, elles doivent produire un bénéfice individuel ou sociétal suffisant pour dépasser le détriment qu'elles causent.

Optimisation: L'exposition doit être amenée à un niveau aussi bas que raisonnablement possible en prenant en compte les facteurs économiques et sociétaux.

Limitation: La dose totale ne doit pas dépasser une dose limite.

Afin de surveiller l'exposition des travailleurs, des programmes de surveillance sont mis en place. Ils peuvent être formés de mesures d'ambiance surveillant la contamination surfacique ou volumique d'une pièce ou individuelles pour estimer directement la contamination d'un travailleur. Les programmes de surveillance individuelle de routine sont formés de mesures d'activité périodiques.

1.3. Mesure d'activité incorporée

Deux types de mesures peuvent être mis en place pour évaluer l'activité incorporée dans le corps humain. La mesure radiotoxicologique ou *in vitro* est la mesure de l'activité excrétée dans les urines ou les selles pendant une période d'échantillonnage, typiquement une journée. Elle est particulièrement importante pour mesurer la contamination par des émetteurs alpha et béta.

L'anthroporadiamétrie est la mesure *in vivo* par spectrométrie des rayonnements X ou gammas émis par les radionucléides présents dans l'ensemble du corps humain ou dans un organe en particulier.

La sensibilité de ces mesures est quantifiée par leur seuil de décision (SD) et limite de décision (LD). En effet, si un résultat de mesure est supérieur au SD, alors la présence d'activité peut être quantifiée, sinon, il peut être conclu que l'activité mesurée est inférieure à la LD.

Ces deux types de mesures sont sujets aux incertitudes dues à la statistique de comptage de radioactivité qui peut être modélisée par un loi de Poisson d'une part ; et dues à la détermination du bruit de fond, de la calibration, et de l'échantillonnage pour les mesures *in vitro* d'autre part. Ces incertitudes de Type B sont modélisées par une loi lognormale avec un écart-type appelé scattering factor (SF).

Pour remonter de la mesure d'activité excrétée ou retenue dans un organe à l'activité incorporée et à la dose des modèles doivent être utilisés.

1.4. Modèles

Des modèles biocinétiques ont été développés par la CIPR pour prédire le comportement du radionucléide dans le corps humain de son entrée à son excrétion.

- Le modèle respiratoire humain HRTM (ICRP, 1994a) représente le système respiratoire, et prédit le dépôt d'un aérosol dans les voies respiratoires paramétré par son diamètre aérodynamique médian en activité DAMA ; l'épuration du radionucléide soit par transport muco-ciliaire soit par absorption vers le sang. L'absorption est modélisée par trois paramètres : la fraction rapidement dissoute f_r, la vitesse d'absorption rapide s_r et lente s_s ; ou par les vitesses s_p, s_{pt}, s_t.
- Le système gastro-intestinal est modélisé soit par le GITM (ICRP, 1979), soit par le HATM (ICRP, 2006). Une fraction f_1 ou f_A de l'activité dans le système gastro-intestinal est absorbée vers le sang.
- Le comportement du radionucléide depuis son entrée dans le sang jusqu'à son excrétion est modélisé par les modèles systémiques. La CIPR a défini des modèles spécifiques de chaque radionucléide : U (ICRP, 1995a), Pu (ICRP, 1993). Leggett *et al* (2005) a développé un nouveau modèle systémique du Pu.

Des modèles dosimétriques sont utilisés pour calculer les doses absorbées par les différents tissus à partir des activités retenues dans les tissus prédites par les modèles biocinétiques. Pour cela, une représentation géométrique du corps humain est nécessaire (Cristy and Eckerman, 1987, ICRP, 2002b, 2009).

Cependant, ces modèles sont définis pour l'homme de référence de la CIPR et non pour un individu particulier. Les prédictions des modèles sont donc sujettes aux incertitudes dues à la variabilité inter-individuelle.

1.5. Calcul de la dose interne

Pour quantifier l'exposition des travailleurs, les mesures de l'activité retenue ou excrétée doivent être interprétées en termes de dose efficace engagée par l'utilisation des modèles biocinétiques et dosimétriques. D'un point de vue pratique, la dose est estimée en deux étapes : 1) l'incorporation i est estimée en divisant la valeur d'activité mesurée M t jours après l'incorporation par la fonction de rétention ou d'excrétion à la date t, $m(t)$; 2) la dose efficace engagée E est calculée en multipliant l'incorporation par le coefficient de dose e_{50} :

$$i = \frac{M}{m(t)} \qquad E = i \times e_{50}\,.$$

La fonction de rétention ou d'excrétion est la prédiction des modèles biocinétiques pour la quantité mesurée (rétention dans le corps entier, dans un organe ou l'excrétion journalière) pour

une incorporation unitaire. Le coefficient de dose est la dose efficace engagée reçue par l'homme de référence pour une incorporation unitaire.

Pour choisir les fonctions d'excrétion et de rétention ainsi que le coefficient de dose adaptés à la situation, il est nécessaire de connaître ou de faire des hypothèses sur les conditions d'exposition :

- radionucléide(s),
- composition isotopique,
- date(s) de contamination,
- voie(s) de contamination: inhalation, ingestion, blessure,
- propriétés physico-chimique du matériau radioactif: type d'absorption, DAMA pour un aérosol.

Les valeurs exactes de tous ou certains de ces paramètres sont en général inconnues et souvent difficiles à déterminer. La CIPR recommande l'utilisation des valeurs par défaut pour ces paramètres.

En l'absence d'information spécifique, l'individu est représenté par l'homme de référence (ICRP, 1975, 2002b); un travailleur exerce une activité professionnelle 8 heures par jour avec un débit respiratoire de 1,2 $m^3.h^{-1}$ (ICRP, 1994a); l'absorption pulmonaire du matériel est soit de type F, M, ou S (ICPR, 1994b); l'absorption de l'intestin vers le sang est quantifiée par des valeurs proposées de f_1 or f_A (ICRP, 1979, 2006); le DAMA de l'aérosol radioactive est de 5 µm pour les travailleurs avec un écart-type géométrique de 2,5 et une densité de 3 $g.cm^{-3}$ (ICRP, 1994a); dans le cadre d'une surveillance de routine, la contamination est supposée avoir lieu au milieu de l'intervalle de surveillance (ICRP, 1997b).

1.6. Approche de cette étude

La surveillance individuelle des contaminations internes susceptibles de résulter d'une exposition professionnelle est réalisée par des mesures anthroporadiamétriques et radiotoxicologiques, interprétées en termes d'activité incorporée et de dose efficace engagée à l'aide de modèles biocinétiques et dosimétriques. Le risque de contamination est quantifié *a priori* par l'identification des radionucléides présents au poste de travail, de leurs activités, de la fréquence et de la durée d'exposition potentielle. Une technique de mesure, associée à une période de surveillance, sont déterminées en fonction de l'exposition potentielle. Pour faciliter ces choix, la norme ISO 20553 (ISO, 2006a) recommande des programmes de surveillance spécifiques pour certains composés radioactifs, permettant la détection de toute incorporation annuelle induisant une dose efficace engagée sur 50 ans de plus de 1 mSv. Des valeurs nominales y sont attribuées aux différents paramètres intervenant dans l'évaluation dosimétrique. Malgré ces normes, des incertitudes dans l'interprétation dosimétrique des mesures radiotoxicologiques peuvent subsister de par la variabilité de la mesure d'activité et la connaissance quelquefois incomplète des conditions de contamination. Les incertitudes sur la dose évaluées à partir de conditions

d'exposition ont été évaluées pour une exposition potentielle à l'uranium durant la fabrication du combustible et dans les mines.

La sensibilité d'un programme de surveillance en termes de dose efficace peut être déterminée en prenant en compte les incertitudes relatives aux conditions d'expositions et à la mesure. Le seuil de décision et la fréquence de la mesure permettent de définir une incorporation et une dose minimales détectables par le programme de surveillance en fonction des modèles biocinétiques et dosimétriques appliqués. La dose minimale détectable (DMD) est définie de telle manière que si la mesure est inférieure au seuil de décision, la dose efficace correspondante est inférieure à la DMD avec un niveau de confiance de 95%. Elle est ainsi un critère de sensibilité du programme de surveillance et peut être utilisée comme un outil d'aide au choix du programme le plus pertinent pour une exposition donnée, en procédant à un compromis entre le poids des mesures (coût, contraintes,..) et la sensibilité de la surveillance.

Le calcul de la DMD relative à une exposition et un programme de surveillance donnés et l'optimisation de ce programme a été réalisé pour les installations d'extraction du plutonium sur le site AREVA NC de La Hague.

2. Modélisation et propagation des incertitudes

2.1. Représentation de l'incertain

Dans le cadre de cette étude, différentes représentation de l'incertain ont été utilisées :

- Les probabilités sont définies par l'axiomatique de Kolmogorov. Cependant, attribuer une distribution de probabilité à une variable incertaine est un choix subjectif qui devrait reposer sur des connaissances précises de la variabilité du paramètre.
- Si ces informations ne sont pas connues, des possibilités (Dubois and Prade, 1988) peuvent être utilisées. Au lieu d'attribuer un poids de vraisemblance à une valeur d'une variable, il est assigné à un intervalle. Ceci permet de limiter l'information apportée par le choix de la distribution de possibilité car elle contient toutes les distributions de probabilité ayant le même intervalle de variation et le même mode. Ainsi, au lieu de choisir une seule distribution de probabilité pour une variable, une famille de probabilité est choisie, limitant ainsi le poids des hypothèses.
- Afin de pouvoir modéliser certaines variables par des distributions de probabilité quand les informations sur cette variable sont suffisantes et d'autres par des possibilités, les plausibilités dans le cadre de la théorie de Dempster-Shafer (Shafer, 1976) ont été utilisées dans cette étude.

2.2. Techniques de propagation directe

La propagation directe des incertitudes est le calcul de l'incertitude sur une variable de sortie à partir des incertitudes sur les variables d'entrée. Pour cette étude, cela revient à estimer l'incertitude sur la dose efficace engagée à partir des incertitudes sur les paramètres définissant les conditions d'exposition : l'incorporation, la date de contamination, le DAMA et l'absorption vers le sang de l'aérosol radioactif.

Si le modèle reliant les variables de sortie aux variables d'entrée n'est pas une expression analytique, la méthode reine de propagation des incertitudes modélisées par des probabilités est la technique de Monte-Carlo. Cette méthode échantillonne aléatoirement des valeurs de chaque paramètre d'entrée suivant sa loi de probabilité. Ensuite, pour chaque jeu de ces valeurs, la variable de sortie est calculée en appliquant le modèle pour ce jeu de paramètre. Une distribution de probabilité de la variable de sortie peut donc être évaluée.

Afin de propager les incertitudes sur les variables d'entrée modélisées par des possibilités et des probabilités, la méthode RaFu (Chojnacki *et al*, 2010), adaptation des techniques de Monte-Carlo peut être utilisée. Pour les variables probabilistes et possibilistes, sont tirées aléatoirement suivant leurs distributions des valeurs fixes pour les premières et des intervalles pour les secondes. Ensuite la variable de sortie est calculée pour tous les jeux de variables d'entrée formés par les valeurs fixes ou les bornes des intervalles de chaque paramètre d'entrée. Ainsi une distribution de plausibilité de la dose est obtenue à partir des incertitudes sur les conditions d'exposition. Cette distribution est obtenue sous la forme de probabilités cumulées haute et basse.

2.3. Techniques de propagation indirecte

La propagation indirecte d'incertitudes est le calcul des incertitudes sur les paramètres d'entrée à partir de l'incertitude sur les paramètres de sortie. Pour ce travail, l'incertitude sur l'incorporation est obtenue à partir des incertitudes sur les autres paramètres de l'exposition et sur la mesure et à partir d'un résultat de mesure d'activité. L'incertitude sur la dose est également évaluée.

Pour propager indirectement les incertitudes, une première méthode, dite classique, considère l'incorporation éventuelle comme une valeur fixe mais inconnue. Elle permet de calculer un intervalle de confiance sur l'incorporation à partir d'un résultat d'analyse radiotoxicologique et d'hypothèses probabilistes sur les paramètres incertains que sont la date de contamination, le DAMA, les paramètres d'absorption des particules inhalées et les variations d'échantillonnage biologique et de mesure (Molokanov *et al*, 2009). Si le modèle biocinétique est fixé, l'intervalle de confiance sur la dose est proportionnel à celui de l'incorporation. En revanche, si les paramètres biocinétiques sont incertains, l'intervalle de confiance sur la dose ne peut plus être estimé rigoureusement en raison de la corrélation entre l'estimation de l'incorporation et le coefficient de dose.

C'est pourquoi une seconde méthode, dite Weighted Likelihood MonteCarlo Sampling (WeLMoS), développée par la Health Protection Agency (HPA, Royaume-Uni ; Puncher and Birchall, 2008) a été appliquée. Elle s'appuie sur la statistique bayésienne pour actualiser la connaissance *a priori* de la probabilité de l'incorporation en une connaissance *a posteriori* des probabilités de l'incorporation et de la dose après l'observation d'une valeur de mesure :

$$P(i|M) = \frac{\int_L \int_t P(M|i,L,t) \times P(L) \times P(t) \times dL \times dt}{\int_i \int_L \int_t P(M|i,L,t) \times P(i) \times P(L) \times P(t) \times dL \times dt \times di} \times P(i),$$

$$P(E|M) = \frac{\int_L \int_t P(M|E,L,t) \times P(L) \times P(t) \times dL \times dt}{\int_i \int_L \int_t P(M|E,L,t) \times P(i) \times P(L) \times P(t) \times dL \times dt \times di} \times P(i) \text{ with } E = i \times e_{50}(L)$$

P(i), *P(L)* et *P(t)* sont les probabilités *a priori* de l'incorporation *i*, des propriétés physico-chimiques de l'aérosol *L* et de la date de contamination *t* : elles représentent l'information connue ou supposée relative à ces variables préalablement à toute mesure. *P(M|i, L, t)* est la vraisemblance de la mesure sachant *i*, *L* et *t*: c'est la probabilité d'obtenir la mesure M à partir des valeurs données de *i*, *L* et *t*. *P(i | M)* t *P(E | M)* sont les probabilités *a posteriori*. Elles sont la mise à jour des probabilités *a priori* par la connaissance apportée par la mesure. Le théorème de Bayes peut être appliquée en utilisant des variables continues comme pour la méthode WeLMoS ou pour des variables discrètes en remplaçant les intégrales par des sommes.

Enfin, un réseau bayésien discrétisé a été développé dans le cadre de cette étude (Davesne *et al*, 2010) pour calculer les probabilités *a posteriori* de l'incorporation et de la dose à partir d'une mesure (Fig. 1). La dose *E* est seulement corrélée avec les propriétés physico-chimiques du contaminant *L* et avec l'incorporation *i*. L'activité mesurée *M* est complètement corrélée avec la quantité biologique *S* (par exemple, l'activité dans un échantillon urinaire) mais est différente de la mesure à cause des incertitudes de comptage : la probabilité *P(M | S)* d'obtenir *M* sachant *S* est ainsi modélisée par une distribution de Poisson de moyenne *S*. La quantité biologique *S* est définie par *i*, *L* et *t*, modulée par des incertitudes de Type B : la probabilité de *S* sachant *i*, *L* et *t* suit une distribution lognormale de moyenne géométrique $i \times m(L,t)$ où *m* est la fonction d'excrétion ou de rétention correspondant à la quantité mesurée et avec un écart-type géométrique égal au SF dépendant de l'échantillonnage et de la calibration des systèmes de mesures pour l'anthroporadiamétrie. Chacune des six variables est discrétisée et la vraisemblance globale associée à une incorporation ou dose spécifique est obtenue en sommant les vraisemblances obtenues pour chaque combinaison des valeurs discrètes des différentes variables.

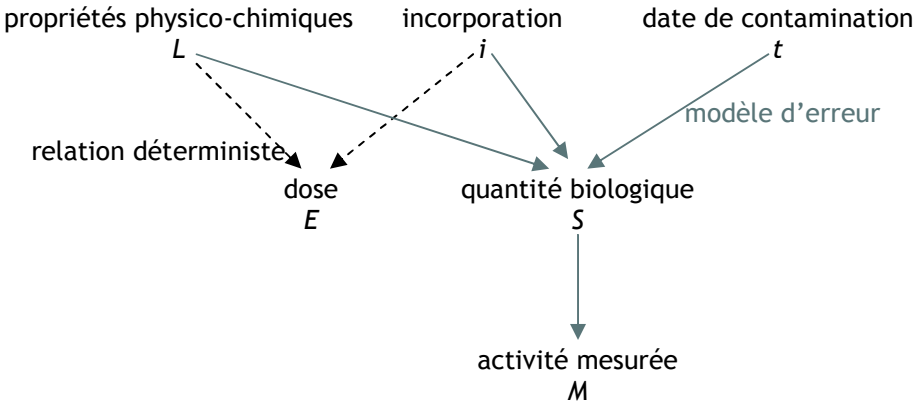

Figure 1 : Structure du réseau bayésien développé pour obtenir les probabilités *a posteriori* de l'incorporation et de la dose

Ces méthodes ont été mises en place pour l'évaluation des incertitudes en dosimétrie prospective (propagation directe) et rétrospective (propagation indirecte).

3. Dosimétrie prospective : propagation directe d'incertitudes

3.1. Objectif et cadre de l'étude

L'objectif de cette étude est l'application de la méthode RaFu pour l'évaluation des incertitudes et de démontrer son utilité en dosimétrie prospective de l'exposition interne. Elle est plus prudente que les habituelles approches probabilistes et est particulièrement bien adaptée à la modélisation de l'information imprécise relative aux conditions d'exposition.

Le cas de contamination étudié ici est l'inhalation de poussière de ^{234}U par un travailleur du nucléaire. Seules les incertitudes liées aux paramètres caractérisant la forme physico-chimique du contaminant ont été prises en compte. Ce sont le diamètre aérodynamique médian en activité DAMA des particules formant la poussière et leurs vitesses d'absorption des voies respiratoires, s_p, s_{pt} et s_t et digestives vers le sang f_1. Les résultats recherchés sont les doses efficace ou équivalentes engagées sur 50 ans aux poumons h_{poumon}, à la région extrathoracique des voies respiratoires h_{ET} ou à la moelle osseuse h_{MO}, par unité d'incorporation et avec leurs incertitudes associées.

Cette approche a été appliquée à la contamination par inhalation de poussières d'uranium par :

- la caractérisation de l'exposition interne à différents postes de travail par l'estimation de la dose reçue pour une incorporation unitaire,
- l'estimation des doses reçues dans les mines et durant le traitement du minerai pour une exposition d'une heure avec une concentration d'uranium dans l'air unitaire.

3.2. Modélisation des incertitudes

Pour propager les incertitudes, le logiciel Statistical UNcertainty and SEnsitivity Tools (SUNSET, IRSN, France) a été utilisé. SUNSET a été connecté à DCAL (Eckerman *et al*, 2006) pour calculer la dose correspondante aux jeux de paramètres échantillonnés par SUNSET. L'analyse statistique et les graphiques ont été réalisés avec Excel® (Microsoft®, USA).

Trois approches déterministe, probabiliste et de Dempster-Shafer ont été appliquées pour évaluer les incertitudes sur la dose. Elles ont été quantifiées comme le rapport entre :

- les bornes des intervalles obtenus par le calcul déterministe,
- le 95ème percentile et le 5ème percentile de la courbe de probabilité cumulée (CDF) obtenue par l'approche probabiliste,
- le 95ème percentile de la CDF basse et le 5ème percentile de la CDF haute obtenues avec l'approche de Dempster-Shafer.

Pour la comparaison entre les approches purement probabiliste et de Dempster-Shafer, la même fonction mathématique a été utilisée pour représenter l'information sur un paramètre comme soit une distribution de probabilité soit une distribution de possibilité.

Une revue de la littérature a été réalisée pour collecter les connaissances actuelles du DAMA, s_p, s_{pt}, s_t et f_1. Cette information a été utilisée pour modéliser les incertitudes sur les paramètres en attribuant des lois de possibilités aux paramètres quand peu d'information a été recueillie ou de probabilité si une connaissance importante a été mise en évidence. Les distributions utilisées pour ce travail sont regroupées dans le Tableau 1 et 2.

Tableau 1 : Distributions de possibilités et de probabilités utilisées pour évaluer les incertitudes pour une contamination à différents postes de travail en appliquant l'approche de Dempster-Shafer. GSD, écart-type géométrique.

Composé et poste de travail	Paramètre	Théorie	Distribution
U_3O_8 à COMURHEX Malvesi	DAMA	Possibilité	Trapézoïdale avec pour support 2,2–15 µm et pour noyau 5–10 µm
	s_p	Possibilité	Uniforme sur 0,02-0,11 j^{-1}
	s_{pt}	Possibilité	Uniforme sur 0,3–2,6 j^{-1}
	s_t	Possibilité	Triangulaire avec pour support 3,5 x 10^{-4}-9,5 x 10^{-3} j^{-1} et pour mode 1,3 x 10^{-3} j^{-1}
	f_1	Probabilité	Lognormale avec une moyenne géométrique de 0,01 et GSD de 2,46
UF_4 à COMURHEX Malvesi	DAMA	Possibilité	Trapézoïdale avec pour support 2,2–15 µm et pour noyau 5–10 µm
	s_p	Possibilité	Triangulaire avec pour support 5,5 x 10^{-2}-0,5 j^{-1} et pour mode 0,15 j^{-1}
	s_{pt}	Possibilité	Trapézoïdale avec pour support 0,05–0,14 j^{-1} et pour noyau 0,09-0,12 j^{-1}
	s_t	Possibilité	Triangulaire avec pour support 8,0 x 10^{-4}-8,0 x 10^{-3} j^{-1} et pour mode 3,0 x 10^{-3} j^{-1}
	f_1	Probabilité	Lognormale avec une moyenne géométrique de 0,01 et GSD de 2,46

UO_2 à COMURHEX Malvesi	DAMA	Possibilité	Trapézoïdale avec pour support 2,2–15 µm et pour noyau 5–10 µm
	s_p	Possibilité	Uniforme sur 0,01-0,06 j^{-1}
	s_{pt}	Possibilité	Triangulaire avec pour support 0-1,6 j^{-1} et pour mode 1,2 j^{-1}
	s_t	Possibilité	Triangulaire avec pour support 1,0 x 10^{-4}-1,7 x 10^{-3} j^{-1} et pour mode 6,0 x 10^{-4} j^{-1}
	f_1	Probabilité	Lognormale avec une moyenne géométrique de 0,01 et GSD de 2,46
U_3O_8 à FBFC Pierrelatte	DAMA	Possibilité	Trapézoïdale avec pour support 2,2–15 µm et pour noyau 3–7 µm
	s_p	Possibilité	Uniforme sur 0,02-0,11 j^{-1}
	s_{pt}	Possibilité	Uniforme sur 0,3–2,6 j^{-1}
	s_t	Possibilité	Triangulaire avec pour support 3,5 x 10^{-4}-9,5 x 10^{-3} j^{-1} et pour mode 1,3 x 10^{-3} j^{-1}
	f_1	Probabilité	Lognormale avec une moyenne géométrique de 0,01 et GSD de 2,46
UO_2 à FBFC Pierrelatte	DAMA	Possibilité	Trapézoïdale avec pour support 2,2–15 µm et pour noyau 3–7 µm
	s_p	Possibilité	Uniforme sur 0,01-0,06 j^{-1}
	s_{pt}	Possibilité	Triangulaire avec pour support 0-1,6 j^{-1} et pour mode 1,2 j^{-1}
	s_t	Possibilité	Triangulaire avec pour support 1,0 x 10^{-4}-1,7 x 10^{-3} j^{-1} et pour mode 6,0 x 10^{-4} j^{-1}
	f_1	Probabilité	Lognormale avec une moyenne géométrique de 0,01 et GSD de 2,46
U_3O_8 à COGEMA Pierrelatte	DAMA	Possibilité	Trapézoïdale avec pour support 2,2–15 µm et pour noyau 4–9 µm
	s_p	Possibilité	Uniforme sur 0,02-0,11 j^{-1}
	s_{pt}	Possibilité	Uniforme sur 0,3–2,6 j^{-1}
	s_t	Possibilité	Triangulaire avec pour support 3,5 x 10^{-4}-9,5 x 10^{-3} j^{-1} et pour mode 1,3 x 10^{-3} j^{-1}
	f_1	Probabilité	Lognormale avec une moyenne géométrique de 0,01 et GSD de 2,46
UO_4 à COGEMA Pierrelatte	DAMA	Possibilité	Trapézoïdale avec pour support 2,2–15 µm et pour noyau 4–9 µm
	s_p	Possibilité	Uniforme sur 0,15-0,9 j^{-1}
	s_{pt}	Possibilité	Triangulaire avec pour support 0,1-0,14 j^{-1} et pour mode 0,12 j^{-1}
	s_t	Possibilité	Uniforme sur 8,0 x 10^{-3}-2,5 x 10^{-2} j^{-1}
	f_1	Probabilité	Lognormale avec une moyenne géométrique de 0,01 et GSD de 2,46
UO_2 à COGEMA Pierrelatte	DAMA	Possibilité	Trapézoïdale avec pour support 2,2–15 µm et pour noyau 4–9 µm
	s_p	Possibilité	Uniforme sur 0,01-0,06 j^{-1}
	s_{pt}	Possibilité	Triangulaire avec pour support 0-1,6 j^{-1} et pour mode 1,2 j^{-1}
	s_t	Possibilité	Triangulaire avec pour support 1,0 x 10^{-4}-1,7 x 10^{-3} j^{-1} et pour mode 6,0 x 10^{-4} j^{-1}
	f_1	Probabilité	Lognormale avec une moyenne géométrique de 0,01 et GSD de 2,46
U_3O_8 à COMURHEX Pierrelatte	DAMA	Possibilité	Trapézoïdale avec pour support 2,2–17 µm et pour noyau 4–10 µm
	s_p	Possibilité	Uniforme sur 0,02-0,11 j^{-1}
	s_{pt}	Possibilité	Uniforme sur 0,3–2,6 j^{-1}
	s_t	Possibilité	Triangulaire avec pour support 3,5 x 10^{-4}-9,5 x 10^{-3} j^{-1} et pour mode 1,3 x 10^{-3} j^{-1}
	f_1	Probabilité	Lognormale avec une moyenne géométrique de 0,01 et GSD de 2,46

UF_4 à COMURHEX Pierrelatte	DAMA	Possibilité	Trapézoïdale avec pour support 2,2–17 µm et pour noyau 4–10 µm
	s_p	Possibilité	Triangulaire avec pour support 5,5 x 10^{-2}-0,5 j^{-1} et pour mode 0,15 j^{-1}
	s_{pt}	Possibilité	Trapézoïdale avec pour support 0,05–0,14 j^{-1} et pour noyau 0,09-0,12 j^{-1}
	s_t	Possibilité	Triangulaire avec pour support 8,0 x 10^{-4}-8,0 x 10^{-3} j^{-1} et pour mode 3,0 x 10^{-3} j^{-1}
	f_1	Probabilité	Lognormale avec une moyenne géométrique de 0,01 et GSD de 2,46
U_3O_8 à FBFC Romans	DAMA	Possibilité	Trapézoïdale avec pour support 0,75–17,5 µm et pour noyau 0,9–10 µm
	s_p	Possibilité	Uniforme sur 0,02-0,11 j^{-1}
	s_{pt}	Possibilité	Uniforme sur 0,3–2,6 j^{-1}
	s_t	Possibilité	Triangulaire avec pour support 3,5 x 10^{-4}-9,5 x 10^{-3} j^{-1} et pour mode 1,3 x 10^{-3} j^{-1}
	f_1	Probabilité	Lognormale avec une moyenne géométrique de 0,01 et GSD de 2,46
UO_4 à FBFC Romans	DAMA	Possibilité	Trapézoïdale avec pour support 0,75–17,5 µm et pour noyau 0,9–10 µm
	s_p	Possibilité	Uniforme sur 0,15-0,9 j^{-1}
	s_{pt}	Possibilité	Triangulaire avec pour support 0,1-0,14 j^{-1} et pour mode 0,12 j^{-1}
	s_t	Possibilité	Uniforme sur 8,0 x 10^{-3}-2,5 x 10^{-2} j^{-1}
	f_1	Probabilité	Lognormale avec une moyenne géométrique de 0,01 et GSD de 2,46
UO_2 à FBFC Romans	DAMA	Possibilité	Trapézoïdale avec pour support 0,75–17,5 µm et pour noyau 0,9–10 µm
	s_p	Possibilité	Uniforme sur 0,01-0,06 j^{-1}
	s_{pt}	Possibilité	Triangulaire avec pour support 0-1,6 j^{-1} et pour mode 1,2 j^{-1}
	s_t	Possibilité	Triangulaire avec pour support 1,0 x 10^{-4}-1,7 x 10^{-3} j^{-1} et pour mode 6,0 x 10^{-4} j^{-1}
	f_1	Probabilité	Lognormale avec une moyenne géométrique de 0,01 et GSD de 2,46
mines	DAMA	Possibilité	Triangulaire avec pour support 3–23 µm et pour mode 6 µm
	s_p	Possibilité	Polygonale définie par (abscisse (j^{-1}), ordonnée): (0,005, 0); (0,05, 1); (0,5, 0,1); (5, 0,067); (50, 6,7 x 10^{-4}); (500, 0)
	s_{pt}	Possibilité	Polygonale définie par (abscisse (j^{-1}), ordonnée): (0,05, 0); (0,5, 1); (5; 0,0167); (5, 0,005); (50, 0)
	s_t	Possibilité	Uniforme sur 0,001-0,029 j^{-1}
	f_1	Probabilité	Lognormale avec une moyenne géométrique de 0,01 et GSD de 2,46
traitement du minerai d'uranium	DAMA	Possibilité	Uniforme sur 0,5–15 µm
	s_p	Possibilité	Polygonale définie par (abscisse (j^{-1}), ordonnée): (5 x 10^{-5}, 0); (5 x 10^{-4}, 1); (0,005, 0,5); (0,05, 0,21); (0,5, 0,007); (5, 4 x 10^{-4}); (50, 1 x 10^{-5}); (500, 0)
	s_{pt}	Possibilité	Polygonale définie par (abscisse (j^{-1}), ordonnée): (5 x 10^{-5}, 0); (5 x 10^{-4}, 0,1); (5 x 10^{-3}, 0,2); (0,05, 0,01); (0,5, 3,67 x 10^{-3}); (5, 5,44 x 10^{-4}); (50, 0)
	s_t	Possibilité	Polygonale définie par (abscisse (j^{-1}), ordonnée): (5 x 10^{-6}; 0); (5 x 10^{-5}; 0,77); (5 x 10^{-4}; 1); (0,005; 0,18); (0,05; 1,54 x 10^{-3}); (0,5; 0)
	f_1	Probabilité	Lognormale avec une moyenne géométrique de 0,01 et GSD de 2,46

Tableau 2 : Distributions de probabilités utilisées pour évaluer les incertitudes pour une contamination dans les mines et pour le traitement du minerai d'uranium pour l'approche probabiliste. GSD : écart-type géométrique.

	Paramètre	Théorie	Distribution
mines	DAMA	Probabilité	Triangulaire avec pour support 3–23 µm et pour mode 6 µm
	s_p	Probabilité	Polygonale définie par (abscisse (j^{-1}); ordonnées cumulées): (0,005; 0); (0,05; 0,5); (0,5; 0,95); (5; 0,999); (50; 0,9995); (500; 1)
	s_{pt}	Probabilité	Polygonale définie par (abscisse (j^{-1}); ordonnées cumulées): (0,05; 0); (0,5; 0,5); (5; 0,99); (50; 0,999); (500; 1)
	s_t	Probabilité	Uniforme sur 0,001-0,029 j^{-1}
	f_1	Probabilité	Lognormale avec une moyenne géométrique de 0,01 et GSD de 2,46
traitement du minerai d'uranium	DAMA	Probabilité	Uniforme sur 0,5–15 µm
	s_p	Probabilité	Polygonale définie par (abscisse (j^{-1}); ordonnées cumulées): (5 x 10^{-5}; 0); (5 x 10^{-4}; 0,5); (0,005; 0,7); (0,05; 0,9); (0,5; 0,995); (5; 0,9999); (500; 1)
	s_{pt}	Probabilité	Polygonale définie par (abscisse (j^{-1}); ordonnées cumulées): (5 x 10^{-5}; 0); (5 x 10^{-4}; 0,5); (5 x 10^{-3}; 0,9); (0,05; 0,995); (0,5; 0,999); (5; 0,9999); (50; 1)
	s_t	Probabilité	Polygonale définie par (abscisse (j^{-1}); ordonnées cumulées): (5 x 10^{-6}; 0); (5 x 10^{-5}; 0,2); (5 x 10^{-4}; 0,5); (0,005; 0,9); (0,05; 0,999); (0,5; 1)
	f_1	Probabilité	Lognormale avec une moyenne géométrique de 0,01 et GSD de 2,46

La dose engagée équivalente *H*, en $Sv.h^{-1}$, reçue par un tissu durant une heure de travail dans une mine ou au traitement du minerai due à une inhalation de ^{234}U est calculée par

$$H = C \times B \times h ,$$

où *C* est la contamination de l'air en $Bq.m^{-3}$, *B* est le débit respiratoire en $m^3.h^{-1}$, et *h* est la dose équivalente reçue par le tissu pour une incorporation unitaire de ^{234}U en $Sv.Bq^{-1}$. Les incertitudes sur la dose par unité d'incorporation ont été estimées puis propagées aux incertitudes sur la dose reçue par un travailleur pour une exposition d'une heure pour une contamination de l'air unitaire.

Les incertitudes sur la mesure de la contamination de l'air sont modélisées par une distribution de probabilité normale avec une moyenne de 1 $Bq.m^{-3}$ et un écart-type relatif de 0,5 (Duport, 1994).

Le débit respiratoire varie avec la pénibilité du travail. Quatre situations ont été considérées : pénibilité grande, intermédiaire, faible ou inconnue. Les distributions de possibilité pour le débit respiratoire sont présentées sur la Fig. 2. A des fins de comparaisons, un calcul probabiliste a été réalisé avec une distribution normale avec une moyenne de 1,3 $m^3.h^{-1}$ et un écart-type de 0,19 $m^3.h^{-1}$ (ICRP, 1994a), pour modéliser le débit respiratoire pour une pénibilité inconnue.

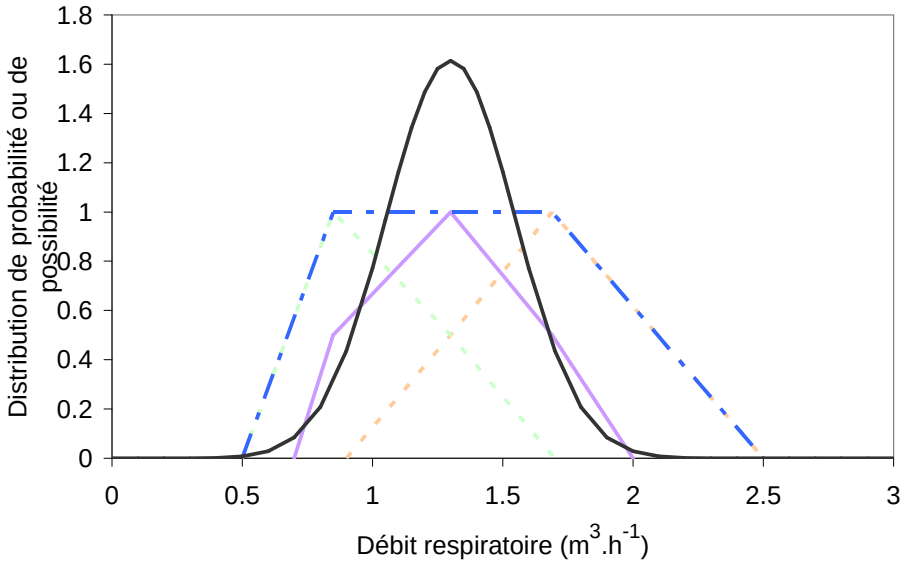

Figure 2 : Distributions de possibilité pour modéliser le débit respiratoire pour une pénibilité grande (pointillés orange), intermédiaire (violet), faible (pointillés verts) et inconnue (pointillés bleus). Distribution de probabilité pour une pénibilité inconnue (courbe noire)

3.3. Résultats et discussion

Les résultats (Tableaux 3 et 4) montrent que l'incertitude estimée par la méthode de Dempster-Shafer est plus large que celle obtenue par une modélisation purement probabiliste mais plus réduite que l'intervalle entre les valeurs de dose extrêmes envisageables. De plus, les hypothèses faites sur la dépendance ou l'indépendance entre les paramètres a une importance moindre dans le cadre de la méthodologie de Dempster-Shafer que dans un calcul purement probabiliste.

Tableau 3 : Facteurs d'incertitudes de la dose par unité d'incorporation pour différents postes de travail

Composé et poste de travail	Dose ($Sv.Bq^{-1}$) \ Méthode	Déterministe	Probabiliste	Dempster-Shafer
U_3O_8 à COMURHEX Malvesi	e_{50}	13	3	10
	h_{ET}	11	5	9
	h_{poumon}	15	4	12
	h_{MO}	36	5	13
UF_4 à COMURHEX Malvesi	e_{50}	27	5	15
	h_{ET}	9	10	17
	h_{poumon}	43	6	22
	h_{MO}	19	4	8
UO_2 à COMURHEX Malvesi	e_{50}	32	3	6
	h_{ET}	53	2	3
	h_{poumon}	36	4	9

	h_{MO}	75	6	16
U_3O_8 à FBFC Pierrelatte	e_{50}	14	4	10
	h_{ET}	11	5	10
	h_{poumon}	15	4	12
	h_{MO}	36	5	12
UO_2 à FBFC Pierrelatte	e_{50}	32	3	6
	h_{ET}	53	2	3
	h_{poumon}	36	4	9
	h_{MO}	75	6	19
U_3O_8 à COGEMA Pierrelatte	e_{50}	14	4	10
	h_{ET}	11	5	10
	h_{poumon}	15	4	12
	h_{MO}	36	5	13
UO_4 à COGEMA Pierrelatte	e_{50}	17	5	14
	h_{ET}	9	7	9
	h_{poumon}	25	6	21
	h_{MO}	12	4	7
UO_2 à COGEMA Pierrelatte	e_{50}	32	3	6
	h_{ET}	53	2	3
	h_{poumon}	36	4	9
	h_{MO}	75	6	17
U_3O_8 à COMURHEX Pierrelatte	e_{50}	16	4	12
	h_{ET}	10	5	9
	h_{poumon}	19	5	14
	h_{MO}	44	6	15
UF_4 à COMURHEX Pierrelatte	e_{50}	32	5	18
	h_{ET}	9	10	17
	h_{poumon}	52	7	28
	h_{MO}	23	5	10
U_3O_8 à FBFC Romans	e_{50}	16	4	12
	h_{ET}	20	5	19
	h_{poumon}	23	6	19
	h_{MO}	43	7	20
UO_4 à FBFC Romans	e_{50}	23	6	19
	h_{ET}	12	7	13
	h_{poumon}	34	9	30
	h_{MO}	15	5	10
UO_2 à FBFC Romans	e_{50}	48	3	7
	h_{ET}	90	2	6

	h_{poumon}	55	6	15
	h_{MO}	88	8	28
mines	e_{50}	9	11	35
	h_{ET}	60	39	71
	h_{poumon}	95	18	57
	h_{MO}	151	7	8
traitement du minerai d'uranium	e_{50}	17	24	90
	h_{ET}	60	178	265
	h_{poumon}	234	34	163
	h_{MO}	151	40	98

Tableau 4 : Facteurs d'incertitudes estimés pour la dose équivalente aux poumons reçues pour une contamination de l'air unitaire et une heure d'exposition dans les mines et lors du traitement du minerai d'uranium. H_{95}, 95ème percentile. H_5, 5ème percentile

	Pénibilité	H_{95} (Sv,h^{-1})	H_5 (Sv,h^{-1})	Facteur d'incertitude
mines	Grande	$1,2 \times 10^{-4}$	$2,3 \times 10^{-7}$	540
	Intermédiaire	$9,9 \times 10^{-5}$	$1,6 \times 10^{-7}$	610
	Faible	$7,9 \times 10^{-5}$	$1,2 \times 10^{-7}$	660
	Inconnue	$1,2 \times 10^{-4}$	$1,2 \times 10^{-7}$	1020
	Calcul probabiliste	$2,4 \times 10^{-5}$	$4,3 \times 10^{-7}$	55
traitement du minerai d'uranium	Grande	$3,4 \times 10^{-4}$	$2,8 \times 10^{-7}$	1211
	Intermédiaire	$2,8 \times 10^{-4}$	$2,0 \times 10^{-7}$	1365
	Faible	$2,2 \times 10^{-4}$	$1,5 \times 10^{-7}$	1497
	Inconnue	$3,4 \times 10^{-4}$	$1,5 \times 10^{-7}$	2340
	Calcul probabiliste	$2,2 \times 10^{-4}$	$2,8 \times 10^{-7}$	782

3.4. Conclusion

La méthodologie de Dempster-Shafer permet d'améliorer la modélisation de l'information sur les paramètres considérés et l'estimation de l'incertitude sur le résultat du calcul de dose par rapport au calcul probabiliste, qui tend à sous-estimer les incertitudes, et au calcul déterministe, qui ne fournit qu'un intervalle peu informatif entre les valeurs extrêmes. L'application de la méthodologie de Dempster-Shafer peut être facilement utilisée pour modéliser d'une manière réaliste les incertitudes sur les conditions d'exposition pour un poste de travail donné afin d'obtenir une juste estimation de la dose.

Cependant, cette méthodologie ne permet pas pour l'instant d'estimer les incertitudes sur la dose à partir d'un résultat de mesure par propagation inverse.

4. Exposition potentielle à une contamination par du plutonium à R4-T4

Un programme de surveillance spécifique a été choisi comme support à cette étude.

4.1. Travailler à R4-T4

Les ateliers d'extraction du plutonium sur le centre de retraitement AREVA NC de La Hague (R4 et T4) reçoivent la solution de nitrate de plutonium provenant de la séparation de l'uranium et des produits de fission. Dans un premier temps, le Pu est extrait par extraction liquide-liquide puis concentré et purifié sous forme de précipité d'oxalate. L'oxalate est ensuite filtré puis séché et placé dans un four pour être oxydé. Le dioxyde de plutonium est successivement homogénéisé puis conditionné dans des boîtes avant entreposage (Fig. 3).

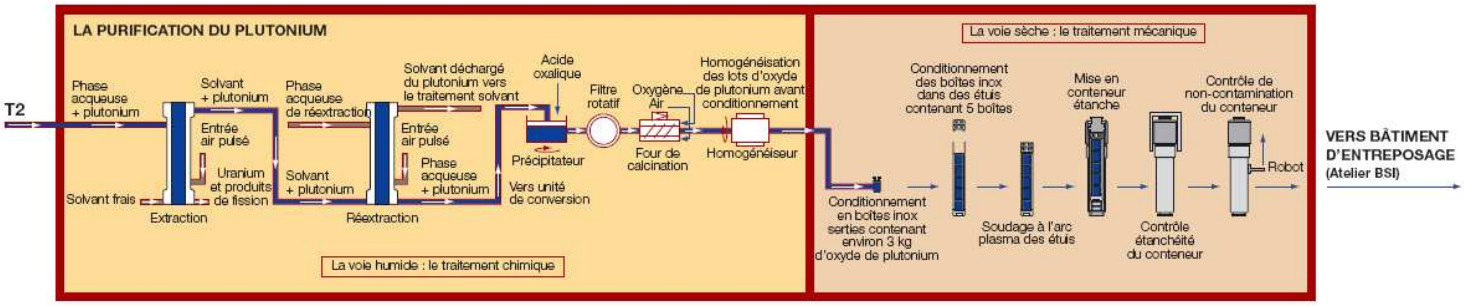

Figure 3 : Procédé d'extraction et de purification du plutonium sur le centre AREVA NC de La Hague (source : http://www.lahague.areva-nc.fr)

Grâce à l'automatisation du procédé, les travailleurs restent la plupart du temps en salle de conduite. Une contamination ne pourrait avoir lieu que lors d'interventions en boîte à gant pour le nettoyage hebdomadaire du filtre rotatif, le recyclage une à deux fois par semaine des reliquats de plutonium provenant d'analyse, ou la maintenance en cas de problème particulier comme le mauvais placement d'une boîte de conditionnement. En cas de rupture de confinement d'une boîte à gant, les travailleurs sont susceptibles d'inhaler de l'oxalate ou du dioxyde de plutonium lors de ces opérations.

4.2. Surveillance de la contamination interne

Surveillance d'ambiance

Afin de détecter une possible contamination au poste de travail, le Service de Prévention et de Radioprotection (SPR) réalise des mesures d'ambiance sur toutes les installations. Le contrôle de la

contamination surfacique est effectué par frottis, le résultat doit être inférieure à 0,01 $Bq.cm^{-2}$ pour de l'activité alpha dans des conditions de travail normal. Au-delà, le port du masque est obligatoire. De plus, les salles sont équipées de préleveurs d'air dont le filtre est mesuré toutes les semaines pour surveiller la contamination atmosphérique. Ces deux mesures permettent de surveiller périodiquement la propreté radiologique des installations.

Parallèlement, un suivi en temps réel est réalisé par des balises CRP qui analysent l'air en continu. Des Limites Moyennes Admissibles (LMA) sont définies pour être très inférieures aux Limites Annuelles d'Incorporations (LAI) correspondant aux limites de dose réglementaires.

Surveillance individuelle

Le programme de surveillance en place sur le centre AREVA NC de La Hague utilise des mesures anthroporadiamétriques des émetteurs gamma comme les produits de fission et l'américium, ainsi que des mesures radiotoxicologiques des émetteurs alpha comme l'U et le Pu. La période et la technique de mesure sont adaptées au risque individuel de contamination (Tableau 5). Tous les travailleurs bénéficient d'une mesure biannuelle par anthroporadiamétrie en corps entier pour s'assurer de l'absence de contamination par des produits de fission. Les différents intervalles de surveillance et techniques de mesure sont indiqués dans le Tableau 5. Le Pu manipulé en voie sèche (partie rouge de la Fig. 3), principalement du dioxyde, est un composé supposé insoluble et faiblement absorbé vers le sang ; c'est pourquoi il est surveillé par des mesures fécales contrairement au Pu en voie humide (partie orangée de la Fig. 3, Pu-TBP, ou nitrate), sous forme supposée soluble et facilement absorbée vers le sang qui est surveillé par des mesures urinaires. Le tritium ne fait pas l'objet d'une surveillance individuelle mais d'une surveillance de groupe par la mesure d'un échantillon représentatif de travailleurs exposés.

Tableau 5 : Procédures de surveillance individuelle de la contamination interne sur le centre AREVA NC de La Hague et forme du composé manipulé générant le risque.

Forme du composé manipulé à l'origine du risque de contamination	Procédure de surveillance
Plutonium en voie sèche (dioxyde)	Mesure fécale tous les 6 mois Anthroporadiamétrie pulmonaire tous les 6 mois
Plutonium en voie humide (nitrate, Pu-TBP)	Mesure urinaire tous les 6 mois
Produits de fission	Anthroporadiamétrie corps entier tous les 6 mois
Uranium pur (dioxyde, solution nitrique ou TBP)	Mesure urinaire tous les 6 mois
Tritium (HTO)	Mesure urinaire tous les mois

Mesures anthroporadiamétriques

Deux types de mesure anthroporadiamétrique sont réalisés sur le centre AREVA NC de La Hague. Leur niveau de dépistage (ND) est la limite de détection susceptible d'être obtenue pour la mesure la moins favorable c'est-à-dire pour des conditions de mesure pénalisantes en termes de limite de

détection. Les travailleurs classés B sont surveillés par des mesures corps entier selon un temps de comptage de 3 minutes réalisées avec un système de type Fast Scan (Canberra) avec un ND de 300 Bq pour le ^{137}Cs, lequel peut servir de traceur pour d'autres radionucléides.

Pour les travailleurs classés A, les mesures sont réalisées pendant 15 minutes sur un autre système de mesure dans des cellules blindées. Le ND est alors compris entre 3000 et 15000 Bq pour le ^{239}Pu en fonction de la morphologie du travailleur. Il est de 12 Bq pour le comptage pulmonaire de l'^{241}Am et de 85 Bq pour le ^{137}Cs en configuration corps entier.

Mesures radiotoxicologiques

Les mesures radiotoxicologiques *in vitro* sont réalisées sur des échantillons de selle ponctuelle ou sur au moins 1,5 L d'urine prélevée pendant une durée maximale de 10 jours pour une surveillance de routine. Dans le cadre d'une surveillance post-incidentelle, des urines de 24 heures ainsi que des selles de 72 h sont recueillies. La mesure par spectrométrie alpha des actinides après traitement chimique des échantillons permet de quantifier les activités des isotopes ^{238}U, ^{236}U, ^{235}U, ^{234}U, ^{240}Pu, ^{239}Pu, ^{238}Pu, ^{241}Am, ^{242}Cm, ^{244}Cm. Compte tenu de la proximité des pics, les isotopes ^{239}Pu et ^{240}Pu ne peuvent être séparés en spectrométrie alpha, leur activité est donc mesurée globalement ; de même que celle en ^{242}Cm et ^{244}Cm. Des quantités connues de ^{242}Pu et de ^{233}U sont ajoutées aux échantillons comme traceurs pour calculer le rendement chimique R_c de préparation (Tableau 6).

Tableau 6 : Rendement chimique moyen et écart-type pour les mesures radiotoxicologiques de l'uranium et du plutonium sur le site AREVA NC de La Hague

	Mesure urinaire		Mesure fécale
Traceur	^{242}Pu	^{233}U	^{242}Pu
Valeur moyenne du R_c	78,6 %	70,9 %	86,0 %
Ecart-type du R_c	10,9 %	11,8 %	13,6 %

Les échantillons biologiques obtenus après incident sont comptés durant une nuit en cas de surveillance post-incidentelle ; pour la surveillance de routine, le temps de comptage est de 48 h. Le rendement de comptage dépend de l'épaisseur de l'échantillon en couche mince pour le comptage et de l'angle solide selon lequel il est vu par le détecteur. Ce rendement est en moyenne égal à 32,5 % avec un écart-type de 2,7 %.

A partir de mesures du bruit de fond alpha de 24 h, le bruit de fond moyen a été estimé à 12,2 impulsions par 24 h sur une plage de mesure en énergie de 2200 keV. La largeur de la région d'intérêt pour la mesure du ^{239}Pu est de 200 keV. Pour un comptage de routine du ^{239}Pu, le bruit de fond moyen est donc de 2,2 impulsions par 48 h. Pour le ^{239}Pu, ceci implique un seuil de décision de 4,2 impulsions par 48 h.

4.3. Composition isotopique et taille des particules d'un aérosol

Le centre AREVA NC de La Hague retraite des combustibles de diverses origines impliquant différentes compositions isotopiques du plutonium : combustibles irradié dans des réacteurs à eau pressurisée ou à eau bouillante ou MOX. La variabilité de la composition isotopique est présentée dans le Tableau 7.

Tableau 7 : Composition isotopique en Pu et Am dans les combustibles retraités à R4-T4 provenant de réacteurs à eau pressurisée (REP1 et REP2), à eau bouillante (REB), d'un combustible MOX irradié (MOX) qui peut être mélangé avec un ancien Pu retraité (MOX_RP)

Origine du combustible	Isotope	Distribution en masse (%)	Distribution en activité (%)	Distribution en activité α (%)
REP1	^{238}Pu	2,805	5,3	$8,3 \times 10^{1}$
	^{239}Pu	52,479	$3,6 \times 10^{-1}$	5,7
	^{240}Pu	27,684	$6,9 \times 10^{-1}$	$1,1 \times 10^{1}$
	^{241}Pu	8,198	$9,4 \times 10^{1}$	
	^{242}Pu	8,834	$3,7 \times 10^{-3}$	$6,1 \times 10^{-2}$
	^{241}Am	$2,18 \times 10^{-4}$	$8,3 \times 10^{-5}$	$1,3 \times 10^{-3}$
REP2	^{238}Pu	2,982	4,4	$8,5 \times 10^{1}$
	^{239}Pu	52,532	$2,8 \times 10^{-1}$	5,4
	^{240}Pu	25,771	$5,1 \times 10^{-1}$	9,7
	^{241}Pu	10,53	$9,5 \times 10^{1}$	
	^{242}Pu	8,185	$2,8 \times 10^{-3}$	$5,4 \times 10^{-2}$
	^{241}Am	$2,07 \times 10^{-4}$	$6,2 \times 10^{-5}$	$1,2 \times 10^{-3}$
REB	^{238}Pu	2,94	5,4	$8,3 \times 10^{1}$
	^{239}Pu	47,672	$3,2 \times 10^{-1}$	4,9
	^{240}Pu	30,818	$7,6 \times 10^{-1}$	$1,2 \times 10^{1}$
	^{241}Pu	8,371	$9,4 \times 10^{1}$	
	^{242}Pu	10,199	$4,4 \times 10^{-3}$	$6,7 \times 10^{-2}$
	^{241}Am	$1,85 \times 10^{-4}$	$6,8 \times 10^{-5}$	$1,1 \times 10^{-3}$
MOX	^{238}Pu	3,15	5,3	$8,4 \times 10^{1}$
	^{239}Pu	40,554	$2,5 \times 10^{-1}$	3,9
	^{240}Pu	34,793	$7,8 \times 10^{-1}$	$1,2 \times 10^{1}$
	^{241}Pu	9,204	$9,4 \times 10^{1}$	
	^{242}Pu	12,299	$4,8 \times 10^{-3}$	$7,6 \times 10^{-2}$
	^{241}Am	$2,40 \times 10^{-4}$	$8,1 \times 10^{-5}$	$1,3 \times 10^{-3}$

MOX_RP	^{238}Pu	1,863	4,5	$7,6 \times 10^{1}$
	^{239}Pu	53,647	$4,7 \times 10^{-1}$	7,9
	^{240}Pu	30,788	$9,9 \times 10^{-1}$	$1,7 \times 10^{1}$
	^{241}Pu	6,414	$9,4 \times 10^{1}$	
	^{242}Pu	7,288	$4,1 \times 10^{-3}$	$6,9 \times 10^{-2}$
	^{241}Am	$1,79 \times 10^{-4}$	$8,7 \times 10^{-5}$	$1,5 \times 10^{-3}$

Les distributions en taille des particules composant les poudres de dioxyde de plutonium ont été recueillies pour les différents types de combustible. Leur diamètre médian varie entre 6,2 et 10,5 µm. Cependant, il est difficile de relier cette distribution en taille à celle qu'aurait un aérosol générer à partir de ces poudres par une rupture de confinement.

4.4. Absorption pulmonaire du Pu sous différentes formes chimiques

L'absorption pulmonaire du plutonium a été estimée à partir de données expérimentales *in vitro*, animales ou à partir de cas de contamination, publiées.

Des valeurs spécifiques des 3 paramètres d'absorption f_r, s_r et s_s ont été calculées (Fig. 4 et Tableau 8) pour différentes formes chimiques du plutonium en utilisant des modèles spécifiques aux conditions expérimentales. La Fig. 4 permet d'observer que les absorptions vers le sang des différents composés sont proches des types d'absorption de référence de la CIPR. Cependant, une certaine variabilité de l'absorption peut être notée.

D'autre part, en appliquant les critères d'assignation d'un composé à un type de référence de la CIPR (ICRP, 1995c), le dioxyde de plutonium, le MOX, les sols de Maralingua, les poussières de Palomares et le graphite d'oxyde de Pu peuvent être considérés comme des composés insolubles de référence (Type S) ; le Type M peut être attribué au complexe Pu-TBP (tributyl phosphate), aux résidus, au nitrate de Pu, au chlorure de Pu, aux alliages Pu-Na et Pu-Mg ; le Type F au citrate de Pu.

La variabilité du coefficient de dose a également été estimée ; de même que les corrélations entre les paramètres.

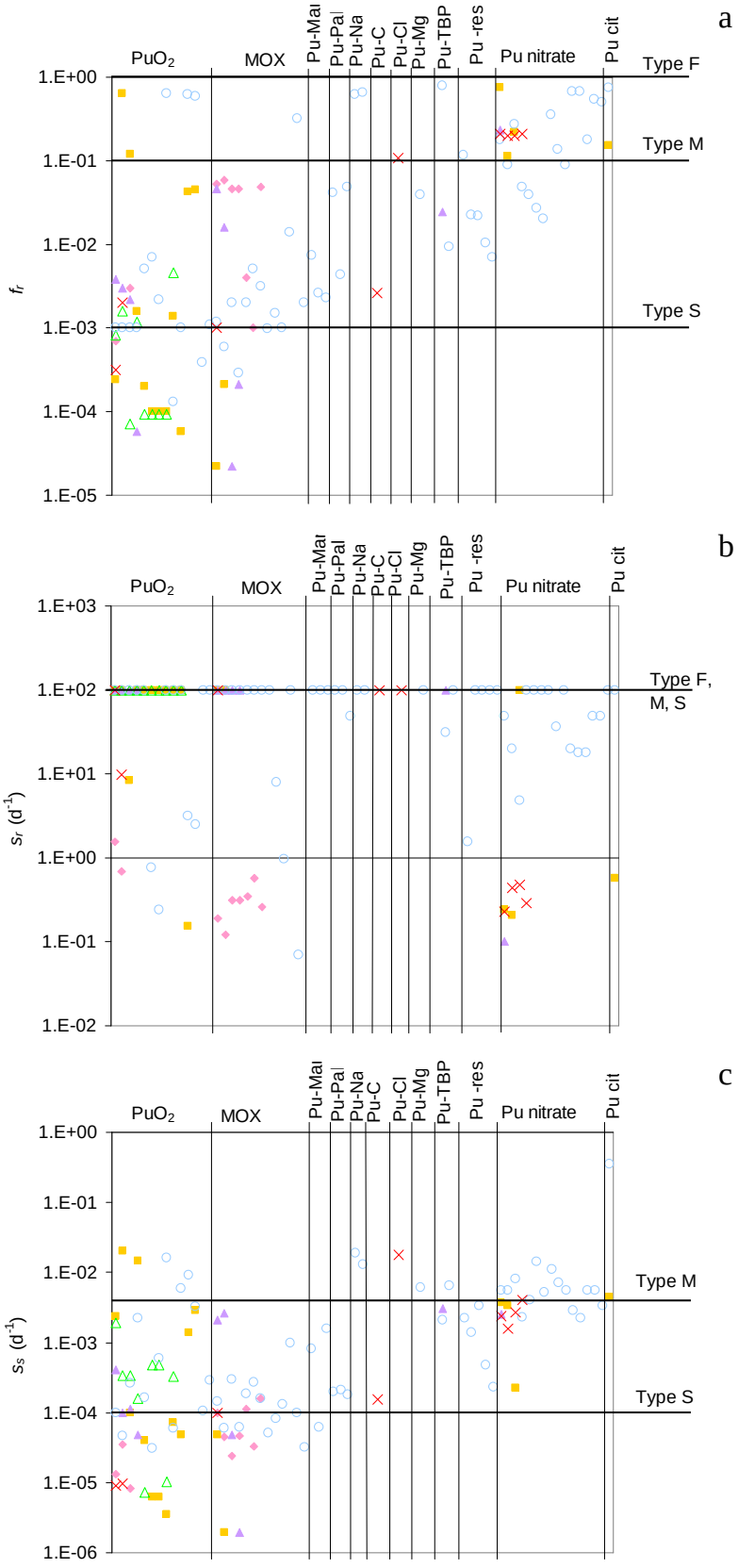

Figure 4 : Fraction rapidement dissoute f_r (a), vitesse de dissolution rapide s_r (b) et vitesse de dissolution lente s_s (c) pour différents composés de Pu. Pu-Mar: sols de Maralinga; Pu-Pal: poussières de Palomares; Pu-Na : alliage de Pu sodium; Pu-C: graphite d'oxyde de Pu; Pu-Cl: chlorure de Pu; Pu-Mg: alliage de Pu magnésium; Pu-res: résidus; Pu cit: citrate de Pu. Expériences menées *in vitro* (◆), sur le chien (■), le singe (▲), la souris (△), le rat (○); données de contaminations humaines (✖).

Tableau 8 : Moyennes, médianes et écart-type géométriques (GSD) de f_r, s_r et s_s pour les différents composés de plutonium ; Type de référence attribué selon les critères de la CIPR (ICRP, 1995c)

Composé		f_r	s_r (j^{-1})	s_s (j^{-1})
PuO_2[a]	moyenne	$6,4 \times 10^{-2}$	3	$1,9 \times 10^{-3}$
(Type S)	médiane	$1,1 \times 10^{-3}$	1,6	$1,0 \times 10^{-4}$
	GSD	14,3	4,3	10,7
MOX	moyenne	$3,2 \times 10^{-2}$	1,1	$3,0 \times 10^{-4}$
(Type S)	médiane	$2,0 \times 10^{-3}$	0,3	$1,0 \times 10^{-4}$
	GSD	11,2	3,7	5
sols de	moyenne	$4,0 \times 10^{-3}$	-	$8,4 \times 10^{-4}$
Maralinga	médiane	$2,3 \times 10^{-3}$	-	$8,2 \times 10^{-4}$
(Type S)	GSD	1,9	-	5,6
poussières	moyenne	$3,1 \times 10^{-2}$	49	$2,0 \times 10^{-4}$
de Palomares	médiane	$4,2 \times 10^{-2}$	49	$2,0 \times 10^{-4}$
(Type S)	GSD	3,9	-	1,1
alliage de	moyenne	$6,3 \times 10^{-1}$	-	$1,6 \times 10^{-2}$
Pu-Na	médiane	$6,3 \times 10^{-1}$	-	$1,6 \times 10^{-2}$
(Type M)	GSD	1	-	1,3
Pu-TBP	moyenne	$2,7 \times 10^{-1}$	31,5	$3,9 \times 10^{-3}$
(Type M)	médiane	$2,4 \times 10^{-2}$	31,5	$3,1 \times 10^{-3}$
	GSD	10,3	-	1,8
résidus de Pu	moyenne	$2,8 \times 10^{-2}$	1,8	$1,6 \times 10^{-3}$
(Type M)	médiane	$1,4 \times 10^{-2}$	1,8	$1,4 \times 10^{-3}$
	GSD	2,9	-	3
nitrate de Pu	moyenne	$2,6 \times 10^{-1}$	16,7	$5,1 \times 10^{-3}$
(Type M)	médiane	$2,0 \times 10^{-1}$	11,4	$4,0 \times 10^{-3}$
	GSD	2,7	11,2	2,3
citrate de Pu	moyenne	$4,5 \times 10^{-1}$	0,6	$1,8 \times 10^{-1}$
(Type F)	médiane	$4,5 \times 10^{-1}$	0,6	$1,8 \times 10^{-1}$
	GSD	3,1	-	22,3

[a] PuO_2 regroupe les résultats pour $^{238}PuO_2$, $^{239}PuO_2$ et $^{(238, 239, 240)}PuO_2$

4.5. Conclusion

L'objectif de cette partie était de présenter les informations recueillies sur le programme de surveillance de la contamination interne mis en place sur le site AREVA NC à La Hague et de présenter une synthèse de l'étude sur les conditions d'exposition des travailleurs réalisant l'extraction et la purification du plutonium, notamment concernant l'absorption du dioxyde de

plutonium. Les résultats de cette étude ont été utilisés pour modéliser les paramètres incertains liés à l'évaluation dosimétrique et pour déterminer la dose minimale détectable à un niveau de confiance donné pour le programme de surveillance en place pour les travailleurs des ateliers R4 et T4 de l'installation AREVA NC de La Hague.

5. Evaluation du programme de surveillance

5.1. Objectif

La sensibilité d'un programme de surveillance en termes de dose efficace peut être déterminée en prenant en compte les incertitudes relatives aux conditions d'expositions et à la mesure. Le seuil de décision et la fréquence de la mesure permettent de définir une incorporation et une dose minimales détectables par le programme de surveillance en fonction des modèles biocinétiques et dosimétriques appliqués.

La dose minimale détectable (DMD) est définie de telle manière que si la mesure est inférieure au seuil de décision, la dose efficace correspondante est inférieure à la DMD avec un niveau de confiance de 95%. Elle est ainsi un critère de sensibilité du programme de surveillance.

La DMD est définie ici comme étant le 95ème percentile de la distribution de probabilité de la dose efficace annuelle, pour une mesure observée au seuil de décision et compte-tenu des incertitudes sur l'estimation dosimétrique.

5.2. Paramètres de l'étude

Un cas de contamination envisageable suite à une éventuelle rupture de confinement dans une installation d'extraction du plutonium de l'usine AREVA NC de La Hague serait une inhalation ponctuelle de particules de dioxyde de ^{239}Pu ($^{239}PuO_2$).

- La date de contamination inconnue pendant l'intervalle de surveillance est représentée par une loi de probabilité uniforme entre 0 et 180 jours avant la mesure fécale biannuelle.
- L'incertitude sur le diamètre des particules est modélisée par une probabilité uniforme du DAMA entre 1 et 10 µm.
- L'incertitude sur la solubilité du PuO_2 est quantifiée en utilisant les résultats présentés sur la Fig. 4 pour le dioxyde de Pu et le MOX.
- Le modèle d'incertitude de mesure est de type Poisson, avec un bruit de fond moyen de 2,2 coups/48 h.

- L'incertitude d'échantillonnage suit une loi lognormale d'écart-type géométrique 3 (Marsh *et al*, 2008b).
- L'événement minimal détecté par la technique de mesure correspond alors à l'observation de 5 coups/48 h.

Trois hypothèses de probabilité *a priori* de l'incorporation *P*(*i*) ont été considérées : une densité constante $P(i) = 1$ suppose que toutes les valeurs d'activité incorporée sont équiprobables entre 0 et 10000 Bq ; des densités décroissantes $P(i) = e^{-i}$ et $P(i) = a.i^{a-1}$ avec $a = 0{,}001$ supposent que les incorporations les plus faibles sont les plus vraisemblables. Le paramètre α représente la fréquence de mesures positives pour un groupe de travailleur donné (Miller *et al*, 2001). Ces probabilités *a priori* ont été choisies comme des hypothèses extrêmes pouvant être faite avant toute mesure.

5.3. Méthodes utilisées

La méthode classique a été utilisée pour calculer la DMD à partir des niveaux de confiance de l'incorporation. La méthode WeLMoS a également été appliquée mais dans une version légèrement modifiée par rapport à celle de Puncher and Birchall (2008). Finalement, la DMD a été calculée grâce à un réseau bayésien prenant en compte une ou deux mesures. Sa discrétisation a été développée spécialement pour l'étude et pour limiter le temps de calcul.

De plus, la méthode WeLMoS et le réseau font tous deux utilisation du théorème de Bayes mais la modélisation des variables est différente : continues pour la méthode WeLMoS et discrétisées pour le réseau. Les deux méthodes ont été comparées sur un cas simple et leurs résultats sont similaires.

5.4. DMD pour un intervalle de surveillance

Les résultats obtenus par les méthodes classique et WeLMoS permettent une interprétation qualitative similaire en termes de niveaux de confiance à 95% (Tableau 9).

Dans tous les cas, les incertitudes relatives sont importantes mais les DMD restent inférieures à la limite réglementaire de 20 mSv. Les différentes estimations de la DMD reflètent l'importance des hypothèses faites sur les paramètres incertains, notamment la probabilité *a priori* de l'incorporation. Supposer *a priori* que toutes les incorporations de 0 à 10000 Bq sont équiprobables est une hypothèse très, voire trop, prudente. Elle résulte en une DMD de 11 mSv. En revanche, supposer *a priori* que les faibles incorporations sont les plus probables conduit à une DMD de l'ordre de 0,3 mSv pour $P(i) = e^{-i}$ et inférieure à 1 nSv pour $P(i) = a.i^{a-1}$. $P(i) = a.i^{a-1}$ est peu influencée par les autres paramètres du calcul et parait trop informative. La probabilité *a priori* exponentielle est ainsi un choix intermédiaire raisonnable bien que subjectif.

Le point limitant de la méthode classique, supposant l'incorporation fixe, est que la DMD n'est pas calculée directement, mais par une estimation prudente. De plus, supposer l'incorporation comme fixe confère un poids plus important sur les autres modélisations des variables devenant des hypothèses implicites. La méthode WeLMoS tout comme le réseau bayésien a l'avantage d'expliciter complétement toutes les hypothèses, permettant ainsi une lecture facile des résultats.

Tableau 9 : Intervalles de confiance de l'incorporation et de la dose

Méthode	Incorporation (Bq)			Dose (mSv)		
	Médiane	IMD (95ème percentile)	Facteur d'incertitude	Médiane	DMD (95ème percentile)	Facteur d'incertitude
classique	0,7	7,3	10	$7,8 \times 10^{-2}$	$3,2 \times 10^{-1}$	4,0
WeLMoS, *P(i)* exponentielle	0,6	2,4	4,0	$7,2 \times 10^{-3}$	$5,2 \times 10^{-2}$	7,2
WeLMoS, *P(i)* uniforme	7,3	92	13	$7,5 \times 10^{-1}$	$1,1 \times 10^{+1}$	15
WeLMoS, alpha *P(i)*		$< 10^{-9}$			$< 10^{-6}$	

5.5. Analyse de sensibilité de la DMD

Les différentes estimations de la DMD reflètent l'importance des hypothèses faites sur les paramètres incertains. En effet, une étude de sensibilité (Fig. 5) montre que la probabilité *a priori* de l'incorporation et la solubilité du composé influent fortement sur la DMD. En revanche la variation du DAMA a peu d'effet sur le résultat.

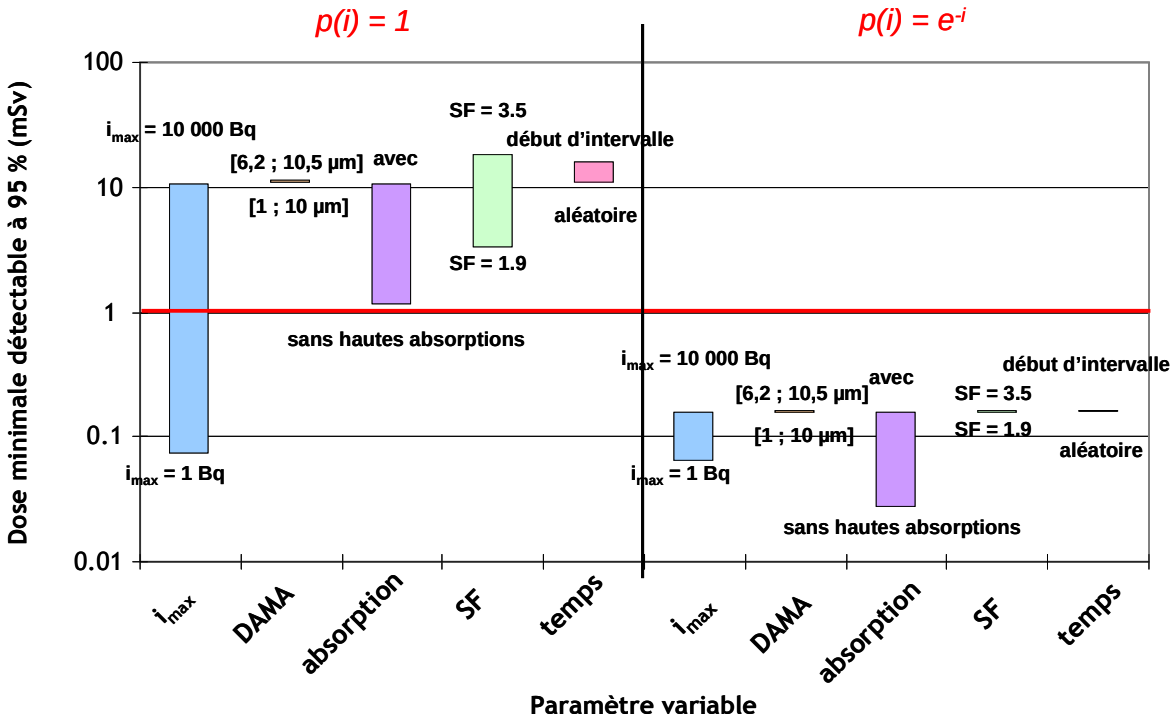

Figure 5 : Analyse de sensibilité de la DMD avec un niveau de confiance de 95 % utilisant la méthode WeLMoS avec une probabilité *a priori* uniforme (à gauche) ou exponentielle (à droite). Un paramètre à la fois a été modifié les autres étant fixés aux valeurs décrites dans le texte.

5.6. DMD annuelle pour R4-T4

Tableau 10 : DMD annuelles calculées par la méthode WeLMoS et le réseau bayésien avec des probabilités *a priori* de l'incorporation uniforme, exponentielle, ou alpha. Application aux travailleurs de R4-T4 pour une mesure fécale égale au seuil de décision pour différents combustibles

Probabilité *a priori* de l'incorporation	Méthode	Combustible	DMD (mSv)
P(i) uniforme	WeLMoS	REP1	17
		REP2	20
		REB	20
		MOX	24
		MOX_RP	13
	Réseau bayésien	REP1	8 < MDD < 9
		REP2	9 < MDD < 10
		REB	9 < MDD < 10
		MOX	10 < MDD < 15
		MOX_RP	6 < MDD < 7
P(i) exponentielle	WeLMoS	REP1	$3{,}4 \times 10^{-1}$
		REP2	$3{,}5 \times 10^{-1}$
		REB	$3{,}6 \times 10^{-1}$
		MOX	$4{,}2 \times 10^{-1}$
		MOX_RP	$2{,}4 \times 10^{-1}$
	Réseau bayésien	REP1	0,5 < MDD < 1
		REP2	0,5 < MDD < 1
		REB	0,5 < MDD < 1
		MOX	1 < MDD < 2
		MOX_RP	0,5 < MDD < 1
P(i) alpha	WeLMoS	REP1	MDD < 10^{-6}
		REP2	MDD < 10^{-6}
		REB	MDD < 10^{-6}
		MOX	MDD < 10^{-6}
		MOX_RP	MDD < 10^{-6}
	Réseau bayésien	REP1	MDD = 0[a]
		REP2	MDD = 0[a]
		REB	MDD = 0[a]
		MOX	MDD = 0[a]
		MOX_RP	MDD = 0[a]

[a] La dose 0 mSv correspond à un percentile supérieur au 95eme

La DMD annuelle est calculée en prenant en compte les différentes mesures de routine qui sont réalisées par an et en écartant les valeurs d'absorption pulmonaire jugées irréalistes. Sinon, la modélisation des incertitudes est la même que celle présentée précédemment. Les résultats sont présentés dans le Tableau 10 pour les différents combustibles.

Les différences entre les DMD calculées par la méthode WeLMoS et le réseau bayésien sont induites par la définition du problème physique. En effet, pour la méthode WeLMoS, les probabilités *a priori* sont continues pour tous les paramètres incertains sauf l'absorption vers le sang qui est modélisé par les résultats de l'étude des données publiées. Pour le réseau bayésien, les paramètres incertains ainsi que leurs probabilités *a priori* sont discrétisées et l'absorption par le sang est modélisée par un mélange de Type M et S de référence de la CIPR. Cette étude prouve donc l'importance de la modélisation du problème et du choix des hypothèses sur le résultat.

5.7. Conclusion

La DMD a été calculée pour les travailleurs des ateliers R4-T4 en utilisant la méthode classique, la méthode WeLMoS et le réseau bayésien pour un intervalle de surveillance ou sur une année complète. La composition isotopique a été prise en compte pour estimer précisément la DMD pour le programme de surveillance en place. L'influence des paramètres incertains sur la DMD a été quantifiée. Les méthodes qui ont été comparées permettent d'estimer la DMD et d'évaluer la qualité d'un programme de surveillance en comparant la DMD avec les contraintes de dose, car le programme assure la détection de dose supérieure à la DMD avec un certain niveau de confiance.

La méthode classique souffre d'un manque de flexibilité et d'hypothèses implicites sur les différents paramètres. D'autre part, pour estimer la DMD avec la méthode WeLMoS ou avec le réseau bayésien, une probabilité *a priori* de l'incorporation doit être choisie. Comme plusieurs probabilités *a priori* peuvent souvent être sélectionnées, une analyse de sensibilité de la DMD pour les différentes probabilités *a priori* devrait être réalisée. Dans cette étude, nous avons jugé que la probabilité *a priori* exponentielle est un choix raisonnable mais subjectif.

6. Optimisation du programme de surveillance

Dans la partie précédente, différentes méthodes pour calculer la DMD du programme de surveillance en place pour les ateliers R4-T4 de l'usine AREVA NC de La Hague ont été présentées avec leurs résultats. Comme la DMD est une mesure de la sensibilité d'un programme de surveillance, elle peut être utilisée pour optimiser le programme en réalisant un compromis entre les DMD de différents programmes et les coûts associés aux mesures nécessaires.

6.1. Paramètres de l'étude

Un cas de contamination envisageable suite à une éventuelle rupture de confinement dans une installation d'extraction du plutonium de l'usine AREVA NC de La Hague serait une inhalation ponctuelle de particules de dioxyde de Pu (PuO_2).

- La date de contamination inconnue pendant l'intervalle de surveillance est représentée par une loi de probabilité uniforme sur l'intervalle de surveillance.
- L'incertitude sur le diamètre des particules est modélisée par une probabilité uniforme du DAMA entre 1 et 10 µm.
- L'incertitude sur la solubilité du PuO_2 est quantifiée en utilisant un type M de référence avec une probabilité de 0,162 et un type S avec une probabilité de 0,838.
- Le modèle d'incertitude de mesure est de type Poisson, avec un bruit de fond moyen de 2,2 coups/48 h.
- L'incertitude d'échantillonnage suit une loi lognormale d'écart-type géométrique 3 (Marsh *et al*, 2008b).
- L'événement minimal détecté par la technique de mesure correspond alors à l'observation de 5 coups/48 h.

Trois hypothèses de probabilité *a priori* de l'incorporation (i) ont été considérées : une densité constante $P(i) = 1$ entre 0 et 10000 Bq ; des densités décroissantes $P(i) = e^{-i}$ et $P(i) = a.i^{a-1}$ avec $a = 0{,}001$.

6.2. Programmes de surveillance envisagés

Après avoir évalué le programme de surveillance en place par le calcul de la DMD, les DMD de différents programmes envisageables ont été calculées :

a) une mesure fécale tous les 2 ans
b) une mesure fécale tous les ans,
c) une mesure fécale tous les 6 mois,
d) une mesure urinaire tous les 6 mois,
e) une mesure urinaire annuelle suivie d'une mesure fécale 6 mois après,
f) une mesure fécale annuelle suivie d'une mesure urinaire 6 mois après,
g) une mesure urinaire et une mesure fécale tous les 6 mois,
h) une mesure fécale tous les 3 mois,
i) une mesure urinaire tous les 3 mois.

6.3. Méthodes

Trois réseaux bayésiens ont été utilisés pour cette étude pour modéliser les faibles connaissances sur les paramètres incertains par des probabilités discrètes plutôt que continues. Ils comprennent 1, 2 ou 4 mesures. Leurs discrétisations sont présentées dans le Tableau 11.

Tableau 11 : Discrétisations des variables dans le réseau bayésien

Nombres de mesures par an	Variable	Discrétisation
1	Incorporation (Bq)	0; 10^{-4}; $5x10^{-4}$; 10^{-3}; $5x10^{-3}$; 10^{-2}; $5x10^{-2}$; 10^{-1}; $5x10^{-1}$; 1,0; 5; 10; 20; 30; 40; 50; 100; 150; 300; 600; 1000
	DAMA (µm)	1; 3; 5; 10
	Absorption pulmonaire	Type M; Type S
	Date de contamination (j)	0; 10; 20; 30; 40; 50; 60; 70; 80; 90; 100; 110; 120; 130; 140; 150; 160; 170; 180
	Quantité biologique (Bq)	0; 10^{-7}; 10^{-6}; $5x10^{-6}$; 10^{-5}; $2x10^{-5}$; $3x10^{-5}$; $4x10^{-5}$; $5x10^{-5}$; $6x10^{-5}$; $7x10^{-5}$; $8x10^{-5}$; $9x10^{-5}$; 10^{-4}; $2x10^{-4}$; $3x10^{-4}$; $4x10^{-4}$; $5x10^{-4}$; $6x10^{-4}$; $7x10^{-4}$; $8x10^{-4}$; $9x10^{-4}$; 10^{-3}; $2x10^{-3}$; $3x10^{-3}$; $4x10^{-3}$; $5x10^{-3}$; $6x10^{-3}$; $7x10^{-3}$; $8x10^{-3}$; $9x10^{-3}$; 10^{-2}; $2x10^{-2}$; $3x10^{-2}$; $4x10^{-2}$; $5x10^{-2}$; $6x10^{-2}$; $7x10^{-2}$; $8x10^{-2}$; $9x10^{-2}$; 10^{-1}; $2x10^{-1}$; $3x10^{-1}$; $4x10^{-1}$; $5x10^{-1}$; $6x10^{-1}$; $7x10^{-1}$; $8x10^{-1}$; $9x10^{-1}$; 1; 2; 3; 4; 5; 6; 7; 8; 9; 10; 20; 30; 40; 50; 60; 70; 80; 90; 100; 200; 300; 400; 500; 600; 700; 800; 900; 1000
	Dose (mSv)	0; 10^{-3}; 10^{-2}; 10^{-1}; $5x10^{-1}$; 1; 2; 3; 4; 5; 6; 7; 8; 9; 10; 15; 20; 50; 100; 500; 1 000; 10 000
2	Incorporation (Bq)	0; 10^{-4}; $5x10^{-4}$; 10^{-3}; $5x10^{-3}$; 10^{-2}; $5x10^{-2}$; 10^{-1}; $5x10^{-1}$; 1; 5; 10; 20; 30; 40; 50; 100; 150; 300; 600; 1000
	DAMA (µm)	1; 3; 5; 10
	Absorption pulmonaire	Type M; Type S
	Date de contamination (j)	0; 10; 20; 30; 40; 50; 60; 70; 80; 90; 100; 110; 120; 130; 140; 150; 160; 170; 180
	Quantité biologique (Bq)	0; 10^{-6}; 10^{-5}; 10^{-4}; $5x10^{-4}$; 10^{-3}; $5x10^{-3}$; 10^{-2}; $5x10^{-2}$; 10^{-1}; $5x10^{-1}$; 1; 5; 10; 50; 100; 200; 500; 1000
	Dose (mSv)	0; 10^{-3}; 10^{-2}; 10^{-1}; $5x10^{-1}$; 1; 2; 3; 4; 5; 6; 7; 8; 9; 10; 15; 20; 50; 100; 500; 1 000; 10 000
4	Incorporation (Bq)	0; 10^{-4}; 10^{-3}; 10^{-2}; 10^{-1}; 1; 10; 100; 1000
	DAMA (µm)	1; 5; 10
	Absorption pulmonaire	Type M; Type S
	Date de contamination (j)	0; 10; 90; 180

Quantité biologique (Bq)	0; 10^{-6}; 10^{-5}; 10^{-4}; $5x10^{-4}$; 10^{-3}; $5x10^{-3}$; 10^{-2}; $5x10^{-2}$; 10^{-1}; $5x10^{-1}$; 1; 5; 10; 50; 100; 1000
Dose (mSv)	0; 10^{-3}; 10^{-1}; $5x10^{-1}$; 1; 5; 10; 20; 1 000; 10 000

6.4. Résultats et discussion

Les résultats sont regroupés dans le Tableau 12. L'exploitant veut assurer la détection d'incorporation correspondant à une dose efficace annuelle de 1 mSv. En se basant sur $P(i) = e^{-i}$ comme probabilité *a priori* de l'incorporation la plus raisonnable, seuls les programmes c et h permettent d'assurer que la DMD est inférieure à 1 mSv. Or, le programme h implique 2 fois plus de mesures fécales que le programme c. Ainsi, cette étude permet de conclure que le programme en place (c) est un bon compromis entre le nombre de mesures et la sensibilité du programme de surveillance.

Tableau 12 : DMD calculées pour les différents programmes de surveillance utilisant le réseau bayésien avec la modélisation et la discrétisation présentées dans le texte.

Composition isotopique	Dose minimale détectable avec un niveau de confiance de 95 % (mSv)			
	Programme	*P(i)* uniforme	*P(i)* exponentielle	*P(i)* alpha
REP1	a	20 < MDD	1 < MDD < 2	MDD = 0[a]
	b	20 < MDD < 50	1 < MDD < 2	MDD = 0[a]
	c	8 < MDD < 9	0,5 < MDD < 1	MDD = 0 [a]
	d	50 < MDD < 100	3 < MDD < 4	MDD = 0 [a]
	e	10 < MDD < 15	1 < MDD < 2	MDD = 0 [a]
	f	10 < MDD < 15	2 < MDD < 3	MDD = 0 [a]
	g	5 < MDD < 10	1 < MDD < 5	MDD = 0 [a]
	h	1 < MDD < 5	0,1 < MDD < 0,5	0 < MDD < 0,001
	i	20 < MDD < 1000	5 < MDD < 10	1 < MDD < 5
REP2	a	20 < MDD	1 < MDD < 2	MDD = 0[a]
	b	20 < MDD < 50	1 < MDD < 2	MDD = 0[a]
	c	9 < MDD < 10	0,5 < MDD < 1	MDD = 0 [a]
	d	50 < MDD < 100	3 < MDD < 4	MDD = 0 [a]
	e	10 < MDD < 15	1 < MDD < 2	MDD = 0 [a]
	f	10 < MDD < 15	3 < MDD < 4	MDD = 0 [a]
	g	5 < MDD < 10	1 < MDD < 5	MDD = 0 [a]
	h	1 < MDD < 5	0,1 < MDD < 0,5	0 < MDD < 0,001
	i	20 < MDD < 1000	5 < MDD < 10	1 < MDD < 5

REB	a	20 < MDD	1 < MDD < 2	MDD = 0[a]
	b	20 < MDD < 50	1 < MDD < 2	MDD = 0[a]
	c	8 < MDD < 9	0,5 < MDD < 1	MDD = 0 [a]
	d	50 < MDD < 100	4 < MDD < 5	MDD = 0 [a]
	e	10 < MDD < 15	1 < MDD < 2	MDD = 0 [a]
	f	10 < MDD < 15	3 < MDD < 4	MDD = 0 [a]
	g	5 < MDD < 10	1 < MDD < 5	MDD = 0 [a]
	h	1 < MDD < 5	0,1 < MDD < 0,5	0 < MDD < 0,001
	i	20 < MDD < 1000	5 < MDD < 10	1 < MDD < 5
MOX	a	20 < MDD	2 < MDD < 3	MDD = 0[a]
	b	50 < MDD < 100	2 < MDD < 3	MDD = 0[a]
	c	10 < MDD < 15	1 < MDD < 2	MDD = 0 [a]
	d	50 < MDD < 100	5 < MDD < 6	MDD = 0 [a]
	e	15 < MDD < 20	2 < MDD < 3	MDD = 0 [a]
	f	15 < MDD < 20	4 < MDD < 5	MDD = 0 [a]
	g	5 < MDD < 10	5 < MDD < 10	0 < MDD < 0,001
	h	1 < MDD < 5	0,5 < MDD < 1	0 < MDD < 0,001
	i	20 < MDD < 1000	5 < MDD < 10	1 < MDD < 5
MOX_RP	a	20 < MDD	0,5 < MDD < 1	MDD = 0[a]
	b	20 < MDD < 50	0,5 < MDD < 1	MDD = 0[a]
	c	6 < MDD < 7	0,5 < MDD < 1	MDD = 0 [a]
	d	50 < MDD < 100	2 < MDD < 3	MDD = 0 [a]
	e	8 < MDD < 9	1 < MDD < 2	MDD = 0 [a]
	f	9 < MDD < 10	1 < MDD < 2	MDD = 0 [a]
	g	1 < MDD < 5	1 < MDD < 5	MDD = 0 [a]
	h	1 < MDD < 5	0,1 < MDD < 0,5	0 < MDD < 0,001
	i	10 < MDD < 20	1 < MDD < 5	1 < MDD < 5

[a] La dose 0 mSv correspond à un percentile supérieur au 95ème

6.5. Conclusion

Cette étude souligne l'intérêt de la DMD comme une aide à la décision pour le choix du programme de surveillance le mieux adapté à la contamination potentielle en intégrant les incertitudes sur l'exposition et sur la mesure d'activité.

7. Développement d'OPSCI et validation

Le logiciel OPSCI (Optimisation du Programme de Surveillance de la Contamination Interne) a été développé afin d'aider à la mise en place et à l'évaluation d'un programme de surveillance. Il permet dans un premier module de calculer la dose efficace en appliquant les recommandations de la Commission Internationale de Protection Radiologique (ICRP, 1997a).

Un second module estime, pour un programme de surveillance donné, la DMD en prenant en compte les incertitudes sur le calcul de dose. Pour cela, il utilise la méthode WeLMoS et la connaissance (incertaine) de l'utilisateur sur la mesure et sur les conditions d'exposition.

Le dernier module permet le calcul des DMD relatives aux différents programmes de surveillance que l'utilisateur veut évaluer. En prenant en considération ces DMD et le coût des analyses à effectuer, il pourra juger de la pertinence des programmes. Pour cela, le réseau bayésien est utilisé. Si nécessaire, l'utilisateur peut préciser la DMD du programme qu'il juge le plus pertinent avec le deuxième module.

OPSCI a été validé en comparant à chaque étape de son développement ses résultats avec la littérature et IMBA (Puncher and Birchall, 2007).

8. Discussions et perspectives

8.1. Discussions et voies d'amélioration

Propagation des incertitudes

La méthode classique est pénalisée par les hypothèses implicites qu'elle implique et par le fait que l'on ne puisse calculer qu'approximativement la DMD pour une seule mesure et que plusieurs mesures ne peuvent pas être intégrées pour l'instant.

Le choix entre l'utilisation de la méthode WeLMoS ou du réseau bayésien se base sur la précision de l'information sur les différents paramètres incertains. Si une information conséquente est obtenue, des probabilités continues peuvent être choisies pour modéliser les incertitudes sur les paramètres. C'est pourquoi la méthode WeLMoS est une méthode de choix donnant une DMD très précise. Cependant, si seulement une information incomplète est recueillie, on ajoute moins d'information en pondérant de larges intervalles par leur vraisemblance en utilisant des probabilités

discrètes qu'en utilisant des probabilités continues. Par conséquent, dans ce cas, l'utilisation du réseau bayésien est mieux adaptée. Il serait intéressant de comparer les résultats obtenus par ces deux méthodes avec ceux obtenus par l'UF code (Miller, 2008) utilisant un jeu de modèles biocinétiques et un algorithme de chaîne de Markov.

Enfin, une meilleure modélisation des incertitudes est l'utilisation de probabilités imprécises. Il serait donc intéressant de les intégrer au sein d'un réseau bayésien imprécis.

Probabilité a priori *de l'incorporation*

La probabilité *a priori* de l'incorporation est une modélisation subjective de l'utilisateur de la connaissance de l'incorporation avant toute mesure. Cette subjectivité est inévitable mais elle peut être assise sur des données historiques (Miller *et al*, 1993) ou déterminée à partir d'un cas de contamination similaire (James *et al*, 2008).

Dans cette étude, la subjectivité du choix a été quantifiée en utilisant plusieurs probabilités *a priori* modélisant des visions extrêmes de la contamination potentielle. De telles approches sont nécessaires pour évaluer l'influence de la probabilité *a priori* sur le résultat. Les probabilités *a priori* pourraient également être pondérées pour intégrer toutes les modélisations dans une seule estimation de la DMD.

Finalement, la probabilité *a priori* de l'incorporation peut être améliorée en intégrant les mesures de la contamination d'ambiance des postes de travail.

Mesure

Lors de ce travail, le résultat de mesure négatif a été modélisé comme étant égal au seuil de décision. Il est donc traité comme un intervalle où seulement la valeur la plus pénalisante est considérée. Une meilleure modélisation serait d'attribuer au résultat de mesure une probabilité *a priori* uniforme entre 0 et le SD.

De plus, la dose a été déterminée en considérant que seul le ^{239}Pu était mesuré, la dose due aux autres isotopes étant déterminée à partir de cette mesure et de la composition isotopique. Cependant, sur le centre AREVA NC de La Hague, le ^{238}Pu est également mesuré. Il faudrait donc intégrer cette mesure à l'étude.

Incertitudes relatives aux modèles biocinétiques et dosimétriques

Cette étude n'intègre pas les incertitudes relatives à la variabilité inter-individuelle car elle se place dans le contexte de la radioprotection des travailleurs et non pour la détermination de dose

individuelle. Cependant, la mesure radiotoxicologique ou anthroporadiamétrique est spécifique de l'individu contaminé. Cette source d'incertitude devrait être également intégrée. Mais, l'utilisation dans ce travail d'un scattering factor de 3 peut en partie prendre en compte cette incertitude.

8.2. Perspectives

Les méthodes développées peuvent être appliquée à tout programme de surveillance. Il serait donc particulièrement intéressant de les appliquer à la surveillance de l'uranium pour évaluer la qualité du programme de surveillance en termes de concentration rénale tout en intégrant l'apport alimentaire en uranium pour les mesures radiotoxicologiques.

Elles pourraient également aider à la mise en place de programme de surveillance adaptée pour les équipes médicales présentes dans les centres de médecine nucléaire.

Finalement, il serait nécessaire d'intégrer les incertitudes pour la détermination des courbes doses par unité de mesure (Hodgson *et al,* 2007) permettant le tri d'une population suite à un accident radiologique.

Optimisation of monitoring programme of internal contamination by the study of uncertainty related to the dose assessment

Abstract

To optimise the protection of workers against ionizing radiations, the International Commission on Radiological Protection recommends the use of dose constraint and limits. To verify the compliance of the means of protection with these values when a risk of internal contamination exists, monitoring programmes formed of periodic bioassay measurements are performed. However, uncertainty in the dose evaluation arises from the variability of the activity measurement and from the incomplete knowledge of the exposure conditions.

This uncertainty was taken into account by means of classical, Bayesian and possibilist statistics. The developed methodology was applied to the evaluation of the potential exposure during nuclear fuel preparation or mining; and to the analysis of the monitoring programme of workers purifying plutonium in AREVA NC La Hague reprocessing plant.

From the measurement decision threshold, the minimum dose detectable (MDD) by the programme with a given confidence level can be calculated through the software OPSCI. It is shown to be a useful support in the optimisation of monitoring programmes when seeking a compromise between their sensitivity and their costs.

Key words: radiological protection, internal dosimetry, uncertainty, uranium, plutonium

List of notation

abs	absorption into blood
AMAD	Activity Median Aerodynamic Diameter
BWR	Boiling Water Reactor
CDF	Cumulative Distribution Function
DT	Decision threshold
E	Committed effective dose
e_{50}	Dose coefficient
f	Type B measurement uncertainty
f_1	Absorbed fraction in the GITM
f_r	Rapidly dissolved fraction in the HRTM
GITM	Gastro-Intestinal Tract Model
HRTM	Human Respiratory Tract Model
HATM	Human Alimentary Tract Model
i	Intake
ICRP	International Commission on Radiological Protection
M	Measurement result
MDD	Minimum Detectable Dose with a level of confidence of 95 %
MDI	Minimum Detectable Intake with a level of confidence of 95 %
MOX	Mixed Oxide fuel
PDF	Probability Density Function
Pu	Plutonium
PWR	Pressurised Water Reactor
RaFu method	Dempster-Shafer approach using Monte-Carlo simulations
S	Bioassay quantity
SF	Scattering Factor
s_r	Rapid dissolution rate in the HRTM
s_s	Slow dissolution rate in the HRTM
t	Time of contamination
Type F, M, S	Fast, Moderate or Slow reference absorption Type
U	Uranium
WeLMoS method	Weighted Likelihood Monte-Carlo Sampling method

Contents

General introduction

The workers of the nuclear industry can be exposed to ionizing radiation either by external irradiation or by internal contamination. The exposure is quantified by the resulting dose.

Prospective dosimetry is used for preventive and planning purpose, to quantify the potential health risk and to check if the protection and safety at a workplace is in conformity with the regulation or radiation protection policy. For internal exposure, such dosimetry is based on the results of assessments at design or planning stages, on the measurement of the ambient air or surface contamination at the workplace.

On the other hand, retrospective dosimetry is usually based on individual bioassay measurement. In case of significant potential occupational exposure by internal contamination, a routine monitoring programme is designed to verify and document that the worker's protection complies with the regulatory dose limits and dose constraints. After a prospective evaluation of exposure at the workplace, a monitoring programme is implemented by periodic *in vivo* or *in vitro* measurements at a frequency consistent with the sensitivity of the measurement technique, the biokinetics of the radionuclide and the dose constraint.

To calculate dose from the conditions of exposure in prospective dosimetry or from bioassay measurements in retrospective dosimetry, the behaviour of a radionuclide in the human body has to be known or assumed. The International Commission on Radiological Protection (ICRP) provides reference models for this behaviour from the entry into the body through the excretion. The Human Respiratory Tract Model (HRTM) deals with the deposition of the radionuclide and its clearance after an inhalation intake. Ingestion is described by the Human Alimentary Tract Model (HATM). The behaviour of a radionuclide in body tissues since its uptake into blood can be estimated by a systemic model specific to the element. The ICRP also provides radiation transport models to calculate energy absorbed in different tissues and the resulting effective dose.

All these models have various parameters. Some are related to the physico-chemical properties of the radionuclides and others to the individual physiology. The ICRP recommends default values for these parameters, considering a reference person and a standard situation of exposure. By using these models for inhalation or ingestion of different radionuclides with the default parameters, the ICRP calculated dose coefficients, which are effective dose per unit intake, for workers. These dose coefficients are reference values for radiation protection purpose and are not associated, by definition, with any uncertainty.

However, the degree of knowledge on the parameters varies in specific situations of exposure. Firstly, the exposure conditions which affect the model predictions are usually not well defined: from a routine measurement, the intake rate (acute or chronic) and the contamination time are difficult to assess; the aerosol size distribution and its absorption kinetics are rarely known. Secondly, the activity measurement is subject to Poisson variability and, in case of *in vitro* measurement, uncertainty on the result is influenced by the sampling of excreta. By modelling and propagating the uncertainty in exposure conditions and measurements, the uncertainty in dose assessed from prospective or retrospective calculation can be estimated.

Moreover, the sensitivity of a routine monitoring programme can be evaluated through the determination of the minimum dose detectable by this programme. It is usually calculated using reference values of exposure and biokinetic parameters. However, a more accurate minimum detectable dose (MDD) should be evaluated by integrating the uncertainty regarding the dose evaluation. In addition, MDDs of different programmes can be compared to optimise the monitoring of workers.

After a presentation of the exposure to radiation in the nuclear industry, the first chapter of this manuscript presents the radiological protection system, the activity measurement techniques, the biokinetic and dosimetric models, the dose calculation, and the design of a monitoring programme. All these topics are investigated along with a discussion of their associated uncertainties. In the second chapter, the different modelling of uncertainty are presented. The direct and inverse uncertainty propagation techniques are highlighted. A special attention is paid to the methods used in this work.

The aim of chapter 3 is to demonstrate the usefulness of “Dempster-Shafer” approach in prospective dosimetry of internal exposure. It is more conservative than the usual probabilistic approach and is well suited to process imprecise information. This approach is applied to the issue of occupational inhalation of uranium dust through the cases of fuel processing facilities and of uranium mines and mills. The results are compared to those obtained from other mathematical approaches.

The next part of this work is dedicated to the evaluation of the sensitivity of a monitoring programme by integrating uncertainty in dose assessment. This study is applied to the monitoring of a specific group of workers of AREVA NC La Hague reprocessing plant. In chapter 4, their job is presented along with their monitoring programme, including a description of the measurement characteristics and of the physico-chemical properties of the handled plutonium (Pu). Moreover, a large part of this work is interested in the determination of the variability of Pu absorption in the respiratory tract.

In chapter 5, the modelling of the uncertainties is used to determine the MDD for the current monitoring programme. The different inverse propagation methods are compared as well as the influence of the respective sources of uncertainty. In chapter 6, the MDDs of different possible monitoring programmes are calculated to determine the best compromise between the number of measurements and the sensitivity.

All computations were performed with the OPSCI software developed during this work. It is presented in details with its validation in chapter 7. Finally, a general discussion of the results and perspectives is proposed in chapter 8.

CHAPTER 1

Monitoring internal exposure of workers

1.1 Exposure to ionizing radiation in the nuclear industry

1.1.1 Nuclear reactions in fuel

The production of electric power in a nuclear reactor is based on the fission reaction of ^{235}U nuclei after absorption of neutrons. The fission reaction is the splitting of an unstable heavy nucleus into two fission products of lesser mass. ^{235}U fission releases 200 MeV and between 2 and 3 neutrons (Fig. 1.1). This reaction is a source of a considerable amount of energy. The neutrons are slowed down to be absorbed by other ^{235}U nuclei and to continue the chain reaction.

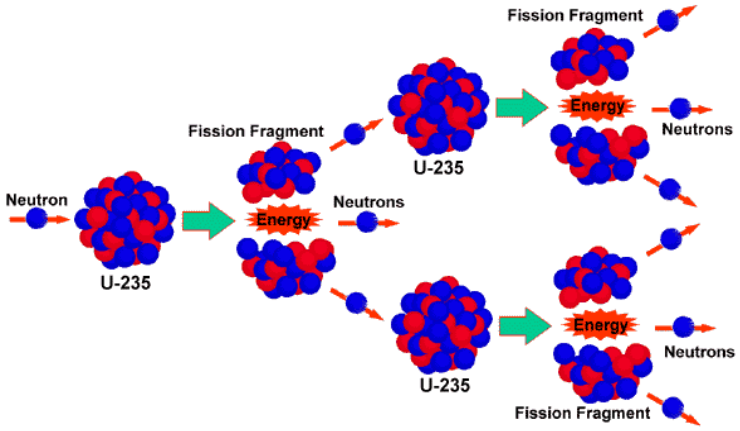

Figure 1.1: ^{235}U fission chain reaction

The fission of ^{235}U generates fission fragments with a number of nucleons between 80-110 and 125-155 with 95 and 138 being the most probable. The fission fragments initiate decay chains which daughters are called fission products. The most common are: ^{85}Kr, ^{90}Sr, ^{95}Sr, ^{106}Ru, ^{129}I, ^{131}I, ^{133}Xe, ^{137}Cs, ^{144}Ce, ^{147}Pm; but they include overall 300 different isotopes. They are the main contributors to the radiotoxicity of spent fuel during the first decades.

In addition, ^{238}U and ^{235}U can capture some of the neutrons and generate nuclei of higher mass from ^{236}Np to ^{246}Cm which are called transuranic elements (Fig. 1.2). These are responsible for most of the radiotoxicity of spent fuel for hundreds of years after irradiation.

Finally, stable nuclei present in the reactor constituents can be activated by neutron capture. For example, the activation products ^{58}Co and ^{60}Co are formed by activation of iron and nickel.

The spent fuel therefore contains uranium which has not reacted (about 94 % in weight), plutonium (1 %), neptunium, americium, curium (0.1 %) and fission products (5 %). As they can initiate fission reaction, uranium and plutonium can be retreated and reprocessed as Mixed Oxide

(MOX) fuel, a mixture of ^{235}U depleted UO_2 and PuO_2 reintroduced in the nuclear cycle. The remaining elements are treated as waste of high activity.

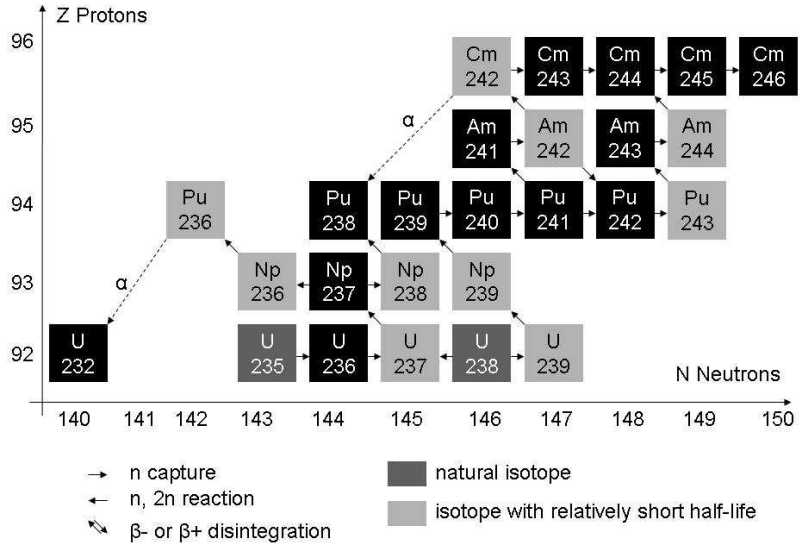

Figure 1.2: Formation of transuranic elements in a nuclear reactor from ^{235}U and ^{238}U (Patarin, 2002)

1.1.2 Nuclear cycle

The process of using uranium to make fuel and the treatment of spent fuel is called the nuclear cycle (Fig. 1.3). It groups uranium ore extraction, conversion into yellow cake, enrichment, fuel fabrication, treatment of spent fuel and MOX fuel preparation.

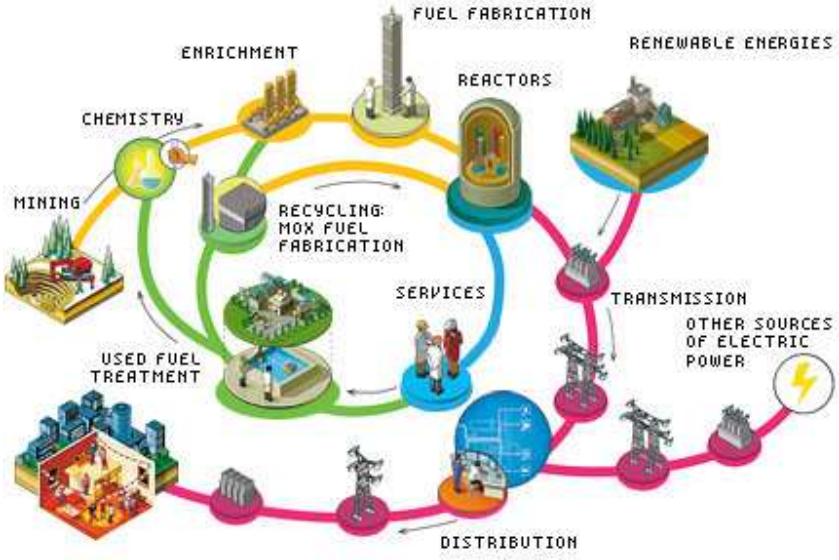

Figure 1.3: Nuclear cycle (source www.areva.com)

Mining

Naturally occurring uranium ore is extracted from the soil. The most common ore is the pechblende formed of U_3O_8 uranium oxide. It contains three isotopes:

- ^{238}U at 99.28 % in mass or 49 % in activity (half-life: $4.5x10^9$ y)
- ^{235}U at 0.718 % in mass or 2 % in activity (half-life: $7.0x10^8$ y)
- ^{234}U at 0.0056 % in mass or 49 % in activity (half-life: $2.4x10^5$ y) (Patarin, 2002)

Milling

The uranium ore is first crushed. Then the uranium oxide is dissolved in a strong oxidising acid solution or by a strong alkaline solution depending on the ore. Uranium is separated from solid residues by filtration and purified by ion exchange. After extraction, uranium is precipitated and removed from the solution by NH_4OH or $Mg(OH)_2$. After drying, magnesia or ammonium diuranate (MgU_2O_7 or $(NH_4)_2U_2O_7$), called yellow cake, is obtained.

Conversion

At this stage, uranium concentrate is prepared for the enrichment process. Firstly, yellow cake is dissolved in nitric acid. Secondly, uranyl nitrate is extracted by tributyl phosphate (TBP). Then uranium is precipitated by adding ammonia. The diuranate is filtered and dried before being converted into UO_3 by calcinations. UO_3 is then reduced by NH_3 and H_2 before adding HF to obtain UF_4, and F_2 to produce UF_6. UF_6 is finally crystallized at -15 °C and -25°C.

Enrichment

In order to use uranium oxide as a nuclear fuel, the concentration of ^{235}U must be around 4 % in contrast with the 0.7 % percent present in the ore. Enrichment in ^{235}U is performed by gaseous diffusion or ultracentrifugation of UF_6. In gaseous diffusion, the isotopic separation is based on the difference of molecular diffusion rates of ^{235}U and ^{238}U in a 0.01 µm porous medium. Ultracentrifugation is based on weight difference between the two isotopes.

Fuel fabrication

Enriched UF_6 is converted into UO_2 in a rotative oven in presence of water vapour and hydrogen. The density of the oxide is adjusted by adding U_3O_8 in order to obtain UO_2 pellets. The powder is then pre-compacted, crushed, granulated and put into pellets. The pellets are heated to 1700°C under reductive atmosphere and their size are rectified and controlled. They are finally loaded into long rod-like metallic tubes which are gathered to form fuel assemblies.

Reprocessing

For countries which have chosen to reprocess spent fuel, reprocessing starts at least 4 years after the end of the fuel irradiation to evacuate most of the residual heat caused by short half-live

radionuclides disintegration. The first step is the shearing of the rods and the dissolution of spent fuel in nitric acid. The solution is then clarified by extracting insoluble fission products and shearing fines. The solution then contains only soluble fission products, uranium, plutonium and other transuranic elements. In France, uranium and plutonium are extracted from the solution by the PUREX process using liquid-liquid extraction with TBP. The solution containing the fission products and the transuranic elements except plutonium is calcined and vitrified before stocking.

Plutonium is selectively extracted from the organic solution containing uranium and plutonium by selective reduction of plutonium. Finally, uranium and plutonium are converted into PuO_2 and UO_2oxides by calcinations.

MOX fabrication

The MOX fuel is a mixture of depleted uranium oxide and plutonium oxide. MOX fuel preparation is the same as for uranium with two powders instead of one, the mixture having to be homogeneous in the pellets.

1.1.3 Exposure pathways

Handling uranium, transuranic elements, fission or activation products, cleaning or dismantling facilities can lead to irradiation or contamination at the workplace. External irradiation is caused by a radioactive source lying outside of the body while contamination is the incorporation of a radionuclide into the body by inhalation, ingestion or wound. For workers, inhalation of radioactive aerosol is the most likely pathway of contamination.

1.2 Effects of ionizing radiation

1.2.1 Emission of radiation

Disintegration of a radionuclide leads to the emission of particles depending on the radionuclide decay scheme. Heavy nuclei like ^{238}U, ^{235}U, ^{239}Pu, ^{240}Pu, ^{241}Am, decay by α particle emission:

$$^{238}_{92}U \rightarrow ^{234}_{90}Th + \alpha \,. \qquad \text{Equation 1.1}$$

α particles are helium nucleus made of 2 protons and 2 neutrons of relatively heavy weight and very small range : a few centimetres in the air and about 40 microns in water. Their toxicity is therefore to be considered only in case of internal contamination when the α-emitting radionuclide is close to sensitive cells.

Some fission products like ^{90}Sr, ^{90}Y, ^{106}Ru, ^{129}I, ^{131}I, ^{137}Cs or ^{241}Pu emit ß particles. In case of $ß^-$ disintegration, a neutron is transformed into a proton with the emission of a $ß^-$ particle (electron) and of an antineutrino:

$$^{137}_{55}Cs \rightarrow ^{137}_{56}Ba + \beta^- + \bar{\nu} \; . \qquad \text{Equation 1.2}$$

For ß$^+$ disintegration, a proton is transformed into a neutron with emission of a ß$^+$ particle (positron) and of a neutrino:

$$^{58}_{27}Co \rightarrow ^{58}_{26}Fe + \beta^+ + \nu \; . \qquad \text{Equation 1.3}$$

ß particles have a range of about few metres in the air and a few millimetres in water, depending on the spectrum of emitted ß particles energy.

Electron capture is a decay mode for a nucleus with an excess of protons and insufficient energy to emit a ß$^+$ particle. One of the orbital electrons, usually from the K or L electron shell is captured by a proton in the nucleus, forming a neutron and a neutrino:

$$^{83}_{37}Rb + e^- \rightarrow ^{83}_{36}Kr + \nu \; . \qquad \text{Equation 1.4}$$

The atom moves into an excited state with the inner shell missing an electron. When transiting to the ground state, the atom will emit an X-ray photon and/or Auger electrons. Auger electrons can be emitted following the transition of an electron filling in an inner-shell vacancy.

Internal conversion is a radioactive decay process where an excited nucleus interacts with an electron in one of the lower atomic orbitals, causing the electron to be emitted from the atom. Thus, in an internal conversion process, a high-energy electron is emitted from the radioactive atom, but without beta decay taking place

The excited nucleus can reach a stable state by emission of γ particles which are photons of high energy. γ particles have a very high penetrating power and will be stopped only by large width of concrete or lead. The local energy deposition in material along the path is small.

Some nuclei like ^{252}Cf can decay by spontaneous fission and generate fission products.

The emission scheme of a nucleus is characterised by the nucleus and the yield of emission and the energy of emitted radiations and particles. Emission schemes have been documented by ICRP (2008).

1.2.2 Biological effect of radiation

α, ß and γ particles can interact with the cell constituents, mainly by ionisation, and induce biological effects.

Most of the damage caused to the cells by particles is assumed to be through the alteration of DNA. DNA strand breaks are due to direct action of primary or secondary charged particles on DNA or by induced free radicals. If the break is perfectly repaired, it has no effect. If damage is beyond repair, the cell dies either by apoptosis (self-destruction of the cell to prevent abnormal behaviour) or by necrosis (destruction of the cell caused by external factors), possibly leading to inflammatory reaction or loss of function of tissues (deterministic effects). If DNA damage is not correctly repaired, a DNA mutation occurs. This can either lead to hereditary effects (in case the germ line is affected) or to cancer (stochastic effects, Fig. 1.4) or have unnoticeable effect.

Deterministic effects appear within a few hours or months after irradiation if the dose received is higher than a certain threshold. They are caused by the destruction of many cells in the same tissue and their severity increases with the dose. The most sensitive tissues are the skin, bone marrow, gut, gonads and eye lenses. The first deterministic effect after a whole-body irradiation is the destruction of white blood cells. From a localised irradiation, the skin is usually the first damaged tissue.

Stochastic effects appear randomly with frequencies depending on the exposure, after a few years or few decades. No dose threshold has been found for their appearance. Therefore it is commonly assumed that the risk of stochastic effects is proportional to the dose down to the slightest directly irradiation: this is known as the linear-non-threshold model (ICRP, 2007) and currently forms the basis of radiological protection practices.

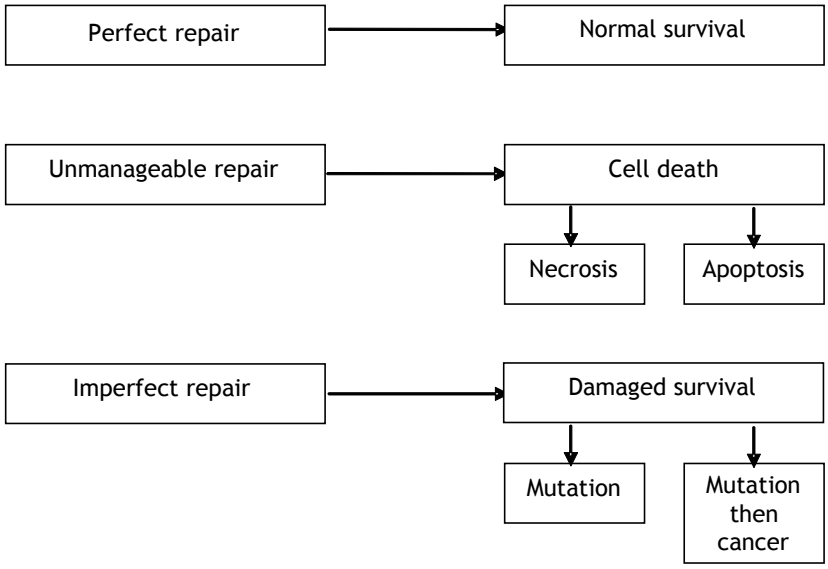

Figure 1.4: Biological effects of ionizing radiation (Métivier, 2006)

The United Nations Scientific Committee on Effects of Atomic Radiation (UNSCEAR) reviews the evidence of health effects of radiations based on biological and epidemiological studies.

1.3 Radiological Protection

1.3.1 Institutions in charge of radiological protection

To protect people against health effects of ionizing radiation, radiological protection policy have been developed since the 1920's. The International Commission on Radiological Protection (ICRP) published recommendations based on the available scientific knowledge. The International Atomic Energy Agency (IAEA) publishes standards, guidelines and recommendations approved by member states representatives, often following the recommendations of ICRP. IAEA International Standards are adapted in state regulations. In France, this is done through the transposition of the European Union regulation. Finally, employers, supported by occupational health and radiation

protection departments, are responsible for the radiological protection of workers. Moreover, national authorities (Autorité de Sûreté Nucléaire in France) ensure that radiological protection complies with regulation for public and for workers.

1.3.2 Dose definition

In its recommendations (ICRP, 2007), the ICRP defines the concept of dose to quantify the exposure to ionizing radiation. The International Commission on Radiation Units and measurements (ICRU, 1998) also introduces the concept of absorbed dose.

Absorbed dose

Ionizing radiation interacts with matter by imparting energy. The quantity of imparted energy by unit of mass is the absorbed dose. Its SI unit is $J.kg^{-1}$ and its special name is gray (Gy). It is an average of energy imparted by point interactions over a defined volume and time per unit mass.For radiation protection purpose, the absorbed dose is averaged over an organ (liver), a tissue (muscle) or sensitive target cells within a tissue (endosteal surfaces of skeleton) when those are identified.

Equivalent dose

In order to account for the fact that some types of radiation are more harmful than others, the concept of equivalent dose is used. The equivalent dose in an organ or tissue, H_T, is defined as:

$$H_T = \sum_R w_R D_{T,R} \ , \qquad \text{Equation 1.5}$$

where $D_{T,R}$ is the average absorbed dose in the target organ or tissue T, due to radiation of type R.. w_R is the radiation weighting factor for radiation R (Table 1.1). The unit of equivalent dose is the sievert (Sv). w_R values result from a judgment based on the knowledge of the relative biological effectiveness of the different radiations. w_R is equal to 1 for photons and ß, and to 20 for α particles.

Table 1.1: Reference values for the radiation weighting factors (ICRP, 2007)

Radiation type	Radiation weighting factor, w_R
Photons	1
Electrons and muons	1
Protons and charged pions	2
Alpha particles, fission fragments, heavy ions	20
Neutrons	$2.5+18.2e^{-(\ln(E_n)^2/6}$, for E_n < 1 MeV $5.0+17.0e^{-(\ln(2E_n)^2/6}$, for 1 MeV ≤$E_n$ ≤ 50 MeV $2.5+3.25e^{-(\ln(0.04E_n)^2/6}$, for E_n > 50 MeV

Radionuclides incorporated in the body may irradiate the tissues for days, months or years depending on their physical half-life and their biological retention. So the committed equivalent dose $H_T(\tau)$ is defined as the total dose delivered in a tissue over the time period τ following intake of a radionuclide. τ is usually set to 50 years for adults and up to the age of 70 for children so as to cover life-long irradiation.

Effective dose

In order to account for the fact that some tissues are more radiosensitive, the concept of effective dose is used. The effective dose *E* is defined as a weighted average of equivalent doses to radiosensitive tissues of the body:

$$E = \sum_T w_T H_T = \sum_T \sum_R w_T w_R D_{T,R} \,, \qquad \text{Equation 1.6}$$

where w_T is the tissue weighting factor for T, with the sum of w_T being 1 (Table 1.2). The values of w_T are set by judgment on the basis of epidemiological data of Hiroshima-Nagasaki survivors considering the frequency of stochastic effects and their severity in the different tissues at a given level of exposure.

Table 1.2: Reference values for tissue weighting factors (ICRP, 2007)

Tissue	Tissue weighting factor, w_T
Bone marrow (red), colon, lungs, stomach, breast, remainder tissues[a]	0.12
gonads	0.08
Bladder, oesophagus, liver, thyroid	0.04
Bone surface, brain, salivary glands, skin	0.01

[a] Adrenals, extrathoracic region, gall bladder, heart, kidneys, lymphatic nodes, muscle, oral mucosa, pancreas, prostate, small intestine, spleen, thymus, uterus

Equivalent and effective doses are related to the risk of stochastic effects for a reference person (ICRP, 2002b) after low-dose irradiation. They are defined for radiological protection purpose and to enable the comparison of different sources of exposure. Effective dose is defined for a reference person, taking account of the conditions of exposure but not of the characteristics of a specific exposed individual, such as sex, age or health status. It therefore cannot be used for assessment of individual risk. Instead, effective dose is a tool in the management of radiation protection for prospective dose assessment in order to plan and optimise protection, and for retrospective dose assessment in order to demonstrate compliance with dose constraints and limits.

Committed effective dose is calculated from committed equivalent doses. The annual effective dose refers to the effective dose committed over 50 years or up to the age of 70 years due to intakes occurred during the year.

1.3.3 Principles of radiological protection

A system of radiological protection was developed by the ICRP in order to provide an adequate level of protection for workers and members of the public without unnecessarily limiting the benefit from practices involving exposure to ionizing radiation. Only occupational exposure is considered in this thesis.

Planned exposure to ionizing radiation should follow the three principles of justification, optimisation and limitation (ICRP, 2007). These principles are integrated in the French regulation (Code du travail, 2008a):

Justification: Only useful or needed practices involving exposure should be performed; furthermore these should achieve sufficient individual or societal benefit to offset the detriment they cause.

Optimisation: Exposure should be kept at a level as low as reasonably achievable, taking into account economic and societal factors. The individual dose resulting from exposure to a given source should be restricted below a dose constraint by undertaking actions such as shielding, reduction of exposure time or confinement of radionuclides.

Limitation: The total dose should not exceed a dose limit fixed to ensure that occurrences of stochastic effects are below unacceptable levels and that tissue reactions are avoided. The annual effective dose limit for workers is 20 mSv (Code du travail, 2008b).

These principles lead to a diminution of collective occupational effective dose every year (IRSN, 2009) consistently with their objective.

1.3.4 Monitoring

In order to demonstrate compliance with regulatory requirements, the occupational exposure must be assessed. Workplace studies can be carried out to determine the handled radionuclide, their activity and chemical form and in some case, the size distribution of the released aerosol and its solubility. Therefore, it forms part of overall radiation protection programme, which starts with an assessment to identify work situations in which there is a risk of radionuclide intake by workers, and to quantify the likely intake of radioactive material and the resulting committed effective dose received. From this workplace study, an adapted monitoring programme can be designed based on collective or individual measurements.

Individual monitoring gives information needed to assess the exposure of a single worker by measuring individual body activities, excretion rates or activity inhaled (using personal air samplers). Workplace monitoring, which includes collective monitoring, provides exposure assessments for a group of workers assuming identical working conditions i.e. risks of intake as well as all factors influencing the resulting doses. It uses measurements made in the working environment such as air monitoring to assess the air contamination and surface activities. Intake i (Bq) can be assessed from air contamination by:

$$i = C \times B \times t\,, \qquad \text{Equation 1.7}$$

where C is the air concentration in Bq.m^{-3}, B the worker breathing rate in m^3.h^{-1} and t the exposure time in h.

Where significant intakes of radionuclides can be expected, individual monitoring of workers is required to detect and quantify exposure, to verify and document that the workers are adequately protected, in compliance with legal requirements. When workers are considered likely to receive routinely a significant fraction of relevant dose limit or work in areas where exposures could be significant in an event of an accident, different types of monitoring can be specified (ICRP, 1997a, 1997b):

- Routine monitoring is associated with continuing operations [*e.g.* over more than a year] and intended to demonstrate that working conditions, including the levels of individual dose, remain satisfactory, and meet regulatory requirements. It is performed to quantify exposures where there is the possibility either of undetected accidental intakes or of chronic intakes. Its basis is the assumption that working conditions remain reasonably constant [the risk of exposure to stay the same]. Periodic measurements are made at pre-determined times.
- Special monitoring is performed to quantify significant exposures following actual or suspected abnormal events;
- Task-related monitoring provides information on a specific operation of limited duration, or following major modifications applied to the installations or operating procedures, or to confirm that the routine monitoring programme is suitable.
- Control monitoring may complement workplace monitoring to confirm that no individual routine monitoring is necessary.

1.4 Measurement of incorporated activity

1.4.1 Measurement techniques

In order to quantify individual contamination, two approaches can be applied: *in vivo* or *in vitro* measurements. *In vivo* measurement is the direct measurement of body content of radionuclides by detectors set outside the body (Fig. 1.5). It provides a quick (20-30 minutes) estimate of activity in the body or in a specific organ. But it is feasible only for radionuclides emitting radiation that can escape from the body. In principle, the technique can be used for radionuclides that emit X, γ or energetic ß particles.

In vitro or indirect measurement is the analysis of excreta or another biological sample (nose blow, nasal smear, blood or biopsy). It is the only measurement approach for radionuclides which emit no penetrating radiation (e.g. high energy photons). Urine and faeces measurements are widely used because of their high sensitivity and applicability to any radionuclide. However, α spectroscopy usually requires a one-week-long chemical process and sample counting for several

days. Furthermore, *in vitro* measurement may be performed without the worker leaving the workplace but involves a risk of sample contamination.

Figure 1.5: *In vivo* measurement and efficiency calibration using a physical (bottle) phantom in the mobile in vivo count laboratory of IRSN

For both techniques, activity measurement is requiring a detector in which the emitted radiations interact. These interactions are converted into electric impulses (counts) by the detector. The number of counts (N) can be converted in activity (A in Bq) through the efficiency of detection of the detector (ε), the emission yield of the radiation (Y) and the counting time (T_{count} in seconds):

$$A = \frac{N}{T_{count} \times Y \times \varepsilon}. \qquad \text{Equation 1.8}$$

For *in vitro* measurements, the chemical yield of the preparation Y_c must be added:

$$A = \frac{N}{T_{count} \times Y \times Y_c \times \varepsilon}. \qquad \text{Equation 1.9}$$

The efficiency of detection, or calibration coefficient, is evaluated by measuring a source of known activity with the same geometry as the actual measurement. For *in vivo* measurements, phantoms are used to simulate the human body (Fig. 1.5).

The performance criteria of these measurements can be assessed by applying the ISO standard 12790-1 (2001).

1.4.2 Decision threshold and detection limit

Each radioactive nucleus has an intrinsic constant probability of transition during a given period depending on its half-life. This random phenomenon generates a variability of the measurement result. Another complication of radioactivity measurement is the presence of natural background radiation caused by cosmic and telluric radiation, concentration of radon and its progeny in the atmosphere and dietary ingestion of natural ^{40}K, ^{14}C, ^{232}Th, ^{238}U, ^{235}U and their daughters: a man weighing 70 kg contains around 4,500 Bq of ^{40}K, 3,700 Bq of ^{14}C, 640 Bq of ^{87}Rb, 220 Bq of U-Th-Ra. To limit the contribution of the background, cosmic radiation can be stopped by shielding and radon concentration can be reduced by ventilation. Still, the sensitivity of the measurement techniques depends on the remaining background.

The total or measured number of counts N_S is the sum of counts induced by background radiation N_0 and counts induced by the activity of interest contained in the sample (*in vitro*) or in the body (*in vivo*) (net counting) N_n:

$$N_S = N_0 + N_n \,. \qquad \text{Equation 1.10}$$

N_0 is determined by measuring the counts from the background in the absence of other activity. However, the background is variable and fluctuates around its mean value according to a Poisson distribution. Therefore a measured low but positive count N_n may be the consequence of a mere fluctuation of the background rather than the presence of an activity of interest.

Hence a decision threshold (*DT*) is defined such that if $N_n > DT$, the sample or the body contains a radionuclide. If this decision rule is observed, a wrong decision occurs with the probability *a* that there is a sample or body contribution when, in fact, only a background effect exists (ISO, 2000). It is calculated under the hypothesis of a Poisson background, by:

$$DT = k_{1-\alpha}\sqrt{R_0(\frac{1}{t_0}+\frac{1}{t_S})} \text{ (ISO, 2000).} \qquad \text{Equation 1.11}$$

for adequate size of $R_0 t_S$ where k_{1-a} is the desired 1- *a* percentile of the Poisson distribution, R_0 the background effect counting rate, quotient of the counts N_0 counted during the preselected duration of the background effect measurement t_0, t_S is the duration of the gross effect measurement. When N_0 is large enough (> about 30) to approximate the Poisson distribution by a normal distribution, an *a* risk of 2.5 % is obtained for k_{1-a} =1.96. Then if 1,000 background effects measurements are carried out, 25 on average would be greater than DT and lead to erroneously conclude that the radionuclide of interest is present in the sample or in the body. *DT* is the highest number of counts which would be interpreted as the absence of the activity of interest.

On the other hand, the overall variability of the counting may lead one to erroneously conclude that the radionuclide of interest is absent (β risk of false negative). A detection limit (DL) is hence defined to specify the minimum sample or body contribution which can be detected with a given probability *β* of error using the measuring procedure in question. This allows a decision to be made as to whether a measuring method satisfies certain requirements and is consequently suitable for the given purpose of measurement (ISO, 2000). The DL shall refer to the smallest expectation of the net counting rate for which a wrong decision occurs with a probability *β* that there is no sample contribution but only a background effect. Under assumption of Poisson background,

$$DL = (k_{1-\alpha} + k_{1-\beta})\sqrt{R_0(\frac{1}{t_0}+\frac{1}{t_S})} \text{ (ISO, 2000).} \qquad \text{Equation 1.12}$$

Typical DLs are gathered in Table 1.3.

Table 1.3: Typical detection limits (DL) for in vivo and in vitro measurements of various radionuclides (ICRP, 1997b).

Radionuclide	Method of Measurement		Typical DL
^{238}Pu	X-ray spectrometry *in vivo*	Lung	1,000 Bq
	Radiochemical separation and α-ray spectrometry	Urine	1 mBq.L^{-1}
		Faeces	1 mBq
^{239}Pu	X-ray spectrometry *in vivo*	Lung	2,000 Bq
	Radiochemical separation and α-ray spectrometry	Urine	1 mBq.L^{-1}
		Faeces	1 mBq
^{241}Am	γ-ray spectrometry *in vivo*	Lung	20 Bq
		Skeleton	20 Bq
	Radiochemical separation and α-ray spectrometry	Urine	1 mBq.L^{-1}
		Faeces	1 mBq
^{234}U, ^{235}U,	γ-ray spectrometry *in vivo*	Lung	200 Bq
^{238}U	Radiochemical separation and α-ray spectrometry	Urine	10 mBq.L^{-1}
		Faeces	10 mBq
^{137}Cs	γ-ray spectrometry *in vivo*	Whole body	50 Bq
	Radiochemical separation and α-ray spectrometry	Urine	1 Bq.L^{-1}

1.4.3 Measurement uncertainties

Radioactivity measurement is subject to different sources of uncertainty. Firstly, the result depends on the random transformation of radionuclides according to a Poisson distribution (ISO, 2010). Secondly, the biological excretion of trace elements fluctuates randomly around a trend (Usuda *et al*, 2002). Such fluctuations are averaged to some extend by sampling the excreta over one or several days (Moss et al, 1969) (Fig. 1.6). Thirdly, for *in vivo* measurement, detection efficiency calibration is carried out using phantoms which can have important morphological differences with the measured person, while measurement geometry is critical (Toohey *et al*, 1991, de Carlan *et al*, 2007, Lopez and Navarro, 2003). For instance, the uncertainty on the thoracic thickness (combinaison of muscular and adipous tissue) attenuating radiation can lead to 80 % error on lung measurement (Franck *et al*, 1997). The determination of the yields of the chemical preparation of *in vitro* samples has to be assessed precisely to evaluate the quantity of radionuclide in the original sample from the prepared sample (Hurtgen and Cossonet, 2003) (Fig. 1.7). Finally, the normalisation of a measurement of the bioassay sample to the daily excretion rate often introduces a substantial uncertainty.

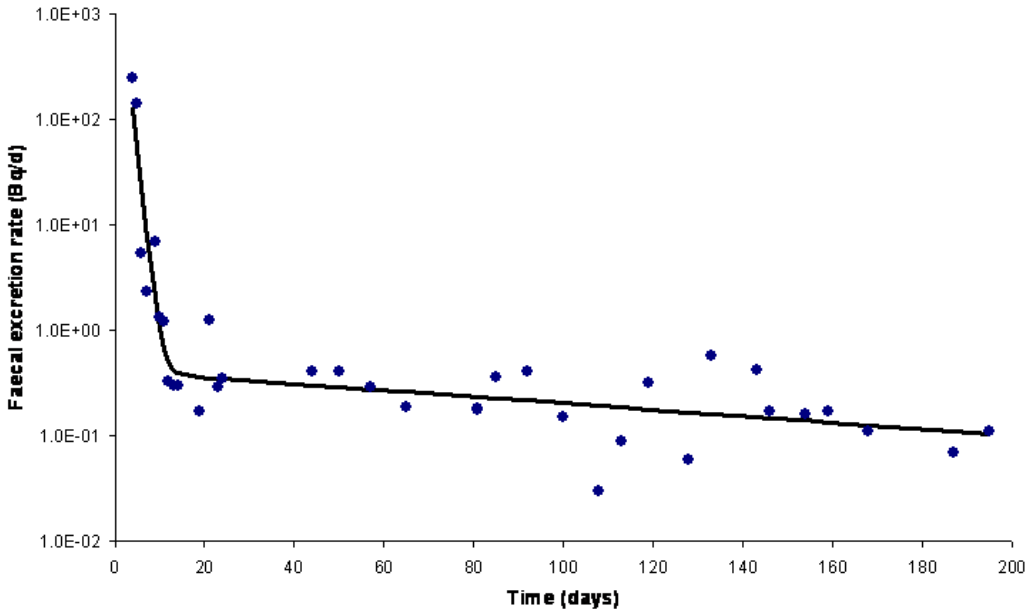

Figure 1.6: Variability of faecal excretion after inhalation of ^{239}Pu for 24 h samples (Marsh et al, 2007)

A report of the IAEA (2004) is intended to assist scientists using nuclear analytical methods in assessing and quantifying the sources of uncertainty of their measurement.

Within the IDEAS guidelines (Doerfel *et al*, 2006) and the CONRAD project (Lopez *et al*, 2008), all of these sources of uncertainty were modelled in terms of one log-normal distribution with a geometric standard deviation called scattering factor (SF). However it is acknowledged that when the activity is very low, close to the DT, the Poisson uncertainty is dominant, while it becomes negligible when the activity is high enough. Values of SF for *in vitro* measurement were determined from the follow-up of actual contamination cases with high excretion data so that Poisson variability would have little influence on the measurement (Marsh *et al*, 2007). Therefore, the determined SFs model all measurement uncertainties except Poisson variability. The suggested default SF values (Doerfel *et al*, 2006) for various types of measurements are gathered in Table 1.4.

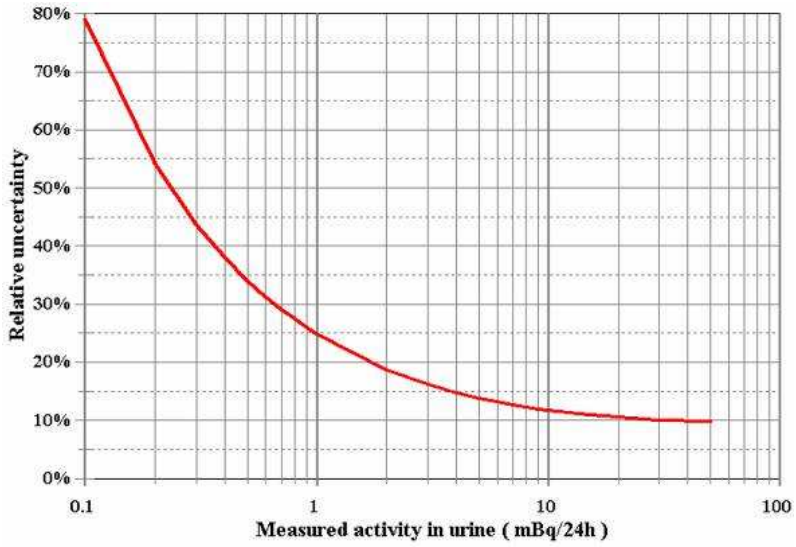

Figure 1.7: Relative measurement uncertainty as a function of the measured activity in urine including Poisson variability and uncertainty in chemical yield (Hurtgen and Cossonnet, 2003)

Table 1.4: Suggested default SF values for various types of measurements. When available, ranges are given in brackets (Doerfel *et al*, 2006; Marsh et al, 2008b).

Quantity	Type B SF
True 24 h urine	1.1
Activity concentration of ^{3}H in urine	1.1
Simulated 24 h urine, creatinine or specific gravity normalised	1.6 (1.3 – 1.8)
Spot urine sample	2.0
Faecal 24 h sample	3 (2 – 4)
Faecal 72 h sample	1.9 (1.5 – 2.2)
Body count (photon energy < 20 keV)	2.3
Body count (20 keV < photon energy < 100 keV)	1.4
Body count (photon energy > 100 keV)	1.2

1.5 Models

To interpret bioassay measurements, the behaviour of radionuclides from intake to elimination are described by biokinetic models. These are made of compartments corresponding to organs, tissues, metabolic states or fractions of activity within a tissue, and transfers of activity between compartments governed by first order kinetics with constant rates estimated from animal experiments or follow-up of human contamination cases. The biokinetic models translate into a set of linear first order differential equations.

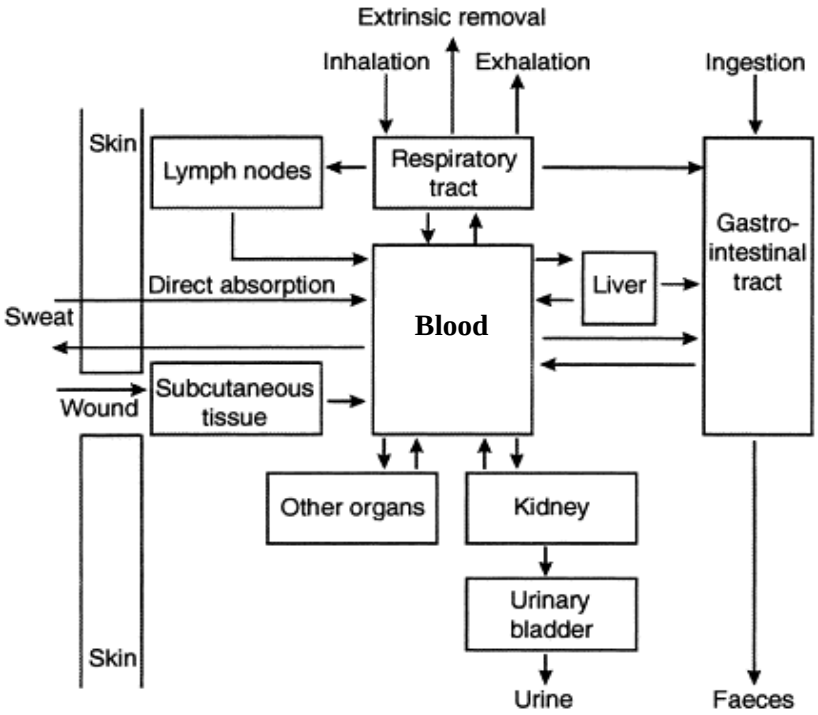

Figure 1.8: Summary of the main routes of intake, transfers and excretion (adapted from ICRP, 1997b)

They allow predicting from a given intake, the retention of activity in organs and the excretion in urine and faeces as functions of time. The integral of retained activity over the commitment period provides the number of nuclear transformations that take place in a region.

Specific models are recommended by ICRP to describe the movement of radionuclides from the site of entry following inhalation, ingestion or wound, its entry into the blood, the element-specific systemic kinetics of exchange between blood and tissues and the excretion (Fig. 1.8).

1.5.1 Human Respiratory Tract Model

The Human Respiratory Tract Model (HRTM) (ICRP, 1994a) describes the morphology and the physiology of the respiratory tract, the deposition of an inhaled radionuclide in the different regions of of the airways (Fig. 1.9), and the clearance of the deposited activity.

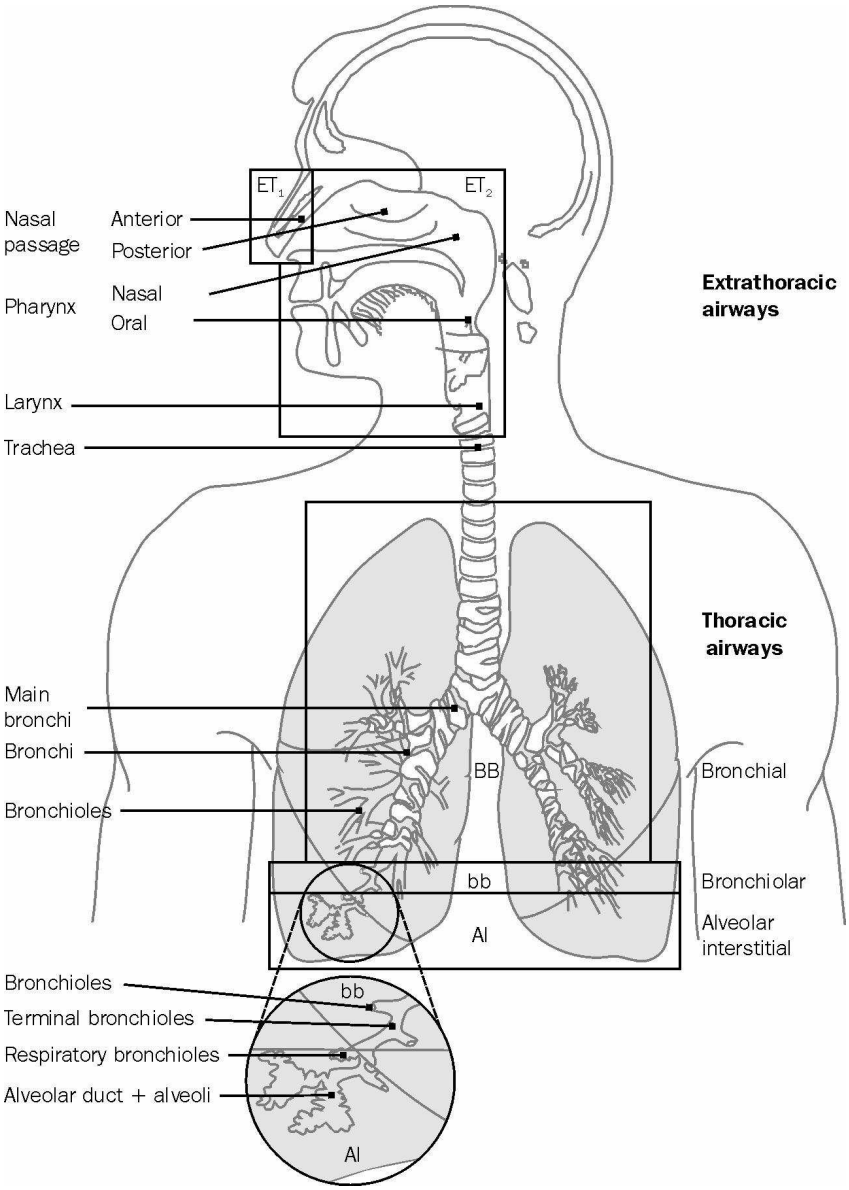

Figure 1.9: Respiratory tract compartments defined in the HRTM (ICRP, 1994a)

Deposition

The morphology of the respiratory tract defines the different compartments used in the model (Fig. 1.9). Deposition is the process that determines how much of the intake initially remains in the regions of the respiratory tract after inhalation and exhalation of an aerosol. The HRTM deposition model represents airways as a succession of filters where a fraction of particles is deposited during inhalation and exhalation. Deposition can occur as a consequence of gravitational sedimentation, inertial impaction and Brownian motion (diffusion) (Fig. 1.10). Sedimentation and impaction are aerodynamic effects that are important for particles with diameters above about 0.1 µm and increase with size. Diffusion is a thermodynamic effect that is important below about 1 µm and increases with decreasing size. Large particle behaviour depends on its aerodynamic equivalent diameter, d_{ae}, which is the diameter of a unit density sphere that has the same terminal settling velocity in air as the particle of interest:

$$d_{ae} \approx \rho^{1/2} d_p \,, \qquad \text{Equation 1.13}$$

where ρ is the particle density in g.cm^{-3} and d_p, the geometric diameter of the particle. For small particles, the thermodynamic equivalent diameter, d_{th}, is used. It is the diameter of a spherical particle that has the same diffusion coefficient in air as the particle of interest. Because diffusion does not depend on particle density, d_{th} is close to d_p.

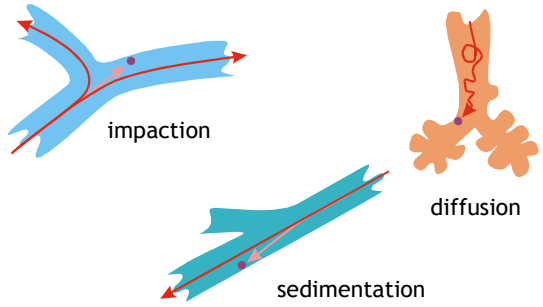

Figure 1.10: Main mechanisms of particle deposition in the respiratory tract (ICRP, 1994a)

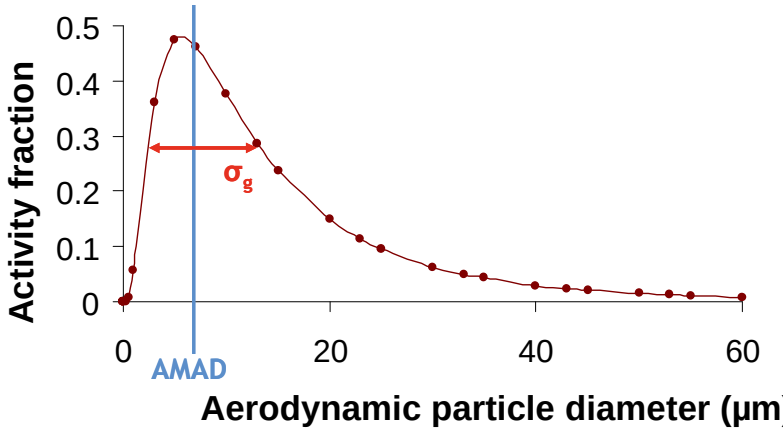

Figure 1.11: U_3O_8 aerosol size distribution measured in FBFC nuclear fuel processing plant in Pierrelate with AMAD and geometric standard deviation (σ_g) adapted from Ansoborlo *et al* (2002).

In practice, aerosols are almost never composed of particles with a single size (monodisperse) but include rather of a mixture of particle sizes (polydisperse). The mass of particles in aerosols is usually log-normally size-distributed (ICRP, 2002a). The log-normal distribution is described by two parameters: the median diameter and the geometric standard deviation (Fig. 1.11). For radioactive aerosols, it is convenient to refer to the activity median diameter of the aerosol. For particles larger than 0.1 μm, the Activity Median Aerodynamic Diameter (AMAD) is used to quantify an aerosol size distribution: 50% of the activity in the aerosol is associated with particles of aerodynamic diameters larger than the AMAD. Activity Median Thermodynamic Diameter (AMTD) is used to characterize particle distributions below 1 μm.

AMAD and AMTD influence the amount and the repartition of deposited particles in the respiratory tract (Fig. 1.12, Table 1.5). In the absence of direct measurements, ICRP recommend reference values of 5 μm and 1 μm for workers and members of the public respectively, with a geometric standard deviation equal to 2.5 (ICRP, 1994a). Physiological parameters such as the breathing rate, which depends on the level of exercise, the regional airways volumes and the fraction of air breathed through the nose also influence deposition and can have reference values suggested by the ICPR (1994a).

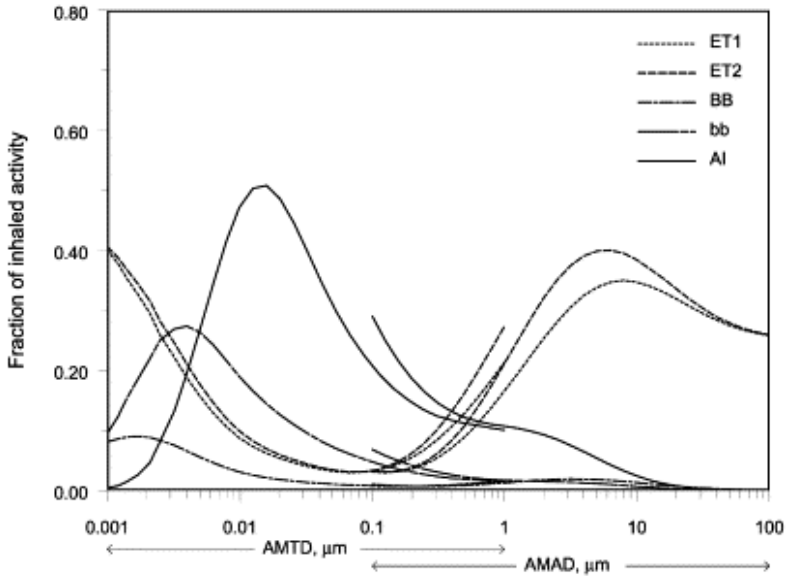

Figure 1.12: Deposition in regions of the HRTM for a standard worker as a function of aerosol median size (ICRP, 1994a)

Table 1.5: Fractional deposition in regions of the respiratory tract for reference worker normal nose breather with an AMAD of 5 μm (ICRP, 1994a)

Respiratory tract region	Fractional deposition
ET1	3.4×10^{-1}
ET2	4.0×10^{-1}
BB	1.8×10^{-2}
bb	1.1×10^{-2}
AI	5.3×10^{-2}
Total	8.2×10^{-1}

Clearance

Clearance is due to the mucociliary transport of the deposited particles up to the alimentary tract in competition with transport to the regional lymph nodes and absorption into blood (Fig. 1.13).

Mechanical particle transport rates are determined by ongoing biological processes, such as the flow of fluids over airway surfaces, which are generally unaffected by the deposited material. Particle transport rates are therefore assumed to be the same for all materials (Fig. 1.14).

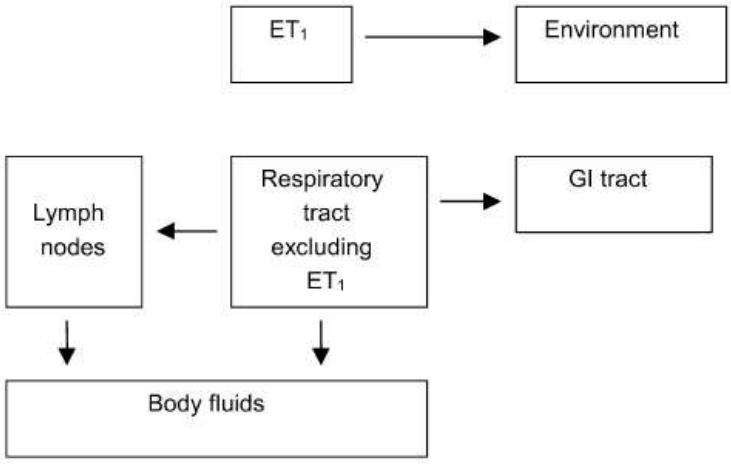

Figure 1.13: Routes of clearance from the respiratory tract (ICRP, 2002a)

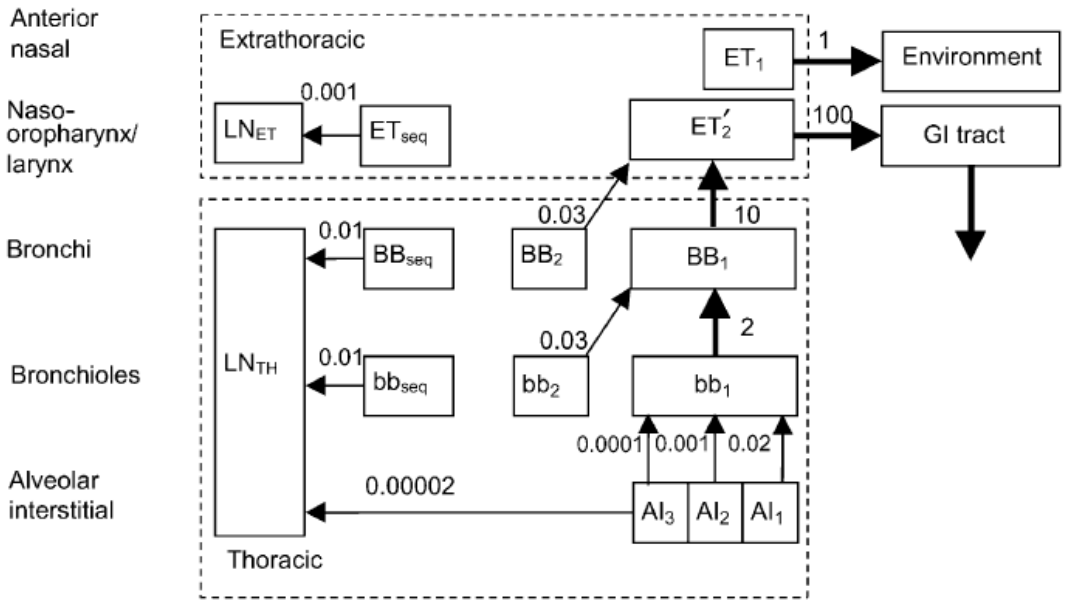

Figure 1.14: Compartmental model representing time-dependent particle transport from regions of the respiratory tract and transfer rates (d^{-1})(ICRP, 1994a)

Absorption is assumed to take place at the same rate throughout the respiration tract and to depend on the physical and chemical form of the deposited material. It is a two-stage process: dissociation of material that can be absorbed into blood (dissolution); and uptake into blood.

Dissolution may be modelled by three parameters: a fraction f_r of the activity is rapidly dissolved at a rate s_r, the remaining fraction (1 – f_r) is dissolved at a slower rate s_s (Fig. 1.15).

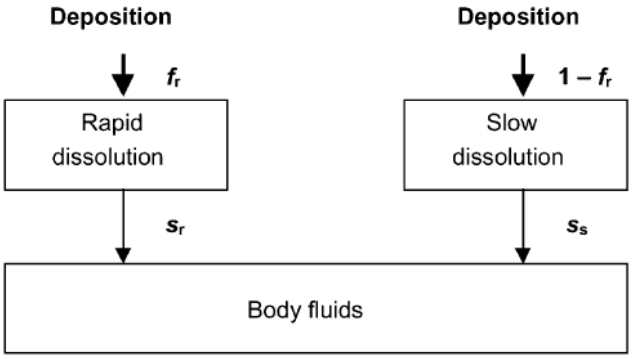

Figure 1.15: First compartment model representing time-dependent dissolution, followed by instantaneous uptake to body fluids (ICRP, 2002a)

A limitation of the system in Fig. 1.15, however, is that it can only readily represent an overall fractional dissolution rate that decreases with time. To overcome this, the HRTM uses an equivalent system with the same number of variables, but which gives greater flexibility, shown in Fig. 1.16. In this, the material deposited in the respiratory tract is assigned to compartments labelled 'Particles in initial state' in which it dissolves at a constant rate s_p. Material is simultaneously transferred (at a constant rate s_{pt}) to a corresponding compartment labelled 'Particles in transformed state' in which it has a different dissolution rate, s_t. With this system, the initial dissolution rate is approximately s_p and the final dissolution rate is approximately s_t. Thus with suitable choice of parameters, including $s_t > s_p$, an increasing dissolution rate can be represented. The ratio of s_p to s_{pt} approximates to the fraction that dissolves rapidly.

If the dissolution rate decreases with time, as is usually the case, either system could be used, and would give the same results, with the following values:

$$s_p = s_s + f_r(s_r - s_s), \qquad \text{Equation 1.14}$$

$$s_{pt} = (1 - f_r)(s_r - s_s), \qquad \text{Equation 1.15}$$

$$s_t = s_s. \qquad \text{Equation 1.16}$$

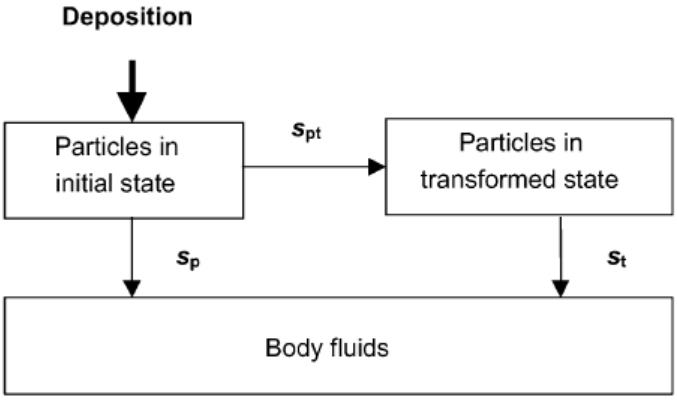

Figure 1.16: Second compartment model representing time-dependent dissolution, followed by instantaneous uptake to body fluids (ICRP, 2002a)

In many circumstances the system in Fig. 1.15 has advantages. In particular, it is generally more straightforward to estimate from experimental data the values of the parameters in Fig. 1.15 than those of Fig. 1.16

The ICRP recommends default values of these parameters for reference absorption types : Type F (fast), corresponds to rapid absorption of the radionuclide with a half-time of about 10 min (f_r = 1, s_r = 100 d^{-1}); for Type M (moderate), 10 % of the activity is absorbed with a half-time of 10 min and 90 % with a half-time of 140 d (f_r = 0.1, s_r = 100 d^{-1} and s_s = 0.005 d^{-1}); for Type S (slow), 0.1 % is absorbed with a half-time of 10 min and 99.9 % with a half-time of 7000 d (f_r = 0.001, s_r = 100 d^{-1}, s_s = 0.0001 d^{-1}) (ICRP, 1994a). In the absence of more specific information, one of the reference types can be chosen according to the chemical form of the radionuclide. For example, insoluble oxides of Pu are commonly associated with Type S (ICRP, 1994b).

Uptake of dissolved material into blood is usually treated as instantaneous. In some situations, however, a significant fraction of the dissolved material may be bound to airway tissues and slowly absorbed into blood. The HRTM therefore allows for a bound fraction f_b of dissolved activity to be retained in each region. However, f_b is set to zero for reference absorption types.

1.5.2 Gastro-Intestinal Tract Model

Material may reach the gastrointestinal tract (GIT) either directly by ingestion or indirectly by transfer from the respiratory tract or from systemic circulation, mostly through the liver. The Gastro-Intestinal Tract Model (GITM) of ICRP (ICRP, 1979) consists of four sections (Fig. 1.17) to predict faecal excretion, absorption into blood and number of nuclear transformations of radionuclides. The transfer rates between sections are gathered in Table 1.6. The small intestine (SI) is assumed to be the only site of absorption from gastro-intestinal tract to blood in the absence of radioactive decay or endogenous input to the tract. The absorption is quantified by the fraction f_1 of activity reaching blood following entry in the GIT. The transfer rate from the small intestine to body fluids, λ_B, is calculated by:

$$\lambda_B = \frac{f_1 \lambda_{SI}}{1 - f_1}, \qquad \text{Equation 1.17}$$

with λ_{SI}, the transfer rate from the small intestine to the upper large intestine, if f_1 is not equal to 1. The value of f_1 is specific to the radionuclide and its chemical form (Table 1.7).

Table 1.6: GITM parameters and transfer rate (ICRP, 1979)

Section of GITM	Mean residence time (day)	λ (d^{-1})
Stomach (ST)	1/24	24
Small Intestine (SI)	4/24	6
Upper Large Intestine (ULI)	13/24	1.8
Lower Large Intestine (LLI)	24/24	1

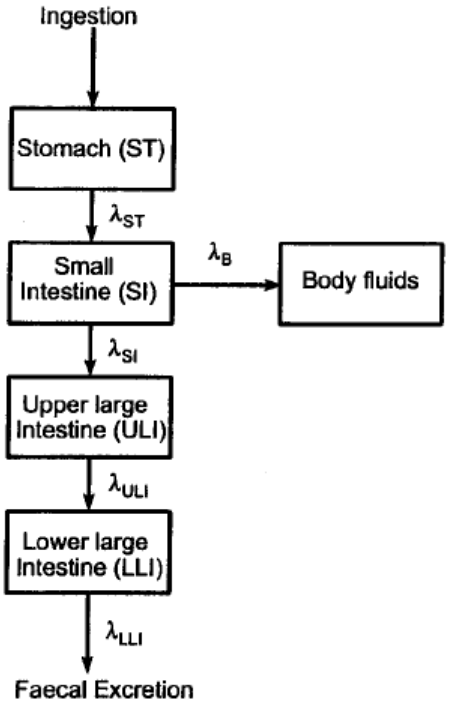

Figure 1.17: Structure of the GITM (ICRP, 1979)

Table 1.7: f_1 values for plutonium and uranium compounds (ICRP, 1997b)

Intake	f_1	Compounds
Ingestion	5.0×10^{-4}	Pu unspecified compounds
Ingestion	1.0×10^{-4}	Pu nitrates
Ingestion	1.0×10^{-5}	Pu insoluble oxides
Inhalation, Type M	5.0×10^{-4}	Pu unspecified compounds
Inhalation, Type S	1.0×10^{-5}	Pu insoluble oxides
Ingestion	0.02	U unspecified compounds
Ingestion	0.002	U most tetravalent compounds, *e.g.* UO_2, U_3O_8, UF_4
Inhalation, Type F	0.02	U soluble compounds including hexavalent compounds, *e.g.* UF_6, UO_2F_2, $UO_2(NO_3)_2$
Inhalation, Type M	0.02	U less soluble compounds, e.g. UO_3, UF_4, UCl_4, and most other hexavalent compounds
Inhalation, Type S	0.002	U highly insoluble compounds, e.g. UO_2, and U_3O_8

1.5.3 Human Alimentary Tract Model

The GITM was replaced by the Human Alimentary Tract Model (HATM) (ICRP, 2006; Fig. 1.18). In the HATM, some local retention and absorption to blood may occur in the mouth, stomach, colon and small intestine. The total fractional absorption in the alimentary tract is quantified by f_A. The transfer rates for alimentary transit depend on the age, diet and sex (Table 1.8).

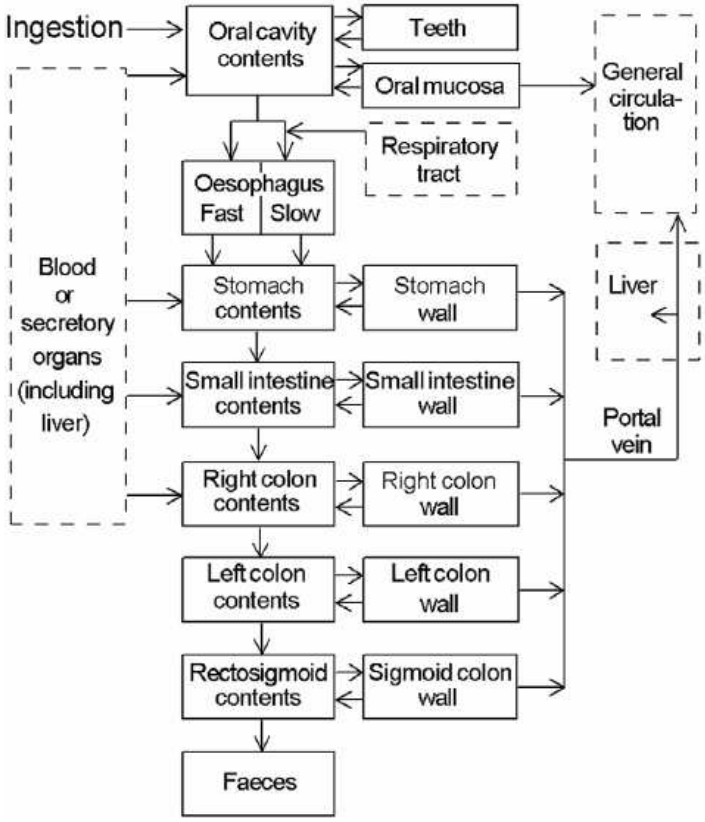

Figure 1.18: Structure of the HATM .The dashed boxes show connections with the other models (ICRP, 2006)

Table 1.8: Transfer rates (d^{-1}) for the movement of alimentary tract contents in HATM (ICRP, 2006)

Region	Adult male	Adult female
Mouth		
Solids	5,760	5,760
Liquids	43,200	43,200
Total Diet	7,200	7,200
Oesophagus (fast)		
Solids	10,800	10,800
Liquids	17,280	17,280
Total diet	12,343	12,343
Oesophagus (slow)		
Solids	1,920	1,920
Liquids	2,880	2,880
Total diet	2,160	2,160

Region	Adult male	Adult female
Stomach		
Solids	19.2	13.71
Caloric liquids	32	24
Non-caloric liquids	48	48
Total diet	20.57	15.16
Small intestine	6	6
Right colon	2	1.5
Left colon	2	1.5
Rectosigmoid	2	1.5

1.5.4 Wound Model

A biokinetic model for radionuclide-contaminated wounds was developed by the US National Council on Radiological Protection and Measurements (NCRP) (NCRP, 2006). The NCRP wound model (Fig. 1.19, Table 1.9) consists of seven compartments describing metabolic states of activity retained within the wound site and clearance to blood and lymph-nodes.

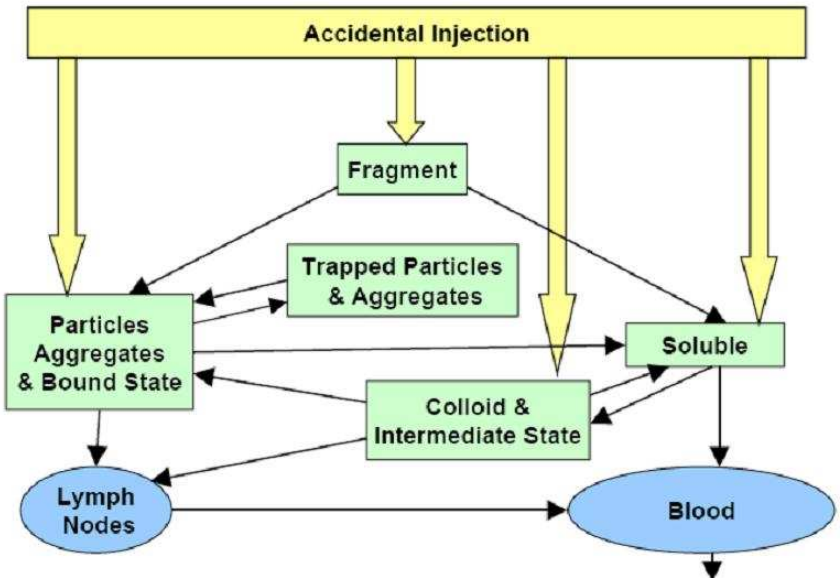

Figure 1.19: NCRP wound model (NCRP, 2006)

Table 1.9: Default transfer rates of the wound model for the reference categories of radionuclides in wounds. CIS: Colloid and Intermediate State; PABS: Particle, Aggregates and Bound State; TPA: Trapped Particles and Aggregates (NCRP, 2006).

Transfer	Transfer rate (d^{-1})						
	Radionuclides initially in Solution				Colloids (injection to CIS)	Particles (injection to PABS)	Fragments (injection to fragment)
	Weak	Moderate	Strong	Avid			
Soluble to blood	45	45	0.67	7.0	0.5	100	–
Soluble to CIS	20	30	0.6	30	2.5	–	–
CIS to blood	2.8	0.4	2.4×10^{-2}	3×10^{-2}	2.5×10^{-2}	–	–
CIS to PABS	0.25	6.5×10^{-2}	1.0×10^{-2}	10	5×10^{-2}	–	–
CIS to lymph nodes	2×10^{-5}	2×10^{-5}	2×10^{-5}	2×10^{-5}	2×10^{-3}	–	–
PABS to soluble	8×10^{-2}	2×10^{-2}	1.2×10^{-3}	5×10^{-3}	1.5×10^{-3}	2×10^{-4}	0.0
PABS to lymph nodes	2×10^{-5}	2×10^{-5}	2×10^{-5}	2×10^{-5}	4×10^{-4}	3.6×10^{-3}	4×10^{-3}
PABS to TPA	–	–	–	–	–	4×10^{-2}	0.7
TPA to PABS	–	–	–	–	–	3.6×10^{-3}	5×10^{-4}
Lymph nodes to blood	–	–	–	–	3×10^{-2}	6×10^{-4}	3×10^{-2}
Fragment to soluble	–	–	–	–	–	–	0.0
Fragment to PABS	–	–	–	–	–	–	8×10^{-3}

Repartition between the compartments, retention at the wound site and transfer to the lymph nodes depends on the physical (solution, colloid, particles, fragment) and chemical form of the compounds. Four default categories for soluble compounds are defined: weak, moderate, strong and avid in which radionuclides may be grouped roughly according to their tendencies for hydrolysis or forming stable complexes with biological ligands at neutral pH. Insoluble compounds are retained much longer at the wound site, with significant transfer of particles to the lymph nodes and tissue reaction around fragments. The model allows the estimation of retention of radionuclide at the wound site and its uptake into blood as a function of time.

1.5.5 Systemic models

A Systemic model describes the behaviour of a radionuclide following its uptake to blood. Systemic circulation distributes the radionuclide in different body tissues where it can be retained for a period depending on the element. Fig. 1.20 and 1.21 present the structures of ICRP biokinetic models for uranium and plutonium, with associated transfer rates in tables 1.10 and 1.11. Their main target organs are skeleton and liver. Plutonium is strongly retained in the skeleton and very slowly excreted.

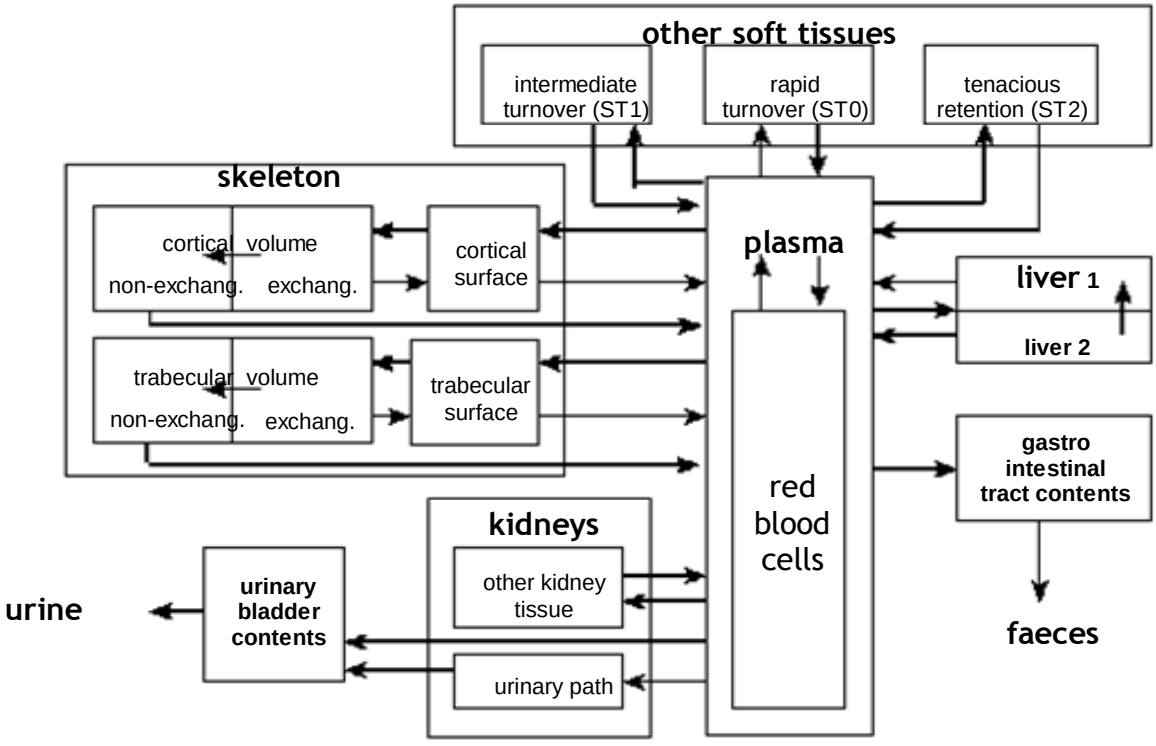

Figure 1.20: Structure of the biokinetic model for strontium, radium and uranium (ICRP, 1995a)

Table 1.10: Transfer rates (d^{-1}) for uranium model (ICRP, 1995a)

Transfer	Adult	Transfer	Adult
Plasma to ST0	1.050×10^{1}	Other kidney tissue to Plasma	3.800×10^{-4}
Plasma to RBC	2.450×10^{-1}	Liver 1 to Plasma	9.200×10^{-2}
Plasma to Urinary bladder	1.543×10^{1}	Liver 2 to Plasma	1.900×10^{-4}
Plasma to Urinary path	2.940	ST1 to Plasma	3.470×10^{-2}
Plasma to Other kidney tissue	1.220×10^{-2}	ST2 to Plasma	1.900×10^{-5}
Plasma to ULI contents	1.220×10^{-1}	Bone surfaces to Plasma	6.930×10^{-2}
Plasma to Liver 1	3.670×10^{-1}	Nonexch trab. vol. to Plasma	4.930×10^{-4}
Plasma to ST1	1.630	Nonexch cort. vol. to Plasma	8.210×10^{-5}
Plasma to ST2	7.350×10^{-2}	Urinary path to Urinary bladder	9.900×10^{-2}
Plasma to Trabecular surfaces	2.040	Liver 1 to Liver 2	6.930×10^{-3}
Plasma to Cortical surfaces	1.630	Bone surfaces to Exch. volume	6.930×10^{-2}
ST0 to Plasma	8.320	Exch. bone vol. to Bone surfaces	1.730×10^{-2}
RBC to Plasma	3.470×10^{-1}	Exch. bone vol. to Nonexch vol.	5.780×10^{-3}

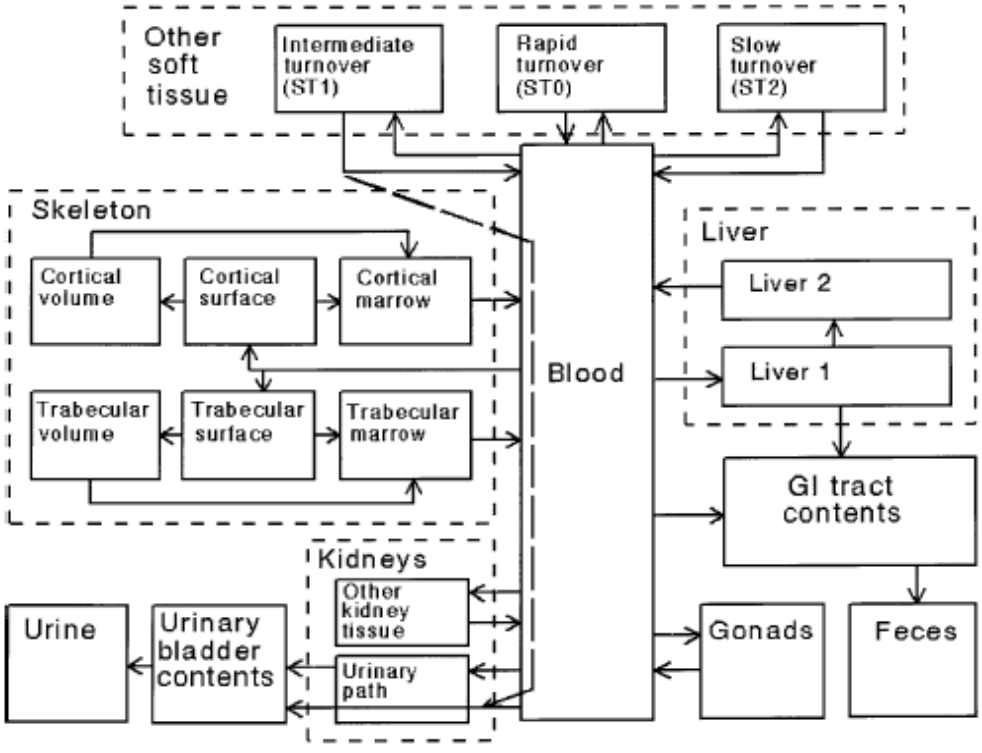

Figure 1.21: Structure of the biokinetic model plutonium (ICRP, 1993)

Table 1.11: Transfer rates (d^{-1}) for plutonium model (ICRP, 1993)

Transfer	Adult	Transfer	Adult
Blood to Liver 1	1.941×10^{-1}	ST1 to Blood	4.75×10^{-4}
Blood to Cortical surface	1.294×10^{-1}	ST1 to Urinary bladder contents	4.75×10^{-4}
Blood to Trabecular surface	1.941×10^{-1}	ST2 to Blood	1.9×10^{-5}
Blood to Urinary bladder content	1.29×10^{-2}	Trabecular surface to Volume	2.47×10^{-4}
Blood to Kidney (urinary path)	6.47×10^{-3}	Trabecular surface to Marrow	4.93×10^{-4}
Blood to Other kidney tissue	3.23×10^{-3}	Cortical surface to Volume	4.11×10^{-5}
Blood to ULI contents	1.29×10^{-2}	Cortical surface to Marrow	8.21×10^{-5}
Blood to testes	2.3×10^{-4}	Trabecular volume to Marrow	4.93×10^{-4}
Blood to ovaries	7.1×10^{-5}	Cortical volume to Marrow	8.21×10^{-5}
Blood to ST0	2.773×10^{-1}	Cort/Trab marrow to Blood	7.6×10^{-3}
Blood to ST1	8.06×10^{-2}	Liver 1 to Liver 2	1.77×10^{-3}
Blood to ST2	1.29×10^{-2}	Liver 1 to Small intestine	1.33×10^{-4}
ST0 to Blood	6.93×10^{-1}	Liver 2 to Blood	2.11×10^{-4}
Kidneys (urinary path) to Bladder	1.386×10^{-2}	Gonads to Blood	1.9×10^{-4}
Other kidney tissue to Blood	1.39×10^{-3}		

In the ICRP plutonium model, a portion of ST1 activity is directly excreted into urine. Luciani and Polig judged it to lack physiological justification (Luciani and Polig, 2000). They propose a modified plutonium model avoiding this direct excretion pathway and including a different representation of skeletal kinetics (Fig. 1.22 and Table 1.12).

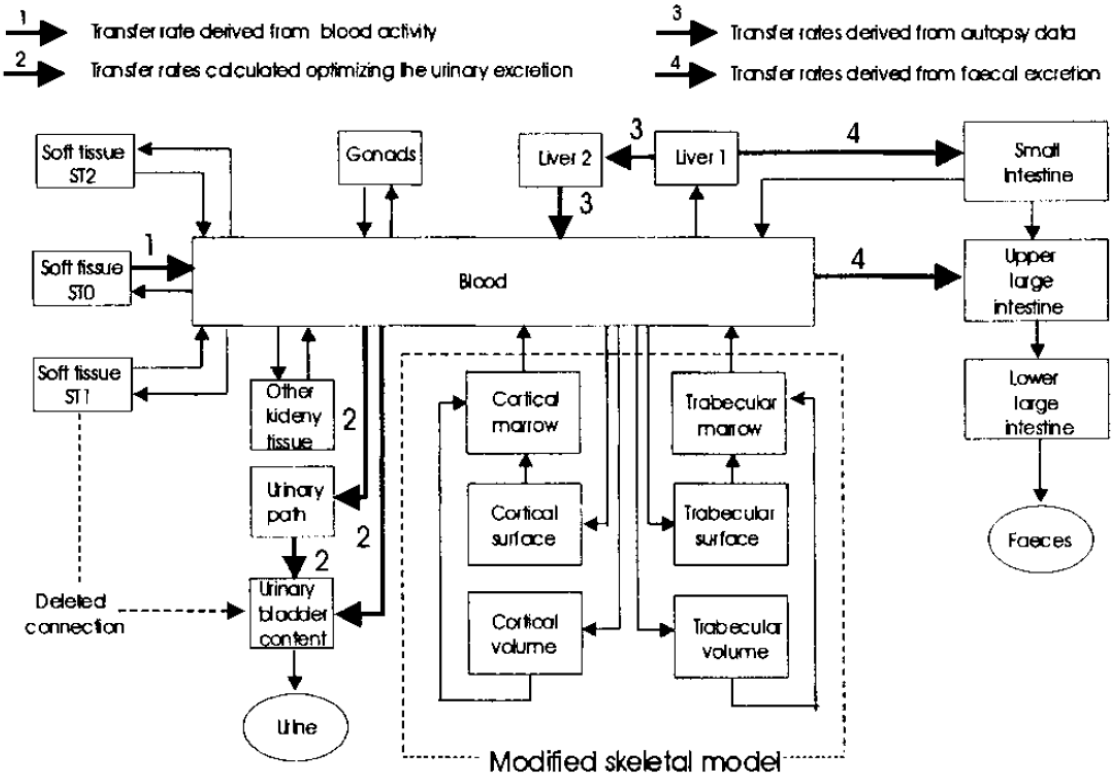

Figure 1.22: Plutonium model proposed by Luciani and Polig (2000)

Table 1.12: Transfer rates (d^{-1}) for Luciani and Polig proposed plutonium model (Luciani and Polig, 2000). Differences with ICRP model are highlighted in bold.

Transfer	Transfer rates (d^{-1})	Transfer	Transfer rates (d^{-1})
Blood to Liver 1	**1.20×10^{-1}**	Urinary bladder content to excretion	12
Blood to Cortical surface	**9.52×10^{-2}**	Other kidney tissue to Blood	1.39×10^{-3}
Blood to Trabecular surface	**2.26×10^{-1}**	ST1 to Blood	**9.50×10^{-4}**
Blood to Cortical volume	**4.48×10^{-3}**	ST1 to Urinary bladder content	**Deleted**
Blood to Trabecular volume	**7.16×10^{-2}**	ST2 to Blood	1.9×10^{-5}
Blood to Urinary bladder content	**9.46×10^{-3}**	Trabecular surface to Marrow	**1.59×10^{-3}**
Blood to Urinary path	**9.92×10^{-3}**	Trabecular volume to Marrow	**1.59×10^{-3}**
Blood to Other kidney tissue	3.23×10^{-3}	Cortical surface to Marrow	**1.56×10^{-4}**
Blood to ULI contents	**8.0×10^{-2}**	Cortical volume to Marrow	**8.22×10^{-5}**
Blood to testes	2.3×10^{-4}	Cortical marrow to Blood	**7.6×10^{-3}**
Blood to ST0	**2.773×10^{-1}**	Trabecular marrow to Blood	**7.6×10^{-3}**
Blood to ST1	**8.06×10^{-2}**	Liver 1 to Liver 2	**1.0×10^{-2}**
Blood to ST2	**1.29×10^{-2}**	Liver 1 to Small intestine	**4.0×10^{-4}**
ST0 to Blood	**1.39×10^{-1}**	Liver 2 to Blood	**4.0×10^{-4}**
Urinary path to Urinary bladder content	**1.02×10^{-2}**	Gonads to Blood	1.9×10^{-4}

From recent plutonium injection studies and follow-up of Mayak plutonium workers, Leggett and others developed an improved systemic model (Leggett *et al*, 2005) (Fig. 1.23). The proposed model contains separate blood compartments for uptake and recycling of activity and a third liver compartment, resulting in increased early and intermediate retention in liver. The transfer rates are shown in Table 1.13.

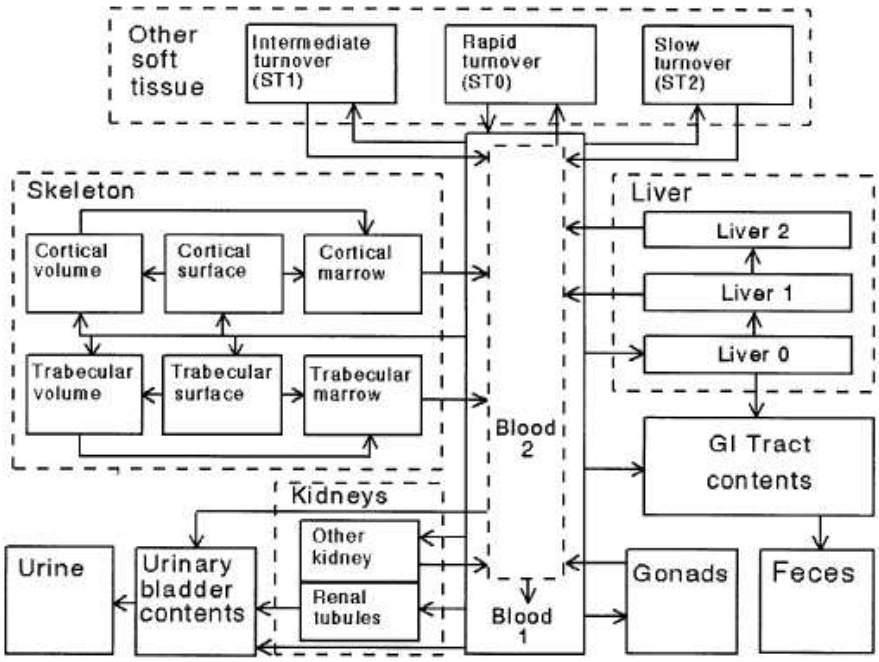

Figure 1.23: Plutonium model proposed by Leggett *et al* (2005)

Table 1.13: Transfer rates (d^{-1}) for Leggett et al proposed plutonium model (Leggett *et al*, 2005).

Transfer	Transfer rate (d^{-1})	Transfer	Transfer rate (d^{-1})
Blood 1 to Liver 0	4.6200×10^{-1}	Other kidney tissue to Blood 2	1.2660×10^{-4}
Blood 1 to Cortical surface	8.7780×10^{-2}	ST1 to Blood 2	1.3860×10^{-3}
Blood 1 to Cortical volume	4.6200×10^{-3}	ST2 to Blood 2	1.2660×10^{-4}
Blood 1 to Trabecular surface	1.2474×10^{-1}	Liver 0 to Small intestine	9.2420×10^{-4}
Blood 1 to Trabecular volume	1.3860×10^{-2}	Liver 0 to Liver 1	4.5286×10^{-2}
Blood 1 to Urinary bladder contents	1.5400×10^{-2}	Liver 1 to Blood 2	1.5200×10^{-3}
Blood 1 to Renal tubules	7.7000×10^{-3}	Liver 1 to Liver 2	3.8000×10^{-4}
Blood 1 to Other kidney tissue	3.8500×10^{-4}	Liver 2 to Blood 2	1.2660×10^{-4}
Blood 1 to ULI contents	1.1550×10^{-2}	Testes to Blood 2	3.8000×10^{-4}
Blood 1 to Testes	2.6950×10^{-4}	Ovaries to Blood 2	3.8000×10^{-4}
Blood 1 to Ovaries	8.4700×10^{-5}	Cortical surface to Cortical marrow	8.2100×10^{-5}
Blood 1 to ST1	1.8511×10^{-2}	Cortical surface to Cortical volume	2.0500×10^{-5}
Blood 1 to ST2	2.3100×10^{-2}	Cortical volume to Cortical marrow	8.2100×10^{-5}
ST0 to Blood 1	9.9000×10^{-2}	Trabecular surface to Trabecular marrow	4.9300×10^{-4}
Blood 2 to Urinary bladder contents	3.5000×10^{0}	Trabecular surface to Trabecular volume	1.2300×10^{-4}
Blood 2 to Blood 1	6.7550×10^{1}	Trabecular volume to Trabecular marrow	4.9300×10^{-4}
Blood 2 to ST0	2.8950×10^{1}	Cortical marrow to Blood 2	7.6000×10^{-3}
Renal Tubules to Urinary bladder contents	1.7329×10^{-2}	Trabecular marrow to Blood 2	7.6000×10^{-3}

1.5.6 Dosimetric models

In order to assess effective dose, absorbed doses in tissues are calculated by dosimetric models. The absorbed dose $D_{r_T,R}$ in the target region r_T due to radiation type *R*, is calculated as:

$$D_{r_T,R} = \sum_{r_S} \tilde{A}(r_S, T_D) S(r_T \leftarrow r_S) \text{ (Bolch } \textit{et al}\text{, 2009),} \qquad \text{Equation 1.18}$$

where $\tilde{A}(r_S, T_D)$ is the time-integrated activity (or total number of nuclear transformations) in the source region r_S over commitment period T_D and $S(r_T \leftarrow r_S)$, the radionuclide-specific quantity representing the mean absorbed dose due radiations of type R to r_T per nuclear transformation in r_S. $\tilde{A}(r_S, T_D)$ is calculated by integrating over T_D the activity in r_S predicted by the biokinetic models. $S(r_T \leftarrow r_S)$ is evaluated by:

$$S(r_T \leftarrow r_S) = \frac{1}{M(r_T)} \sum_i E_{R,i} Y_{R,i} \phi(r_T \leftarrow r_S, E_{R,i})$$ (Bolch *et al*, 2009), Equation 1.19

where $E_{R,i}$ and $Y_{R,i}$ are the energy and yield, respectively, of the i[th] radiation of type R (ICRP, 2008), $\phi(r_T \leftarrow r_S, E_{R,i})$ is the absorbed fraction, $M(r_T)$ is the mass of r_T in the reference individual. The absorbed fraction is the fraction of energy $E_{R,i}$ emitted within r_S that is deposited in r_T. For penetrating radiations, it is calculated by applying Monte-Carlo codes of radiation transport to anthropomorphic computational phantoms representing reference individuals whose parameters organ sizes and densities are mean or median values of the adult population (ICRP, 2002b). The current dose coefficients of ICRP publication 68 (ICRP, 1994b) and French regulation (arrêté du 1er septembre 2003) are based on stylized phantoms described by mathematical equations (Cristy and Eckerman, 1987). These are now replaced by voxel phantoms based on medical images of real persons (ICRP, 2009, Fig. 1.24).

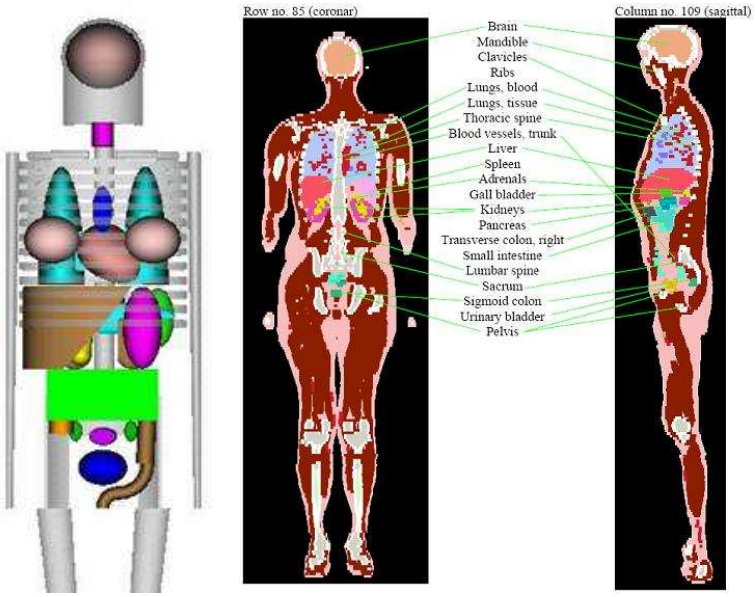

Figure 1.24: Left, front view of ORNL mathematical phantom (Cristy and Eckerman, 1987), right, coronar and sagittal slices of ICRP reference male computational phantom (ICRP, 2009).

For non-penetrating radiations (α, β), the absorbed fraction is either 0 for $r_T \neq r_S$ or 1 for $r_T = r_S$ when the radiosensitive cells are not specifically identified in r_T. In the skeleton (ICRP, 1995b) and walls of the gut (ICRP, 2006) and airways (ICRP, 1994a), the absorbed fraction is evaluated on the basis on the energy deposited in the radiosensitive target cells.

1.5.7 Uncertainty in models

Uncertainty in biokinetic models may arise because the model structure provides an oversimplified representation of the known processes, because unknown processes have been omitted from the model, or because part or all of the model formulation is based on mathematical

convenience rather than consideration of processes (Leggett, 2001). As it was presented for plutonium (Leggett, 2003), different mathematical modelling can agree with observed data.

The main source of uncertainty in models is the reliability of observed data. If the biokinetic model is constructed from direct human data, uncertainties in model predictions arise from limitations in the quality, completeness, and relevance of the data. In most cases, study groups are small and large inter-subject variability in the biokinetics of an element is observed. During the short observation periods, large intra-subject variability is possible (Table 1.14). The use of unhealthy subjects whose diseases may alter the biokinetics of the element and the paucity of observations for women and children induce difficulties to interpret data. The collection of small potentially non-representative samples of tissue and inaccuracies in measurement techniques introduce measurement uncertainty. Sometimes, the exposure conditions such as the pattern or level of intake of the element are not well controlled. Finally, data may be used despite atypical study conditions and inconsistency in reported values.

For biokinetic model constructed from observations of the behaviour of chemically similar elements in human subjects or from observations in non-human species, uncertainties associated with inter-species or inter-element extrapolation of that data must be added (Leggett, 2001).

In addition to the reliability of the reference biokinetic model, the inter-individual variability should be considered when comparing the prediction of the model with the bioassay data from a given individual (Table 1.14).

Table 1.14: Examples of variability of biokinetics of radionuclides in adult humans (Leggett, 2001)

Study	n	Geometric mean (%)	Geometric SD	Observed maximum (%)
Reeve and Hesp (1976), Whole-body ^{45}Ca retention in osteoporotic patients on day 15 post injection	8	63 %	1.2	85 %
Likhtarev *et al* (1975), ^{85}Sr, young adult males:				
Whole-body retention, 50 d post injection	7	25 %	1.4	38 %
Whole-body retention, 50 d post ingestion	8	5.0 %	1.6	10 %
Urinary excretion, 4 d post injection	5	1.7 %	1.2	2.3 %
Urinary excretion, 4 d post ingestion	9	0.41 %	1.6	0.57 %
Newton *et al* (1991), ^{133}Ba, adult males:				
Whole-body retention, 50 d post injection	6	7.8 %	1.4	12 %
Whole-body retention, 200 d post injection	6	5.6 %	1.4	8.9 %
Whole-body retention, 500 d post injection	6	4.4 %	1.4	7.0 %
Urinary excretion on d 1 post injection	6	5.5 %	1.3	8.2 %
Urinary excretion on d 5 post injection	6	0.17 %	1.9	0.51 %
Urinary excretion on d 14 post injection	6	0.03 %	2.0	0.10 %

ICRP Publication 20 (1973), Whole-body retention of ^{226}Ra in Elgin patients:				
Ages 17-23 y, 30 d post injection	7	8.0 %	1.4	14 %
Ages 17-23 y, 4-7 mo post injection	6	3.1 %	1.5	5.4 %
Ages 24-63 y, 4-7 mo post injection	14	3.5 %	1.8	10 %
Maletskos *et al* (1966), Whole-body retention of ^{224}Ra in subjects aged 63-83 y:				
9-10 d post injection	6	22 %	1.2	28 %
20 d post injection	5	15 %	1.3	21 %
Hursh *et al* (1969), Retention of ^{212}Pb in red blood cells of adults:				
1 d after end of inhalation	10	46 %	1.2	57 %
3 d after end of inhalation	5	46 %	1.3	60 %
Heard and Chamberlain (1984), Retention of ^{203}Pb in feet of adults:				
1 d post injection	4	1.2 %	1.3	1.7 %
4 d post injection	4	1.1 %	1.5	1.8 %
10 d post injection	4	1.4 %	1.5	2.4 %
Hursh and Spoor (1973), whole-body retention in unhealthy subjects receiving uranium by injection:				
1 d post injection	23	37 %	1.6	84 %
3 d post injection	14	31 %	1.7	77 %
6 d post injection	9	31 %	1.7	76 %

The dosimetric models are based on sound principles of radiation transport but involve simplified anatomical structures and geometric considerations that also introduce uncertainty into dose estimates. Notably, the assumption of homogeneous distributions of radionuclides, target cells and dose within most tissues may be oversimplifying. Moreover, the reference individual of the ICRP (ICRP, 2002b) has mean anatomical parameters which can be very different from the parameters of a specific individual. The NRCP (1998) considers that the uncertainties in the dosimetric models are associated with:

- incomplete information on masses, compositions, shapes and locations of the organs and tissue of the human body,
- limitations in the physical data (e.g. energy and intensity of radiations emitted by the radionuclides, photon interaction coefficients; etc.),

- limitations in computational procedures for evaluating the energy deposition of penetrating radiations,
- oversimplifications of the representations of certain complex anatomical structures in the body when calculating the energy deposition.

It evaluated the uncertainties associated with items 2 and 3 to be typically less than 20 % assuming proper application of the available data and computational methods. The uncertainties related to items 1 and 4 are typically an order-of-magnitude, although for some combination of organs and radionuclides they might be higher (NCRP, 1998). However, since 1998, the new voxel reference phantoms (ICRP, 2009) have reduced the uncertainties from items 1 and 4.

In the calculation of equivalent and effective dose, radiation weighting factors w_R result from expert judgment on relative biological effect of radiation which is often difficult to assess from available human and animal data, while the extrapolation from *in vitro* experiments to human cancer may be questionable. Similarly, tissue weighting factors w_T involve a strong simplification of the epidemiological information relative to the contribution from each type of cancer and hereditary diseases to the global detriment (ICRP, 2007).

1.6 Internal dose calculation

1.6.1 Principle

In order to quantify the exposure of workers, the measurement of retained or excreted activity must be interpreted in terms of committed effective dose using biokinetic and dosimetric models. Practically, the dose is assessed in two steps:

1) the intake *i* is estimated by dividing the value of activity *M* measured *t* days after incorporation by the retention or excretion function at *t*, *m(t)*, prediction of the biokinetic models of the measured parameter (body content, organ content or daily excretion) for a unit intake. For *in vitro* measurements, the measured activity may sometimes be converted into activity daily excreted which is the predicted quantity;

2) the committed effective dose *E* is calculated by multiplying the intake by the dose coefficient e_{50}:

$$i = \frac{M}{m(t)} \qquad E = i \times e_{50}\,. \qquad \text{Equations 1.20 and 1.21}$$

If multiple measurements are available, a best estimate of intake may be obtained by applying a statistical fitting method. The dose coefficient is the committed effective dose received by the reference man for a unit intake. The retention and excretion functions and the dose coefficient depend on:

- radionuclide(s),
- isotopic composition,
- intake time(s),
- intake route(s): inhalation, ingestion, wound,

- physico-chemical properties of the radioactive material: absorption type, AMAD for an aerosol.

1.6.2 Reference values

Individual parameter values assumed in the dose calculation are, in general, unknown and often difficult to assess. The ICRP therefore recommends the use of default values for such parameters which represent the mean of published values.

In the absence of specific information, the individual is represented by the reference man of the ICRP (ICRP, 1975, 2002b); a worker has an occupational activity 8 hours a day, with a breathing rate of 1.2 $m^3.h^{-1}$ (ICRP, 1994a); the pulmonary absorption of the material is either type F, M, or S (ICPR, 1994b); the absorption from the gut is quantified by a proposed value of f_1 or f_A (ICRP, 1979, 2006); the AMAD of a radioactive aerosol is 5 µm for workers with a geometric standard deviation of 2.5 and a density of 3 $g.cm^{-3}$ (ICRP, 1994a); in routine monitoring, the intake is assumed to have occurred at the middle of the monitoring interval (ICRP, 1997b).

1.6.3 Tools

The corresponding retention and excretion functions are available in ICRP publication 78 (ICRP, 1997b) and on the website of the Japanese National Institute of Radiological Sciences (Ishigure *et al*, 2003). Dose coefficients are tabulated in publications 68 (ICRP, 1994b) and 78 (ICRP, 1997b) for workers and gathered in a CD-ROM (ICRP, 1998). These coefficients are integrated in the French regulation (Arreté du 1er septembre 2003).

The calculation of retention and excretion functions and of dose coefficients with specific parameter values requires dedicated software such as LUDEP (HPA, UK, Birchall *et al*, 1991), IMBA (HPA, UK, Birchall *et al*, 2007), IMIE (RPI, Ukraine, Berkovski *et al*, 2007), MONDAL2 (NIRS, Japan, Ishigure *et al*, 2004), MMK-01 (FMBC, Russia, Molokanov *et al*, 2003), AIDE (http://aidesoftware.com/), DCAL (Eckerman *et al*, 2006) or CYCLOMOD (IRSN, France, Malarbet, 1998). IMBA, IMIE, MMK-01 and AIDE also include algorithms to adjust the parameter values to the bioassay data.

1.6.4 IDEAS project

The third European intercomparison exercise on internal dose assessment (Doerfel *et al*, 2000) proposed seven contamination cases, covering different scenarios of intake of ^{3}H, ^{90}Sr, ^{125}I, ^{137}Cs, ^{210}Po, ^{238}U and ^{239}Pu and all monitoring techniques. On average, there were 35 responses per case, providing a good overview of the state of the art of internal dosimetry. The results in terms of intake and committed effective dose appeared to be log-normally distributed with geometric

standard deviations ranging from 1.15 for the cases dealing with ^{3}H and ^{137}Cs, up to 2.4 for the case dealing with ^{239}Pu. These figures reflect large differences in individual results which varied in the worst case over five orders of magnitude. Several reasons for the differences in the results were identified, including numerical errors but also different assumptions about the pattern of intake and the choice of model. The IDEAS project proposed guidelines based on three principles to limit such differences in dose calculation (Doerfel *et al*, 2006):

- harmonisation: by following the guidelines any two assessors should obtain the same estimate of dose from a given data set,
- accuracy: the best estimate of dose should be obtained from the available data,
- proportionality: the effort applied to the evaluation should be proportionate to the dose – the lower the dose, the simpler the process.

Consistently, four levels of task were proposed:

- Level 0: Annual dose <0.1 mSv. No evaluation of dose needed.
- Level 1: Annual dose typically 0.1 to 1 mSv. Simple, reference evaluation with ICRP defaults used for all parameter values, except where there is better *a priori* information available.
- Level 2: Annual dose typically 1 to 6 mSv. Sophisticated evaluation using additional information to give more realistic assessment of dose: typically a special assessment of an accidental intake. Comparisons are made of the model predictions with the data, to choose between alternative parameter values, or to find optimum parameter values. At this level, the parameters adjusted typically relate to the material (for inhalation intakes the AMAD and absorption Type), and the time of intake if unknown.
- Level 3: Annual dose typically > 6 mSv. More sophisticated evaluation which applies to cases where there are comprehensive data available, as would be the situation after an accident. The evaluation is an extension of level 2, typically to parameters relating to the subject. The fundamental approach at this level is to adjust the model parameter values systematically, in a specific order, until the model prediction is consistent with the data.

The consistency of the model with the data is judged at each step by a chi-squared test: If M_i for $i=1,\ldots, n$ are the n bioassay data measured at time t_i after intake I, $m(t_i)$ the corresponding predictions of the l parameters biokinetic model for a 1 Bq intake and SF_i the scattering factor associated with M_i, the chi-squared is :

$$\chi_0^2 = \sum_{i=1}^{n} \left[\frac{\ln(M_i) - \ln[I \cdot m(t_i)]}{\ln(SF_i)} \right]^2 . \qquad \text{Equation 1.22}$$

The model is judged to be inconsistent with the data if the theoretical probability to observe a value of chi-squared with $n-l-1$ degrees of freedom higher than χ_0^2 is less than 5%. The theoretical values of chi-squared distribution are provided by statistical tables and software. It is also

recommended not to retain the model if the plot of its prediction appears inconsistent with the measurement data to the eye of the expert.

After the publication of these recommendations, the statistical rho-square test has been judged to replace the eye of the expert (Puncher *et al*, 2007).

Finally, the best estimate of intake can be considered as maximizing the likelihood of the observed data under the hypothesis of the retained model. When the conditions of exposure are fixed and the same log-normal uncertainty is associated with all measurement data, the most likely intake is the geometric mean of the intakes estimated from each individual measurement data.

The application of the IDEAS guidelines were shown to result in a slight reduction of the dispersion of doses assessed for a same case (Hurtgen *et al*, 2005).

1.6.5 Uncertainties

As shown by the IDEAS project, the choice of appropriate parameters for the models can introduce significant uncertainty in internal dose calculation. The application of models to the dose assessment requires knowing or making assumptions on the conditions of exposure. Incomplete information may therefore lead to an important uncertainty on the dose result. A major source of uncertainty is the solubility of the incorporated radionuclide (Harrison *et al*, 1998, 2001) which determines its absorption into blood from the respiratory tract (ICRP, 2002a) or from the wound (NCRP, 2006). Another physico-chemical property which rarely well characterized is the size distribution (AMAD) of an inhaled aerosol. When the contamination is discovered as the consequence of a routine or control bioassay measurement, the time(s) of intake may be unknown while restricted to a period of potential exposure and/or to a monitoring interval. Finally, the biokinetics of an actual contamination may differ significantly from the reference model because of inter-individual variability.

1.7 Design of monitoring programme

1.7.1 ISO standard

The International Organization of Standardization (ISO) published a standard relative to the "monitoring of workers occupationally exposed to a risk of internal contamination with radioactive material" (ISO, 2006a). It recommends workplace monitoring if the likely annual committed effective dose exceeds 1 mSv and individual monitoring if it exceeds 6 mSv (Fig. 1.25).

The standard defines requirements to be followed in the design of a routine monitoring programme:

- The consequence resulting from an unknown time interval between intake and measurement shall be limited so that:

- on average over many monitoring intervals, doses are not underestimated, and
- the maximum underestimate of the dose resulting from a single intake does not exceed a factor of three.

- The detection of all annual exposures that can exceed 1 mSv shall be ensured.
- At least two measurements shall be performed annually.

These criteria are in agreement with the recommendations of the IAEA (IAEA, 1999) and of the ICRP (ICRP, 1997b). They are applied to select measurement techniques and monitoring intervals. Consistently, suitable monitoring programmes are proposed for different radionuclides: for routine

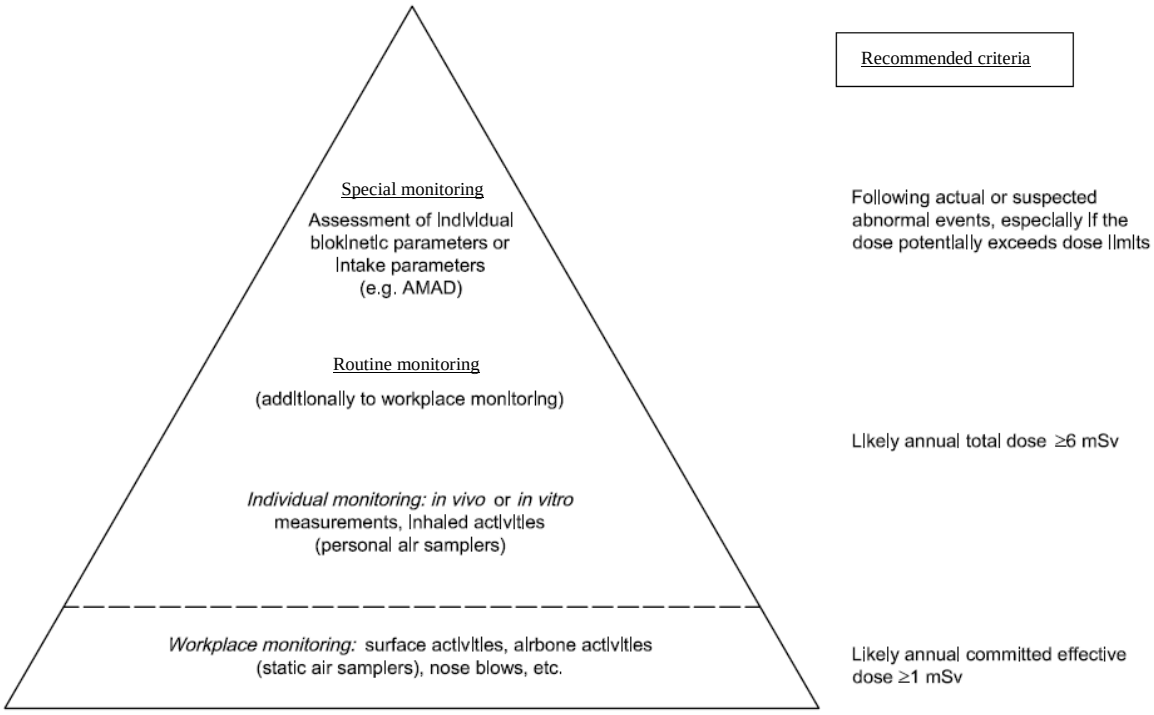

Figure 1.25: Need for monitoring programmes for the internal exposure (ISO, 2006a)

1.7.2 OMINEX project

The European project OMINEX (Optimisation of Monitoring for Internal Exposure) provided advice and recommendations on design and implementation of monitoring programmes for occupational internal exposure in order to enable the best use of available resources, while minimising costs (Etherington *et al*, 2004).

A survey of current monitoring practices within the European Union (EU) was carried out, and summarized by Rahola *et al* (2004). In many instances, there appeared to be little consensus across the EU on the optimum design of an internal dose monitoring programme for particular radionuclides and compounds (Etherington *et al*, 2004).

Surveys were carried out to compile descriptions of the procedure used for *in vivo* or *in vitro* measurements, followed by recommendations on optimum parameters values and quantification of

the resulting overall uncertainty on bioassay measurement (Hurtgen and Cossonnet, 2003 and Génicot, 2003). For example, less than half of the laboratories reach the targeted relative uncertainty of 10 % for a 100 mBq/24 h sample and DL of 1 mBq/24 h for analysis of actinides in faeces (Etherington *et al*, 2004).

Advice was provided on the choice of measurement technique, monitoring interval, required measurement sensitivity and accuracy, measurement parameters needed to achieve such performance, resulting uncertainty in assessed intakes and doses (accuracy), and minimum detectable dose (sensitivity) for individual monitoring of tritium, ^{60}Co, radioiodine, ^{137}Cs, uranium, plutonium and thorium.

1.7.3 Minimum detectable dose

In order to quantify the capability of an individual monitoring programme, Carbaugh (2003) defined the concepts of Minimum Detectable Intake (MDI) and Minimum Detectable Dose (MDD). The MDI is the hypothetical acute intake that would yield a bioassay measurement at the DL (Eq. 1.12, Eq. 1.23)

$$MDI = \frac{DL}{m(t)} \qquad \text{Equation 1.23}$$

The MDD is derived from the MDI by Eq. 1.24:

$$MDD = MDI \times e_{50} = \frac{DL}{m(t)} \times e_{50}\,. \qquad \text{Equation 1.24}$$

The MDD can be compared to dose limits, dose constraints or recording level fixed by the employer or the regulation. It is a measure of the sensitivity of the monitoring programme.

1.8 Approach of this study

Routine monitoring is performed on a regular basis to quantify exposure from undetected accidental intakes in order to verify that the mean of protection complies with regulation and radiation protection policy. However, the activity measurement is subject to uncertainty and possesses an intrinsic sensitivity. Moreover, effective dose assessment from the measurement result is subject to uncertainty through the knowledge of conditions of exposure. Therefore, in the same way as the sensitivity of a measurement technique should be quantified, it is important to determine the sensitivity of a monitoring programme in term of dose by considering the associated uncertainty.

In this study, the sensitivity of a routine monitoring programme is quantified by an extension of the MDD defined by Carbaugh (2003) such as if the measurement result is below the DT, it can be concluded that the corresponding committed effective dose is below the MDD with a level of

confidence of 95 % when taking into account the uncertainty on the measurement itself and on the conditions of exposure.

It is acknowledged that the quality of the absorbed dose estimation depends on the realism of the biokinetic and dosimetric models. Absorbed dose is used for risk evaluation into epidemiological study. For these studies, it is important to integrate the uncertainty relative to the individual and to the biokinetic and dosimetric models.

However, the purpose of this work being limited to the frame of radiation protection and effective dose assessment, uncertainty of the biokinetic and dosimetric models are not considered here. Indeed effective dose is used for managing the risks for workers in general rather than for an individual: "the biokinetic and dosimetric models which are needed for the purpose of dose assessment are defined as reference data and, therefore, are also fixed and not applied with an uncertainty" (ICRP, 2007). Therefore, no individual biokinetic parameters are considered as uncertain in this study. On the other hand, the exposure conditions of the workers defined by the particle size of the inhaled aerosol modelled by the AMAD, and the absorption into blood are biokinetic parameters defining the exposure conditions and not the individual behaviour of the radioactive material. The same values of these parameters can be used for all the workers belonging to the same group. That is why only these biokinetic parameters are varied here and only these ones.

Finally, in the ALARA approach and according to ICRP recommendations (ICRP, 2007), protection has to be optimised. Additionally, as monitoring of exposure is carried out by measurements within a monitoring programme, the programme has to be optimised. Usually, monitoring of internal exposure induces significant economical costs because of the measurement techniques and psycho-social costs relative to the sampling of excreta and to the time needed for measurements. To assure that exposure is low, a high sensitivity of the monitoring is needed in many cases. As the sensitivities of different monitoring programmes can be measured by the values of their MDDs, the optimal monitoring programme for internal exposure is a programme which complies:

- with design criteria on MDD, uncertainty and variability dose assessments,
- with technical constraints of available methods and equipments;

and provides a most cost-effective and reliable solution for the retrospective dose assessments. The optimal programme is a result of the compromise between the numbers of measurements and the measurement techniques and the sensitivity of the programme.

After a presentation of the different uncertainty modelling and their propagation techniques, the uncertainty in the committed effective dose from exposure to uranium in fuel preparation and mines and mills is estimated. After, this study is focused on the calculation of the MDD for the monitoring programme of workers handling the purification of plutonium in AREVA NC reprocessing plant and its possible optimisation.

CHAPTER 2

Uncertainty modelling and propagation

In order to calculate the minimum detectable dose of a monitoring programme, the uncertainties on the measurement and on the conditions of exposure must be quantified and propagated to derive the uncertainty on the effective dose. In this chapter, different mathematical representations of uncertainty are presented together with consistent techniques for propagation.

2.1 Representation of uncertainty

2.1.1 Deterministic representation

A specific value of an uncertain variable may be chosen as a best estimate, central or reference value while the uncertainty may conservatively be represented by the interval between the extreme values the variable can have.

2.1.2 Probability theory

Probability can be used to model the uncertainty on a variable considered as the outcome of a random experiment. An experiment is qualified as random if its outcome cannot be predicted in advance and if, repeated in identical conditions, it can lead to different outcomes. The outcome of the experiment is represented as an element ω of the sample space Ω of all possible outcomes. An event A is a logical proposition regarding the outcome of the experiment. The event is proven if and only if the proposition agrees with the outcome of the experiment. Therefore to each event can be associated with the corresponding elements ω, part of Ω. From now, an event A is identified as the part of Ω for which the event A is true.

Each event A regarding the sample space Ω is associated with a probability $P(A)$ which follows Kolmogorov's axioms:

Axiom 1: $0 \leq P(A) \leq 1$ Equation 2.1

Axiom 2: $P(\Omega) = 1$ Equation 2.2

Axiom 3: any countable sequence of pairwise disjoint events A_1, A_2, ..., A_n satisfies:

$P(\cup A_i) = \sum_i P(A_i)$, where $\cup$ means "or". Equation 2.3

The mathematic theory of probability does not provide a single procedure to assign a specific probability distribution to a set Ω. Instead, different concepts exist to relate the quantification of uncertainty with the probability of an event.

Classical approach

The classical approach is derived from games of chance. The sample set Ω is discrete and finite with each element ω having the same weight.

The probability of an event A is calculated from the enumeration of favourable elements under which it is realised:

$$P(A) = \frac{Number\ \ of\ \ favorable\ \ elements}{Number\ \ of\ \ elements}. \qquad \text{Equation 2.4}$$

This approach is grounded on an idealised conception of random experiment and can no longer be applied if Ω is not enumerable

Frequentist approach

Within the frequentist approach, an experiment being repeated a large number of times; the probability of A is the limit of the frequency f when the number of repetitions tends towards infinity:

$$\frac{Number\ \ of\ \ times\ A\ is\ true}{Number\ \ of\ \ repetition\ s} = f \qquad \text{Equation 2.5}$$

The frequentist approach suffers from several drawbacks: From a practical point of view, it does not allow fully accurate calculation of a probability because the infinite repetition of an experiment is physically unmanageable. Also, it is impossible to define a probability from an unrepeatable experiment.

Subjectivist approach

As the classical definition is limited and the frequentist definition may be questionable, the very existence of probability was denied by De Finetti: "Probability does not exist" (De Finetti, 1974). In the subjectivist approach, the probability is no longer an objective quantity like the mass of an object, but a measure of uncertainty which can vary with circumstances and observers. It is a subjective quantity which satisfies Kolmogorov's axioms. As repetition is no longer needed, probabilities can be assigned to events of unrepeatable experiments. In the Bayesian school of thought, a probability can be assigned to any uncertain event whether it is random or not. The probability is then a measure of the degree of belief that an event will occur.

2.1.3 Possibility theory

Another representation of uncertain knowledge is possibility. The possibility theory (Dubois and Prade, 1988), like probability, provides a set-function that quantifies the uncertainty of events. As for probability, the possibility π of any event A regarding the sample set Ω satisfies:

Axiom 1: $0 \le \pi(A) \le 1$ Equation 2.6

Axiom 2: $\pi(\Omega) = 1$ Equation 2.7

But, unlike probability, possibility is not an additive measure. Axiom 3 is then modified into:

Axiom 3: $\pi(\cup A_i) = \max_i(\pi(A_i))$. Equation 2.8

Therefore, several events may be fully possible (possibility = 1).

From a possibility measure, a dual measure called the necessity *N* of the event *A* can be defined by:

$$N(A) = 1 - \pi(\overline{A}), \quad \text{Equation 2.9}$$

with $\overline{A}$ the complementary event of *A*. From this definition, it can be seen that for any event A, $N(A) \le \pi(A)$. The possibility indicates to which extent the event *A* is possible while the necessity indicates to which extent it is certain.

In this way, it appears that a possibility distribution π and its dual form, the necessity distribution *N*, define a set of probabilities *P*:

$$\mathrm{P}(\pi) = \{P, \forall A, N(A) \le P(A) \le \pi(A)\}. \quad \text{Equation 2.10}$$

In this way, a possibility distribution constitutes a way to model a whole family of probability distributions and may be seen as an imprecise modelling of probability. The imprecision of an event is then defined as the difference between the possibility (upper probability) and the necessity (lower probability) of this event.

2.1.4 Dempster-Shafer theory

Dempster-Shafer theory (Shafer, 1976) is a generalisation of the probability theory. Its main point is to extend the third axiom of probability. To do so, Shafer defined the plausibility measure *Pl* with the axioms:

Axiom 1: $0 \le Pl(A) \le 1$ Equation 2.11

Axiom 2: $Pl(\Omega) = 1$ Equation 2.12

Axiom 3: $\max_i(Pl(A_i)) \le Pl(\cup A_i) \le \sum_i Pl(A_i)$. Equation 2.13

From this definition, possibility and probability are particular plausibility measures. It can be shown that plausibility measures are defined from mass functions on subsets. For probability, the mass functions are based on singletons. As a probability measure is additive, the probability of a set *A* is the sum of probabilities of each of its single elements. For possibility measures, the mass functions are based on nested intervals.

The Dempster-Shafer uncertainty methodology consists in associating a probability distribution with an uncertain variable when actual knowledge is accurate enough to determine it, and in associating a possibility distribution when it is not, both of them seen as plausibility. Since both probability and possibility are used to model uncertainty on the input of an experiment or a calculation, the uncertainty associated with the result can no more be described by only probability

or possibility. The uncertainty on the result derived from this methodology is a plausibility which can be described by its lower and upper probabilities; both representing variability introduced by probability, while the difference between these probabilities represents the imprecision (or lack of knowledge) introduced by possibility.

2.2 Probabilistic quantities

2.2.1 Definitions

Random variable

A random variable is a variable which can take any value from a set of determined values. A random variable which can take only isolated values is discrete and a variable which can take any values in a finite or infinite interval is continuous (ISO, 2006b).

Probability density function

The probability density function (PDF) of a random variable X is the function P determining the probability that the random variable equals a value x_i (discrete random variable) or belongs to an interval (continuous random variable) (ISO, 2006b):

Discrete: $P(x_i)$ = probability that X equals x_i;

Continuous: $P(x)dx$ = probability that X is between x and $x+dx$.

The PDF is normalised, for a discrete random variable, by:

$$\sum_i P(x_i) = 1, \qquad \text{Equation 2.14}$$

or for a continuous variable, by:

$$\int_{-\infty}^{+\infty} P(x)dx = 1. \qquad \text{Equation 2.15}$$

Cumulative distribution function

The cumulative distribution function (CDF) of a random variable X is the function that associates to each value a, the probability that X is lower than or equal to a (ISO, 2006b). For a discrete variable, it is defined by:

$$F(a) = \sum_{x_i \le a} P(x_i), \qquad \text{Equation 2.16}$$

or for a continuous variable, by:

$$F(a) = \int_{-\infty}^{a} P(x)dx. \qquad \text{Equation 2.17}$$

The p^{th} percentile x_p with $0 \leq p \leq 100$ is defined by

$$F(x_p) = \frac{p}{100} \qquad \text{Equation 2.18}$$

Median

The median (x50) is the 50th percentile:

$$F(x_{50}) = 0.5. \qquad \text{Equation 2.19}$$

X has 50 % chance to be less than x50 and 50 % chance to be more than x50. The median is an estimate of the central value which is mostly insensitive to extreme values.

Mean

The mean (μ) of the random variable *X* is defined by, for a discrete random variable:

$$\mu = \sum_i P(x_i) \times x_i \ , \qquad \text{Equation 2.20}$$

or for a continuous variable:

$$\mu = \int_{-\infty}^{+\infty} P(x) \times x \, dx \, . \qquad \text{Equation 2.21}$$

It is an assessment of the central value of the PDF but is very sensitive to extreme values of X.

Standard deviation

The standard deviation (SD or σ) describes the dispersion of the random variable *X* around its mean. It is calculated by, for a discrete random variable:

$$\sigma^2 = \sum_i (x_i - \mu)^2 P(x_i) \, , \qquad \text{Equation 2.22}$$

or for a continuous variable

$$\sigma^2 = \int_{-\infty}^{+\infty} (x - \mu)^2 P(x) dx \, . \qquad \text{Equation 2.23}$$

Confidence interval

The 5^{th} (x_5) and 95^{th} (x_{95}) percentiles are such that $F(x_5) = 0.05$ and $F(x_{95}) = 0.95$. *X* has 5 % chance to be less than x_5 and 5 % chance to be more than x_{95}. Consequently there are 90 % chances that *X* belongs to the 90 % confidence interval $[x_5, x_{95}]$.

Mode

The mode of a PDF is the value the most probable for a discrete variable or the most probable interval for a continuous variable. It is difficult to determine and depends on the intervals used to estimate the probability. For a perfect symmetrical PDF, the mean is equal to the median, equals to the mode.

2.2.2 Usual PDFs

Poisson

The Poisson PDF of a positive or null integer variable with parameter λ is defined by:

$$P(x_i) = e^{-\lambda} \frac{\lambda^{x_i}}{x_i!}. \qquad \text{Equation 2.24}$$

μ and σ equal respectively λ and $\sqrt{\lambda}$. The Poisson PDF with $\lambda = 2$ is represented in Fig. 2.1. The probability of nuclear transformation over time intervals follows a Poisson PDF.

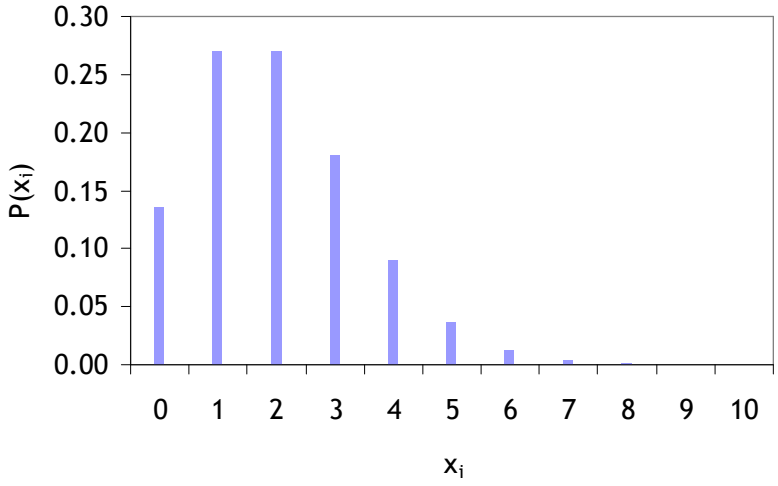

Figure 2.1: Poisson PDF with $\lambda = 2$

Uniform

A uniform PDF models constant probability between two extreme values *a* and *b*. It is often used in the absence of knowledge and is defined by:

$$P(x) = \frac{1}{b-a}, \text{ for } a \le x \le b, \qquad \text{Equation 2.25}$$

$$P(x) = 0 \text{ else.} \qquad \text{Equation 2.26}$$

The uniform PDF between 0 and 10 is plotted in Fig. 2.2.

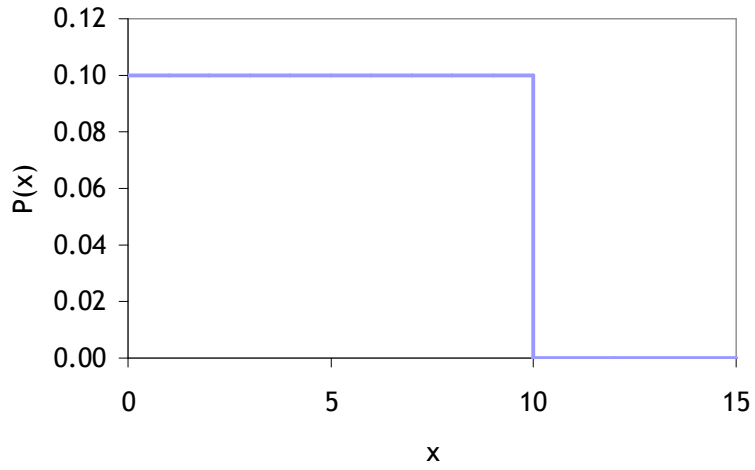

Figure 2.2: Uniform PDF between 0 and 10

Triangular

A triangular PDF is often used when the most probable value (mode) *b* and extreme values *a* and *c* are known. It is defined by:

$$P(x) = \frac{2}{c-a} \times \frac{x-a}{b-a}, \text{ for } a \le x \le b, \qquad \text{Equation 2.27}$$

$$P(x) = \frac{2}{c-a} \times \frac{c-x}{c-b}, \text{ for } b \le x \le c, \qquad \text{Equation 2.28}$$

$$P(x) = 0 \text{ else.} \qquad \text{Equation 2.29}$$

The triangular PDF between 0 and 10 with a mode of 3 is shown in Fig. 2.3.

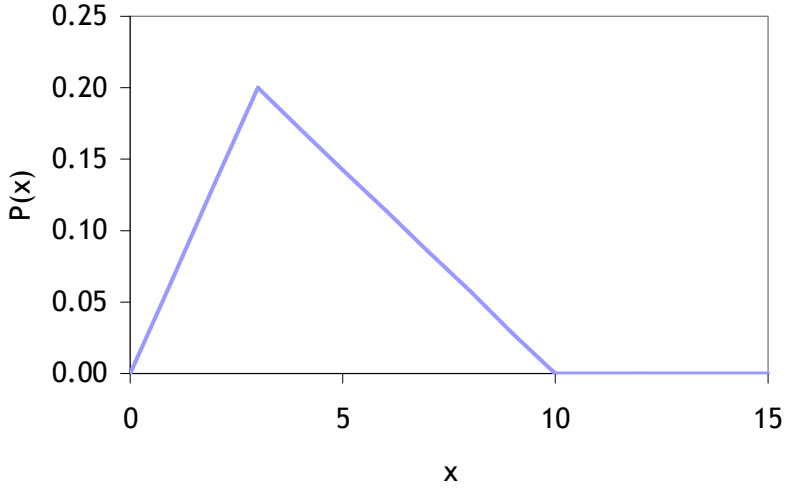

Figure 2.3: Triangular PDF between 0 and 10 with a mode of 3

Trapezoidal

If an interval [*b*, *c*] is the most probable and extreme values *a* and *d* are known, a trapezoidal PDF can be applied. It is calculated by:

$$P(x) = \frac{2}{d+c-b-a} \times \frac{x-a}{b-a}, \text{ for } a \le x \le b, \qquad \text{Equation 2.30}$$

$$P(x) = \frac{2}{d+c-b-a}, \text{ for } b \le x \le c, \qquad \text{Equation 2.31}$$

$$P(x) = \frac{2}{d+c-b-a} \times \frac{d-x}{d-c}, \text{ for } c \le x \le d, \qquad \text{Equation 2.32}$$

$$P(x) = 0 \text{ else.} \qquad \text{Equation 2.33}$$

Fig. 2.4 represents the trapezoidal PDF between 0 and 10 with most probable values between 3 and 5.

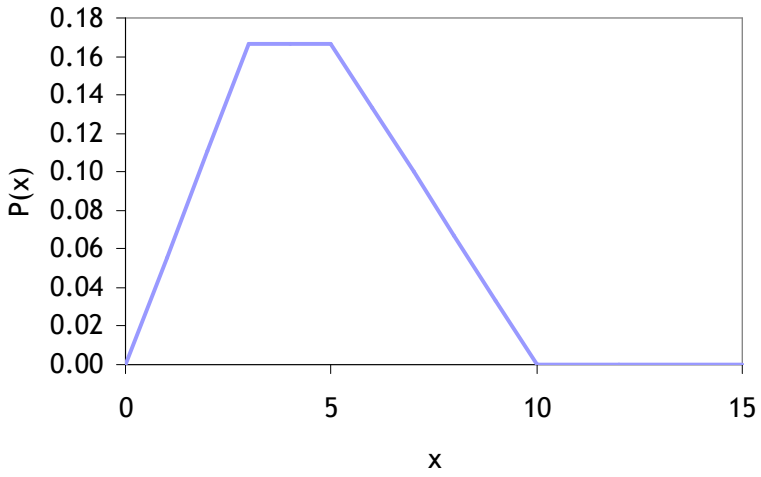

Figure 2.4: Trapezoidal PDF between 0 and 10 with a most probable interval of [3, 5]

Normal

The normal PDF is the PDF of the sum of independent uniform random variables. Therefore, it is widely used to model uncertainty resulting from multiple additive sources of uncertainty. Moreover, it is good approximation of a Poisson PDF with λ above 30. *X* follows a normal PDF with a mean of μ and a SD of σ if:

$$P(x) = \frac{1}{\sigma\sqrt{2\pi}} e^{-\frac{1}{2}(\frac{x-\mu}{\sigma})^2}. \qquad \text{Equation 2.34}$$

The normal PDF with $\mu = 2$ and $\sigma = 0.5$ is plotted on Fig. 2.5.

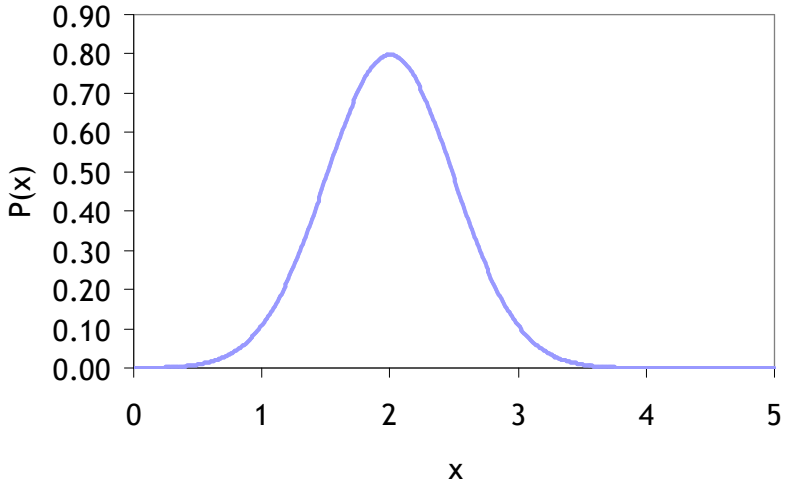

Figure 2.5: Normal PDF with μ = 2 and σ = 0.5

Lognormal

The lognormal PDF describes the probability of a positive variable which natural logarithm follows a normal PDF. This PDF is often used to model uncertainty resulting from multiplicative sources of uncertainty. The lognormal PDF with mean μ and SD σ is calculated by:

$$P(x) = \frac{1}{\sigma x\sqrt{2\pi}} e^{-\frac{1}{2}\left(\frac{\ln(x)-\mu}{\sigma}\right)^2} . \qquad \text{Equation 2.35}$$

Usually, the lognormal PDF is parameterised by its geometric mean μ_g and geometric standard deviation σ_g which are the mean and SD of the normal PDF of the natural logarithm of:

$$P(x) = \frac{1}{\ln(\sigma_g)x\sqrt{2\pi}} e^{-\frac{1}{2}\left(\frac{\ln(x)-\ln(\mu_g)}{\ln(\sigma_g)}\right)^2} . \qquad \text{Equation 2.36}$$

Fig. 2.6 represents the lognormal PDF with μ_g = 1 and σ_g = 3.

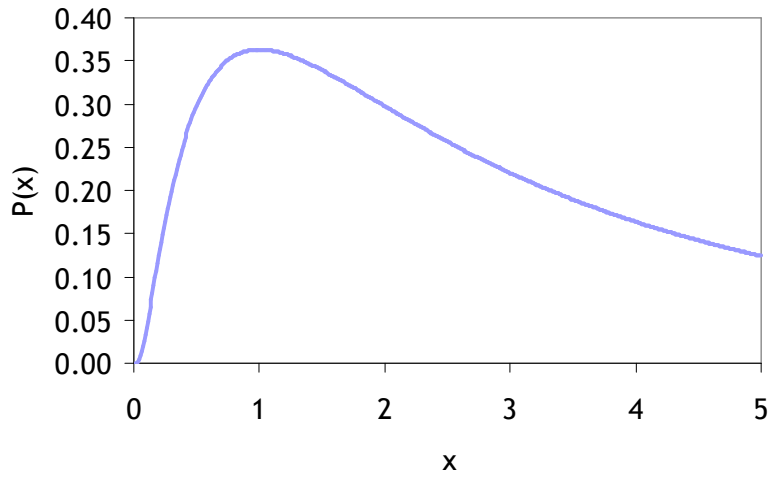

Figure 2.6: Lognormal PDF with μ_g = 1 and σ_g = 3

Exponential

An exponential PDF parameterised by λ is equal to:

$$P(x) = \frac{1}{\lambda} e^{-\lambda x}. \qquad \text{Equation 2.37}$$

It is plotted on Fig. 2.7 for $\lambda = 1$.

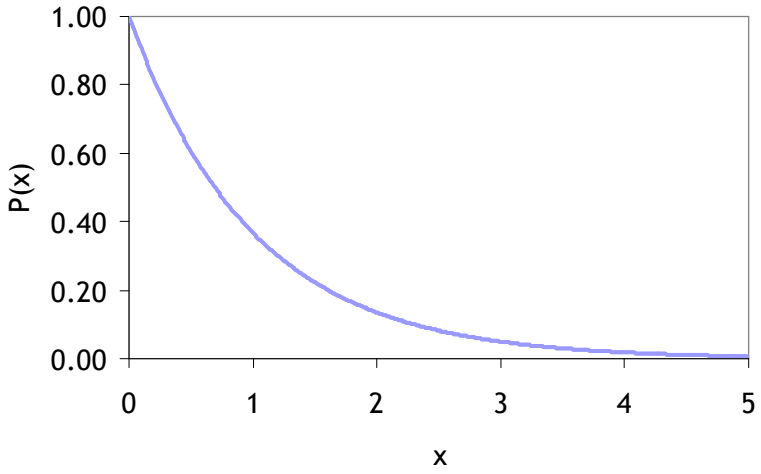

Figure 2.7: Exponential PDF with λ = 1

Alpha

The alpha PDF was defined by Miller *et al* (2001). It models high probability of low values and is calculated as:

$$P(x) = \frac{\alpha}{x}\left(\frac{x}{A}\right)^{\alpha}. \qquad \text{Equation 2.38}$$

It is truncated for *x* higher than *A*. The value of α changes the PDF to

$$P(x) = \frac{1}{x} \text{ when } \alpha \text{ tends to 0,} \qquad \text{Equation 2.39}$$

to

$$\text{uniform } P(x) \text{ when } \alpha = 1. \qquad \text{Equation 2.40}$$

The PDF for *A = 10000* and $\alpha = 0.001$ is represented on Fig. 2.8.

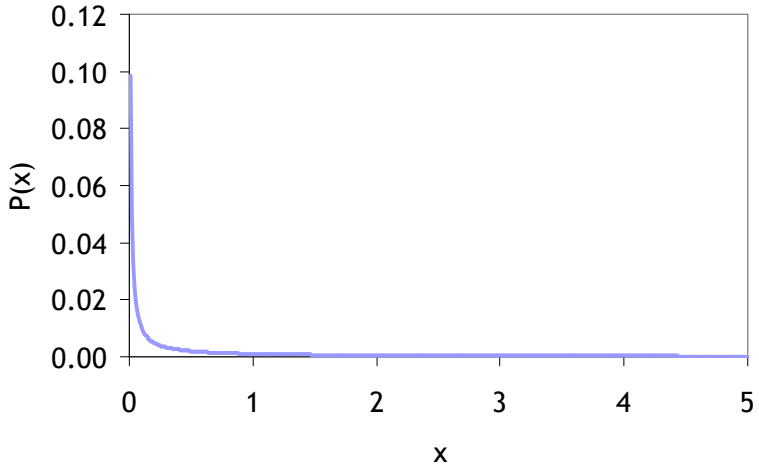

Figure 2.8: Alpha PDF for A = 10000 and α = 0.001

2.2.3 For couples of random variables

In case several random variables are considered, it is useful to define additional concepts. In this section, only two discrete random variables are considered but the following definitions can be expanded to situations where more random variables or continuous variables are used.

Here, two random variables X and Y may take a finite or denumerable values x_i and y_j.

Joint probability

The joint probability P_{XY} is the probability of the couple (X, Y), defined by:

$$P_{XY}(x_i, y_j) = P(X = x_i \cap Y = y_j) = p_{ij} \text{ with } \sum_i \sum_j p_{ij} = 1, \text{ where } \cap \text{ means "and"} \quad \text{Equation 2.41}$$

It is the probability to observe at the same time $X = x_i$ and $Y = y_j$, which can be tabulated (Fig. 2.9).

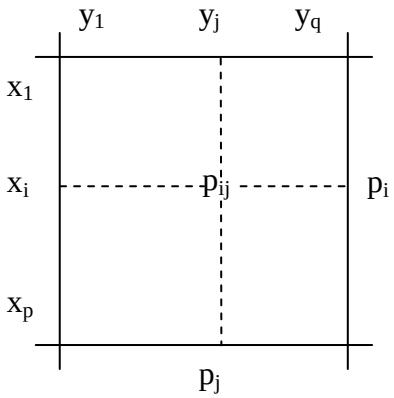

Figure 2.9: Joint and marginal probabilities of X and Y

Marginal probability

The marginal probability is the probability of X or Y considered separately (Fig. 2.9). The marginal probability of X is:

$$P(X = x_i) = \sum_j p_{ij} = p_i . \quad \text{Equation 2.42}$$

For Y, it is:

$$P(Y = y_j) = \sum_i p_{ij} = p_j . \quad \text{Equation 2.43}$$

Conditional probability

If $P(X = x_i)$ and $P(Y = y_j)$ are non-null, two conditional probabilities can be defined: the probability $P(X = x_i \mid Y = y_j)$ to observe $X = x_i$ given the observation $Y = y_j$, and the probability $P(Y = y_j \mid X = x_i)$ to observe $Y = y_j$ given the observation $X = x_i$. They are calculated by:

$$P(X = x_i \mid Y = y_j) = \frac{p_{ij}}{p_j} = \frac{P(X = x_i \cap Y = y_j)}{P(Y = y_j)}, \quad \text{Equation 2.44}$$

$$P(Y = y_j \mid X = x_i) = \frac{p_{ij}}{p_i} = \frac{P(X = x_i \cap Y = y_j)}{P(X = x_i)}. \quad \text{Equation 2.45}$$

The conditional probability is often easier to evaluate than the joint probability and it can be used to derive the latter as well as the marginal probability:

$$P(X = x_i) = \sum_j P(X = x_i \cap Y = y_j) = \sum_j P(X = x_i \mid Y = y_j) \times P(Y = y_j), \quad \text{Equation 2.46}$$

$$P(Y = y_j) = \sum_i P(X = x_i \cap Y = y_j) = \sum_i P(Y = y_j \mid X = x_i) \times P(X = x_i). \quad \text{Equation 2.47}$$

2.3 Possibilistic quantities

Possibility distributions allow modelling in a convenient way families of PDFs so that it is not required to choose a specific probability when not enough information is available to support this choice. For example a uniform possibility distribution encodes all the PDFs which have the same support. A triangular possibility distribution encodes all the PDFs which have the same support and the same mode. A trapezoidal possibility distribution encodes the family of PDFs which have the same support and which mode is in the core. However, where it is applicable, the use of specific PDFs for random variables allows the representation of more precise information and limits the conservatism of interval calculation.

Upper and lower Cumulative Distribution Function (CDF)

In radiation protection, events of the form: “to be lower than a threshold value” obviously are of particular interest. Indeed, this threshold value often corresponds to a limit of a quantity which must not be exceeded. In case the quantity of interest is modelled by a random variable, the

probability of such event is determined by its CDF. If possibility distributions are considered, the CDF is then replaced by a couple of two extreme CDF:

- the upper CDF, *F** which is equal to the possibility distribution:

$$F^*(x) = \pi(]-\infty, x]), \qquad \text{Equation 2.48}$$

- the lower CDF, F_* which is equal to the necessity distribution:

$$F_*(x) = N(]-\infty, x]) = 1 - \pi([x, +\infty[). \qquad \text{Equation 2.49}$$

The difference between the same percentile of the lower and upper CDF corresponds to the imprecision on the exact value of this percentile, so that without imprecision the lower and upper CDF are merged. On the other hand, the differences between the values of any CDF included in the band defined by the lower and upper CDF reflect the variability of the random quantity. The overall uncertainty comes from both the variability and the imprecision, and may be quantified by the difference between a (e.g. 5th) percentile of the upper CDF and a (e.g. 95th) percentile of the lower CDF (Fig. 2.10).

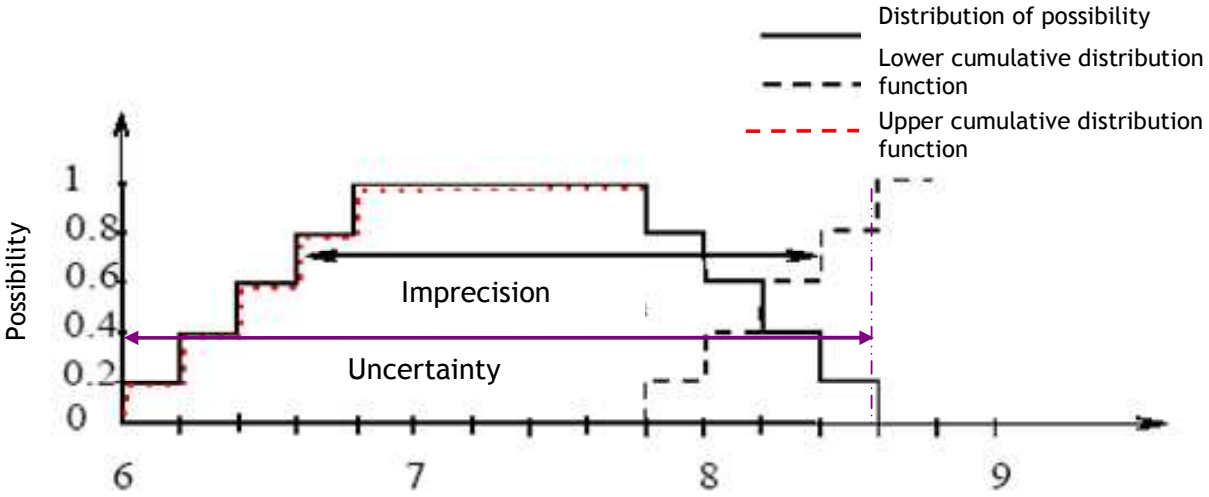

Figure 2.10: Example of an arbitrary possibility distribution, its lower and upper CDF and the derived imprecision and uncertainty.

α-cut

An α-cut $[\underline{x}_\alpha, \overline{x}_\alpha]$ of the possibility distribution π (Fig. 2.11) is the interval containing values which possibility is higher than α:

$$[\underline{x}_\alpha, \overline{x}_\alpha] = \{x,\ \pi(x) \geq \alpha\}. \qquad \text{Equation 2.50}$$

The degree of certainty that the α-cut contains the true value of *X* is:

$$N([\underline{x}_\alpha, \overline{x}_\alpha]) = 1 - \alpha\ . \qquad \text{Equation 2.51}$$

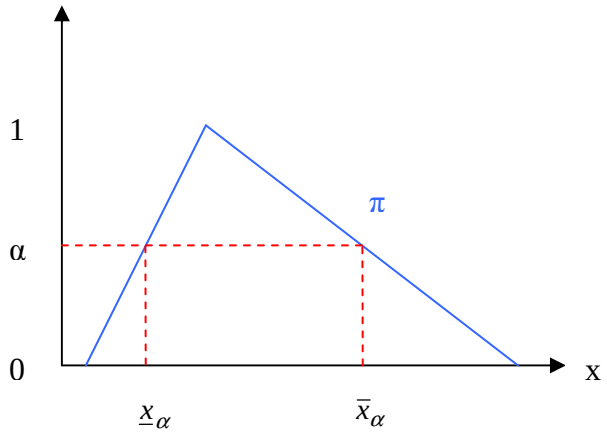

Figure 2.11: α-cut of the possibility distribution π

2.4 Direct propagation techniques

2.4.1 Definition

Direct propagation of uncertainty is deriving the uncertainty in consequences from known uncertainty in the causes.

The committed effective dose resulting from an intake depends on the magnitude of the intake *I* and on the biokinetic parameters *L*, while a following bioassay measurement *M* also depends on the time of contamination *t* (Eq. 1.20 and 1.21). The relationships between the variables are represented by a graph in Fig. 2.12: the internal exposure is parameterised by *i*, *L*, *t* and has for consequences the committed effective dose *E* and the bioassay quantity *M*.

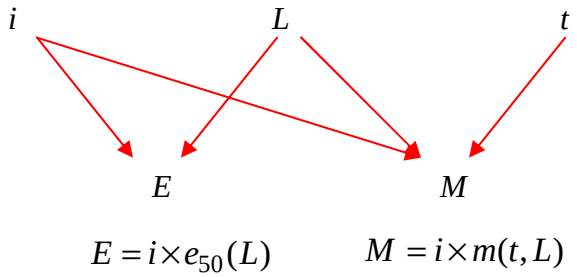

Figure 2.12: Relationships between the characteristics of exposure (intake *i*, biokinetic parameters *L*, time of contamination *t*) and its consequences: committed effective dose *E* and measured activity *M*. $e_{50}(L)$ is the dose coefficient calculated for the biokinetic parameters *L*; $m(t, L)$ is the retention or excretion function at time *t* following intake, calculated with the biokinetic parameters *L*.

The uncertainty in the causes *i*, *L* and *t* may be propagated to the uncertainty in the consequences *E* and *M* (Fig. 2.13).

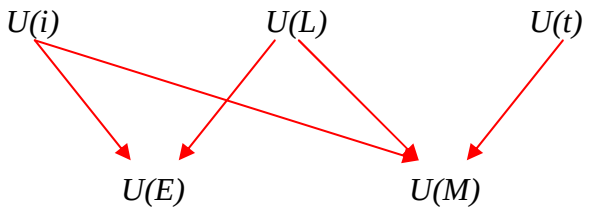

Figure 2.13: Direct propagation of the uncertainty *U* in the exposure characteristics (intake *i*, biokinetic parameters *L*, time of contamination *t*) to the exposure consequences: committed effective dose *E* and measured activity *M*.

Since different representations of uncertainty exist, different direct propagation techniques have to be consistently applied.

2.4.2 Deterministic propagation

From a deterministic point of view, the variables *i*, *L* and *t* are modelled by reference values or intervals between extreme values. Calculating *E* and *M* through Eq. 1.20 and 1.21 for the reference or extreme values, reference estimates or intervals of *E* and *M* are obtained. The reference estimate is not necessarily the most probable value but could be the result of an expert judgement. The deterministic interval calculation is very conservative since all possible outcomes are included in the resulting interval and no information is provided on the relative probability of values within this interval.

2.4.3 Probabilistic approach

In probabilistic methods, a PDF is selected to quantify the degree of belief associated with each value of the parameter *i*, *L* and *t*. If dependencies between uncertain parameters are known and judged to be potentially important, then they need to be quantified. In this method, each value of the uncertainty domain is weighted by its degree of belief. The probabilistic methods consist in evaluating from this knowledge the likelihood associated with each possible result of *E* and *M* as a PDF.

Accurate results require precise knowledge of the PDF of each uncertain parameter and of the possible correlations. Such knowledge is rarely available in practice and some information has often to be subjectively added based on expert judgment. In practical studies, some particular choices of PDFs are commonly made to represent the lack of knowledge on uncertain parameters. For example, a uniform probability distribution is often used when no information but the extreme values is available. A triangular distribution can be used when the extreme values and the mode are known.

However, subjective information may lead to less realistic results and arbitrarily change the confidence interval. Indeed, when the variability of a parameter is not well known, several

different PDFs could be applied and the overall uncertainty may be underestimated by considering only one. In the same way, unknown correlations may lead to unrealistic estimation of the uncertainty.

Analytic techniques

If an analytical relationship *f* between the uncertain parameters x_j (e.g. *i*, *L* and *t)*, and the model outcome *y* (e.g. *E* or *M)* is available:

$$y = f(x_1, x_2 \ldots x_N) . \qquad \text{Equation 2.52}$$

then the uncertainty in *y* can be derived from the uncertainty in x_j by:

$$\sigma^2(y) = \sum_{j=1}^{N} \left[\frac{\partial f}{\partial x_j} \right]^2 \sigma^2(x_j) + 2 \sum_{j=1}^{N-1} \sum_{k=j+1}^{N} \frac{\partial f}{\partial x_j} \frac{\partial f}{\partial x_k} \sigma(x_j, x_k) \text{ (ISO, 2008).} \qquad \text{Equation 2.53}$$

However, it implies knowing the covariance $\sigma(x_j, x_k)$ and restraining x_j to small variations.

Perturbation theory

In this approach applied by Krahenbuhl *et al* (2005) and Bess *et al* (2007), the uncertainties on each x_j are combined using first order perturbation theory to determine the uncertainty of *y*. The uncertainty in a reported value determined from a complex system of equations can be estimated by separately perturbing each variable by its specific uncertainty. The results from the perturbed solution are then subtracted from the standard solution. The differences are squared and summed. The method results in an estimation of the total uncertainty in the reported value through the general equations:

$$y_0 = f(\mu_{x_1}, \mu_{x_2}, \ldots, \mu_{x_N}) , \qquad \text{Equation 2.54}$$

$$y_j{}^{+} = f(\mu_{x_1}, \mu_{x_2}, \ldots, x_j + \sigma_j \ldots, \mu_{x_N}) , \qquad \text{Equation 2.55}$$

$$y_j{}^{-} = f(\mu_{x_1}, \mu_{x_2}, \ldots, x_j - \sigma_j \ldots, \mu_{x_N}) , \qquad \text{Equation 2.56}$$

$$\sigma^{2+}(y) = \sum_{j=1}^{N} (y_0 - y_j{}^{+})^2 , \qquad \text{Equation 2.57}$$

$$\sigma^{2-}(y) = \sum_{j=1}^{N} (y_0 - y_j{}^{-})^2 . \qquad \text{Equation 2.58}$$

The perturbation techniques allow for non-symmetrical uncertainties on both the parameters and the outcome.

Monte-Carlo techniques

The Monte Carlo method is a numerical technique of integral calculation which converges faster than other methods in several dimensional space. It consists in generating a large number of random sets of input parameters according to their probability and in estimating the output of interest from discrete sums approximating the integrals to be calculated. In Monte-Carlo simulation, a physical model is applied repeatedly, using different values for each of the uncertain parameters each time. The values of each of the uncertain parameters are drawn from its PDF:

If $F(x)$ is the CDF of X, then the variable $Y = F(X)$ is uniformly distributed between 0 and 1. n numbers, $r_1, r_2, \ldots, r_n$ are drawn randomly between 0 and 1. The sample of X $(x_1, x_2, \ldots, x_n)$ is determined by $x_i = F^{-1}(r_i)$ where F^{-1} is the inverse function of F. The sample of X is therefore distributed according to $F(x)$.

For the model of Fig 2.13, a set (i_j, L_j, t_j) is obtained at the j^{th} simulation. Then the model is solved for each set of the uncertain parameters leading to sets of E and M. This sample can be used to estimate any typical statistics such as the mean or the variance of E and M and to determine the CDF of E and M. It follows from the law of large numbers that the mean, the standard deviation and the CDF can be calculated without knowing the PDF of the result, using a Monte-Carlo simulation:

$$\bar{x} = \frac{1}{N}\sum_{i=1}^{N} x_i \xrightarrow[N\to+\infty]{} \mu = \int_{-\infty}^{+\infty} xP(x)dx \,, \qquad \text{Equation 2.59}$$

$$S^2 = \frac{\sum_{i=1}^{N}(x_i - \bar{x})^2}{N-1} \xrightarrow[N\to+\infty]{} \sigma^2 = \int_{-\infty}^{+\infty}(x-\mu)^2 P(x)dx \,, \qquad \text{Equation 2.60}$$

$$\frac{1}{N}\sum_{i=0, x_i \le a}^{N} x_i \xrightarrow[N\to+\infty]{} F(a) = \int_{-\infty}^{a} P(x)dx \,. \qquad \text{Equation 2.61}$$

The Monte-Carlo simulation is therefore a simple way to obtain useful statistics about the model outputs and can be used for complex model where no analytical solution exists. Two methods for sampling random or pseudo-random sets of number are widely used: In the Simple Random Sampling (SRS) (Cochran, 1977) method, a number between 0 and 1 is randomly drawn for each uncertain parameter to sample its CDF.

In the Latin Hypercube Sampling (LHS) (McKay *et al*, 1979) method, the interval [0, 1] is first divided into sub-intervals from which numbers are randomly or deterministically drawn without replacement. This ensures that each of the uncertain parameters is represented in a fully stratified manner, no matter which component might turn out to be important. Although LHS provides a faster convergence than SRS, it is not a pure random method and the direct estimation of percentiles from order statistics cannot be applied.

Examples of application in internal dosimetry

The propagation of the uncertainty on the model parameter values to the dose coefficient has been studied by Monte-Carlo techniques in several cases. Bolch *et al* (2001, 2003) assessed the uncertainties on parameter values for particle deposition and clearance in the HRTM following inhalation of a mono-dispersed aerosol. These uncertainties were propagated to the dose coefficient.

Fritsch (2006) applied the same method to poly-dispersed aerosols. Farfan *et al* (2003) evaluated the uncertainties on parameters characterising source and target tissues geometry in the HRTM and derived resulting uncertainties on the dose. Farfan *et al* (2005) studied uncertainty in electron absorbed fractions and lung doses from inhaled beta-emitters. Birchall and James (1994) and Marsh *et al* (2002) carried out parameter uncertainty analyses of the weighted equivalent dose to the lung per unit exposure to radon progeny respectively in a home and in a mine.

Other studies have been carried out with specific radionuclides in order to assess the uncertainties on the absorption and on the systemic model. Harrison *et al* (2001) estimated the uncertainty on the fraction of activity absorbed in the gut for 14 radionuclides and observed no direct effect of it on the uncertainty in the dose coefficients. Later, the same authors studied the uncertainties on the parameters describing the systemic model for tritium in order to determine the uncertainty on the dose coefficient from intake of tritiated water and organically bound tritium (Harrison *et al*, 2002).

Uncertainties in dose coefficients from ingestion of iodine and caesium were extensively studied (Dunning and Schwarz, 1981, Schwartz and Dunning, 1982, Hamby and Benke, 1999, Harvey *et al*, 2003, Apostaei and Miller, 2004). Krahenbuhl *et al* (2005) determined the uncertainty on the organ burden of Mayak workers by Monte-Carlo techniques varying the 20 excretion parameters. Bess *et al* (2007) assessed the uncertainty on the dose from plutonium inhalation as a consequence of uncertainties on the parameters of a model modified from ICRP publication to fit the data from Mayak workers. Khursheed (1998) determined the uncertainty in dose coefficients for systemic plutonium by Monte-Carlo technique considering uncertainty on the most sensitive biokinetic parameters.

Blanchardon *et al* (2007) proposed to take into account uncertainty associated with measurements and models as well as the realistic hypotheses on the conditions of exposure to estimate a distribution of possible dose values. This was performed by assuming *a priori* PDF for input data including measurement result, model parameters and conditions of exposure, and by computing the resulting PDF of dose by Monte-Carlo simulation (Molokanov and Blanchardon, 2007). However, this method did not consider the causal relationships between the different quantities.

Etherington *et al* (2006) developed a method to determine the uncertainty in the dose assessments for a population of workers when default assumptions are made about model parameter values and intake patterns. First an intake pattern is generated as a series of single intakes at random times with random magnitudes. A measurement data set is consequently generated with model parameters sampled randomly from their PDFs. Measurement uncertainty is also generated

randomly. Intake and committed effective dose are then assessed for the dataset using default assumptions for model parameters and intake pattern. This process of simulating an intake pattern, generating a corresponding measurement dataset, and assessing intake and dose is repeated a large number of times. Because the true intake and dose associated with each simulated dataset is known, a PDF can be determined for the ratio of assessed dose to true dose. The arithmetic mean of the distribution provides a measure of the bias, while a confidence interval provides a measure of uncertainty. This method was applied to the routine monitoring of tritiated water exposures.

2.4.4 Dempster-Shafer approach: the RaFu method

In a probabilistic Monte-Carlo method, a probabilistic random variable X defined by its CDF *F* is simulated by drawing a_i values from a uniform distribution over [0, 1] and by associating a_i with $x_i = F^{-1}(\alpha_i)$. Regarding possibility, since there is a bijective correspondence between levels $\alpha \in [0,1]$ and the corresponding α-cuts $\left[\underline{x}_\alpha, \overline{x}_\alpha\right]$, a possibility distribution can also be simulated by drawing α_i values from a uniform distribution over [0, 1] and by associating α_i with the corresponding α-cut.

Therefore, Monte-Carlo techniques can be applied to propagate uncertainty modelled by both possibility distributions and PDFs within the Dempster-Shafer theory framework (Fig. 2.14).

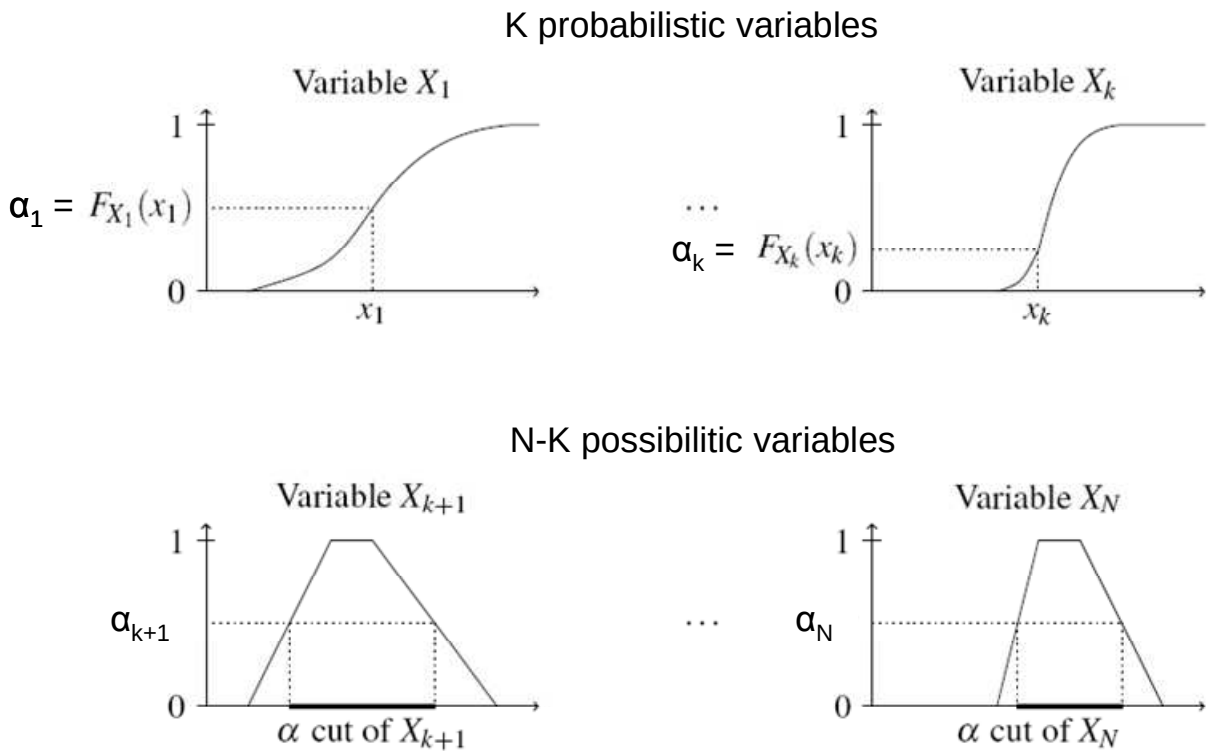

Figure 2.14: Monte-Carlo sampling of probabilistic and possibilist variables in the RaFu approach.

In the Random Fuzzy (RaFu) method (Chojnacki *et al*, 2010), the correlations between the variables, the sampling method and the precision of the outcome or the maximal number of samples are first defined. The propagation of uncertainty is then performed by solving the model (e.g. calculation of dose *E* and measurement *M*) for each set of sampled values, which are point values for probabilistic variables and upper and lower bounds of α-cuts for possibilist variables. For each variable, the less and the more penalizing bounds for the outcome are determined by knowing the influence of the parameter on the outcome. Therefore, by combining all the more (resp. less) penalizing bounds of each parameter, the upper (resp. lower) bound of the model outcome can be determined to form the upper and lower CDF. The result of this method is a plausibility of the outcome variable defined by its lower and upper CDF and taking into account both imprecision and variability.

2.5 Inverse propagation techniques

2.5.1 Definition

In internal dosimetry, the dose *E* and bioassay measurement *M* are consequences of the intake *i*, biokinetic parameters *L* and time of contamination *t* (Eq. 1.20 and 1.21 and Fig. 2.12). However, *i*, *L* and *t* are usually not known in practice. Still, they can be inferred from observed *in vivo* and *in vitro* measurement results *M* by Eq. 1.20 and 1.21. This process is represented in Fig. 2.15.

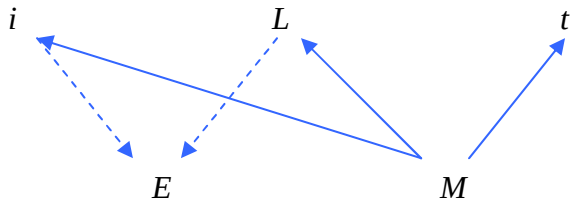

$$E = i \times e_{50}(L)$$

Figure 2.15: Relationships between the exposure characteristics (intake *i*, biokinetic parameters *L*, time of contamination *t*) and the exposure consequences: committed effective dose *E* and measured activity *M*. The directions of the arrows indicate the propagation of information to determine *i* and *E* from *M*. $e_{50}(L)$ is the dose coefficient calculated for the biokinetic parameters *L*.

The inverse propagation of information is inferring the uncertainty in the causes from the uncertain knowledge in the consequences. The uncertainty on *M* can be propagated in the way to *i*, *L* and *t* (Fig. 2.16).

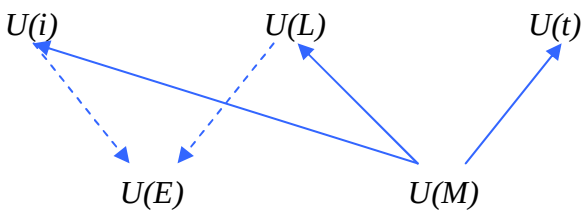

Figure 2.16: Inverse propagation of the uncertainty *U* in the measurement *M* to the exposure conditions: intake *i*, biokinetic parameters *L*, time of contamination *t*

From a probabilistic point of view, the conditional probabilities of *i*, *L*, *t* and *E*, *P(i | M)*, *P(L | M)*, *P(t | M)* and *P(E | M)* can be inferred from the knowledge brought by the measurement result *M*. It can be calculated by applying Bayes' theorem also known as the theorem of conditional probability. Bayes' theorem is used to derive the probability of a cause knowing the probability of a consequence from a priori knowledge of the cause. It is derived from Eq. 2.46 and 2.47:

$$P(X|Y) = \frac{P(X \cap Y)}{P(Y)} = \frac{P(Y|X) \times P(X)}{P(Y)} . \qquad \text{Equation 2.62}$$

For the intake and the dose, it is:

$$P(i|M) = \frac{\iint_{L\ t} P(M|i,L,t) \times P(L) \times P(t) \times dL \times dt}{\iiint_{i\ L\ t} P(M|i,L,t) \times P(i) \times P(L) \times P(t) \times dL \times dt \times di} \times P(i) , \qquad \text{Equation 2.63}$$

$$P(E|M) = \frac{\iint_{L\ t} P(M|E,L,t) \times P(L) \times P(t) \times dL \times dt}{\iiint_{i\ L\ t} P(M|E,L,t) \times P(i) \times P(L) \times P(t) \times dL \times dt \times di} \times P(i) \text{ with } E = i \times e_{50}(L) \qquad \text{Equation 2.64}$$

P(i), *P(L)* and *P(t)* are the prior probabilities of *i*, *L* and *t*: they represent the actual or assumed knowledge on these variables before any measurement is performed. *P(M|i, L, t)* is the probability of the measurement given *i*, *L* and *t*: it is the probability to obtain the measurement *M* from given values of *i*, *L* and *t*. *P(i | M)* and *P(E | M)* are the posterior probabilities. They are the update of the prior probabilities by the knowledge introduced by the measurement. Bayes' theorem may be applied to for discrete variable, replacing integrals with sums in Eq. 2.63 and 2.64.

2.5.2 Classical method

In the so-called classical method of Molokanov *et al* (2010), the intake is modelled by a fixed but unknown value. The following description is adapted from Molokanov *et al* (2010). Its uncertainty is expressed as a confidence interval built from the PDF of the measurement *M* conditional to the intake *i*:

$$P(M|i) = \iint_{L\ t} P(M|i,L,t) \times P(L) \times P(t) \times dL \times dt , \qquad \text{Equation 2.65}$$

The corresponding CDF is used to define a new function of the intake which associates each value *i* with the cumulative probability of the observed measurement *M*:

$$F_M(i) = \int_0^M P(m|i) \times dm . \qquad \text{Equation 2.66}$$

$F_M(i)$ is a decreasing function of *i* because the measured activity is an increasing function of *i*. This integral is calculated by Monte-Carlo techniques. If it is continuous, the value i_α can be defined:

$$i_\alpha = F^{-1}{}_M(\alpha) , \qquad \text{Equation 2.67}$$

such that

$$P(i < i_\alpha) = 1 - \alpha\,, \qquad \text{Equation 2.68}$$

at confidence level 0<α<1. A 90% confidence interval on the intake is bound by the values $i_{0.05}$ and $i_{0.95}$ which correspond to a cumulative probability of the observed measurement *M* equal to 5% and 95 % respectively (Fig. 2.17).

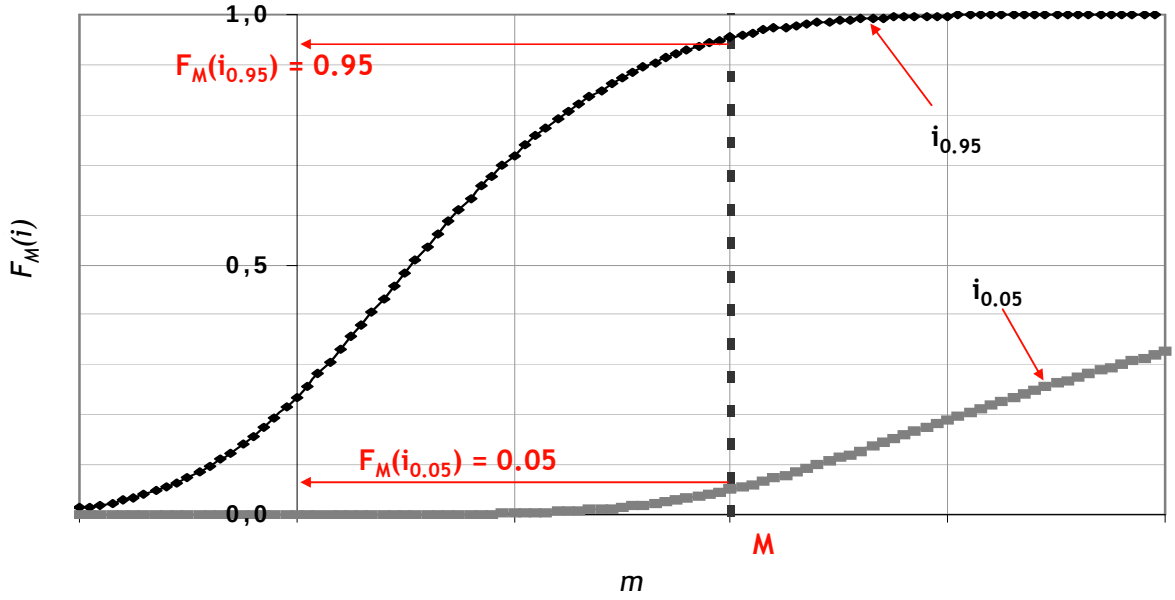

Figure 2.17: Determination of the 90 % confidence interval of intake by the classical method

2.5.3 *WeLMoS method*

The Weighted Likelihood Monte-Carlo Sampling (WeLMoS, Puncher and Birchall (2008)) method is a Bayesian Monte-Carlo method which uses a weighted LHS to calculate the posterior distribution of parameter values including intake and dose. The following description is adapted from Puncher and Birchall (2008). Random samples are generated from the prior distributions of *i*, *L*, and *t* using LHS. Then a weight is assigned to each set of uncertain parameters that is equal to the likelihood of the measurement *M* given the set *i*, *L* and *t*. The weighted values are finally used to compute the posterior distributions according to Eq. 2.63 and 2.64.

Calculating the posterior PDF of the intake P(i | M)

N_i values i_j of the intake are selected over the interval of variation of *i* with equal step Δi. A large number *N* of sets of *L* and *t* are sampled by LHS according to their prior PDF *P(L)* and *P(t)*. The marginal PDF for the intake i_j, $P(i_j \mid M)$ is calculated as:

$$P(i_j|M) = \sum_{k=1}^{N} P(i_j, L_k, t_k|M) = \frac{\sum_{k=1}^{N} P(M|i_j, L_k, t_k) \times P(i_j)}{\sum_{j=1}^{N_i}\sum_{k=1}^{N} P(M|i_j, L_k, t_k) \times P(i_j)}\,. \qquad \text{Equation 2.69}$$

After $P(i_j \mid M)$ is calculated for the $j = 1$ to N_i intakes, the expectation, variance and percentiles of the posterior intake PDF $P(i \mid M)$ can be evaluated.

Calculating the posterior PDF of the dose P(E | M)

The dose E_{jk} corresponding with given i_j and L_k is calculated through the deterministic relation:

$$E_{jk} = i_j \times e_{50}(L_k)\,. \qquad \text{Equation 2.70}$$

Hence, the PDF of the dose given the measurement data $P(E_{jk} \mid M)$ is the same as $P(i_j, L_k, t_k \mid M)$:

$$P(E_{jk} \mid M) = P(i_j, L_k, t_k \mid M)\,. \qquad \text{Equation 2.71}$$

2.5.4 Bayesian network

A discrete Bayesian network was developed in this study (Davesne *et al*, 2010) to calculate the posterior probabilities of intake and dose from the measurement (Fig. 2.18). The dose E is only correlated with the exposure parameters L and with the intake i. The measured activity M is completely correlated with the bioassay quantity S (e.g. activity in a urine sample) but is different from it because of the counting statistics: the probability $P(M \mid S)$ to obtain M given S is therefore modelled by a Poisson distribution of mean S. The bioassay quantity S is defined by i, L and t, modulated by Type B uncertainty: the probability of S given i, L and t follows a lognormal distribution of geometric mean $i \times m(L,t)$ where m is the retention or excretion function corresponding to the measured quantity and with a geometric standard deviation equal to a scattering factor (SF) depending on the bioassay sampling or on the *in vivo* detector calibration.

Each of the six variables is discretised and the global likelihood associated to a specific intake or dose is determined by summing the likelihood obtained for each combination of the discrete values of the different variables.

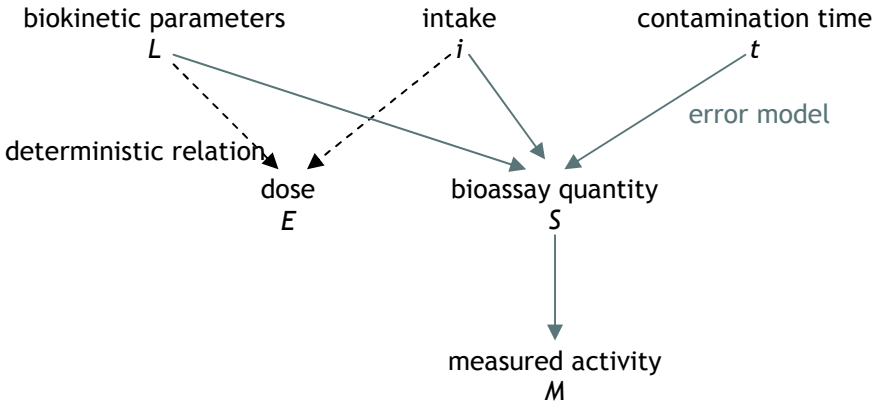

Figure 2.18: Structure of the Bayesian network used to infer the posterior probabilities of intake and dose from the measured activity.

In order to calculate the posterior probability of *i* and *E*, the first step is to evaluate the joint probability of each combination of discrete values i_j, L_k, t_n, S_o and E_p:

$$P(i_j, L_k, t_n, S_o, E_p) = P(S_o | i_j, L_k, t_n) \times P(E_p | i_j, L_k) \times P(i_j) \times P(L_k) \times P(t_n) \text{ . Equation 2.72}$$

The joint probabilities of *i* and S, and *E* and *S*, and *S* alone are then calculated:

$$P(i_j, S_o) = \sum_p \sum_k \sum_n P(i_j, L_k, t_n, S_o, E_p) \text{ , Equation 2.73}$$

$$P(S_o, E_p) = \sum_j \sum_k \sum_n P(i_j, L_k, t_n, S_o, E_p) \text{ , Equation 2.74}$$

$$P(S_o) = \sum_p \sum_j \sum_k \sum_n P(i_j, L_k, t_n, S_o, E_p) \text{ . Equation 2.75}$$

Finally, the posterior probabilities are evaluated by Bayes' theorem:

$$P(i_j | M) = \frac{\sum_o P(M | S_o) \times P(i_j, S_o)}{\sum_o P(M | S_o) \times P(S_o)} \text{ , Equation 2.76}$$

$$P(E_p | M) = \frac{\sum_o P(M | S_o) \times P(S_o, E_p)}{\sum_o P(M | S_o) \times P(S_o)} \text{ . Equation 2.77}$$

2.5.5 Markov Chain Monte-Carlo

In order to calculate posterior probabilities of intake and effective dose, Miller *et al* (1999) developed the Los Alamos UF code in which the retention/excretion functions *m* and dose coefficients e_{50} for each biokinetic model *L* are tabulated. This code was developed to determine if a plutonium measurement in Los Alamos monitoring programme is positive.

The posterior PDF are calculated through a Markov Chain Monte-Carlo algorithm (Miller *et al* 2002) considering up to about 200 biokinetic models to solve the integrals of Eq. 2.63 and 2.64. The main problem of Markov Chain Monte-Carlo is the calculation time which can be prohibitive. Puncher and Birchall (2008) showed that the WeLMoS method and the UF code obtain the same results for the same study and that the WeLMoS method is quicker. As this method is not used in this study, its algorithm is not detailed here.

2.6 Conclusion

Different tools are available to model uncertainty: interval, probability, possibility or plausibility. They are representations of the knowledge of imprecise or variable quantities. These tools can be used to directly propagate uncertainty from the intake and biokinetic model to the

dose. Alternatively, the uncertainty on the intake and dose can be inferred from prior knowledge on uncertain quantities and from an observed measurement result by inverse propagation.

The direct propagation of probability and possibility was presented in detail, highlighting the advantages of Monte-Carlo methods. For inverse propagation, Bayesian methods appear as well adapted and efficient.

In this study, uncertainties on the conditions of exposure characterized by the AMAD and the absorption kinetics were propagated using the RaFu method to the effective dose for prospective dosimetry of internal exposure to uranium. The MDD for the routine monitoring programme of plutonium workers at AREVA NC La Hague reprocessing plant was evaluated using the classical method, the WeLMoS method and the Bayesian network, from the uncertainty of measurement and the prior probabilities of intake and conditions of exposure (AMAD, absorption, time of contamination).

CHAPTER 3

Prospective dosimetry: direct propagation of uncertainty

3.1 Introduction

Prospective dosimetry is used at the design and planning stages for preventive purpose, to quantify the potential health risk, to set up appropriate means of protection, and to check if the exposure at a workplace will be in conformity with the regulation and radiation protection policy. For internal exposure, this is based on the assessments of ambient air or surface contamination at the workplace or on such information if available.

As it was specified above, some biokinetic parameters are related to the physico-chemical properties of the radionuclide such as the AMAD and the absorption rates; while others relate to the individual physiology. The absorption into blood is quantified by three rates (s_p, s_{pt} and s_t)[1] in the HRTM and by the absorbed fraction (f_A) of the ingested activity in the HATM. However, the degree of knowledge of these parameters varies with specific situations of exposure; and it can therefore be useful to quantify the resulting uncertainty on the foreseen dose by direct propagation methods.

The aim of this study is to apply the RaFu approach to evaluate uncertainties and to demonstrate its usefulness in prospective dosimetry of internal exposure. It is more conservative than the usual probabilistic approach and is well suited to process imprecise information about the exposure. This approach was applied to the issue of occupational inhalation of uranium dust through:

- the characterisation of internal exposure at different workplaces by the estimation of internal dose received from a unit intake,
- the estimation of doses received in mines and mills for an hour exposure to a unit air contamination.

The results were compared to those obtained from deterministic and probabilistic approaches.

3.2 Uncertainty modelling

3.2.1 General approach

The possibilist and probabilistic methods for direct propagation of uncertainty were applied in prospective dosimetry to the common case of an occupational contamination by inhalation of

[1] Some dissolved material can be retained in the airways parenchyma before dissolution: it is the bound fraction f_b dissolving at a rate s_b. From lack of concluding evidence, it is ignored (f_b =0) unless specific inofrmation is available (ICRP, 1994a).

uranium. The dose due to ^{234}U in various chemical forms was estimated for the purpose of comparison of the results obtained from the different methods. Consistently with the philosophy of the recommendations of the ICRP, the uncertainty considered here is relative to the nature of the exposure but not to the physiology of the exposed individual. The worker is thus represented by the reference man of the ICRP. The models used are the HRTM (ICRP, 1994a), the reference biokinetic model for uranium as well as the dosimetric models of the ICRP (ICRP, 1979). Because the HATM is not implemented in our software yet, the older gastro-intestinal tract model is applied here. The uncertain parameters concern the physico-chemical form of the uranium: AMAD, absorption rates s_p, s_{pt}, s_t, and fraction f_1 of activity absorbed in the gut (which is equivalent to f_A in the HATM). The other parameters of the models are fixed at their reference value. s_p, s_{pt}, s_t and f_1 are assumed to be highly correlated but independent of the AMAD.

The results of interest are the committed effective dose e_{50}, the committed equivalent doses to the lung h_{lung}, to the extrathoracic airways h_{ET} and to the haematopoietic stem cells (red bone marrow) h_{RBM} per unit intake ($Sv.Bq^{-1}$) for the characterisation of exposure; and the equivalent doses to the lung H_{lung}, and to the red bone marrow H_{RBM} for a one-hour exposure in mines and mills. They were calculated with the software DCAL on the basis of the ICRP models.

To perform the statistical calculations, the software Statistical UNcertainty and SEnsitivity Tools (SUNSET, IRSN, France) was used. It allows random or Latin hypercube sampling of a set of values for a parameter from a given PDF or possibility distribution in order to perform Monte-Carlo, probabilistic or Dempster-Shafer calculation with the RaFu method (Section 2.4.4). SUNSET was connected to DCAL to calculate the dose corresponding to the parameters sets sampled by SUNSET. The statistical analysis and plotting of the results was performed with Excel® (Microsoft®, USA).

Three, deterministic, probabilistic and Dempster-Shafer, approaches were applied to evaluate the uncertainty on the dose. It is quantified by the ratio of the:

- endpoints of the interval from the deterministic calculation,
- 95^{th} percentile to the 5^{th} percentile of the CDF from the probabilistic calculation,
- 95^{th} percentile of the lower CDF to the 5^{th} percentile of the upper CDF from the Dempster-Shafer calculation.

To perform a possibilist calculation, the variation of the result as a function of the variation of each uncertain parameter must be monotonic. This property was verified for each variable parameter of the dose calculation in its range of variation. For the purpose of comparison between the probabilistic and Dempster-Shafer method, the same mathematical function was used to represent the knowledge about the possible values of a parameter as either a PDF or a possibility distribution.

3.2.2 Characterisation of internal exposure at different workplaces

The prime industrial importance of the uranium fuel cycle makes it a major issue for radiation protection. Various chemical forms of uranium with significantly different properties, especially

regarding solubility, are handled during the process of the nuclear fuel which can cause a spectrum of scenarios of internal contamination (Table 3.1). Extensive generic and workplace specific studies were therefore performed to quantify and prevent the risk of contamination by uranium. The significant information reported about uranium processing was the reason to choose it as a situation of interest for testing the different methods of estimation of the uncertainty in prospective dosimetry.

Table 3.1: Compounds processed in five French nuclear facilities (AREVA NC company).

Facility	Handled compounds
COMURHEX Malvesi	U_3O_8, UF_4, UO_2
FBFC Pierrelatte	U_3O_8, UO_2
COGEMA Pierrelatte	U_3O_8, UO_4, UO_2
COMURHEX Pierrelatte	U_3O_8, UF_4
FBFC Romans	U_3O_8, UO_4, UO_2

A literature review was carried out to gather the current knowledge about AMAD, s_p, s_{pt}, s_t and f_1 (Appendixes). This knowledge was used to model the uncertainties on the parameters. The AMAD is assumed independent of the uranium compound but dependent on the considered facility. The absorption rates are assumed to be independent of the plant but dependent on the compound. f_1 is modelled by the same distribution for all plants and compounds.

Chazel *et al* (2001), Ansoborlo *et al* (2002), Stradling *et al* (2002b), Pellow *et al* (2003) have determined values of the absorption rates of U_3O_8, UO_2, UO_4, UF_4 from *in vitro* or *in vivo* measurements. Harrison *et al* (2001), Zamora *et al* (2002, 2003) measured f_1 from environmental contamination by uranium. The AMAD of uranium aerosols at the different facilities were measured by Andre *et al* (1989), Ansoborlo *et al* (1997, 2002), Chazel *et al* (2000).

The available data was judged to be too scarce to support a realistic PDF for AMAD and absorption rates. Therefore a less stringent distribution of possibility was assigned to all parameters except f_1.

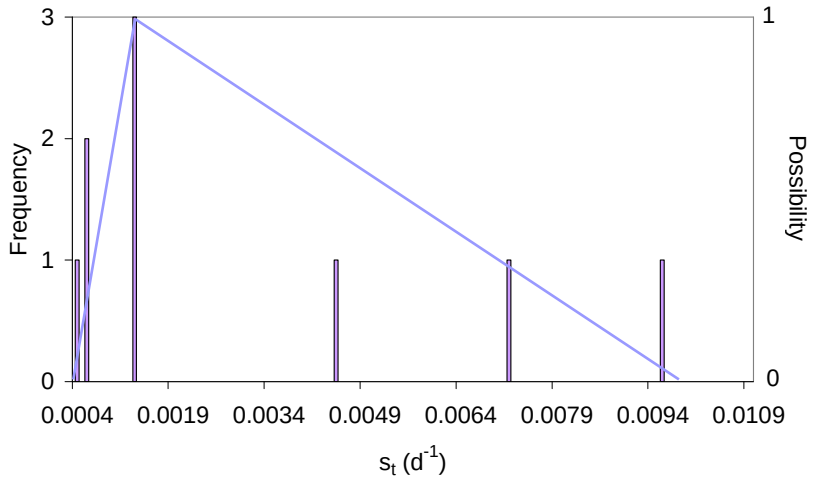

Figure 3.1: Frequency of s_t values for U_3O_8 in three AREVA NC facilities over scaled intervals (bars). Selected distribution of possibility (blue lines).

To determine a proper distribution of possibility, the frequency of values reported in the literature was plotted over consistently scaled ranges. Histograms were obtained as shown in Fig. 3.1 for the absorption rate s_t. The distributions of possibility were selected by expert judgement based on the histograms. Fig. 3.1 presents this selection for s_t for U_3O_8.

Regarding f_1, the numerous measured values reported in the literature justify the use of a PDF. The histogram of these values is consistent with a log-normal distribution of geometric mean 0.01 and geometric standard deviation 2.46 (Fig. 3.2) as confirmed by a successful chi-squared test.

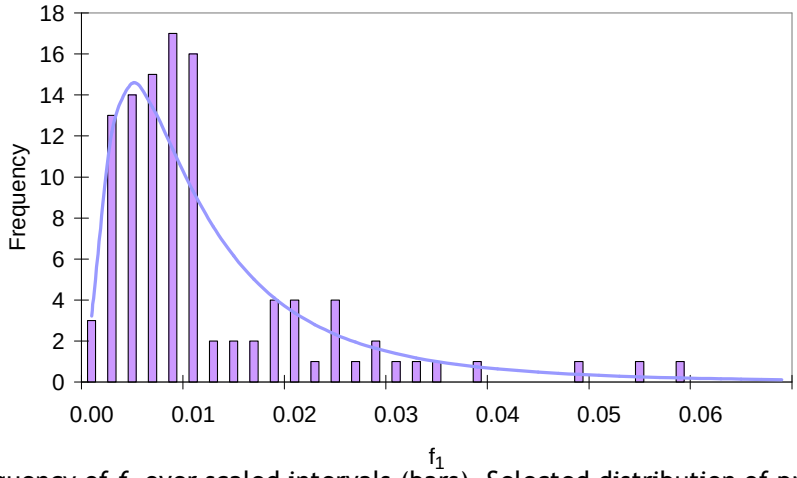

Figure 3.2: Frequency of f_1 over scaled intervals (bars). Selected distribution of probability (blue curve): lognormal distribution with geometric mean 0.01 and geometric standard deviation 2.46.

An aerosol is usually composed of particles with a lognormal distribution of diameters (Dorrian, 1997). This distribution is characterized by its median, AMAD, and geometric standard deviation, σ_g. After summing the diameter distributions observed at each facility, the distribution of possibility for the AMAD at this facility is defined as shown in Fig. 3.3. It is assumed to be trapezoid with the endpoints of its support being the values of 50% frequency and the endpoints of its core being the values of 90% frequency. The possibility is zero out of the support of the trapezoid.

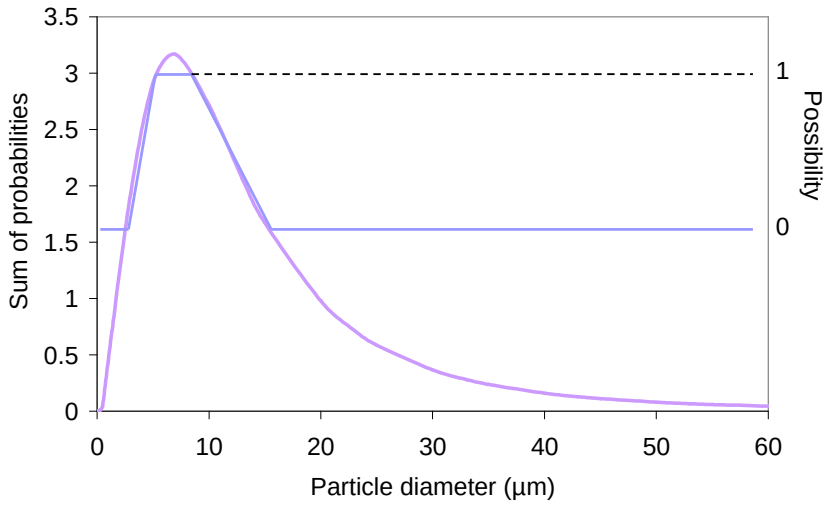

Figure 3.3: Sum of the distributions of the particle diameters observed in the COMURHEX Malvesi plant (purple curve) and distribution of possibility of the AMAD in this facility (blue lines): for diameters with a frequency higher than 90 %, it is totally possible to be the AMAD of a ponctual contamination, diameters with a frequency higher than 50 % can be AMAD of a ponctual contamination but for diameters with frequency lower than 50 %, it is impossible to AMADs.

The retained distributions of possibility and PDFs for the different facilities are summarized in Table 3.2.

Table 3.2: Distributions of possibility and probability used to assess uncertainties from a contamination at different workplaces within the Dempster-Shafer approach. GSD, geometric standard deviation.

Compound and workplace	Parameter	Theory	Distribution
U_3O_8 at COMURHEX Malvesi	AMAD	Possibility	Trapezoid with support 2.2–15 µm and core 5–10 µm
	s_p	Possibility	Uniform over 0.02-0.11 d^{-1}
	s_{pt}	Possibility	Uniform over 0.3–2.6 d^{-1}
	s_t	Possibility	Triangle with support 3.5 x 10^{-4}-9.5 x 10^{-3} d^{-1} and mode 1.3 x 10^{-3} d^{-1}
	f_1	Probability	Lognormal with geometric mean 0.01 and GSD 2.46
UF_4 at COMURHEX Malvesi	AMAD	Possibility	Trapezoid with support 2.2–15 µm and core 5–10 µm
	s_p	Possibility	Triangle with support 5.5 x 10^{-2}-0.5 d^{-1} and mode 0.15 d^{-1}
	s_{pt}	Possibility	Trapezoid with support 0.05–0.14 d^{-1} and core 0.09-0.12 d^{-1}
	s_t	Possibility	Triangle with support 8.0 x 10^{-4}-8.0 x 10^{-3} d^{-1} and mode 3.0 x 10^{-3} d^{-1}
	f_1	Probability	Lognormal with geometric mean 0.01 and GSD 2.46
UO_2 at COMURHEX Malvesi	AMAD	Possibility	Trapezoid with support 2.2–15 µm and core 5–10 µm
	s_p	Possibility	Uniform over 0.01-0.06 d^{-1}
	s_{pt}	Possibility	Triangle with support 0-1.6 d^{-1} and mode 1.2 d^{-1}
	s_t	Possibility	Triangle with support 1.0 x 10^{-4}-1.7 x 10^{-3} d^{-1} and mode 6.0 x 10^{-4} d^{-1}
	f_1	Probability	Lognormal with geometric mean 0.01 and GSD 2.46
U_3O_8 at FBFC Pierrelatte	AMAD	Possibility	Trapezoid with support 2.2–15 µm and core 3–7 µm
	s_p	Possibility	Uniform over 0.02-0.11 d^{-1}
	s_{pt}	Possibility	Uniform over 0.3–2.6 d^{-1}
	s_t	Possibility	Triangle with support 3.5 x 10^{-4}-9.5 x 10^{-3} d^{-1} and mode 1.3 x 10^{-3} d^{-1}
	f_1	Probability	Lognormal with geometric mean 0.01 and GSD 2.46
UO_2 at FBFC Pierrelatte	AMAD	Possibility	Trapezoid with support 2.2–15 µm and core 3–7 µm
	s_p	Possibility	Uniform over 0.01-0.06 d^{-1}
	s_{pt}	Possibility	Triangle with support 0-1.6 d^{-1} and mode 1.2 d^{-1}

UO_2 at FBFC Pierrelatte	s_t	Possibility	Triangle with support 1.0 x 10^{-4}-1.7 x 10^{-3} d^{-1} and mode 6.0 x 10^{-4} d^{-1}
	f_1	Probability	Lognormal with geometric mean 0.01 and GSD 2.46
U_3O_8 at COGEMA Pierrelatte	AMAD	Possibility	Trapezoid with support 2.2–15 µm and core 4–9 µm
	s_p	Possibility	Uniform over 0.02-0.11 d^{-1}
	s_{pt}	Possibility	Uniform over 0.3–2.6 d^{-1}
	s_t	Possibility	Triangle with support 3.5 x 10^{-4}-9.5 x 10^{-3} d^{-1} and mode 1.3 x 10^{-3} d^{-1}
	f_1	Probability	Lognormal with geometric mean 0.01 and GSD 2.46
UO_4 at COGEMA Pierrelatte	AMAD	Possibility	Trapezoid with support 2.2–15 µm and core 4–9 µm
	s_p	Possibility	Uniform over 0.15-0.9 d^{-1}
	s_{pt}	Possibility	Triangle with support 0.1-0.14 d^{-1} and mode 0.12 d^{-1}
	s_t	Possibility	Uniform over 8.0 x 10^{-3}-2.5 x 10^{-2} d^{-1}
	f_1	Probability	Lognormal with geometric mean 0.01 and GSD 2.46
UO_2 at COGEMA Pierrelatte	AMAD	Possibility	Trapezoid with support 2.2–15 µm and core 4–9 µm
	s_p	Possibility	Uniform over 0.01-0.06 d^{-1}
	s_{pt}	Possibility	Triangle with support 0-1.6 d^{-1} and mode 1.2 d^{-1}
	s_t	Possibility	Triangle with support 1.0 x 10^{-4}-1.7 x 10^{-3} d^{-1} and mode 6.0 x 10^{-4} d^{-1}
	f_1	Probability	Lognormal with geometric mean 0.01 and GSD 2.46
U_3O_8 at COMURHEX Pierrelatte	AMAD	Possibility	Trapezoid with support 2.2–17 µm and core 4–10 µm
	s_p	Possibility	Uniform over 0.02-0.11 d^{-1}
	s_{pt}	Possibility	Uniform over 0.3–2.6 d^{-1}
	s_t	Possibility	Triangle with support 3.5 x 10^{-4}-9.5 x 10^{-3} d^{-1} and mode 1.3 x 10^{-3} d^{-1}
	f_1	Probability	Lognormal with geometric mean 0.01 and GSD 2.46
UF_4 at COMURHEX Pierrelatte	AMAD	Possibility	Trapezoid with support 2.2–17 µm and core 4–10 µm
	s_p	Possibility	Triangle with support 5.5 x 10^{-2}-0.5 d^{-1} and mode 0.15 d^{-1}
	s_{pt}	Possibility	Trapezoid with support 0.05–0.14 d^{-1} and core 0.09-0.12 d^{-1}
	s_t	Possibility	Triangle with support 8.0 x 10^{-4}-8.0 x 10^{-3} d^{-1} and mode 3.0 x 10^{-3} d^{-1}
	f_1	Probability	Lognormal with geometric mean 0.01 and GSD 2.46
U_3O_8 at FBFC Romans	AMAD	Possibility	Trapezoid with support 0.75–17.5 µm and core 0.9–10 µm
	s_p	Possibility	Uniform over 0.02-0.11 d^{-1}

U_3O_8 at FBFC Romans	s_{pt}	Possibility	Uniform over 0.3–2.6 d^{-1}
	s_t	Possibility	Triangle with support 3.5 x 10^{-4}-9.5 x 10^{-3} d^{-1} and mode 1.3 x 10^{-3} d^{-1}
	f_1	Probability	Lognormal with geometric mean 0.01 and GSD 2.46
UO_4 at FBFC Romans	AMAD	Possibility	Trapezoid with support 0.75–17.5 µm and core 0.9–10 µm
	s_p	Possibility	Uniform over 0.15-0.9 d^{-1}
	s_{pt}	Possibility	Triangle with support 0.1-0.14 d^{-1} and mode 0.12 d^{-1}
	s_t	Possibility	Uniform over 8.0 x 10^{-3}-2.5 x 10^{-2} d^{-1}
	f_1	Probability	Lognormal with geometric mean 0.01 and GSD 2.46
UO_2 at FBFC Romans	AMAD	Possibility	Trapezoid with support 0.75–17.5 µm and core 0.9–10 µm
	s_p	Possibility	Uniform over 0.01-0.06 d^{-1}
	s_{pt}	Possibility	Triangle with support 0-1.6 d^{-1} and mode 1.2 d^{-1}
	s_t	Possibility	Triangle with support 1.0 x 10^{-4}-1.7 x 10^{-3} d^{-1} and mode 6.0 x 10^{-4} d^{-1}
	f_1	Probability	Lognormal with geometric mean 0.01 and GSD 2.46

3.2.3 Uranium mining and milling

The exposure of uranium miners is usually not monitored by individual bioassay analysis but by sampling and measurement of ambient air. The main component of this exposure is radon gas and its short-lived progeny. However, uranium miners are also exposed to inhalation of long-lived radionuclides in the ore dust and to external gamma irradiation. These three sources of exposure were taken into account in a reconstruction of the lung and bone marrow doses received by a cohort of German, Czech and French miners for the purpose of an epidemiological study within the project Alpha-Risk (Marsh *et al*, 2008a). In this study, only the dose due to an inhalation of ^{234}U was considered in order to allow the comparison of the methods of uncertainty assessment on a simple dosimetric problem.

Dorrian and Bailey (1995) published values of AMAD of ore dust in uranium mines and mills. Their results were used to model the uncertainty on the AMAD in the same way as in Fig. 3.3. The values of absorption rates for uranium mines and mills derived from the literature (Eidson and Mewhinney, 1980, Duport *et al*, 1991, Duport, 1994, Stradling *et al*, 2002) are not uniformly distributed. Many small values as well as a few very large values are recorded. As an example, the empirical histogram of s_p values for mines is plotted in Fig. 3.4. The possibility distribution chosen to represent the collected information is a polygon defined by couples of abscissa and ordinates being respectively the middle of the intervals of the histogram in logarithmic scale and their frequencies divided by the width of the corresponding interval (Fig. 3.4). A similar shape of

possibility distribution was retained for s_{pt}, and s_t for mills. s_t for mines is modelled by a uniform possibility distribution between 10^{-3} and 2.9 10^{-2} d^{-1} due to the very scarce available information. The variability of f_1 is modelled by the PDF of Fig. 3.2. The parameters distributions are summarized in Table 3.3.

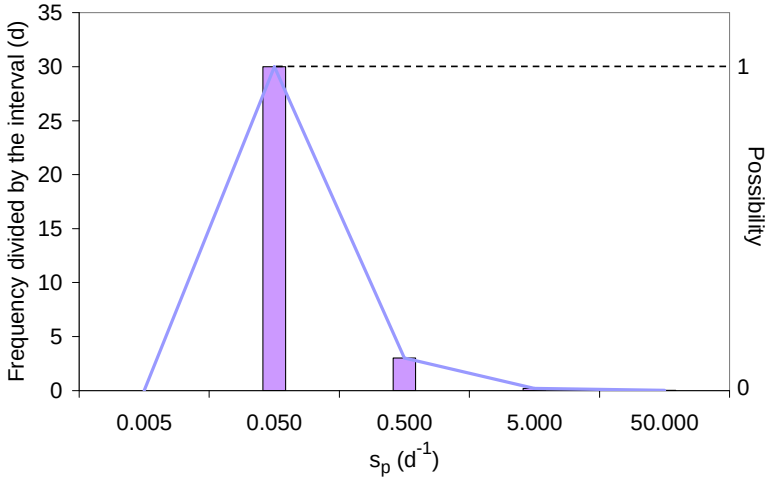

Figure 3.4: Empirical histogram of s_p values in uranium mines on a logarithmic scale (bars). The value of the abscissa is the middle of the interval containing the reported values. The ordinate is the frequency divided by the length of the interval. The lowest observed value is more than 10^{-2} d^{-1}. Polygonal possibility distribution built from the histogram of s_p (blue lines).

Table 3.3: Possibility and probability distributions of the uncertain parameters in the uranium mines and mills for the Dempster-Shafer calculation.

	Parameter	Theory	Distribution
mines	AMAD	Possibility	Triangular with support 3–23 µm and mode 6 µm
	s_p	Possibility	Polygonal defined by (abscissa (d^{-1}), ordinate): (0.005, 0); (0.05, 1); (0.5, 0.1); (5, 0.067); (50, 6.7 x 10^{-4}); (500, 0)
	s_{pt}	Possibility	Polygonal defined by (abscissa (d^{-1}), ordinate): (0.05, 0); (0.5, 1); (5; 0.0167); (5, 0.005); (50, 0)
	s_t	Possibility	Uniform with support 0.001-0.029 d^{-1}
	f_1	Probability	Lognormal with geometric mean 0.01 and GSD 2.46
mills	AMAD	Possibility	Uniform with support 0.5–15 µm
	s_p	Possibility	Polygonal defined by (abscissa (d^{-1}), ordinate): (5 x 10^{-5}, 0); (5 x 10^{-4}, 1); (0.005, 0.5); (0.05, 0.21); (0.5, 0.007); (5, 4 x 10^{-4}); (50, 1 x 10^{-5}); (500, 0)
	s_{pt}	Possibility	Polygonal defined by (abscissa (d^{-1}), ordinate): (5 x 10^{-5}, 0); (5 x 10^{-4}, 0.1); (5 x 10^{-3}, 0.2); (0.05, 0.01); (0.5, 3.67 x 10^{-3}); (5, 5.44 x 10^{-4}); (50, 0)
	s_t	Possibility	Polygonal defined by (abscissa (d^{-1}); ordinate): (5 x 10^{-6}; 0); (5 x 10^{-5}; 0.77); (5 x 10^{-4}; 1); (0.005; 0.18); (0.05; 1.54 x 10^{-3}); (0.5; 0)
	f_1	Probability	Lognormal with geometric mean 0.01 and GSD 2.46

For purely probabilistic calculation, the PDF that appeared to be the most consistent with the empirical data of s_p, s_{pt}, and s_t in the uranium mines and mills are polygonal distributions which are indicated in Table 3.4. To use the same polygonal distribution as for the possibilist study was not possible because the family of probability derived from the possibilist polygonal distribution does not comprise the corresponding probabilistic polygonal distribution. For the other parameters, the same shape as the possibility distributions is used for the distributions of probability (Table 3.4).

Table 3.4: Probability distributions of the parameters used for the probabilistic calculation for uranium mines and mills.

	Parameter	Theory	Distribution
mines	AMAD	Probability	Triangular with support 3–23 µm and mode 6 µm
	s_p	Probability	Polygonal defined by (abscissa (d^{-1}); cumulated ordinate): (0.005; 0); (0.05; 0.5); (0.5; 0.95); (5; 0.999); (50; 0.9995); (500; 1)
	s_{pt}	Probability	Polygonal defined by (abscissa (d^{-1}); cumulated ordinate): (0.05; 0); (0.5; 0.5); (5; 0.99); (50; 0.999); (500; 1)
	s_t	Probability	Uniform with support 0.001-0.029 d^{-1}
	f_1	Probability	Lognormal with geometric mean 0.01 and GSD 2.46
mills	AMAD	Probability	Uniform with support 0.5–15 µm
	s_p	Probability	Polygonal defined by (abscissa (d^{-1}); ordinate): (5 x 10^{-5}; 0); (5 x 10^{-4}; 0.5); (0.005; 0.7); (0.05; 0.9); (0.5; 0.995); (5; 0.9999); (500; 1)
	s_{pt}	Probability	Polygonal defined by (abscissa (d^{-1}); ordinate): (5 x 10^{-5}; 0); (5 x 10^{-4}; 0.5); (5 x 10^{-3}; 0.9); (0.05; 0.995); (0.5; 0.999); (5; 0.9999); (50; 1)
	s_t	Probability	Polygonal defined by (abscissa (d^{-1}); ordinate): (5 x 10^{-6}; 0); (5 x 10^{-5}; 0.2); (5 x 10^{-4}; 0.5); (0.005; 0.9); (0.05; 0.999); (0.5; 1)
	f_1	Probability	Lognormal with geometric mean 0.01 and GSD 2.46

The equivalent dose *H* committed during 50 years, in $Sv.h^{-1}$, received by a tissue during one hour of work in a mine or mill due to inhalation of ^{234}U is calculated as

$$H = C \times B \times h \,, \qquad \text{Equation 3.1}$$

where *C* is the air contamination in $Bq.m^{-3}$, *B* is the breathing rate in $m^3.h^{-1}$, and *h* is the equivalent dose to the organ per unit of intake of ^{234}U in $Sv.Bq^{-1}$. The uncertainty on the dose per unit intake was estimated and then propagated to the uncertainty on the hourly dose received by miners from a unit air contamination. To obtain the dose received for a specific exposure, *H* should be multiplied by the duration of exposure and by the mean air concentration.

The uncertainty on the measurement from a static air sampler was modelled by a normal PDF with a mean of 1 $Bq.m^{-3}$ and a standard deviation of 0.5 (Duport, 1994).

The breathing rate changes according to physical activity of the miner. Breathing rate is considered here as an exposure condition to derive inhaled activity but it is acknowledged that it

can be interpreted as an individual parameter or taken as a fixed value. Four situations were considered: heavy work, intermediate work, light work, unknown work. Each is modelled by a specific possibility distribution. The most possible breathing rate was chosen on the basis of data collected in the Alpha-Risk project (Marsh *et al*, 2008a) including the default values recommended by the ICRP (ICRP, 1994a). The possibility distributions for the breathing rate are described in Fig. 3.5. The unknown work situation corresponds to a total lack of knowledge about the physical activity of the miner. It therefore results in a very large possibility distribution. For comparison purpose, a probabilistic calculation was carried out with a normal PDF with a mean equal to 1.3 $m^3.h^{-1}$ and a standard deviation of 0.19 $m^3.h^{-1}$ (ICRP, 1994a), to model the breathing rate in case of an unknown work.

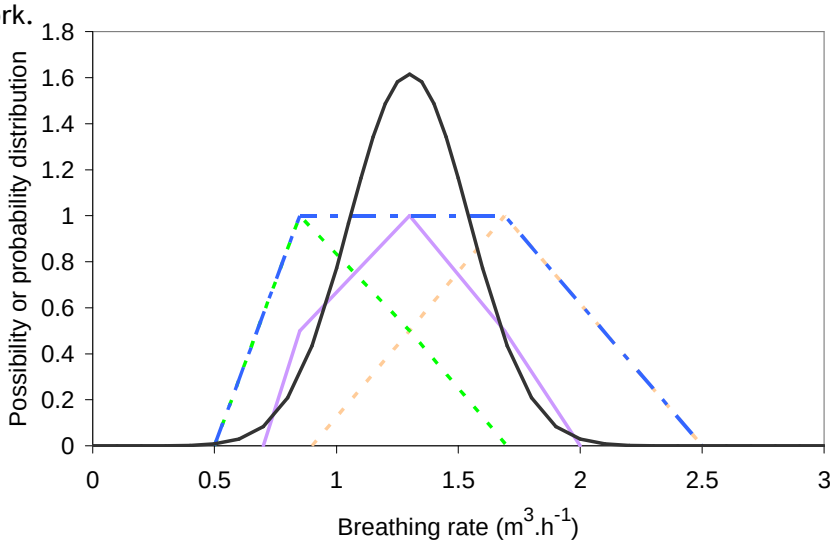

Figure 3.5: Possibility distributions which model the breathing rate for heavy (orange broken lines), intermediate (purple solid lines), light (green broken lines) and unknown work (blue-dashed lines). PDF of the breathing rate for an unknown work (black curve).

3.3 Results

3.3.1 Characterisation of internal exposure at different workplaces

These distributions were used as input into SUNSET and DCAL to assess the uncertainties on the tissue equivalent doses and on the effective dose per unit intake by Dempster-Shafer calculation. For comparison purpose, a deterministic interval calculation was performed with the extreme values of each parameter and a central estimate was determined by choosing the mode values. A fully probabilistic calculation was done through Monte-Carlo method by substituting PDFs for the possibility distributions. The results for e_{50} are presented for COMURHEX Malvesi as the upper and lower CDF from the Dempster-Shafer calculation, the single CDF from the probabilistic calculation, the endpoints of the interval and the central estimate from the deterministic calculation (Fig. 3.6). Within the probabilistic methodology, the uncertainty about any variable is equivalent to its variability. On the other hand, the uncertainty calculated in the Dempster-Shafer framework may be understood as the sum of the imprecision and of the variability of the result. This is represented

by arrows in Fig. 3.6. Table 3.5 summarizes the uncertainty on the doses per unit intake for the different workplaces as calculated by the three different methods.

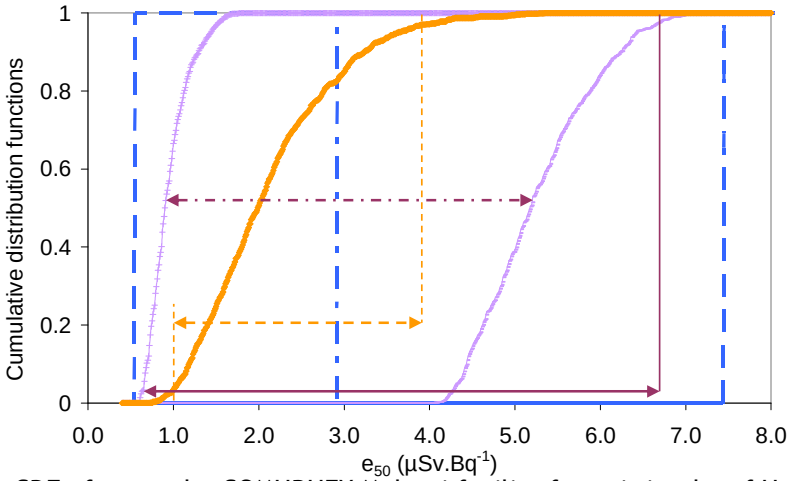

Figure 3.6: CDF of e_{50} at the COMURHEX Malvesi facility for unit intake of U_3O_8. Curves: deterministic (broken blue), probabilisitc (orange), Dempster-Shafer (purple) calculations. Arrows, probabilistic uncertainty (broken orange), Dempster-Shafer uncertainty (solid purple) and imprecision (dotted-dashed purple)

Table 3.5: Uncertainty factors on the dose per unit intake for different workplaces; columns, calculation method; lines, type of dose.

Compound and workplace	Dose ($Sv.Bq^{-1}$) \ Calculation	Deterministic	Probabilistic	Dempster-Shafer
U_3O_8 at COMURHEX Malvesi	e_{50}	13	3	10
	h_{ET}	11	5	9
	h_{lung}	15	4	12
	h_{RBM}	36	5	13
UF_4 at COMURHEX Malvesi	e_{50}	27	5	15
	h_{ET}	9	10	17
	h_{lung}	43	6	22
	h_{RBM}	19	4	8
UO_2 at COMURHEX Malvesi	e_{50}	32	3	6
	h_{ET}	53	2	3
	h_{lung}	36	4	9
	h_{RBM}	75	6	16
U_3O_8 at FBFC Pierrelatte	e_{50}	14	4	10
	h_{ET}	11	5	10
	h_{lung}	15	4	12
	h_{RBM}	36	5	12
UO_2 at FBFC Pierrelatte	e_{50}	32	3	6
	h_{ET}	53	2	3
	h_{lung}	36	4	9
	h_{RBM}	75	6	19

U_3O_8 at COGEMA Pierrelatte	e_{50}	14	4	10
	h_{ET}	11	5	10
	h_{lung}	15	4	12
	h_{RBM}	36	5	13
UO_4 at COGEMA Pierrelatte	e_{50}	17	5	14
	h_{ET}	9	7	9
	h_{lung}	25	6	21
	h_{RBM}	12	4	7
UO_2 at COGEMA Pierrelatte	e_{50}	32	3	6
	h_{ET}	53	2	3
	h_{lung}	36	4	9
	h_{RBM}	75	6	17
U_3O_8 at COMURHEX Pierrelatte	e_{50}	16	4	12
	h_{ET}	10	5	9
	h_{lung}	19	5	14
	h_{RBM}	44	6	15
UF_4 at COMURHEX Pierrelatte	e_{50}	32	5	18
	h_{ET}	9	10	17
	h_{lung}	52	7	28
	h_{RBM}	23	5	10
U_3O_8 at FBFC Romans	e_{50}	16	4	12
	h_{ET}	20	5	19
	h_{lung}	23	6	19
	h_{RBM}	43	7	20
UO_4 at FBFC Romans	e_{50}	23	6	19
	h_{ET}	12	7	13
	h_{lung}	34	9	30
	h_{RBM}	15	5	10
UO_2 at FBFC Romans	e_{50}	48	3	7
	h_{ET}	90	2	6
	h_{lung}	55	6	15
	h_{RBM}	88	8	28

mines	e_{50}	9	11	35
	h_{ET}	60	39	71
	h_{lung}	95	18	57
	h_{RBM}	151	7	8
mills	e_{50}	17	24	90
	h_{ET}	60	178	265
	h_{lung}	234	34	163
	h_{RBM}	151	40	98

3.3.2 *Uncertainty in dose received by a tissue in uranium mining and milling*

It was assumed that the breathing rate, the air contamination and the dose per unit intake were totally independent. SUNSET sampled several values of these parameters according to their distributions which were multiplied in Excel®. A random value from the upper (lower) CDF of *h* was multiplied by a random value from the upper (lower) CDF of *B* and by a random value of the CDF of *C* to obtain the upper (lower) CDF for the dose *H* (Eq. 3.1). Fig. 3.7 presents the CDF of doses to the lung and to the bone marrow for a unit air contamination. The estimated uncertainty factors are summarized in Tables 3.6-3.7.

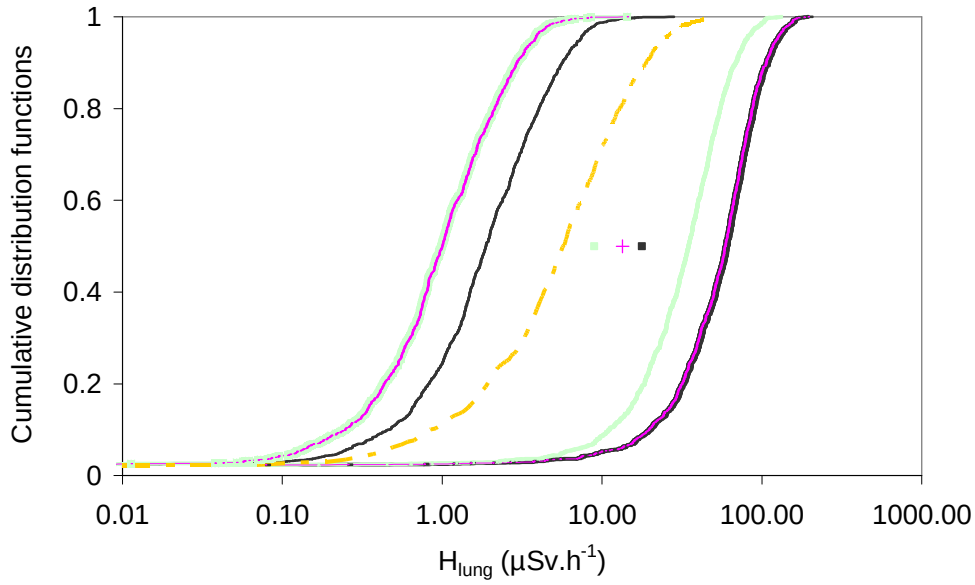

Figure 3.7: CDF of the committed equivalent dose to the lung for one hour of work in a uranium mine contaminated by 1 Bq of ^{234}U per m^3 of air at different levels of physical activity [light (green curves), heavy (black curves) and unknown work (pink curves)]. The upper CDF is on the left of the figure and the lower CDF is on the right. The points are the central estimates of dose for reference values of the parameters (same colors). The CDF of the probabilistic calculation is the orange broken line.

Table 3.6: Uncertainty factors estimated for the equivalent dose to the lung of uranium miners and millers under the same hypotheses as in Fig. 3.7. H_{95}, 95th percentile. H_5, 5th percentile.

	Situation of work	Central estimate (Sv.h^{-1})	H_{95} (Sv.h^{-1})	H_5 (Sv.h^{-1})	Uncertainty factor
mines	Heavy	1.8 x 10^{-5}	1.2 x 10^{-4}	2.3 x 10^{-7}	522
	Intermediate	1.4 x 10^{-5}	9.9 x 10^{-5}	1.6 x 10^{-7}	619
	Light	8.9 x 10^{-6}	7.9 x 10^{-5}	1.2 x 10^{-7}	658
	Unknown	1.3 x 10^{-5}	1.2 x 10^{-4}	1.2 x 10^{-7}	1,020
	Probabilistic calculation	1.3 x 10^{-5}	2.4 x 10^{-5}	4.3 x 10^{-7}	55
mills	Heavy	3.4 x 10^{-5}	3.4 x 10^{-4}	2.8 x 10^{-7}	1,211
	Intermediate	2.6 x 10^{-5}	2.8 x 10^{-4}	2.0 x 10^{-7}	1,365
	Light	1.7 x 10^{-5}	2.2 x 10^{-4}	1.5 x 10^{-7}	1,497
	Unknown	2.6 x 10^{-5}	3.4 x 10^{-4}	1.5 x 10^{-7}	2,340
	Probabilistic calculation	2.6 x 10^{-5}	2.2 x 10^{-4}	2.8 x 10^{-7}	782

Table 3.7: Uncertainty factors estimated for the equivalent dose to the bone marrow of uranium miners and millers under the same hypotheses as in Fig. 3.7. H_{95}, 95th percentile. H_5, 5th percentile.

	Situation of work	Central estimate (Sv.h^{-1})	H_{95} (Sv.h^{-1})	H_5 (Sv.h^{-1})	Uncertainty factor
mines	Heavy	1.7 x 10^{-7}	1.3 x 10^{-6}	6.3 x 10^{-9}	210
	Intermediate	2.2 x 10^{-7}	1.1 x 10^{-6}	4.7 x 10^{-9}	230
	Light	1.5 x 10^{-7}	8.7 x 10^{-7}	3.5 x 10^{-9}	250
	Unknown	2.2 x 10^{-7}	1.3 x 10^{-6}	3.5 x 10^{-9}	390
	Probabilistic calculation	2.2 x 10^{-7}	4.6 x 10^{-7}	1.7 x 10^{-8}	27
mills	Heavy	8.4 x 10^{-8}	1.7 x 10^{-6}	2.8 x 10^{-9}	615
	Intermediate	6.4 x 10^{-8}	1.4 x 10^{-6}	2.0 x 10^{-9}	688
	Light	4.2 x 10^{-8}	1.1 x 10^{-6}	1.5 x 10^{-9}	713
	Unknown	6.3 x 10^{-8}	1.7 x 10^{-6}	1.5 x 10^{-9}	1,140
	Probabilistic calculation	6.3 x 10^{-8}	1.1 x 10^{-6}	3.2 x 10^{-9}	352

3.4 Discussion

3.4.1 Confidence intervals

The results show, except for $h_{ET,}$ that the estimated uncertainty on the dose per unit intake gradually decreases, depending on the approach, from the deterministic interval to the result of the Dempster-Shafer calculation to the probabilistic one and finally to the single deterministic central estimate. The deterministic calculation from the mode values of the parameters provides a central estimate which is usually reasonable but with no information about its reliability. In case the input parameters are badly estimated, the result could be strongly biased. The deterministic interval calculation is very conservative as the true result is to be included within the interval derived from the most and the least penalizing values for each parameter. But it is not accurate since no

information is provided about the likeliness of different values within the interval. The deterministic interval should contain all the values calculated with the probabilistic or Dempster-Shafer methods.

For h_{ET}, the superior bound of the deterministic interval is lower than the extreme values of the lower cumulative distribution function from the Dempster-Shafer calculation (Table 3.5). This inconsistent result can be explained by a non-monotony of the dose with the AMAD in the considered solubility range. To solve this problem, a more accurate parametric study should be carried out in order to find the actual most and least penalizing values of each parameter.

Probabilistic and possibilist approaches provide more information on the uncertainty. Still, a much narrower confidence interval on the dose and a smaller uncertainty factor are estimated by the mean of a probabilistic calculation than by the Dempster-Shafer method. This is explained by the richer information modelled by a PDF than by a possibility distribution, independently of whether this information is actually available or is arbitrarily assumed. The Dempster-Shafer calculation seems more consistent with the real information on the input parameters by making use of a PDF when enough data about the observed frequency of the values are reported and of a possibility distribution to model imprecise information. When dealing with such imprecise information, the possibility distribution induces all the PDFs consistent with the given information and thus does not artificially reduce the confidence interval by providing arbitrary information. However the choice between probabilistic and possibilist modelling of information is subjective and should involve discussion and expert judgment.

The uncertainty on the doses e_{50}, h_{ET} and h_{lung} estimated with the Dempster-Shafer method is close to the deterministic interval, but this is not the case for the committed equivalent dose to the bone marrow, h_{RBM}. The explanation is the modelling of f_1 by a lognormal PDF which has a 90% confidence interval much smaller than the interval between the extreme observed values. The f_1 has little importance for the doses to the respiratory tract but significantly affects the activity entering into the blood and then reaching the bone marrow. Therefore, the PDF assigned to f_1 reduces the confidence interval on h_{RBM} much more than on e_{50} as compared to what would have been obtained from a possibility distribution of f_1.

3.4.2 Influence of the (in)dependence between parameters

The hypotheses of a strong correlation between s_p, s_{pt}, s_t and f_1 and of an independence of these parameters with the AMAD were made. To understand the influence of this hypothesis on the dose calculation, probabilistic and Dempster-Shafer calculations of h_{RBM} were performed under hypotheses of either total correlation or total independence between the parameters s_p, s_{pt}, s_t and f_1 of U_3O_8 at the COMURHEX Malvesi facility. The AMAD remained independent in all cases. The uncertainty factor decreased from 5 to 4 in the probabilistic calculation and from 13 to 12 in the Dempster-Shafer calculation when changing the hypothesis of full correlation to total independence. So the hypothesis of total independence during a Monte-Carlo calculation may reduce the uncertainty on the result. The variation of the uncertainty is lower for the Dempster-

Shafer calculation which is therefore less sensitive to the correlation or independence hypotheses than the probabilistic calculation. The exploration of the feasibility of intermediate hypotheses about correlation of possibilist variables is a topic of current mathematical research.

3.4.3 Uranium mining and milling

In Fig. 3.7, the dose received is dependent on the level of physical activity because it increases the breathing rate and the inhaled activity during a given time in contaminated air. The uncertainty factors estimated by the Dempster-Shafer approach are very large, up to more than a thousand. This accounts for the significant imprecision and/or variability in the information involved at every step of the calculation. The distributions of B, C and h_{RBM} or h_{ET} are consequently quite large and each of them contributes to the width of the composed uncertainty. The breathing rate of a miner of unknown work is modelled by the largest possibility distribution and thus results in the largest dose uncertainty. The uncertainty calculated from a probabilistic calculation is lower than the one from Dempster-Shafer calculation; this is consistent with the narrower distribution of the breathing rate. Further investigation of exposure parameters, such as variability of breathing rate and data from personal air samplers should help in reducing the large uncertainties reported here.

3.5 Conclusion

The Dempster-Shafer method is useful to evaluate the prospective exposure of workers when designing monitoring procedures and protection devices. Moreover, it is also well adapted when only environmental measurements of activity are available, as for uranium mines or to estimate the risk for the public due to a spread contamination of the environment. It provides a consistent tool to model the imprecision in the knowledge of calculation parameters.

As showed by this work, the Dempster-Shafer method can be easily used to realistically assess the prospective uncertainty in internal dose estimates at a characterized workplace. However, this method is presently not suitable for the inverse problem of retrospective dose calculation. Therefore, the next parts of this work, dealing with inverse propagation of uncertainty, will rather use probabilistic methods, acknowledging nonetheless their possible limitations highlighted in this chapter, depending on the quality of the available information.

CHAPTER 4

Exposure to plutonium contamination at R4-T4

A specific monitoring programme was chosen as the support of this study. The possible conditions of exposure of workers and the associated individual monitoring program are analysed in this chapter together with the resulting uncertainty on input parameters for dose calculation.

4.1 Women and men at work

The study presented here is focused on a specific group of workers of the AREVA NC reprocessing plant which extracts uranium (U) and plutonium (Pu) from the spent fuel and vitrifies residual waste (Section 1.1.2, Fig. 4.1). The group is formed of the workers of the (older) R4 and (newer) T4 facilities who perform the purification of Pu and its dispatch for recycling (Fig. 4.1).

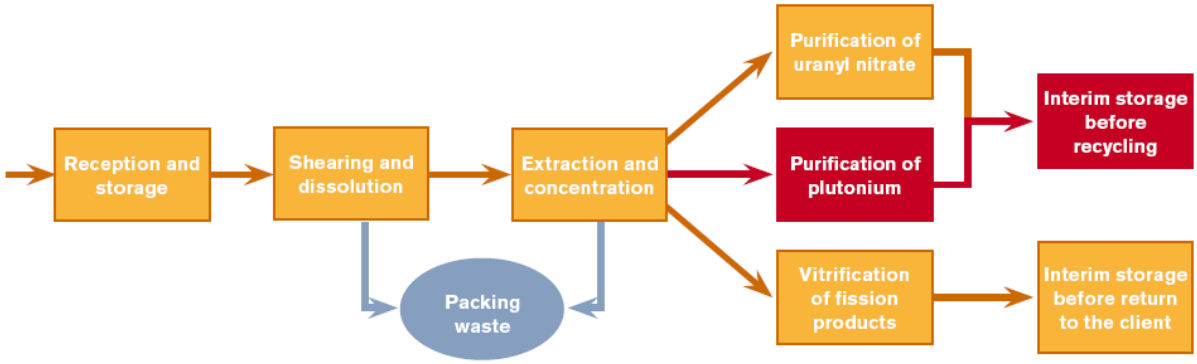

Figure 4.1: Process of the AREVA NC reprocessing plant in La Hague and the situation of R4-T4 facilities in the production line (red) (www.lahague.areva-nc.fr)

4.1.1 Process of the R4-T4 facilities

The first step is the purification of the Pu solution. In T4, purification is carried out through two successive cycles of liquid-liquid extraction and re-extraction in pulsed columns. Traces of U and residual fission products are eliminated. The solvent used is processed in T4, and what remains is sent to organic effluent processing. In R4, purification is carried out in a single extraction and re-extraction cycle using different equipment, by centrifugal extractors. At the end of the purification, Pu nitrate is obtained.

Then, Pu nitrate is extracted from the solution by the precipitation of Pu nitrate in Pu oxalate. The precipitate obtained is filtered, spun, dried and then burned at around 600-650°C during 30 minutes to give Pu dioxide (PuO_2).

After, Pu is homogenised in batches of 120 kg in T4 and 200 kg in R4. PuO_2 is placed in crimped steel cans (approximately 3 kg each). 5 such cans are packed in a case, sealed by welding with a plasma arc. Finally each case is placed in a container. Containers are checked for seals and non-contamination before being stored in workshops BSI and BST1 facilities, from where they are dispatched to plants that manufacture MOX fuel. The process is summarised in Fig. 4.2.

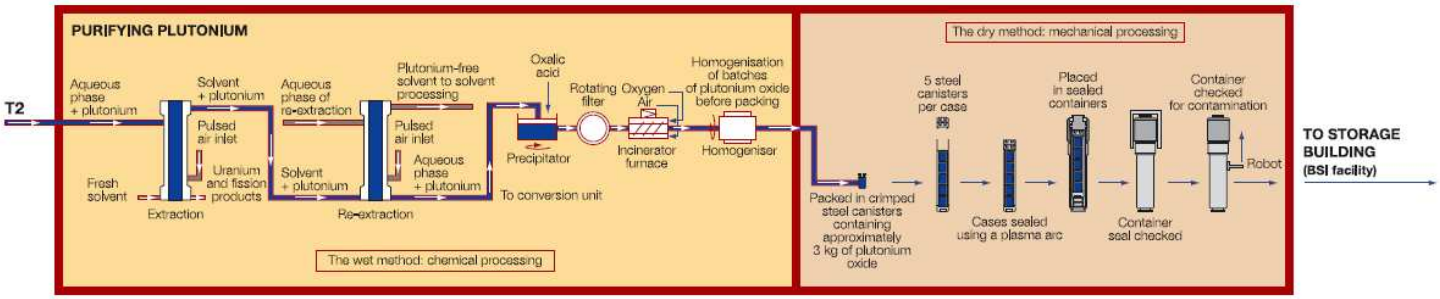

Figure 4.2: Process of R4-T4 facilities (www.lahague.areva-nc.fr)

4.1.2 Workers' occupation

Because of the automation of the process, workers spend most of their time in control room to monitor the process from a distance. No contamination can take place in this room. However, workers could be in contact with radioactive material during maintenance operations, which are:

- weekly cleaning of the rotary filter which isolates Pu oxalate precipitate,
- reintroduction in the process of remaining Pu from analysis once or twice a week,
- maintenance in case of technical disorder such as repositioning a Pu steel can in the conditioning glove box.

During these operations workers are protected from contamination by personal equipment: clothing, gloves and masks. However, inhalation of PuO_2 could still be possible.

4.2 Routine monitoring programme of internal contamination

4.2.1 Workplace monitoring

In order to detect a possible workplace contamination, air monitoring and surface activity measurement are performed in all workplaces. Surface contamination, controlled by wipe tests must be below 0.01 $Bq.cm^{-2}$ of α-activity in normal working conditions. In case of higher surface contamination, masks must be worn. Moreover, the rooms are equipped with air samplers which filters are measured weekly to monitor air contamination. The detection limit of this technique is 0.15 Bq of α-activity on the filter, equivalent to 7.5 10^{-4} $Bq.m^{-3}$ air concentration with a flow of 20 $L.min^{-1}$. These techniques allow periodic monitoring of the radiological contamination of workplaces.

In parallel, a real-time follow-up monitoring is continuously carried out by air samplers with alarm thresholds fixed to detect airborne activity which could lead to significant contamination of workers. The first alarm threshold is set at 0.074 $Bq.m^{-3}$ of α-activity and 3.7 $Bq.m^{-3}$ of ß-activity.

4.2.2 Individual monitoring

The individual bioassay monitoring in AREVA NC La Hague facility uses *in vivo* measurements of γ-emitters such as fission products and ^{241}Am and *in vitro* measurements of α-emitters such as U and Pu and ß-emitters such as tritium. The measurement technique and frequency are adapted to the individual risk of contamination (Table 4.1). A whole-body count is performed every 6 months for all workers to ensure the absence of contamination by fission products. Pu handled in mechanical processing (red part of Fig. 4.2), mainly as PuO_2 powder, is an insoluble compound weakly absorbed to blood. The corresponding risk of contamination is therefore monitored by faecal measurement, while Pu in chemical processing (yellow part of Fig. 4.2) (Pu-TBP or nitrate), soluble and readily absorbed to blood, is monitored by urine measurement. Tritium is collectively monitored by measuring a representative sample of workers.

Table 4.1: Individual monitoring of internal contamination in AREVA NC La Hague facility for the different handled compounds

Compounds	Monitoring programme
Plutonium in mechanical processing (PuO_2)	Faecal measurement every 6 months Lung count every 6 months
Plutonium in chemical processing (nitrate, Pu-TBP)	Urine measurement every 6 months
Fission products	Whole-body count every 6 months
Uranium (dioxide, nitrate or U-TBP)	Urine measurement every 6 months
Tritium (HTO)	Urine measurement every month

In vivo *measurement characteristics*

Two types of *in vivo* count are performed in AREVA NC reprocessing plant. They are characterised by their practical level which is the detection limit under the most penalizing conditions. Workers potentially exposed to less than 6 mSv per year are monitored by 3 minute whole body count carried out with a Fast-Scan system (Canberra) of practical level 300 Bq for ^{137}Cs used as a tracer of other fission products or even actinides. For workers potentially exposed to more than 6 mSv per year, 15 minute count is performed in a shielded facility. The practical level is between 3,000 and 15,000 Bq for ^{239}Pu depending on the worker morphology; 12 Bq for lung count of ^{241}Am; and 85 Bq for ^{137}Cs whole-body count.

In vitro *measurement characteristics*

A routine *in vitro* measurement is performed on a spot faecal sample or on at least 1.5 L of urine sampled over 1 to 10 days. Routine samples are collected at the workplace. For special monitoring, 24 h urine samples and 72 h faecal samples are collected. The measurement of actinides by α spectrometry after chemical preparation allows quantifying the activity of the isotopes ^{238}U, ^{236}U, ^{235}U, ^{234}U, ^{240}Pu, ^{239}Pu, ^{238}Pu, ^{241}Am, ^{244}Cm and ^{242}Cm. Due to the close α emission energies of ^{239}Pu and ^{240}Pu, these isotopes cannot be separated and their total activity is globally measured. The same applies to ^{242}Cm and ^{244}Cm.

A known quantity of ^{242}Pu or ^{233}U is added to the sample as a tracer to determine the chemical yield of the preparation (Table 4.2).

Table 4.2: Mean and standard deviation of chemical yield Y_c for the *in vitro* measurement of U and Pu at AREVA NC La Hague

	Urine measurement		Faecal measurement
Tracer	^{242}Pu	^{233}U	^{242}Pu
Y_c mean	78.6 %	70.9 %	86.0 %
Y_c standard deviation	10.9 %	11.8 %	13.6 %

The counting time is one night for special monitoring and 48 h for routine monitoring. The efficiency of detection depends on the thickness of the sample and of the solid angle between the sample and the detector. The average efficiency is 32.5 % with a standard deviation of 2.7 %.

From 24 h measurements of background, the mean background is estimated as 12.2 counts over an energy range of 2,200 keV. The width of the region of interest for ^{239}Pu is 200 keV. Therefore in routine monitoring of ^{239}Pu, the mean background is 2.2 counts per 48 h. This leads to a decision threshold of 4.2 counts per 48 h and to a practical level of 0.5 mBq of ^{239}Pu. In special monitoring, the practical level is 2 mBq of ^{239}Pu.

4.3 Isotopic composition

The isotopic compositions of the processed materials are gathered in Table 4.3 for a representative sample of different spent fuels. All of them are globally similar.

Table 4.3: Isotopic composition of Pu and Am in spent fuels handled at R4 and T4 from pressurized water reactors (PWR1 and PWR2), boiling water reactor (BWR), mixed oxide spent fuel (MOX), spent mixed oxide fuel mixed with recycled old Pu (MOX_RP)

Spent fuel origin	Isotope	Mass distribution (%)	Activity distribution (%)	α activity distribution (%)
PWR1	^{238}Pu	2.805	5.3	8.3×10^{1}
	^{239}Pu	52.479	3.6×10^{-1}	5.7
	^{240}Pu	27.684	6.9×10^{-1}	1.1×10^{1}
	^{241}Pu	8.198	9.4×10^{1}	
	^{242}Pu	8.834	3.7×10^{-3}	6.1×10^{-2}
	^{241}Am	2.18×10^{-4}	8.3×10^{-5}	1.3×10^{-3}
PWR2	^{238}Pu	2.982	4.4	8.5×10^{1}
	^{239}Pu	52.532	2.8×10^{-1}	5.4
	^{240}Pu	25.771	5.1×10^{-1}	9.7
	^{241}Pu	10.53	9.5×10^{1}	
	^{242}Pu	8.185	2.8×10^{-3}	5.4×10^{-2}
	^{241}Am	2.07×10^{-4}	6.2×10^{-5}	1.2×10^{-3}
BWR	^{238}Pu	2.94	5.4	8.3×10^{1}
	^{239}Pu	47.672	3.2×10^{-1}	4.9
	^{240}Pu	30.818	7.6×10^{-1}	1.2×10^{1}
	^{241}Pu	8.371	9.4×10^{1}	
	^{242}Pu	10.199	4.4×10^{-3}	6.7×10^{-2}
	^{241}Am	1.85×10^{-4}	6.8×10^{-5}	1.1×10^{-3}
MOX	^{238}Pu	3.15	5.3	8.4×10^{1}
	^{239}Pu	40.554	2.5×10^{-1}	3.9
	^{240}Pu	34.793	7.8×10^{-1}	1.2×10^{1}
	^{241}Pu	9.204	9.4×10^{1}	
	^{242}Pu	12.299	4.8×10^{-3}	7.6×10^{-2}
	^{241}Am	2.40×10^{-4}	8.1×10^{-5}	1.3×10^{-3}
MOX_RP	^{238}Pu	1.863	4.5	7.6×10^{1}
	^{239}Pu	53.647	4.7×10^{-1}	7.9
	^{240}Pu	30.788	9.9×10^{-1}	1.7×10^{1}
	^{241}Pu	6.414	9.4×10^{1}	
	^{242}Pu	7.288	4.1×10^{-3}	6.9×10^{-2}
	^{241}Am	1.79×10^{-4}	8.7×10^{-5}	1.5×10^{-3}

4.4 Particle size distribution of an aerosol

For quality control, the size distribution of PuO_2 particles is measured by impedance techniques in R4 and T4 before its conditioning. The measured size is the volume equivalent diameter d_{ev} which

is the diameter of a sphere with the same volume as the particle. The size distributions for the spent fuels are represented in Fig. 4.3.

However, these are the size distributions of the PuO_2 powder rather than the size distribution of an aerosol which could generated from this powder. Therefore, to model the possible exposure of workers, a scenario of aerosol generation is proposed in order to determine its size distribution.

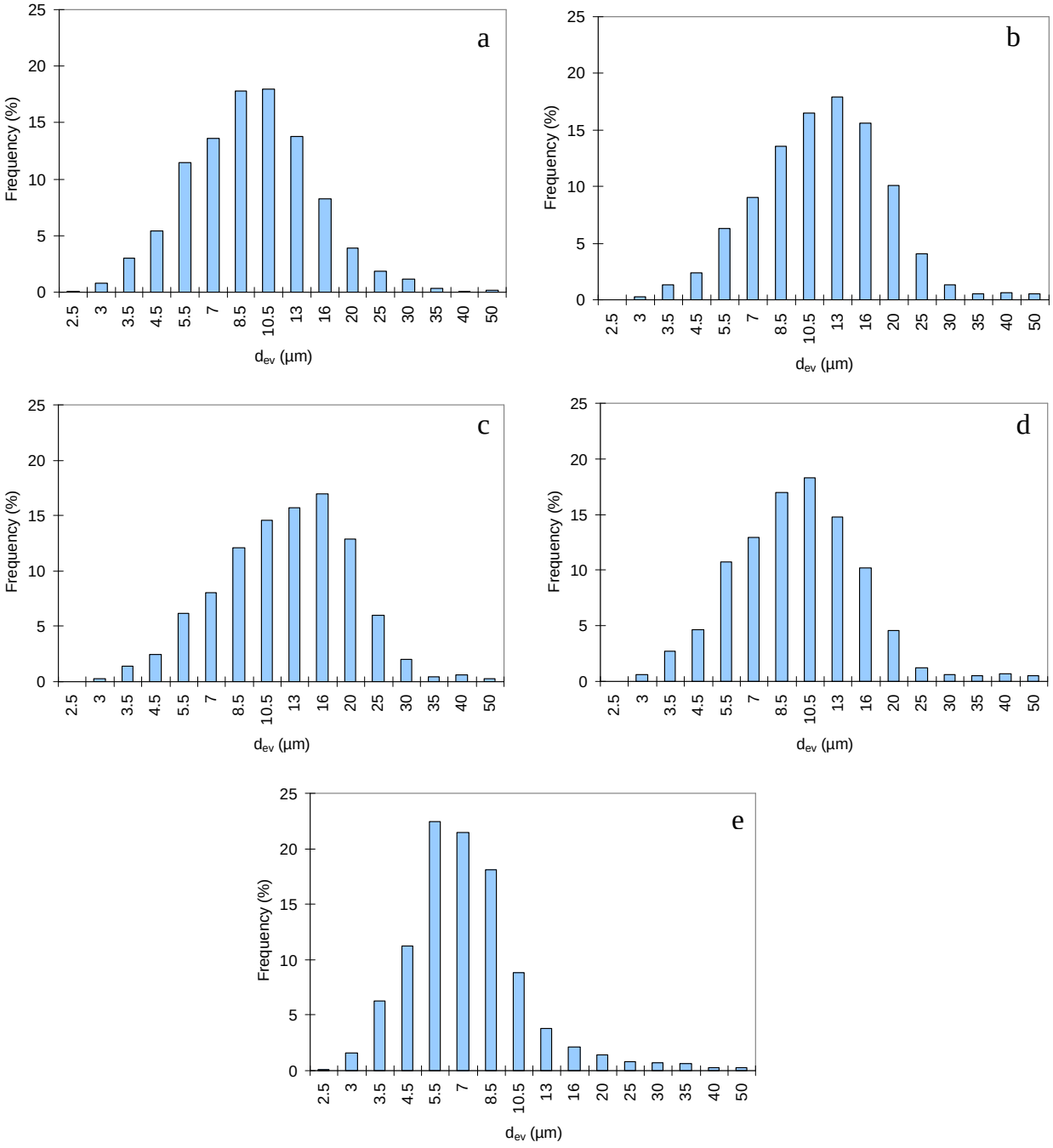

Figure 4.3: Distribution of the volume equivalent diameter (d_{ev}) for Pu dioxide at the end of R4-T4 process for different spent fuels. a: Pressurized Water ReactorPWR1; b: Pressurized Water Reactor PWR2; c: Boiling Water Reactor (BWR); d: Mixed Oxide spent fuel (MOX); e: Mixed Oxide fuel mixed with recycled Pu (MOX_RP)

4.4.1 Scenario of aerosol generation

The most plausible scenario of contamination is inhalation of particles following a leak from a glove while handling PuO_2 in a glove box. Such leak would change the air dynamics in the glove box leading to the suspension of an aerosol from the powder. Then, the aerosol could be transported from the glove box to the worker's nose and mouth (Fig. 4.4). An issue of this study is the modification of the particle size distribution related to the physical processes of suspension from the powder and transport of the aerosol.

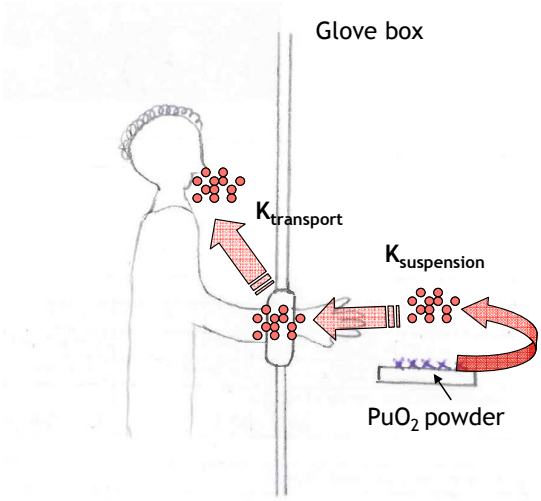

Figure 4.4: Scenario and physical process of the aerosol generation

4.4.2 Suspension

A particle lying on a substrate and caught in an air flow is subject to adhesive force f_a, lift force F_L and drag force F_D (Fig. 4.5). The adhesive and lift forces are respectively proportional to the particle diameter and to the square of this diameter. To suspend a particle, the lift force has to be stronger than the adhesive force. Therefore, larger particles are more easily suspended than smaller ones.

Two different cases were considered: suspension from a powder pile or from a mono-layered powder. Alloul-Marmor (2002) calculated the suspension factor $K_{suspension}$, which is the fraction of powder suspended by the air flow, for different size distributed piles of powder and derived a correlation with the median $d_{50,\,ev}$ of the distribution in volume equivalent diameter:

$$K_{suspension} = 6.4\times10^{-3}\times(d_{50}{}^{+})^{5.7} \text{ with } d_{50}{}^{+} = \frac{d_{50,ev}\times v^{*}}{\nu}, \qquad \text{Equation 4.1}$$

where v^* is the air friction velocity and ν is the air viscosity. However, Eq. 4.1 does not allow evaluating $K_{suspension}$ for each particle size of the powder to determine the size fractions which are suspended in order to derive the resulting size distribution of the aerosol.

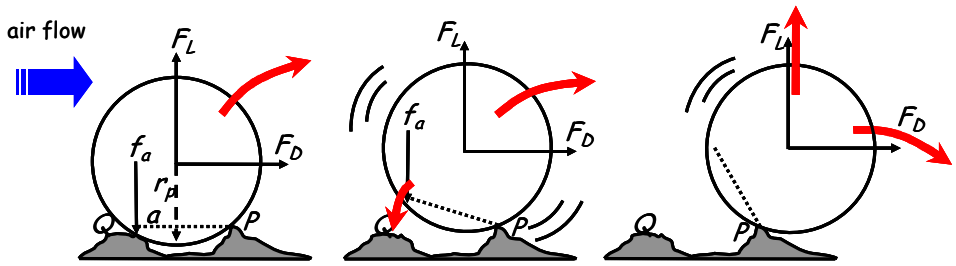

Figure 4.5: Rock 'n' Roll model for suspension of particles (from Alloul-Marmor, 2002)

The Rock 'n' Roll suspension model developed by Biasi *et al* (2001) can be applied to a mono-layered powder. The distribution of asperity contacts of a particle with a rough surface is reduced for simplicity to a two dimensional model of two point asperity contacts *P* and *Q*. The particle exposed to a turbulent flow in a boundary layer will rock about *P* due to the action of the aerodynamic lift and drag couples, counteracted by the adhesive couple at *Q* until it has enough rotational energy to break the contact with *Q*. Once this happens the particle is free to rotate or to fly off the surface if the lift force is sufficient to break the contact with *P*: in either case the particle is considered as suspended (Fig. 4.5). Reeks and Hall (2001) expressed $K_{suspension}$ using the Rock 'n' Roll model by:

$$K_{suspension} = 1 - \int_0^{\infty} \varphi(f_a) \cdot \exp(-p \times \Delta t) df_a \ , \qquad \text{Equation 4.2}$$

where $\varphi(f_a)$ is the distribution of adhesive force, p is the suspension rate constant and Δt is the suspension time. Although this model allows the calculation of $K_{suspension}$ for different particle sizes, it is not straightforward and uses many parameters which values are unknown in our study.

4.4.3 Transport

The size distribution of the aerosol changes with transport because of the sedimentation of particles, large particles being prone to sedimentation more quickly than smaller ones. The transport coefficient $K_{transport}$ is used to relate the flow rate of particles at the source of emission with their concentration at equilibrium in the vessel. Motzkus *et al* (2008) expressed it as:

$$K_{transport}(d_{ae}) = \frac{C_{eq}(d_{ae})}{q(d_{ae})}, \qquad \text{Equation 4.3}$$

where $C_{eq}(d_{ae})$ is the concentration at equilibrium at a given point within the ventilated vessel, which could be the worker airways and $q(d_{ae})$ is the flow rate at the source. d_{ae} is the aerodynamic diameter (Eq. 1.13). The equilibrium concentration C_{eq} at time t is given by:

$$C_{eq}(d_{ae}, t) = \frac{q(d_{ae})}{v_{sed}(d_{ae}) \times S + Q_{ext}}, \qquad \text{Equation 4.4}$$

where S is the settling surface area, Q_{ext} is the extraction flow, and $v_{sed}(d_{ae})$ is the settling velocity of particles of diameter d_{ae} which is proportional to the square of d_{ae}. Combining Eq. 4.3 and 4.4 gives the following expression of the transport coefficient $K_{transport}$

$$K_{transport}(d_{ae}) = \frac{1}{v_{sed}(d_{ae}) \times S + Q_{ext}}. \qquad \text{Equation 4.5}$$

However, S and Q_{ext} are not known for the workers in R4 and T4 facilities. Therefore, the calculation of $K_{transport}$ is not straightforward.

4.4.4 Discussion

Relevant models do therefore exist and can be applied to quantify the fraction of a powder which is suspended by an air flow but the derivation of the size distribution of the resulting aerosol from the size distribution of the powder does not appear feasible in the time frame of this study due to numerous unknown parameter values in the aerosol transport model.

Moreover, the measurement of the size distribution by impedance performed in R4-T4 facilities does not allow measuring particles of size less than 2 µm. Therefore, the measured size distribution could not be fully representative of the particles which could actually be inhaled.

As a conclusion, evaluating the size distribution of an inhalable aerosol from the size distribution of a powder appears as a research subject of its own and beyond the scope of this study. Therefore, no specific information on the AMAD is used here. Practical information may be brought by sampling aerosols in R4-T4 with specific devices close to the position of the workers airways during operation in glove box. However, as long as the static air samplers do not detect activity, it can be assumed that the aerosol concentration at the workplaces is low even during operation.

4.5 Absorption into blood of plutonium compounds

The last but not least important characteristic of a inhaled aerosol is the absorption of deposited particles into the blood. The choice of absorption type can dramatically influence the estimation of the dose from a given inhaled activity. For example, assuming an AMAD of 5 µm, the ^{239}Pu dose coefficient varies from 8.4 x 10^{-6} Sv.Bq^{-1} for Type S to 3.3 x 10^{-5} Sv.Bq^{-1} for Type M and to 1.4 x 10^{-4} Sv.Bq^{-1} for Type F. The actual absorption of a compound is usually intermediate between the reference types. Besides, the knowledge of a compound absorption influences the accuracy of the estimation of the dose from a given exposure as well as the definition of the monitoring programme (e.g. by selecting either urine or faeces measurement).

Therefore, it is desirable to determine specific values of absorption for handled Pu compounds in order to optimise the monitoring of workers and to improve the evaluation of doses. Consistently, the ICRP recommends the use of specific values of the absorption parameters if they are known (ICRP, 2002a) and proposes, when no more precise information is available, reference values (Type F, M, S) (ICRP, 1994a) and criteria to assign materials to Types F, M, S considering experimental data (ICRP, 1995c).

This work intends to derive specific values of f_r, s_r and s_s for different chemical forms of Pu from the literature data. The consequences of the use of these values were investigated by calculating the related e_{50}. The correlations between f_r, s_r and s_s were studied as well.

4.5.1 Models and data used

Information related to the pulmonary absorption of Pu was obtained from published *in vitro* and animal (monkeys, dogs, mice, rats) experiments, and human contamination cases. The literature review was as exhaustive as possible by considering articles referenced by the ICRP (1995c), by the OMINEX report (Stradling *et al,* 2003) and by the RBDATA-EULEP database (Bailey *et al,* 2004).

In order to derive values of absorption parameters for the HRTM from animal data, biokinetic models were adapted to the species and applied to estimate the retained activity in the different organs and its excretion, for comparison with the experimental data. The fit of the model prediction with the data was performed with the software Simulation Analysis And Modeling (SAAM) II (SAAM Institute, University of Washington, USA, Barrett *et al,* 1998) by varying the absorption parameters. The deposition in the compartments of the HRTM was calculated with LUDEP software (Birchall *et al*, 1991).

Furthermore, in the respiratory tract model, the particle transport and the absorption into blood are assumed to be independent, the particle transport is assumed to be the same for all materials in the same species and the absorption into blood is assumed to be uniform in the entire respiratory tract (ICRP, 1994a). The decay of Pu in the body was neglected because of the long half-lives of ^{238}Pu (87.7 y) and of ^{239}Pu (2.41 x 10^{+4} y) compared with the duration of the experiments.

4.5.1.1 *In vitro* studies

The *in vitro* experimental protocol consists of enclosing a sample within a sandwich of two filter papers and suspending it in a solvent. The solvent can be water, acidic solution with or without chelating agents or simulated lung fluid. The solution is renewed at intervals and analysed to measure the quantity of dissolved radionuclide. The time-dependent retention of non-dissolved Pu on the filter *R(t)* is fitted by two exponentials to derive values of f_r, s_r and s_s:

$$R(t) = f_r e^{-s_r t} + (1 - f_r) e^{-s_s t}$$ (Ansoborlo *et al,* 2002). Equation 4.6

The *in vitro* studies used in this work were published by Eidson and Mewhinney (1983), Carbaugh and La Bone (2003), Rateau-Matton *et al* (2004).

4.5.1.2 *In vivo* studies

The exposure of the animals was carried out by aerosol inhalation in most cases or by intratracheal instillation in some experiments involving rats and mice. The same dissolution model

was used for all species (Fig. 1.15). However, species-dependent models were applied to represent the deposition and particle transport in the respiratory tract, as well as the gastro-intestinal and systemic biokinetics of the radionuclide. The model predictions of retention in the lung, liver, skeleton (monkey and dog) and carcass (rodent), and of the faecal and urinary excretions were fitted to the available observed data by varying the values of f_r, s_r, s_s and of the intake (human) (Fig. 4.6).

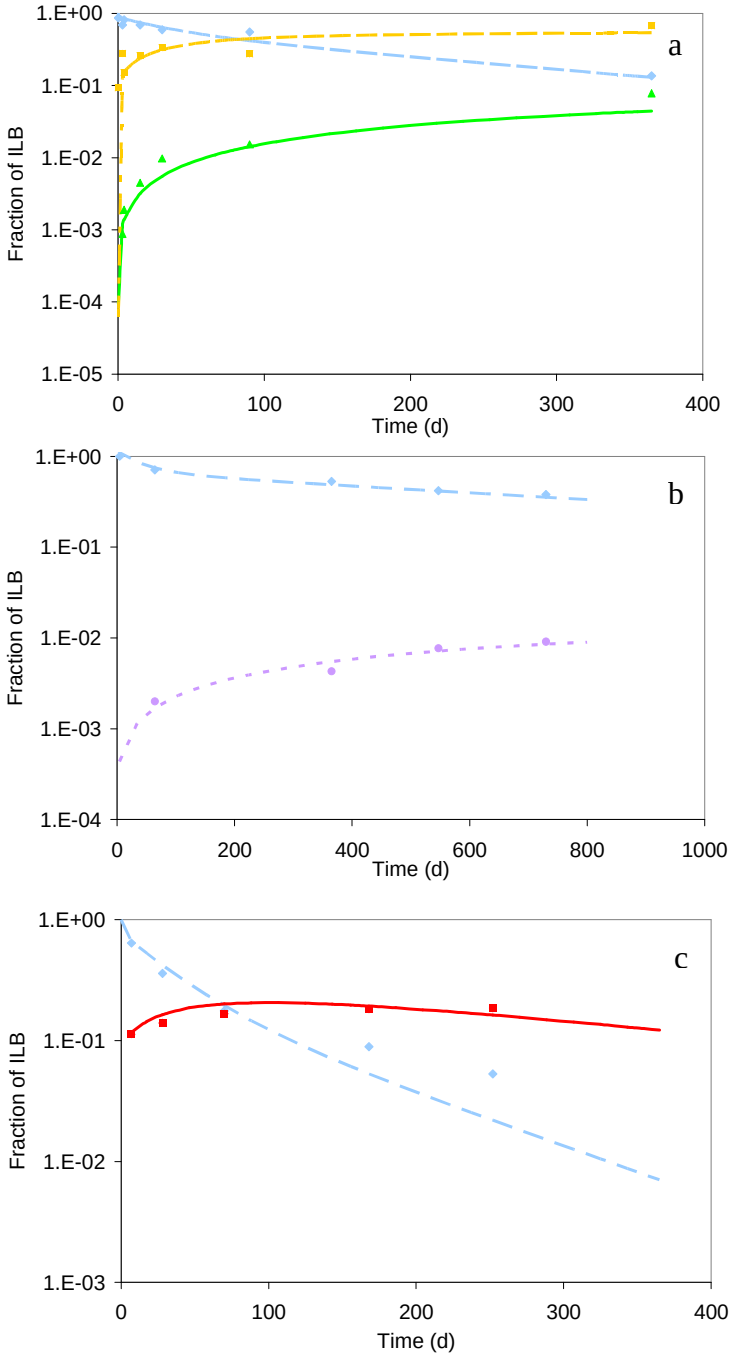

Figure 4.6: Fits obtained with different data: (a) Pu TBP inhaled by baboons, Métivier *et al* (1989); (b) MOX inhaled by dogs, Stanley *et al* (1980a); (c) Pu nitrate in rats, Stradling *et al* (1987). Retained and excreted activity expressed as fraction of Initial Lung Burden (ILB). lung retention: experimental data (◆) with fit (blue broken line); cumulative faecal excretion: experimental data (■) with fit (orange dotted-dashed line); cumulative urine excretion: experimental data (▲) with fit (green solid line); skeleton retention: experimental data (●) with fit (purple dotted line)carcass retention: experimental data (■) with fit (red solid line).

Human

The chelating agent diethylene-triamine pentaacetic acid (DTPA) is often used in Pu decorporation therapy. As DTPA treatment increases the urinary excretion, the published incidental contamination cases were studied when only one intake by inhalation was suspected and no DTPA was administered (Foster, 1991, Ramsden *et al,* 1970) or when DTPA was judged ineffective by the authors (Carbaugh and La Bone, 2003). A human experiment with volunteers was carried out to derive absorption of Pu in human and to compare it with results of animal studies involving the same Pu aerosol (Stradling *et al,* 2002a, Etherington *et al,* 2003). The particle deposition, transport and absorption into blood were modelled using the HRTM. The human alimentary tract model (HATM) (ICRP, 2006) was applied to derive the faecal excretion. No retention in the walls of the alimentary tract was assumed because it is mainly important for dosimetric applications and because radionuclide retention is generally low and may be ignored in most cases (ICRP, 2006). The values of the fractional absorption into blood from the alimentary tract were taken as $f_A = 10^{-5}$ for insoluble compounds and $f_A = 5 \times 10^{-4}$ for unknown compounds (ICRP, 1994b). To derive Pu urinary excretion, its behaviour from the uptake into blood up to elimination was modelled according to Leggett (2005).

Monkey

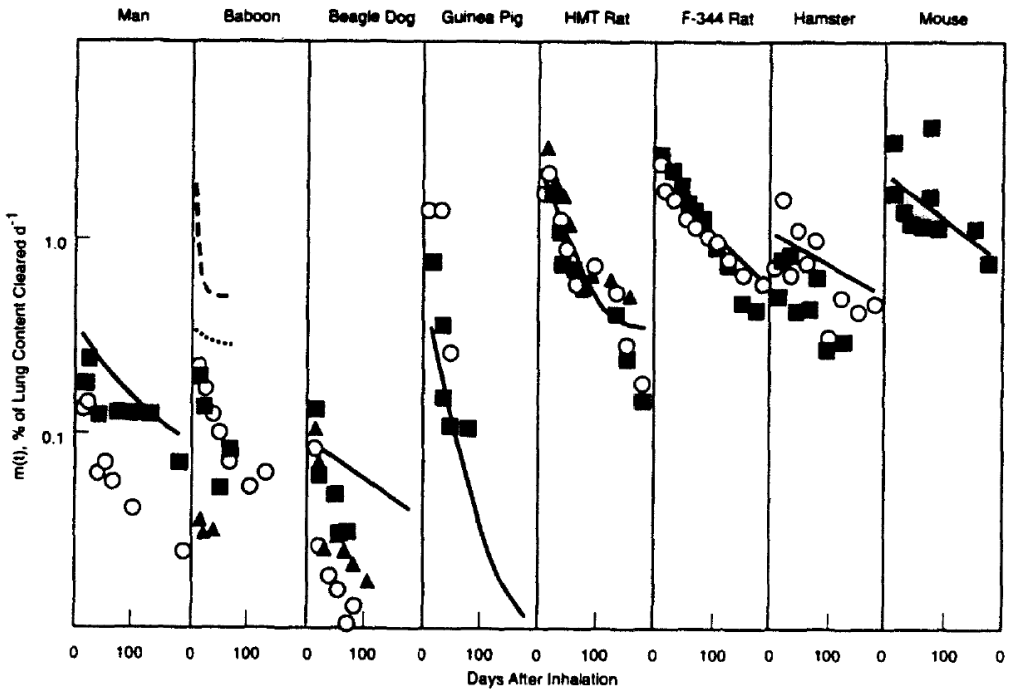

Figure 4.7: (ICRP, 1994a)Estimated particle transport rates from lung to GI tract as percent of cleared lung content per day for 0.8-µm porous Co_3O_4 (■), 1.7-µm porous Co_3O_4 (O), from Bailey *et al* (1989); 0.9-µm solid Co_3O_4 (▲) from Kreyling *et al* (1991); and fused aluminosilicate particles (black curve) from Bailey *et al* (1985a, human, 1985b, HMT rats, hamsters), Kreyling and Schumann (1987, dogs), McClellan *et al* (1984, Hartley guinea pigs), Snipes *et al* (1983, F-344 rats, CD-1 mice). Lung clearance rates for ^{51}Cr-labelled polystyrene (dashed line) and ^{198}Au-labelled colloidal gold (dotted line) from Métivier *et al* (1974).

Since human and monkey share a similar physiology and since particle transport rates in the respiratory tract of both species were shown to be close (Bailey *et al*, 1989, Kreyling *et al*, 1991, Fig. 4.7), the same behaviour of Pu was assumed in monkey and human. The models used to interpret the monkey data were therefore the HRTM, the HATM, and the Leggett (2005) systemic model.

The monkey data (baboons, cynomolgus and rhesus monkeys) interpreted in this study are from experiments of Bair *et al* (1980), Stanley *et al* (1980a, b), Stanley *et al* (1982), Métivier *et al* (1989), Brooks *et al* (1992) and Lataillade *et al* (1995).

Dog

Ballou *et al* (1972), McClellan (1972), Park *et al* (1972), Bair *et al* (1980), Stanley *et al* (1980a, b, 1982), Dagle *et al* (1983), Mewhinney and Diel (1983), Guilmette *et al* (1984, 1987) were interpreted in this work.

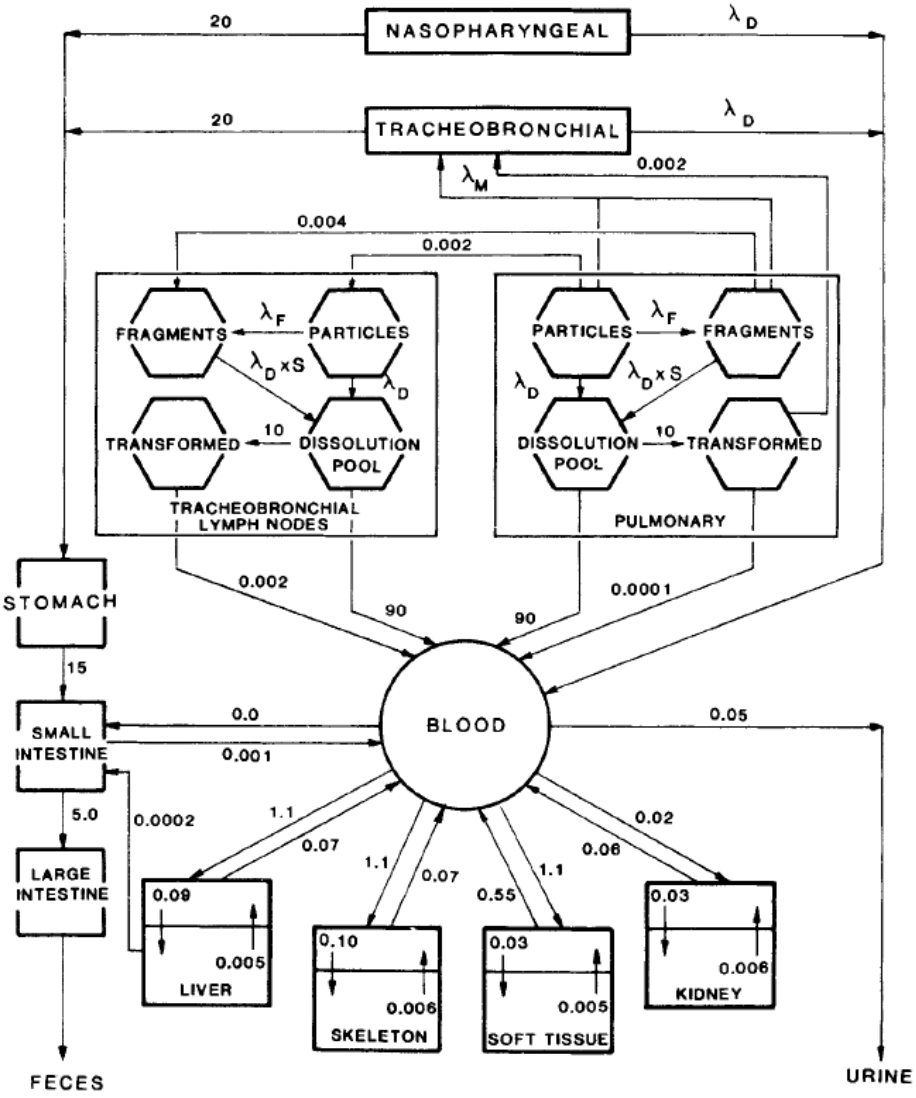

Figure 4.8: Respiratory tract, GI tract and Pu systemic model for dogs (Mewhinney and Diel, 1983)

Rodent

ICRP (2002a) developed models of the respiratory tract and Pu systemic behaviour in rats (Fig. 4.9). These were also applied to mouse studies since Bailey *et al* (1989) suggested that particle transport is similar among rodents (Fig. 4.7). The alveolar deposition was occasionally modified according to the difference of deposition between the different experiments (ICRP, 2002a). This study used the data of Bair *et al* (1961), Morin *et al* (1972), Nénot *et al* (1972), Stather and Howden (1975), Stather *et al* (1975), Ballou *et al* (1977), Smith *et al* (1977), Stradling *et al* (1978a, 1978b), Métivier *et al* (1980), Kanapilly and Boecker (1981), Stanley *et al* (1982), Métivier *et al* (1983), Stradling *et al* (1985), Rhoads *et al* (1986), Stradling *et al* (1987), Morgan *et al* (1988), Stradling *et al* (1989, 1992), Moody *et al* (1993), Birchall *et al* (1995), Lataillade *et al* (1995), Stradling *et al* (1998), Sato *et al* (1999), Ramounet *et al* (2000), ICRP (2002a), Stradling *et al* (2002a), Hodgson *et al* (2003), Ramounet-Le Gall *et al* (2003), Rateau-Matton *et al* (2004)

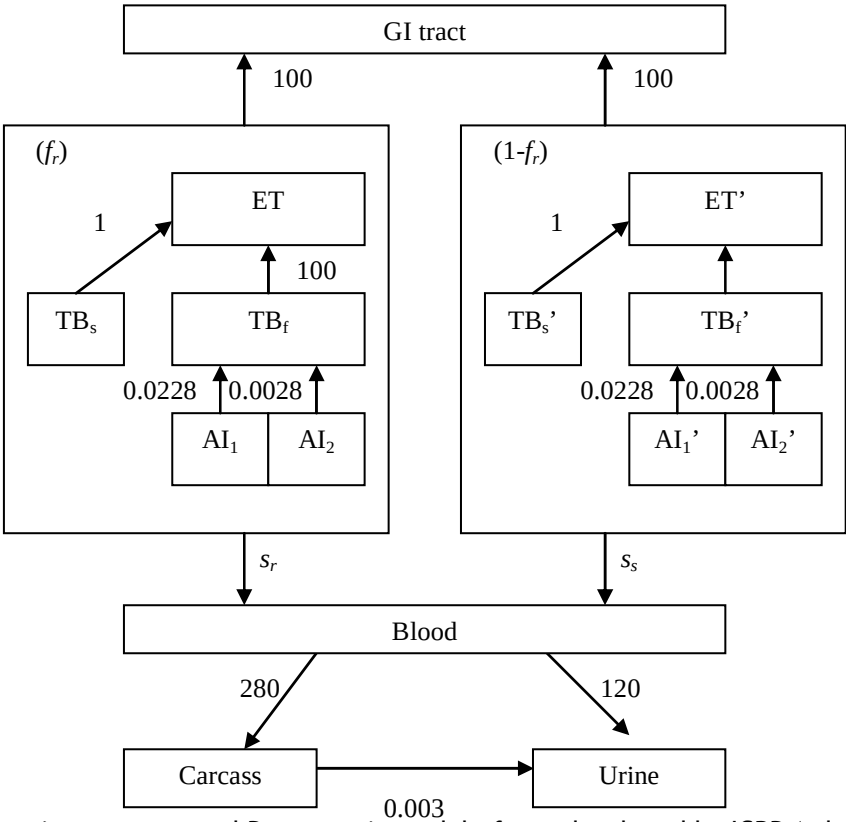

Figure 4.9: Respiratory tract and Pu systemic model of rats developed by ICRP (adapted from ICRP, 2002a). It is assumed that 80 % of the deposit in TB clears in a fast phase (TB_f) and 20 % in a slow phase (TB_s); 66 % of the deposit in AI clears in a faster phase (AI_1) and 34 % in a slower phase (AI_2); 10 % of the ILD is deposited in TB and 90 % in AI. Rates are in d^{-1}.

4.5.2 Results and discussion

The values of the absorption parameters giving the best fit to the data are shown in Fig. 4.10 and Table 4.4 along with some values already provided by the authors of the experiments. When no data provided information about s_r, the default value of 100 d^{-1} was assumed.

Table 4.4: Estimation of the absorption parameter values for Pu in various chemical forms

Compound	*in vitro* or species	f_r	s_r (d^{-1})	s_s (d^{-1})	Reference
$^{238}PuO_2$	dog	2.4×10^{-4}	100	2.4×10^{-3}	Mewhinney and Diel, 1983
	mouse [b]	8.2×10^{-4}	100	1.9×10^{-3}	Morgan *et al*, 1988
	mouse [b]	1.6×10^{-3}	100	3.4×10^{-4}	Morgan *et al*, 1988
	mouse [b]	7.1×10^{-5}	100	3.4×10^{-4}	Morgan *et al*, 1988
	mouse [b]	1.2×10^{-3}	100	1.6×10^{-4}	Morgan *et al*, 1988
	rat	6.0×10^{-1}	2.5	3.3×10^{-3}	Stradling *et al*, 1978a
	rat	6.3×10^{-1}	3.1	9.2×10^{-3}	Stradling *et al*, 1978a
$^{239}PuO_2$	dog	4.2×10^{-2}	100	1.4×10^{-3}	Bair and McClanahan, 1961
	dog	4.5×10^{-2}	0.2	2.9×10^{-3}	Bair and McClanahan, 1961
	dog	6.3×10^{-1}	100	2.1×10^{-2}	Bair and Willard, 1963
	dog	1.2×10^{-1}	8.3	1.0×10^{-4}	Bair and Willard, 1963
	dog	1.6×10^{-3}	100	1.5×10^{-2}	Bair and Willard, 1963
	dog	2.0×10^{-4}	100	4.0×10^{-5}	Bair *et al*, 1980
	dog	1.0×10^{-4}	100	6.2×10^{-6}	Guilmette *et al*, 1984
	dog	1.0×10^{-4}	100	6.2×10^{-6}	Guilmette *et al*, 1987
	dog	1.0×10^{-4}	100	3.5×10^{-6}	Guilmette *et al*, 1987
	dog	1.4×10^{-3}	100	7.6×10^{-5}	Park *et al*, 1972
	monkey (baboon)	3.8×10^{-3}	100	4.1×10^{-4}	Bair *et al*, 1980
	mouse	4.6×10^{-3}	100	3.2×10^{-4}	Bair *et al*, 1961
	mouse [b]	9.2×10^{-5}	100	7.2×10^{-6}	Morgan *et al*, 1988
	mouse [b]	9.2×10^{-5}	100	4.8×10^{-6}	Morgan *et al*, 1988
	mouse [b]	9.2×10^{-5}	100	4.8×10^{-6}	Morgan *et al*, 1988
	mouse [b]	9.2×10^{-5}	100	1.0×10^{-5}	Morgan *et al*, 1988
	rat	3.9×10^{-4}	100	1.1×10^{-4}	Stather *et al*, 1975
	rat	1.1×10^{-3}	100	2.9×10^{-5}	Stather *et al*, 1975
	rat	1.0×10^{-3}	100	6.0×10^{-3}	Rhoads *et al*, 1986
	rat [b]	1.0×10^{-3}	100	2.6×10^{-4}	Sato *et al*, 1999

	rat [b]	1.0×10^{-3}	100	2.2×10^{-3}	Sato *et al,* 1999
	rat [b]	1.0×10^{-3}	100	1.0×10^{-4}	Stradling *et al,* 1987
PuO_2	dog	5.8×10^{-5}	100	4.8×10^{-5}	Stanley *et al,* 1980b
(mixture of ^{238}Pu,	human [b]	3.1×10^{-4}	100	9.2×10^{-6}	Carbaugh and La Bone, 2003
^{239}Pu, ^{240}Pu)	human [a]	2.0×10^{-3}	9.9	9.7×10^{-6}	Carbaugh and La Bone, 2003
	in vitro [a]	7.0×10^{-4}	1.6	1.3×10^{-5}	Carbaugh and La Bone, 2003
	in vitro [a]	0	_	3.5×10^{-5}	Eidson and Mewhinney, 1983
	in vitro [a]	3.0×10^{-3}	0.7	8.2×10^{-6}	Rateau-Matton *et al,* 2004
	monkey (baboon)	3.0×10^{-3}	100	1.0×10^{-4}	Lataillade *et al,* 1995
	monkey (baboon)	2.2×10^{-3}	100	1.1×10^{-4}	Lataillade *et al,* 1995
	monkey (cynomolgus)	5.8×10^{-5}	100	4.8×10^{-5}	Stanley *et al,* 1980b
	rat	1.3×10^{-4}	100	6.0×10^{-5}	Kanapilly and Boecker, 1981
	rat [b]	1.0×10^{-3}	100	1.0×10^{-4}	Lataillade *et al,* 1995
	rat [b]	5.1×10^{-3}	100	1.6×10^{-4}	Ramounet *et al,* 2000
	rat [a]	7.0×10^{-3}	0.8	3.1×10^{-5}	Rateau-Matton *et al,* 2004
	rat [a]	2.2×10^{-3}	0.2	5.9×10^{-4}	Rateau-Matton *et al,* 2004
	rat	6.4×10^{-1}	100	1.6×10^{-2}	Smith *et al,* 1977
MOX	dog	2.2×10^{-5}	100	4.8×10^{-5}	Stanley *et al,* 1980a
	dog	2.1×10^{-4}	100	1.9×10^{-6}	Stanley *et al,* 1982
	human	1×10^{-3}	100	1×10^{-4}	Foster, 1991
	in vitro [a]	4.6×10^{-2}	0.3	4.6×10^{-5}	Eidson and Mewhinney, 1983
	in vitro [a]	4.0×10^{-3}	0.4	1.1×10^{-4}	Eidson and Mewhinney, 1983
	in vitro [a]	1.0×10^{-3}	0.6	3.3×10^{-5}	Eidson and Mewhinney, 1983
	in vitro [a]	5.8×10^{-2}	0.1	4.5×10^{-5}	Rateau-Matton *et al,* 2004
	in vitro [a]	4.6×10^{-2}	0.3	2.4×10^{-5}	Rateau-Matton *et al,* 2004
	in vitro [a]	4.9×10^{-2}	0.3	1.6×10^{-4}	Rateau-Matton *et al,* 2004
	in vitro [a]	5.3×10^{-2}	0.2	1.0×10^{-4}	Rateau-Matton *et al,* 2004
	monkey (baboon)	4.6×10^{-2}	100	2.1×10^{-3}	Lataillade *et al,* 1995
	monkey (baboon)	1.6×10^{-2}	100	2.6×10^{-3}	Lataillade *et al,* 1995
	monkey (cynomolgus)	2.2×10^{-5}	100	4.8×10^{-5}	Stanley *et al,* 1980a

	monkey (cynomolgus, rhesus)	2.1×10^{-4}	100	1.9×10^{-6}	Stanley *et al*, 1982
	rat	1.2×10^{-3}	100	1.5×10^{-4}	Kanapilly and Boecker, 1981
	rat [a]	6.0×10^{-4}	100	6.0×10^{-5}	Ramounet *et al*, 2000
	rat [a]	2.0×10^{-3}	100	3.0×10^{-4}	Ramounet *et al*, 2000
	rat [b]	2.9×10^{-4}	100	6.3×10^{-5}	Ramounet *et al*, 2000
	rat [b]	2.0×10^{-3}	100	1.9×10^{-4}	Ramounet *et al*, 2000
	rat [a]	5.1×10^{-3}	100	2.7×10^{-4}	Ramounet-Le Gall *et al*, 2003
	rat [a]	3.2×10^{-3}	100	1.6×10^{-4}	Ramounet-Le Gall *et al*, 2003
	rat [a]	9.8×10^{-4}	100	5.1×10^{-5}	Ramounet-Le Gall *et al*, 2003
	rat [a]	1.0×10^{-3}	7.9	1.3×10^{-4}	Rateau-Matton *et al*, 2004
	rat [a]	2.0×10^{-3}	0.1	3.2×10^{-5}	Rateau-Matton *et al*, 2004
	rat [a]	1.4×10^{-2}	1	1.0×10^{-3}	Rateau-Matton *et al*, 2004
	rat [b]	3.2×10^{-1}	100	1.0×10^{-4}	Stanley *et al*, 1982
Maralinga soil	rat	7.3×10^{-3}	100	8.2×10^{-4}	Stradling *et al*, 1992
	rat [b]	2.6×10^{-3}	100	6.1×10^{-5}	Stradling *et al*, 1992
	rat [b]	2.3×10^{-3}	100	1.6×10^{-3}	Stradling *et al*, 1992
Palomares dusts	rat [a]	4.2×10^{-2}	100	2.0×10^{-4}	Stradling *et al*, 1998
	rat [a]	4.3×10^{-2}	100	2.1×10^{-4}	Stradling *et al*, 1998
	rat [a, d]	4.8×10^{-2}	49	1.8×10^{-4}	ICRP, 2002a
Pu-Na alloy	rat	6.2×10^{-1}	100	1.9×10^{-2}	Stradling *et al*, 1978b
	rat	6.5×10^{-1}	100	1.3×10^{-2}	Stradling *et al*, 1978b
Pu oxide graphite	human	2.6×10^{-3}	100	1.5×10^{-4}	Ramsden *et al*, 1970
Pu chloride	human	1.1×10^{-1}	100	1.8×10^{-2}	Ramsden *et al*, 1970
Pu-Mg alloy	rat	4.0×10^{-2}	100	6.2×10^{-3}	Métivier *et al*, 1980
Pu-TBP	monkey (baboon)[c]	2.4×10^{-2}	100	3.1×10^{-3}	Métivier *et al*, 1989
	rat	9.3×10^{-3}	100	6.5×10^{-3}	Métivier *et al*, 1983
	rat	7.8×10^{-1}	31.5	2.1×10^{-3}	Stradling *et al*, 1985
nitrate-bearing	rat [b]	1.2×10^{-1}	1.5	2.2×10^{-3}	Moody *et al*, 1993
residues (process	rat [b]	2.3×10^{-2}	100	1.4×10^{-3}	Moody *et al*, 1993
line)	rat [b]	2.2×10^{-2}	100	3.4×10^{-3}	Stradling *et al*, 1987
residues from refining process	rat [b]	1.0×10^{-2}	100	4.8×10^{-4}	Stradling *et al*, 1987
residues from Magnox storage pond	rat	7.1×10^{-3}	100	2.4×10^{-4}	Stradling *et al*, 1989

Pu nitrate	dog	7.5×10^{-1}	0.2	3.7×10^{-3}	Dagle *et al*, 1983
	dog	1.1×10^{-1}	0.2	3.4×10^{-3}	Dagle *et al*, 1983
	dog	2.2×10^{-1}	100	2.2×10^{-4}	McClellan *et al*, 1972
	human [a]	2.1×10^{-1}	0.2	2.4×10^{-3}	Etherington *et al*, 2003
	human [a]	2.0×10^{-1}	0.4	1.6×10^{-3}	Etherington *et al*, 2003
	human [a]	2.0×10^{-1}	0.5	2.7×10^{-3}	Stradling *et al*, 2002a
	human [a]	2.0×10^{-1}	0.3	4.0×10^{-3}	Stradling *et al*, 2002a
	monkey (cynomolgus)	2.3×10^{-1}	0.1	2.5×10^{-3}	Brooks *et al*, 1992
	rat	5.0×10^{-1}	100	3.4×10^{-3}	Ballou *et al*, 1977
	rat [a, d]	1.8×10^{-1}	49.0	5.6×10^{-3}	Birchall *et al*, 1995
	rat [a]	9.0×10^{-2}	20.0	5.5×10^{-3}	Hodgson *et al*, 2003
	rat [b]	2.7×10^{-1}	4.9	8.2×10^{-3}	Moody *et al*, 1993
	rat [b]	4.9×10^{-2}	100	2.3×10^{-3}	Morin *et al*, 1972
	rat [b]	4.0×10^{-2}	100	4.0×10^{-3}	Morin *et al*, 1972
	rat	2.7×10^{-2}	100	1.4×10^{-2}	Nénot *et al*, 1972
	rat [b]	2.1×10^{-2}	100	5.3×10^{-3}	Nénot *et al*, 1972
	rat	3.5×10^{-1}	36.4	1.1×10^{-2}	Stather and Howden, 1975
	rat	1.4×10^{-1}	100	7.1×10^{-3}	Stradling *et al*, 1987
	rat [a]	9.0×10^{-2}	20.0	5.5×10^{-3}	Stradling *et al*, 2002a
	rat [a]	6.8×10^{-1}	18.0	2.9×10^{-3}	Stradling *et al*, 2002a
	rat [a]	6.8×10^{-1}	18.0	2.2×10^{-3}	Stradling *et al*, 2002a
	rat [a, d]	1.8×10^{-1}	49.0	5.6×10^{-3}	ICRP, 2002a
	rat [a, d]	5.5×10^{-1}	49.0	5.6×10^{-3}	ICRP, 2002a
Pu citrate	dog	1.5×10^{-1}	0.6	4.4×10^{-3}	Ballou *et al*, 1972
	rat	7.4×10^{-1}	100	3.6×10^{-1}	Stradling *et al*, 1978a

[a] Data published by the authors

[b] Deposition was modified to fit the data.

[c] Models of deposition and urinary excretion were modified to fit the data (Métivier *et al*, 1989).

[d] Bound state is considered.

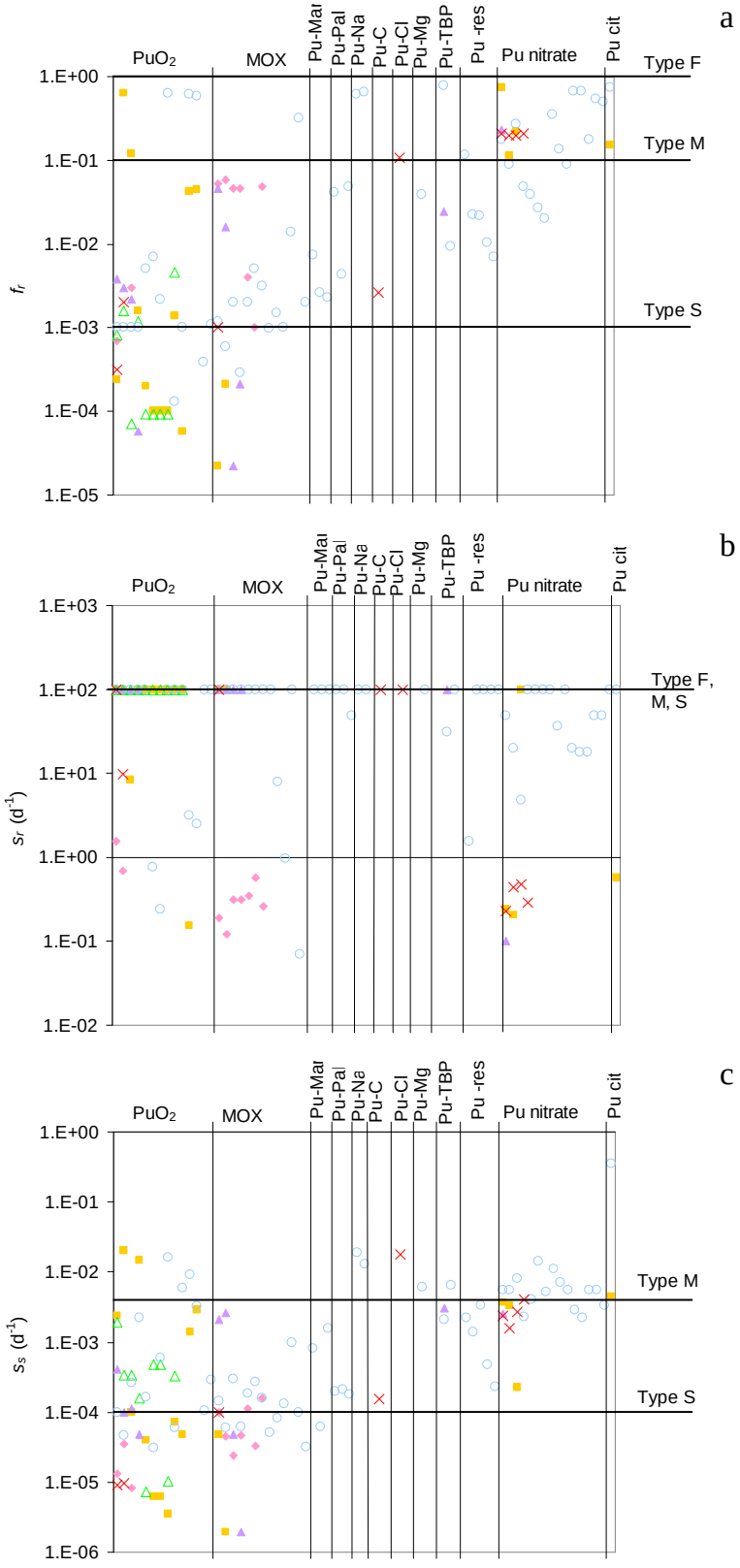

Figure 4.10: Rapidly dissolved fraction f_r (a), fast dissolution rate s_r (b) and slow dissolution rate s_s (c) for different Pu compounds. Pu-Mar: Maralinga soil; Pu-Pal: Palomares dust; Pu-Na : Pu sodium alloy; Pu-C: Pu oxide graphite; Pu-Cl: Pu chloride; Pu-Mg: Pu magnesium alloy; Pu-res: residues; Pu cit: Pu citrate. *In vitro* (◆), dog (■), monkey (▲), mouse (△), rat (○) experiments; human contamination cases (✖)

Parameter values

Mean and median values of f_r, s_r and s_s were calculated for compounds studied in more than one experiment (Table 4.5). Median is judged to be the best central estimate of the distributions because it is less sensitive to extreme values. Moreover it may be used together with the geometric standard deviation as parameters of a log-normal distribution approximating the data.

Table 4.5: Mean, median and geometric standard deviation (GSD) of f_r, s_r and s_s for Pu compounds

Compound		f_r	s_r (d^{-1})[a]	s_s (d^{-1})
PuO_2[b]	mean	6.4×10^{-2}	3	1.9×10^{-3}
(Type S)	median	1.1×10^{-3}	1.6	1.0×10^{-4}
	GSD	14.3	4.3	10.7
MOX	mean	3.2×10^{-2}	1.1	3.0×10^{-4}
(Type S)	median	2.0×10^{-3}	0.3	1.0×10^{-4}
	GSD	11.2	3.7	5.0
Maralinga	mean	4.0×10^{-3}	-	8.4×10^{-4}
soil	median	2.3×10^{-3}	-	8.2×10^{-4}
(Type S)	GSD	1.9	-	5.6
Palomares	mean	3.1×10^{-2}	49	2.0×10^{-4}
dust	median	4.2×10^{-2}	49	2.0×10^{-4}
(Type S)	GSD	3.9	-	1.1
Pu-Na alloy	mean	6.3×10^{-1}	-	1.6×10^{-2}
(Type M)	median	6.3×10^{-1}	-	1.6×10^{-2}
	GSD	1.0	-	1.3
Pu-TBP	mean	2.7×10^{-1}	31.5	3.9×10^{-3}
(Type M)	median	2.4×10^{-2}	31.5	3.1×10^{-3}
	GSD	10.3	-	1.8
Pu residues	mean	2.8×10^{-2}	1.8	1.6×10^{-3}
(Type M)	median	1.4×10^{-2}	1.8	1.4×10^{-3}
	GSD	2.9	-	3.0
Pu nitrate	mean	2.6×10^{-1}	16.7	5.1×10^{-3}
(Type M)	median	2.0×10^{-1}	11.4	4.0×10^{-3}
	GSD	2.7	11.2	2.3
Pu citrate	mean	4.5×10^{-1}	0.6	1.8×10^{-1}
(Type F)	median	4.5×10^{-1}	0.6	1.8×10^{-1}
	GSD	3.1	-	22.3

[a] value calculated without default values at 100 d^{-1}

[b] PuO_2 gathered results for $^{238}PuO_2$, $^{239}PuO_2$ and $^{(238, 239, 240)}PuO_2$

No noticeable differences were found between the short-term absorption of $^{238}PuO_2$ (median f_r = 1.2 x 10^{-3}) and $^{239}PuO_2$ (median f_r = 1.0 x 10^{-3}). However, the long-term absorption of $^{238}PuO_2$ (median s_s = 1.9 x 10^{-3} d^{-1}) is faster than for $^{239}PuO_2$ (median s_s = 2.8 x 10^{-4} d^{-1}). This can be explained by the fragmentation of $^{238}PuO_2$ particles due to their higher specific activity (Mewhinney and Diel 1983, Guilmette *et al*, 1994, Hickman *et al*, 1995). However, considering the variability of s_s values, this difference may not be significant.

The studied chemical forms may be separated in three groups by applying the ICRP Publication 71 criteria (ICRP, 1995c): On the one hand, if Pu retention by assuming no particle transport (Eq. 4.6) is lower than 13 % at 30 d, Type F can be assigned, on the other hand, Type S can be chosen if more than 84 % is retained at 180 d; else the absorption can be associated with Type M. From this study, Type S can be assigned to Pu dioxide, MOX, Maralinga soil, Palomares dust, or Pu oxide graphite; Type M to Pu-TBP complex, residues, Pu nitrate, or chloride, Pu-Na alloy, Pu-Mg alloy; Type F to Pu citrate (Fig. 4.11). Moreover, the median and the standard deviation of f_r, s_r, s_s obtained in this work are consistent with the reference values of the ICRP for each category and the illustrative updated default parameter values derived by Bailey *et al* (2007) (Table 4.6).

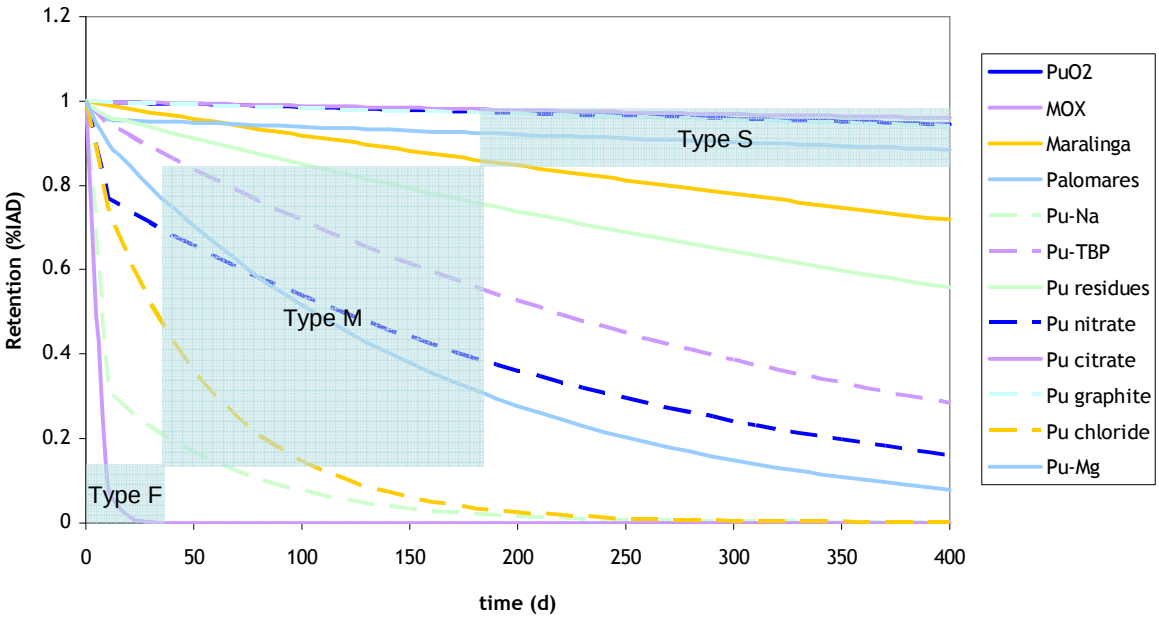

Figure 4.11: Assignation of reference absorption types according to ICRP (1995c) criteria. Retention in lung is expressed as a percentage of the 'initial alveolar deposit' (IAD) following deposition in the alveolar region. For simplicity retention is shown here in the absence of particle transport, similar to the outcome of *in vitro* experiment (Eq. 4.6)

They are also broadly consistent with the absorption into blood calculated for the Mayak workers. Khokhryakov and co-workers (2005) derived values of f_r = 3 x 10^{-3} for Pu dioxide, 1 x 10^{-2} for mixed Pu oxides, chlorides and oxalates, and 3 x 10^{-2} for Pu nitrates from *in vitro* dissolution studies. They also derived values of s_s for smokers (resp. non-smokers) of 3.22 x 10^{-4} d^{-1} (resp. 3.61 x 10^{-4} d^{-1}) for Pu dioxide, 1.17 x 10^{-3} d^{-1} (resp. 4.75 x 10^{-4} d^{-1}) for mixed Pu oxides, chlorides and oxalates, and 7.11 x 10^{-3} d^{-1} (resp 1.77 x 10^{-3} d^{-1}) for Pu nitrates from workers autopsy data (Khokhryakov *et al* 2005).

Table 4.6: Median and geometric standard deviation (GSD) of f_r, s_r, s_s obtained for this study for insoluble and soluble compounds of Pu, reference values of the ICRP (1994a) and updated default values by derived Bailey *et al* (2007)

Type	Reference		f_r	s_r (d^{-1})	s_s (d^{-1})
soluble	this study	median	1.6×10^{-1}	7.3	3.6×10^{-3}
(Type M)		GSD	4.1	4.4	4
	ICRP		1.0×10^{-1}	100	5.0×10^{-3}
	Bailey *et al*		2.0×10^{-1}	3.0	3.0×10^{-3}
insoluble	this study	median	1.6×10^{-3}	0.6	1.0×10^{-4}
(Type S)		GSD	12.3	10.8	7.9
	ICRP		1.0×10^{-3}	100	1.0×10^{-4}
	Bailey *et al*		1.0×10^{-2}	1.0	8.0×10^{-5}

Most of the *in vivo* experiments were not designed to obtain accurate values of s_r, which would require several measurements on the first day after intake. The determination of s_r therefore comes mostly from *in vitro* experiments because they permit the precise measurement of the dissolved activity at early times. These experiments tend to show (Fig. 4.10, Table 4.4) that the default value of 100 d^{-1} is too high for insoluble compounds such as Pu dioxide and MOX. A value of s_r equal to 1 d^{-1} for Type S compounds is consistent with the available data (Fig. 4.10, Table 4.6) and with Ansoborlo *et al* (2002). For Type M Pu compounds, the default value of 10 d^{-1} could be assigned to s_r, in agreement with the provisional updated default value derived by Bailey *et al* (2007). In data analysis, assuming that s_r default value is equal to 1 d^{-1} rather than 100 d^{-1} increases the estimated f_r value to keep the same rapid uptake but s_s value remains unchanged.

Hypothesis discussion

The most relevant data on absorption from the human respiratory tract obviously come from the follow-up of human contamination cases but these are few and often affected by DTPA treatment. Moreover, they are strongly influenced by individual variability since they usually refer to a single person. On the contrary, rat physiology is quite different from the human one but the individual variability is averaged over the several rats sacrificed at each measurement time. Overall, the results show no real correlation between solubility of Pu and studied animal species. For example, the median s_s values for PuO_2 are 9×10^{-5} for dogs, 1×10^{-4} for monkeys, 3×10^{-4} for rats and mice. They are close considering the significant differences in the experimental conditions.

This is in agreement with the findings of Stradling *et al* (2002a) which indicated that absorption parameter values in rat and other mammals, and humans, are reasonably independent of species. However, it should be noted that because of the short life of rodents, and the very small value of s_s, determination of s_s is difficult and will have a large error associated with it. This in turn may inflate the overall uncertainty in s_s when applied to humans.

In vitro studies can provide a quick and rough evaluation of the solubility of a compound in simulated lung fluid, especially for prospective study of exposure at a workplace and help in the design of monitoring programmes. However, obtaining results that can be applied with reasonable confidence to human exposure is not straightforward (ICRP, 2002a). From this study, it appears that *in vitro* studies give faster long-term absorption and slower short-term absorption than *in vivo* studies: for MOX, median f_r = 5 x 10^{-2} and s_s = 5 x 10^{-5} d^{-1} for *in vitro* studies compared to median f_r = 1 x 10^{-3} and s_s = 1 x 10^{-4} d^{-1} for *in vivo*.

It would be interesting to derive central estimate values of f_r, s_r, s_s from this study by weighing differently the data from *in vitro*, *in vivo* studies and from human contamination cases. However, the choice of the different weights is not straightforward.

In this work, only dissolution was studied and uptake was considered as instantaneous. However, it is acknowledged that this simplifying assumption may not always be valid, and that a small fraction of dissolved activity can be retained in the lungs for several years (James *et al,* 2007). The measured systemic retentions and excretions should not be affected since the fraction of dissolved activity bound to lung tissues appears to be less than 8 % (James *et al,* 2007).

Therefore, the dissolution parameter values derived here would not be noticeably modified by considering a bound fraction of activity. Still the actual presence of a bound fraction would have a large effect on the corresponding lung doses (ICRP, 2002a). So, when indication of such bound fraction is available, it can be used together with the dissolution rates to calculate accurate lung doses.

Physically, the dissolution should depend on the particle size through the surface-to-volume ratio (Mercer, 1967, ICRP, 1994a). However, Mewhinney and Diel (1983) observed similar absorption rates for aerosols of different sizes (monodispersed aerosols of 0.7, 1.7, 2.7 µm and poly-dispersed aerosol with an AMAD of 1.4 µm) in dogs. Consistently, Guilmette *et al* (1987) showed that the AMAD had a small influence on the absorption.

However, ultra-fine particles of a few nanometres behave differently from particles of tens of nanometres and are instantaneously absorbed into blood (Stradling *et al* 1979). It can explain the high values of f_r reported by Smith *et al* (1977) and Stradling *et al* (1978a) who studied the absorption of nanometric particles. On the contrary, Kanapilly and Diel (1980) observed the same dissolution rate constant for ultra-fine and micrometric particles using a different aerosol generator from the above authors. Further study of the absorption of nanometric particles would therefore be of high interest.

The other f_r values for PuO_2 and MOX greater than 0.1 were interpreted from Bair and Willard (1963) and Stanley *et al* (1982). The latest compared the retention and absorption of the same PuO_2 in rat, dog and monkeys. The short-term absorption was faster in rat lungs than for dogs and monkeys but no clear explanation was provided. The experimental data of Bair and Willard (1963) are expressed as percent of total Pu intake which includes both the initial lung burden and Pu deposited in the gastro-intestinal tract. This could explain that the lung retention is small just after the exposition leading to a high value of f_r.

The simple absorption model used in this study (Fig. 1.15) could not be applied to a contamination by a ceramic ^{238}Pu compound which displays an increasing solubility over time (Guilmette *et al*, 1994, Hickman *et al*, 1995, James *et al*, 2003). The alternative model of absorption to blood in the HRTM (ICRP, 1994a) (Fig. 1.16) was used by James *et al* to derive rates for dissolution of particles in initial state s_p = 1 x 10^{-6} d^{-1}, for conversion to a transformed state s_{pt} = 1.89 x 10^{-3} d^{-1} and dissolution of transformed particles s_t = 2.57 x 10^{-4} d^{-1}.

Variability of dose

The committed effective dose coefficient (e_{50}) was calculated with each determined set of absorption parameters for an inhaled aerosol of pure ^{239}Pu with an AMAD of 5 µm (Fig. 4.12). The calculations were performed with IMBA (Birchall *et al*, 2007) according to the HRTM, GI tract model and Pu biokinetic model (ICRP, 1993) of ICRP.

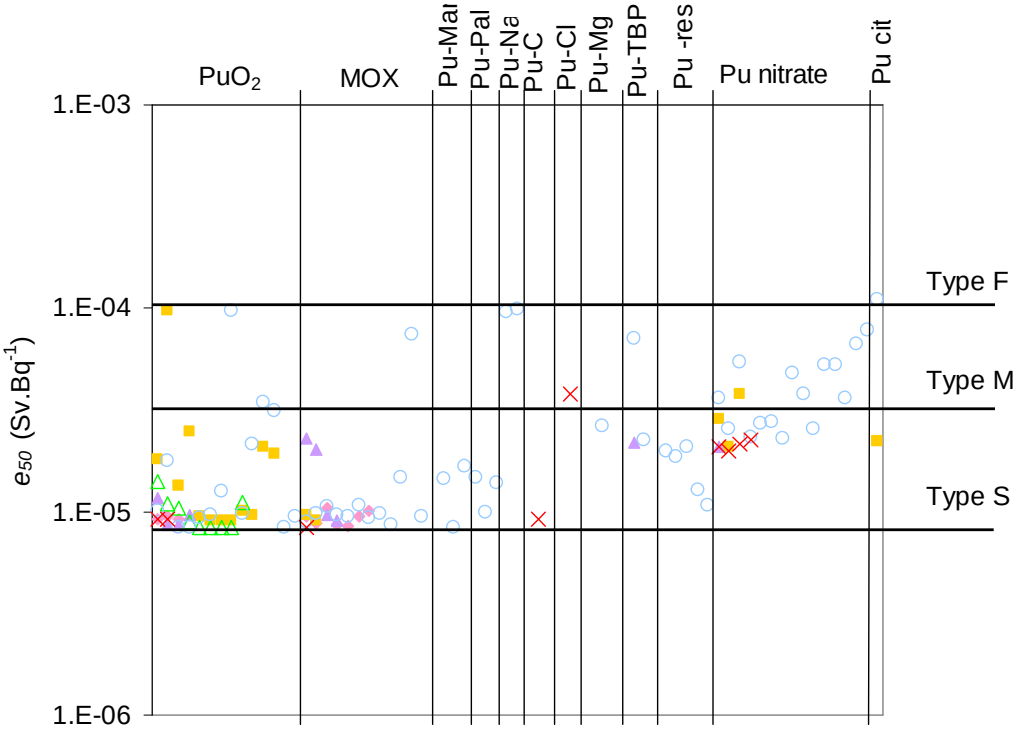

Figure 4.12: Dose coefficient (e_{50}) for different Pu compounds. *In vitro* (◆), dog (■), monkey (▲), mouse (△), rat (○) experiments; human contamination cases (✖)

The e_{50} for insoluble compounds and more soluble compounds respectively are close to the published values of Type S and M dose coefficients (ICRP, 1994b). This is consistent with the trend of the estimated solubility rates as well as with the stability of the e_{50} which is a weighted average of doses over all radiosensitive tissues. However, estimates of lung dose, particularly when assessed from urinary excretion, are considerably more sensitive to absorption into blood and when a best estimate of lung dose is required, case specific parameter values should be preferred to ICRP reference Types.

Correlation between absorption parameters

The uncertainty on the absorption parameters can be propagated to the dose resulting from an inhalation exposure by Monte-Carlo calculation. For lack of information, it is often assumed that f_r, s_r and s_s are independent (Bolch *et al*, 2003, Bess *et al*, 2007). However, unknown correlations between these parameters may significantly affect the reliability of the results. From the number of sets of values presented here, the actual correlation between f_r and s_s was studied by the rank correlation Spearman test (Fig. 4.13).

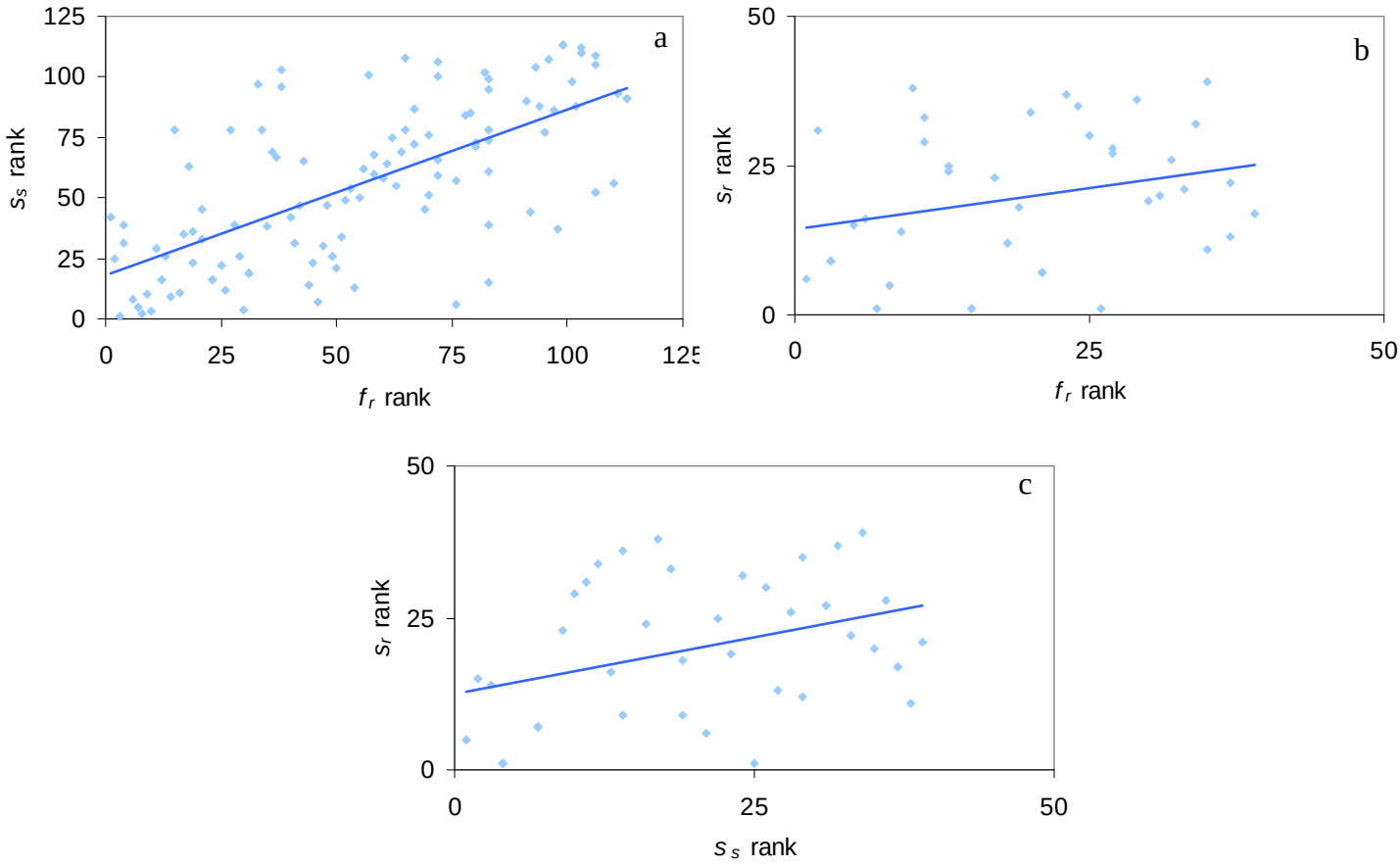

Figure 4.13: Rank correlation of a: f_r and s_s; b: s_r and f_r; c: s_r and s_s. Each point corresponds to a single experiment. The regression line has a slope of a: 0.69; b: 0.27; c: 0.37

As a result, f_r and s_s were found to be significantly correlated ($P < 0.01$) with a correlation coefficient of 0.69. This correlation coefficient may be used to model rank correlation of f_r and s_s in a Monte-Carlo sampling to estimate uncertainty on quantities resulting from an inhalation of Pu, such as the committed dose. On the other hand, no real correlation was found between f_r and s_r, or s_r and s_s: it might be because only few values of s_r were derived in this study. Alternatively, the discrete sets of three dissolution parameters determined in this study can be sampled to represent the variability in absorption, implicitly taking the correlation between f_r, s_r and s_s into account.

4.6 Conclusion

This chapter summarizes the information gathered on the conditions of internal exposure of workers at the R4-T4 facilities handling the purification and expedition of Pu as well as current monitoring programmes at AREVA NC La Hague. The parameters needed for dose assessment of R4-T4 workers were estimated with their associated uncertainty. They are related to the measurement of excreted activity, size distribution of aerosols, isotopic composition and pulmonary absorption of Pu compounds. This information will be used in the next sections of this manuscript to calculate minimum detectable doses in such conditions of exposure and monitoring.

However, no size distribution of the aerosol could be derived from the size distribution of the Pu powder. This may highlight a use for further research in the topic of characterisation of exposure conditions at the workplace.

Specific values of absorption parameters for various chemical forms of Pu were determined from *in vitro* and *in vivo* experiments and from human contamination cases. Pu dioxide, MOX, oxide graphite, Maralinga soil and Palomares dusts may be considered as insoluble compounds, while Pu nitrate, chloride, Pu-Na alloy, Pu-Mg alloy, Pu-TBP complex and industrial residues may be classified as moderately soluble compounds, and citrate as a rapidly soluble compound. Average and median estimates were calculated for f_r, s_r, and s_s for each Pu compound that can be used as better estimates than reference absorption types for a specific chemical form, as recommended by the ICRP (2002a) and Bailey *et al* (2007), especially for lung dose calculation. Such information may be useful in different workplaces within and out of AREVA NC La Hague, along with similar study of other parameters.

CHAPTER 5

Evaluation of a monitoring programme

5.1 Aim

The quality of a monitoring programme may be evaluated by its sensitivity in terms of minimum detectable dose (MDD). To be realistic, the MDD should be assessed taking into account uncertainties regarding dose calculation: from a measurement result at the decision threshold (DT), an effective dose PDF can be calculated through the uncertainties in the bioassay measurement and in the exposure conditions defined by the time of contamination, the AMAD and the absorption rate of the aerosol.

The MDD is then determined as the 95th percentile of this PDF. Applying this approach, it can be assured with a 95 % level of confidence that the MDD is not exceeded when no activity is detected in the sample.

5.2 Parameters of the study

The information on the monitoring program (Section 4) was modelled to derive MDD. Firstly, it was supposed that possible contamination of workers could occur by acute inhalation of ^{239}Pu dioxide particles at a single unknown time during the monitoring interval. Only this plutonium isotope was considered: for simplicity and because it is the most abundant in the spent fuel. Secondly, it was assumed that the observed measurement of a routine faecal sample was equal to 5 counts, first integer above the DT. All uncertain parameters were modelled by PDFs except for Pu absorption.

- The probability of time of contamination was modelled by a uniform PDF between 0 and 180 days, thus conservatively maximizing the uncertainty due to the time of intake (Molokanov and Blanchardon, 2007).
- As no accurate information was available about the AMAD of the aerosol which could be inhaled by workers, it was assumed to take any value between 1 and 10 µm with uniform probability.
- The uncertainty on the absorption of Pu dioxide into blood was modelled using all data of Table 4.4 related to Pu dioxide and MOX.
- The measurement uncertainty is represented by Poisson PDF with a mean background of 2.2 counts per 48 h.

- The measurement uncertainty introduced by Type B uncertainty is modelled by a lognormal PDF with a geometric mean of 1 and a geometric standard deviation of 3 (Marsh *et al*, 2008b).

With the WeLMoS method, three prior PDFs of the intake were compared: a uniform *P(i)* assuming that all intakes between 0 and 10,000 Bq have the same probability to occur; an exponential *P(i)* proportional to e^{-i} (where *i* is expressed in Bq) assuming that the smallest intakes are the most probable; the alpha-prior (Section 2.2.2) with alpha equal 0.001 consistently with the historically observed frequency of positive measurement results in AREVA La Hague. The exponential and alpha priors are also truncated at 10,000 Bq. These three priors were chosen as extreme hypotheses that could be made on the intake before measurement.

5.3 Methods

5.3.1 Classical method

The classical method is used to calculate the intake PDF, of which the 95th percentile is the minimum detectable intake (MDI) with a level of confidence of 95%. If the biokinetic model is fixed, the MDD can be derived by multiplying the MDI by e_{50}. On the other hand, if at least one biokinetic parameter is uncertain, the MDD cannot be easily determined because of the correlation of the MDI with e_{50} through the biokinetic model which is used both to derive the intake from the measurement and to calculate e_{50}. However, the MDD can be conservatively overestimated by multiplying the MDI at a level of confidence of 95% by the PDF of e_{50} for the different biokinetic models; the MDD is then less than the 95th percentile of the resulting PDF.

The detailed algorithm is in Appendixes. For this study, the likelihood of the measurement result given the time of intake *t*, the *AMAD*, the absorption *abs*, and the intake *i* is a Poisson PDF of mean λ with:

$$\lambda = i \times m(t, AMAD, abs) \times f \ , \qquad \text{Equation 5.1}$$

where *f* is a multiplicative error factor modelling Type B uncertainty sampled from a lognormal PDF.

The classical method was used only when one monitoring period was considered as it is not straightforward to integrate knowledge brought by multiple measurement results with this method.

5.3.2 WeLMoS method

The WeLMoS method applied in this study is slightly modified from the algorithm published by Puncher and Birchall (2008). In the published WeLMoS method, for each sampled set of parameters t_k, $AMAD_k$, abs_k, the likelihood of the measurement given the intake *i* and the exposure parameters $P(M \mid i, t_k, AMAD_k, abs_k)$ is calculated for an *a priori* specified set of intake values linearly spaced (Fig. 5.1.a1): the integral of the likelihood is assessed by rectangles. However, the linearly spaced

rectangles are not the best method to integrate and can strongly underestimate the integral (Fig. 5.1.a2).

Therefore, the WeLMoS method was modified to calculate the integral using dichotomy techniques: the interval between intakes is function adapted to the variation of the likelihood. Therefore, a better estimation of the integral of likelihood is obtained (Fig. 5.1.b1 and b2).

To calculate the likelihood of the measurement given the intake $P(M \mid i)$, the different $P(M \mid i, t_k, AMAD_k, abs_k)$ for a fixed value of i are summed for all the values of k. In the published WeLMoS method, the same set of intakes is used to calculate $P(M \mid i, t_k, AMAD_k, abs_k)$ and $P(M \mid i)$ (Fig. 5.1.a3). In the modified WeLMoS method, $P(M \mid i)$ is calculated for a linearly spaced set of intakes (Fig. 5.1.b3). The likelihood assigned to the linearly spaced intakes is equal to the sums of the likelihoods calculated for the dichotomy-determined intakes belonging to the interval between two linearly spaced intakes (Fig. 5.1.b3).

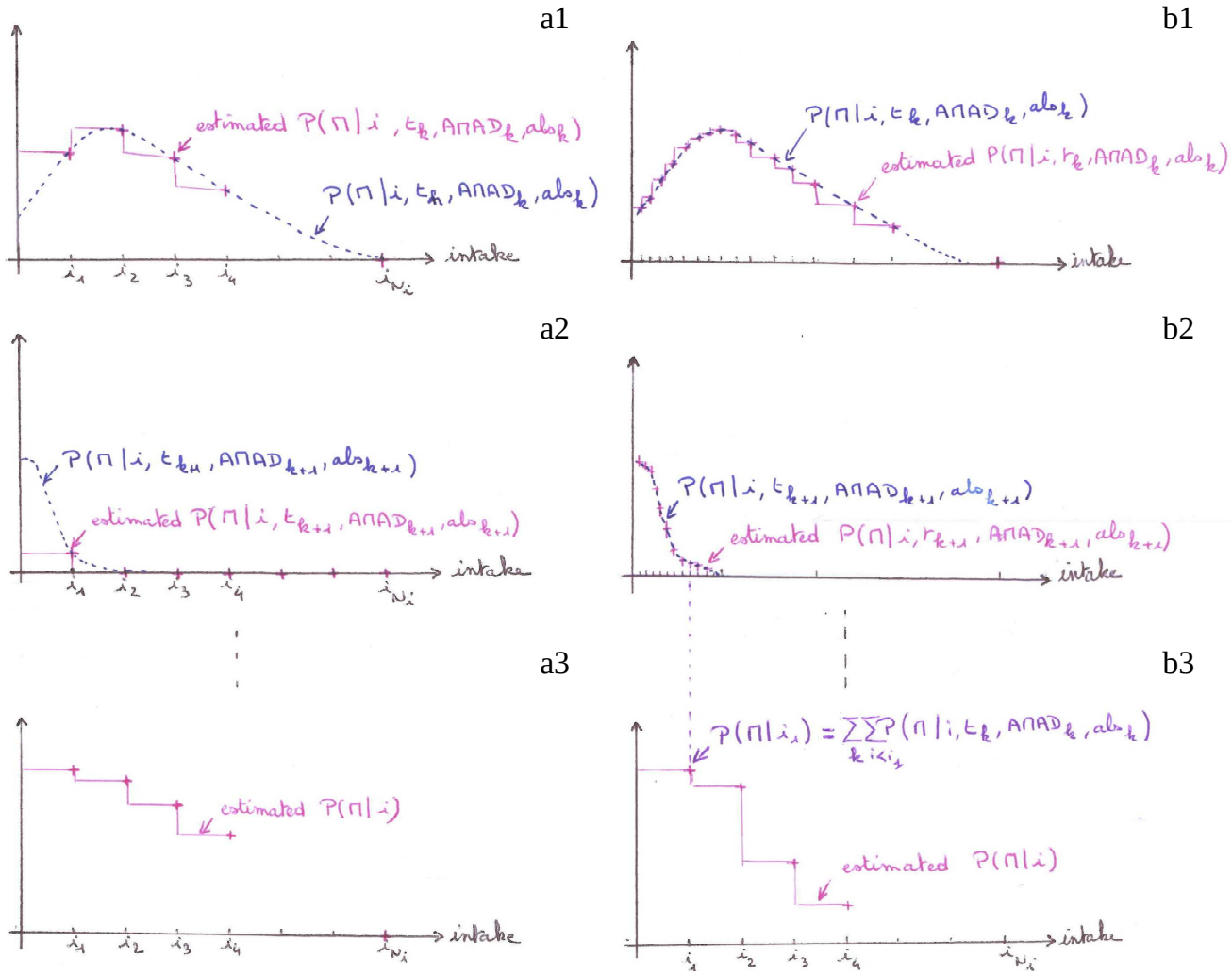

Figure 5.1 : The WeLMoS method published by Puncher and Birchall (2008) (a) and the WeLMoS method modified for this study (b) : calculation of $P(M \mid i, t_k, AMAD_k, abs_k)$ (1); calculation of $P(M \mid i, t_{k+1}, AMAD_{k+1}, abs_{k+1})$ (2); calculation of $P(M \mid i)$ (3)

In this way, the precision in the likelihood is kept in order to obtain representative posterior probabilities for the intake and for the dose. The width of the interval between linearly-spaced

intakes is fixed by the user of the method. With this improvement of the method, good results are obtained. The detailed algorithm is in Appendixes. The same likelihood as for the classical method is used (Eq. 5.1).

Convergence of the results is obtained for more than 100,000 sampling of the exposure conditions and Type B uncertainty. In this study, 100,000 sample sets are used in both the WeLMoS and classical methods.

In the WeLMoS method, the integration of several measurement results is easily done by multiplying the likelihoods of the each measurement for the same sampled set of exposure conditions and the same intake. As an example, the likelihood $P(M_1, M_2 | i, t, AMAD, abs)$of two measurements M_1 and M_2 given the intake i, the time of contamination t and the *AMAD* and the absorption *abs* is calculated by:

$$P(M_1, M_2 | i, t, AMAD, abs) = P(M_1 | i, t, AMAD, abs) \times P(M_2 | i, t, AMAD, abs) \text{ .} \quad \text{Equation 5.2}$$

5.3.3 Bayesian network

The Bayesian network described in Section 2.5.4 was also applied to calculate the MDD. The algorithm is presented in Appendixes. Its main problem is the discretisation of the uncertain parameters. Increasing the number of discrete values improves the accuracy of the calculation but also the number of combinations to be considered and consequently the computation time also increases and can be prohibited in practice.

Its influence was estimated by varying the interval of discretisation for each variable. The best discretisation was selected as the largest intervals yielding the same results as the smallest intervals (Table 5.1). For the time of contamination, an interval of 10 days is the optimised discretion; for the bioassay quantity, they are 19 different values logarithmically distributed.

Table 5.1: Discretisation of the variables in the Bayesian network to calculate the MDD

Variable	Discretisation
Intake (Bq)	0; 10^{-4}; $5x10^{-4}$; 10^{-3}; $5x10^{-3}$; 10^{-2}; $5x10^{-2}$; 10^{-1}; $5x10^{-1}$; 1; 5; 10; 20; 30; 40; 50; 100; 150; 300; 600; 1,000
AMAD (µm)	1; 3; 5; 10
Absorption into blood	Type M; Type S
Time of contamination (d)	0; 10; 20; 30; 40; 50; 60; 70; 80; 90; 100; 110; 120; 130; 140; 150; 160; 170; 180
Bioassay quantity (Bq)	0; 10^{-6}; 10^{-5}; 10^{-4}; $5x10^{-4}$; 10^{-3}; $5x10^{-3}$; 10^{-2}; $5x10^{-2}$; 10^{-1}; $5x10^{-1}$; 1; 5; 10; 50; 100; 200; 500; 1,000
Dose (mSv)	0 10^{-3}; 10^{-2}; 10^{-1}; $5x10^{-1}$; 1; 2; 3; 4; 5; 6; 7; 8; 9; 10; 15; 20; 50; 100; 500; 1,000; 10,000

The discretisations of the intake and dose are adjusted according to the PDF wanted as a result. The 66 sets of f_r, s_r and s_s obtained for Pu dioxide and MOX (Fig. 4.10) are too many for a

manageable computation time. Therefore, a mixture of Type M and S is chosen from Fig. 4.12, modelled as a probability of 0.162 for Type M and 0.838 for Type S (Fig. 5.2). For the AMAD, the standard discretisation of DCAL, which is the same as in the ICRP CD-ROM (ICRP, 1998), is used.

The probabilities assigned to the intervals are the same as for the classical method and as the WeLMoS method.

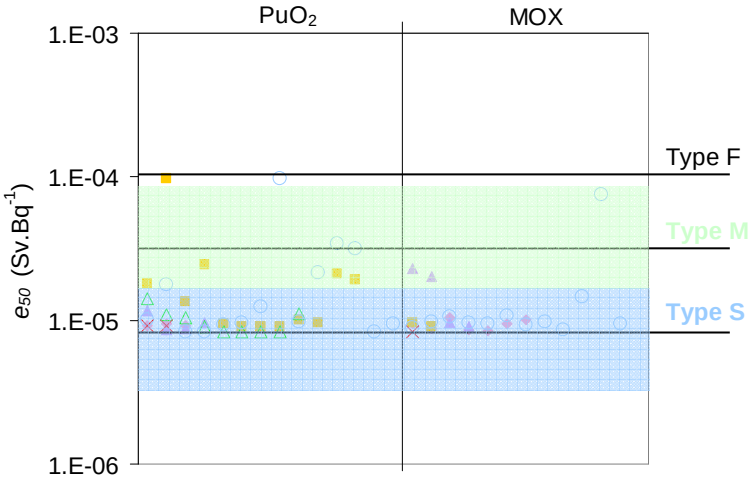

Figure 5.2: Proportions of the sets of f_r, s_r and s_s calculated for Pu dioxide and MOX attributed to Type M (11 values or 16.2 %) and S (57 values or 83.8 %) for modelling probability in the Bayesian network.

To integrate several measurements in the Bayesian network, its structure is modified by adding as many bioassay quantities and measurements as needed. The structure for two measurements M_1 and M_2 is presented in Figure 5.3. Eq. 2.72 to Eq. 2.77 are easily extended to multiple measurement values. The detailed algorithm is presented in Appendixes.

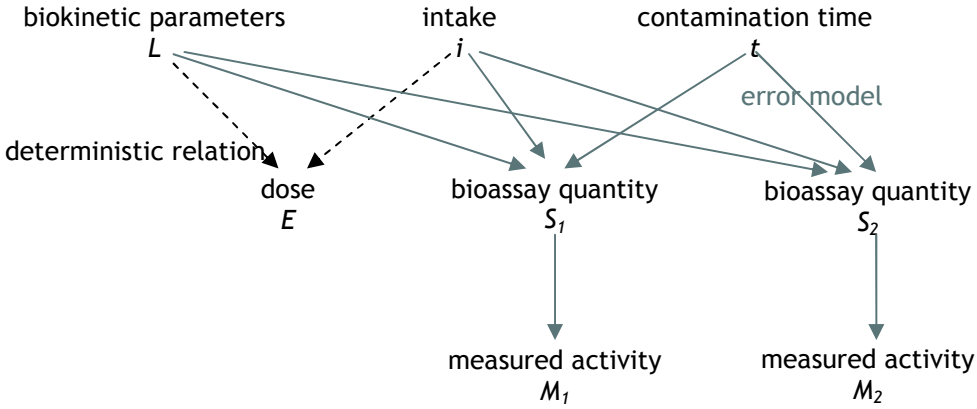

Figure 5.3: Structure of the Bayesian network with two measured activities

5.4 Consistency between Bayesian network and WeLMoS method

5.4.1 Method

The Bayesian network and the WeLMoS method solve the same problem with similar hypotheses except for discrete or continuous variables. The comparison of their results should provide quality

assurance validation of their implementation. Simple model hypotheses were used for a comparison purpose:

- contamination by inhalation of ^{239}Pu aerosol with absorption Type S and AMAD either 1, 5 or 10 µm with equal probability;
- one routine faecal measurement of 50 counts with a mean background of 0.1 count;
- SF = 3;
- prior probability of *i* uniform between 1 and 23 Bq (to obtain 10 values of intake);
- prior probability of *t* uniform between 0 and 180 d.

The discretisation of the Bayesian network is shown in Table 5.2. For this comparison, the sampled sets of time of contamination, AMAD and absorption for the WeLMoS method are the same as the combinations of discrete values of these variables within the Bayesian network. Type B uncertainty is modelled by a lognormal PDF and integrated differently in the two methods. In the Bayesian network, it is represented by the probability *P(S|i, L, t)* (Section 2.5.4). In the WeLMoS method, it is integrated by introducing the multiplicative error *f* distributed according to the lognormal PDF. For this comparison, ten values of *f* are sampled.

Table 5.2: Discretisation of the variables in the Bayesian network for comparison with the WeLMoS method.

Variable	Discretisation
Intake (Bq)	1; 3; 5; 8; 10; 13; 15; 18; 20; 23
AMAD (µm)	1; 5; 10
Absorption into blood	Type S
Time of contamination (d)	1; 20; 40; 60; 90; 110; 130; 150; 170; 180
Bioassay quantity (Bq)	0; 10^{-5}; 10^{-4}; $2x10^{-4}$; $3x10^{-4}$; $5x10^{-4}$; $7x10^{-4}$; $9x10^{-4}$; $1.1x10^{-3}$; $1.3x10^{-3}$; $1.7x10^{-3}$; $3x10^{-2}$; $5x10^{-2}$; 10^{-1}; $5x10^{-1}$; 1; 3; 5; 10
Dose (mSv)	0; 10^{-3}; 10^{-2}; $5x10^{-2}$; 0.1; 0.15; 0.2; 0.25; 0.3; 0.35; 0.4; 0.45; 0.5; 0.55; 0.6; 0.65

5.4.2 Results and discussion

In Fig. 5.4, the result of the comparison shows the consistency between the two methods.

The precision of the WeLMoS method depends only on the number of Monte-Carlo simulations and not on the number of possible combinations of the different variables since only the global likelihood is evaluated. It yields a fast and efficient solution to any uncertain problem provided the probabilities of the combinations are known. On the other hand, the robustness of the result when the probability of an event is changed (for example the probability associated with a contamination time) is difficult to assess because only the likelihood of the Monte-Carlo sampled combinations are evaluated.

The Bayesian network explicitly determines the probability of each possible combination of parameter values. A change of hypothesis in the modelling of an uncertain parameter induces a

different weighting of the sums and its impact can be evaluated directly. The network advantages are therefore its readability and its flexibility in the definition of hypotheses by using discrete probability. However, its calculation time can be prohibitive depending on the number of uncertain parameters and of their discrete values, which dramatically increase the number of possible combinations.

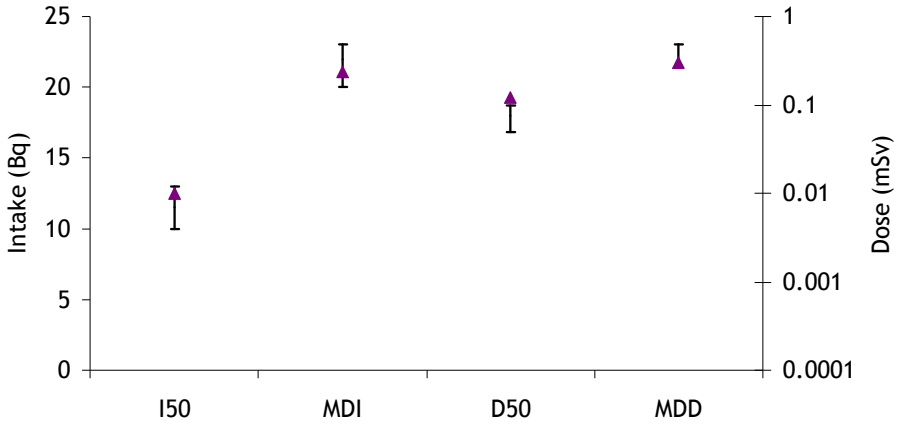

Figure 5.4: Comparison of the results obtained with the WeLMoS method (▲) and with the Bayesian network (intervals) for the same problem described in the text. I50 (respectively D50): median intake (respectively dose); MDI (respectively MDD): minimum detectable intake (respectively dose) with a confidence level of 95 %

The difference between the Bayesian network and the WeLMoS method lies in the definition of the problem. The Bayesian network evaluates the likelihood of an interval between two discrete values, while the WeLMoS method evaluates it for each specific value. Therefore, the WeLMoS method gives results of high precision which is not artificial if the problem definition is based on actual precise knowledge. Still assigning continuous prior probabilities to uncertain parameters is a strong hypothesis which may rely on no specific knowledge such as the uniform prior probability assumed for the contamination time. By assigning discrete priors to intervals, the Bayesian network may limit the strength of the hypotheses to be more consistent with the actual knowledge on uncertain parameters. Because of their complementarities and for comparison purposes, both methods are used in this work.

5.5 MDD for one monitoring period

5.5.1 Preliminary results

The median of the intake and dose PDFs and the MDI and MDD with a confidence level of 95 % calculated by the classical and WeLMoS methods are shown in Fig. 5.5 and Table 5.3. By calculating the ratio of the MDD to the median dose, the relative uncertainties are shown to be significant: between 4 and 15. The MDD from the classical method is in between the MDD obtained from the WeLMoS method with the three prior intake probabilities: this may tend to confirm that these intake priors are extreme visions of the reality.

To assume before any measurement that all intakes between 0 and 10,000 Bq have the same probability to occur is a very conservative hypothesis leading to a MDD greater than 10 mSv. On the other hand, to suppose *a priori* that the lower intakes are more probable by using an exponential prior PDF results in a MDD equal to 0.05 mSv. From the alpha-prior, it can be concluded that the MDD is below 1 nSv.

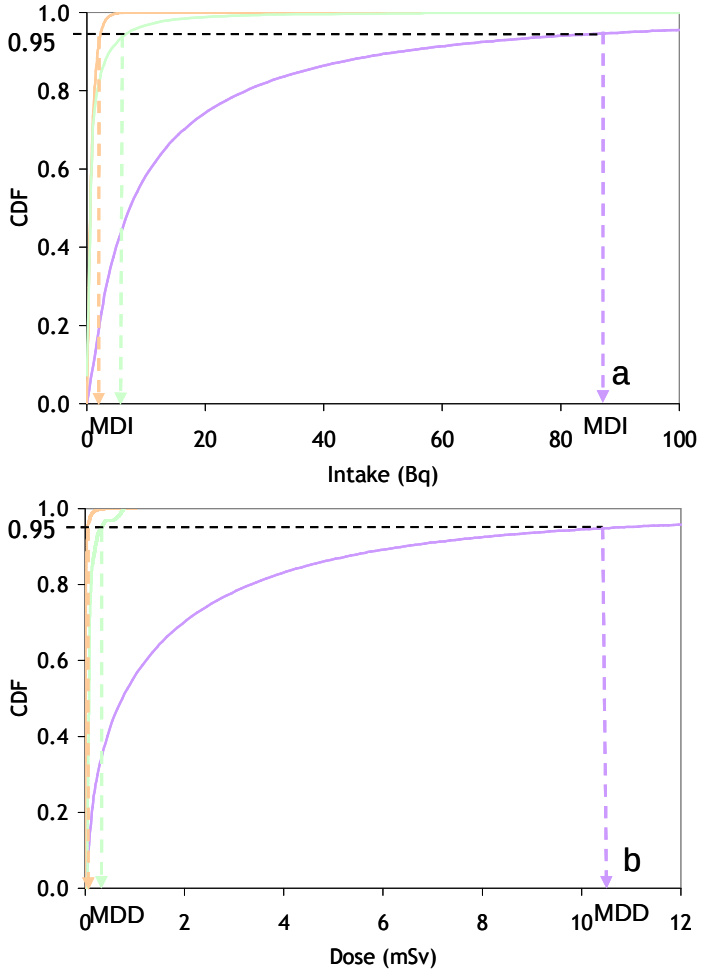

Figure 5.5: Intake (a) and dose (b) CDF obtained from the classical method (green) and from the WeLMoS method with uniform (purple) or exponential (orange) intake prior PDFs; model and parameters as presented in 5.2; MDI (a) and MDD (b) determined with a level of confidence of 95 % (arrows)

Table 5.3: Median and 95th percentile of the intake and dose PDFs obtained from the classical method and from the WeLMoS method with uniform or exponential intake prior PDFs; model and parameters as presented in 5.2. MDI: minimum detectable intake with a level of confidence of 95 %. MDD: minimum detectable dose with a level of confidence of 95 %

Method	Intake (Bq)			Dose (mSv)		
	Median	MDI (95th percentile)	Uncertainty factor	Median	MDD (95th percentile)	Uncertainty factor
classical	0.7	7.3	10	7.8×10^{-2}	3.2×10^{-1}	4.0
WeLMoS, exponential *P(i)*	0.6	2.4	4.0	7.2×10^{-3}	5.2×10^{-2}	7.2
WeLMoS, uniform *P(i)*	7.3	92	13	7.5×10^{-1}	$1.1 \times 10^{+1}$	15
WeLMoS, alpha *P(i)*		$< 10^{-9}$			$< 10^{-6}$	

5.5.2 Difference between classical and WeLMoS methods

The main difference between the classical method and the WeLMoS method is that the intake is assumed to be fixed and unknown in the former while it is associated with a subjective probability in the latter. The classical method calculates levels of confidence on the intake, but the derivation of levels of confidence on the dose is not straightforward. In the WeLMoS method, both posterior probabilities of the intake and of the dose are calculated using Bayes' theorem.

These two methods model and propagate uncertainty in different ways. Their results are therefore difficult to compare. Still, by looking at the algorithm, the classical method may be seen as more conservative that the WeLMoS method, especially regarding the dose. However, the obtained results are not particularly conservative. Indeed, the lack of explicit assumption of prior knowledge of intake is compensated by assumptions on the other variables such as the time of contamination, which become all the stronger. This results in implicit assumptions which make the classical method less reliable than the WeLMoS method where all hypotheses are explicitly expressed.

5.5.3 Sensitivity analysis of the MDD

The influence of the different parameters on the MDD was studied by varying one parameter at a time:

- The intake prior probabilities are defined such as for *i*, expressed in Bq, between 0 and a maximum, *P(i)* is proportional to 1 or to e^{-i}, and for *i* greater than the maximum, *P(i)* equals 0. The maximum intake was varied from 1 to 10,000 Bq.
- Two different distributions of AMAD were tested: (1) uniform probability between 1 and 10 µm; this is a large but plausible interval as no precise information on the AMAD is available; (2) uniform probability between 6.2 and 10.5 µm; these are the two extreme AMAD of the handled Pu powders. In this second case, the assumed size distribution of the aerosol is the same as for the powder.
- Absorption is represented as randomly sampled sets from the study of the absorption of Pu dioxide and MOX with or without the 6 sets of values with a rapidly dissolved fraction higher than 0.1 (Fig. 4.10).
- SF was varied between 1.9 and 3.5; these extreme values were reported by Marsh *et al* (2007) for Pu faecal measurement after contamination by inhalation.
- The time of intake is either randomly sampled from a uniform PDF between 0 and 180 days or fixed at the beginning of the monitoring interval.

The results of the sensitivity study are summarized in Fig. 5.6. The shape of the intake prior probability and its maximum have a strong influence on the MDD. A modification of the prior probability of intake is directly reflected in the posterior intake and dose probabilities because the

single measurement result available in a routine monitoring interval does not bring enough knowledge to balance the influence of the prior, unlike in special monitoring where multiple bioassay data is gathered after an incident.

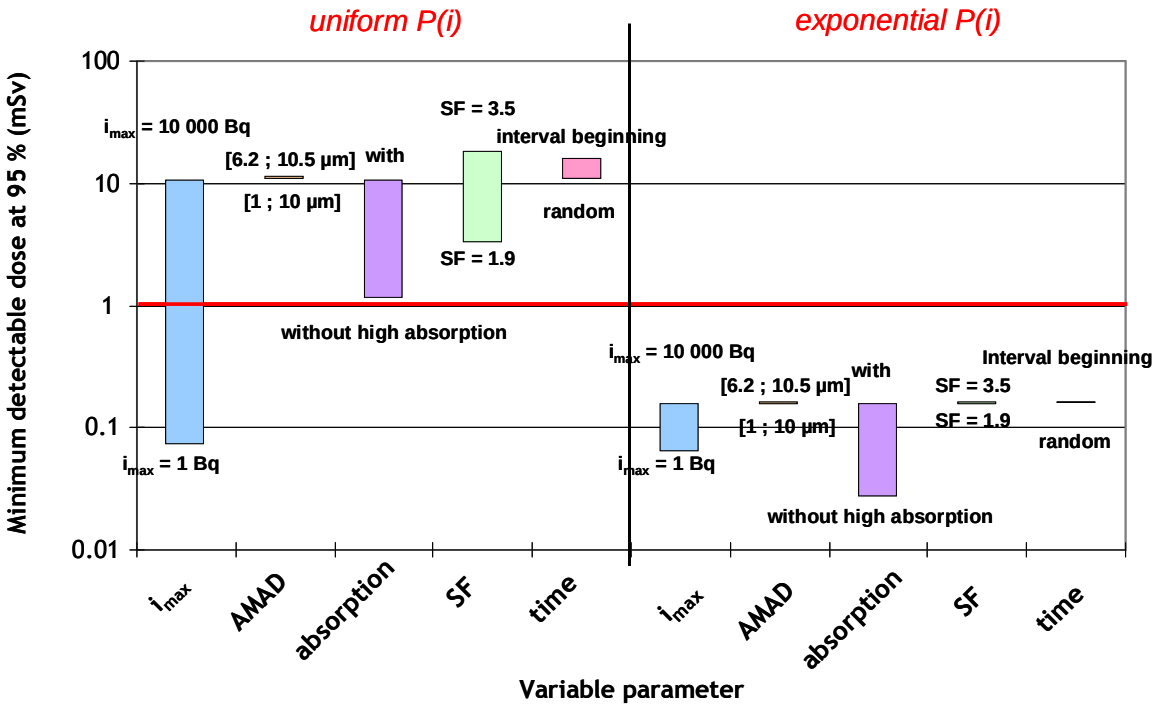

Figure 5.6: Sensitivity study of the MDD with a level of confidence of 95 % using the WeLMoS method with uniform (left) or exponential (right) intake prior probabilities. One parameter was varied at a time; other parameters being fixed at values described in the text.

Changing the interval of possible AMAD from [1, 10 µm] to [6.2, 10.5 µm] leads, in average, to an increase of the AMAD. When the AMAD increases, the faecal excretion goes up in the first 8 days after inhalation and decreases afterwards (Fig. 5.7). So, over 180 days, the faecal excretion mostly decreases with increasing AMAD. As a consequence the MDD, being determined from a fixed measurement result, slightly increases with the AMAD.

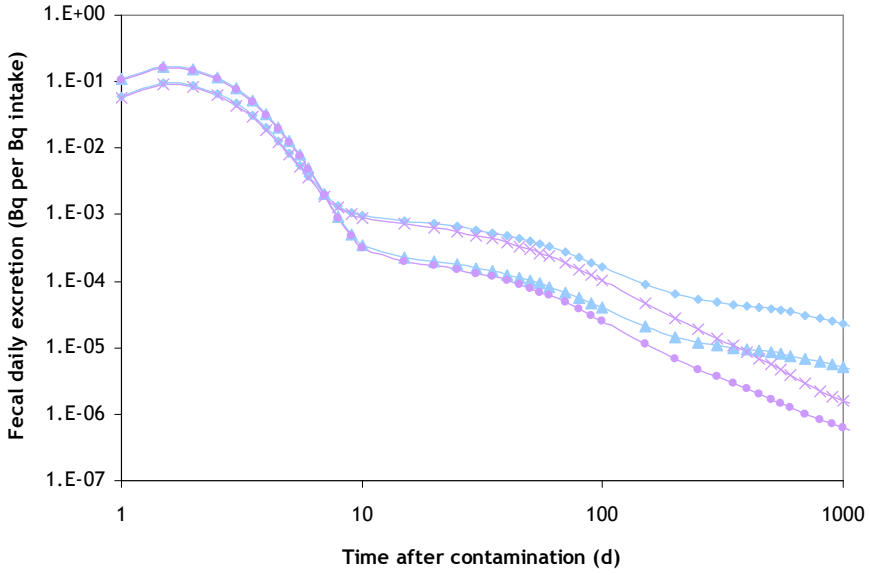

Figure 5.7: Daily faecal excretion of ^{239}Pu after acute inhalation: Type S, AMAD = 1 µm (◆), Type S, AMAD = 10 µm (▲); Type M, AMAD = 1 µm (×); Type S, AMAD = 10 µm (●).

The MDD varies with the data retained for Pu absorption because of some fast absorption values reported in the literature which lead to an increase of the MDD as compared to Type S.

The SF has a strong influence on the MDD because it directly and exponentially affects the uncertainty on the measurement. The higher the SF, the more intake values can fit the measurement results and higher intake values can then be in agreement with the measurement. Thus, a large SF results in a high MDD.

5.5.4 Results for realistic absorption

From the sensitivity study, it can be concluded that the most important parameter is the prior PDF of the intake. To account for his influence, the 3 extreme intake priors are used throughout the study. Pu absorption in airways is a critical factor. As seen in Section 4.5.2, the very fast absorption values obtained for some Pu dioxide or MOX compounds relate to either nanometric particles or questionable experiments. Therefore, these values are considered as unrealistic for the Pu handled in R4-T4 facilities: a new distribution of the absorption is used instead for final calculations (Table 5.4).

Table 5.4: Realistic values of the absorption into blood used to model its variability in this work (from Table 4.4)

Compound	f_r	s_r (d^{-1})	s_s (d^{-1})	Reference
$^{238}PuO_2$	2.4×10^{-4}	100	2.4×10^{-3}	Mewhinney and Diel, 1983
	8.2×10^{-4}	100	1.9×10^{-3}	Morgan *et al*, 1988
	1.6×10^{-3}	100	3.4×10^{-4}	Morgan *et al*, 1988
	7.1×10^{-5}	100	3.4×10^{-4}	Morgan *et al*, 1988
	1.2×10^{-3}	100	1.6×10^{-4}	Morgan *et al*, 1988
$^{239}PuO_2$	4.2×10^{-2}	100	1.4×10^{-3}	Bair and McClanahan, 1961
	4.5×10^{-2}	0.2	2.9×10^{-3}	Bair and McClanahan, 1961
	1.2×10^{-1}	8.3	1.0×10^{-4}	Bair and Willard, 1963
	1.6×10^{-3}	100	1.5×10^{-2}	Bair and Willard, 1963
	2.0×10^{-4}	100	4.0×10^{-5}	Bair *et al*, 1980
	1.0×10^{-4}	100	6.2×10^{-6}	Guilmette *et al*, 1984
	1.0×10^{-4}	100	6.2×10^{-6}	Guilmette *et al*, 1987
	1.0×10^{-4}	100	3.5×10^{-6}	Guilmette *et al*, 1987
	1.4×10^{-3}	100	7.6×10^{-5}	Park *et al*, 1972
	3.8×10^{-3}	100	4.1×10^{-4}	Bair *et al*, 1980
	4.6×10^{-3}	100	3.2×10^{-4}	Bair *et al*, 1961
	9.2×10^{-5}	100	7.2×10^{-6}	Morgan *et al*, 1988
	9.2×10^{-5}	100	4.8×10^{-6}	Morgan *et al*, 1988

	9.2×10^{-5}	100	4.8×10^{-6}	Morgan *et al*, 1988
	9.2×10^{-5}	100	1.0×10^{-5}	Morgan *et al*, 1988
	3.9×10^{-4}	100	1.1×10^{-4}	Stather *et al*, 1975
	1.1×10^{-3}	100	2.9×10^{-5}	Stather *et al*, 1975
	1.0×10^{-3}	100	6.0×10^{-3}	Rhoads *et al*, 1986
	1.0×10^{-3}	100	2.6×10^{-4}	Sato *et al*, 1999
	1.0×10^{-3}	100	2.2×10^{-3}	Sato *et al*, 1999
	1.0×10^{-3}	100	1.0×10^{-4}	Stradling *et al*, 1987
PuO_2	5.8×10^{-5}	100	4.8×10^{-5}	Stanley *et al*, 1980b
(mixture of ^{238}Pu,	3.1×10^{-4}	100	9.2×10^{-6}	Carbaugh and La Bone, 2003
^{239}Pu, ^{240}Pu)	2.0×10^{-3}	9.9	9.7×10^{-6}	Carbaugh and La Bone, 2003
	7.0×10^{-4}	1.6	1.3×10^{-5}	Carbaugh and La Bone, 2003
	0	_	3.5×10^{-5}	Eidson and Mewhinney, 1983
	3.0×10^{-3}	0.7	8.2×10^{-6}	Rateau-Matton *et al*, 2004
	3.0×10^{-3}	100	1.0×10^{-4}	Lataillade *et al*, 1995
	2.2×10^{-3}	100	1.1×10^{-4}	Lataillade *et al*, 1995
	5.8×10^{-5}	100	4.8×10^{-5}	Stanley *et al*, 1980b
	1.3×10^{-4}	100	6.0×10^{-5}	Kanapilly and Boecker, 1981
	1.0×10^{-3}	100	1.0×10^{-4}	Lataillade *et al*, 1995
	5.1×10^{-3}	100	1.6×10^{-4}	Ramounet *et al*, 2000
	7.0×10^{-3}	0.8	3.1×10^{-5}	Rateau-Matton *et al*, 2004
	2.2×10^{-3}	0.2	5.9×10^{-4}	Rateau-Matton *et al*, 2004
MOX	2.2×10^{-5}	100	4.8×10^{-5}	Stanley *et al*, 1980a
	2.1×10^{-4}	100	1.9×10^{-6}	Stanley *et al*, 1982
	1×10^{-3}	100	1×10^{-4}	Foster, 1991
	5.8×10^{-2}	0.1	4.5×10^{-5}	Rateau-Matton *et al*, 2004
	4.6×10^{-2}	0.3	2.4×10^{-5}	Rateau-Matton *et al*, 2004
	5.3×10^{-2}	0.2	1.0×10^{-4}	Rateau-Matton *et al*, 2004
	4.6×10^{-2}	100	2.1×10^{-3}	Lataillade *et al*, 1995
	1.6×10^{-2}	100	2.6×10^{-3}	Lataillade *et al*, 1995
	2.2×10^{-5}	100	4.8×10^{-5}	Stanley *et al*, 1980a
	2.1×10^{-4}	100	1.9×10^{-6}	Stanley *et al*, 1982
	1.2×10^{-3}	100	1.5×10^{-4}	Kanapilly and Boecker, 1981
	6.0×10^{-4}	100	6.0×10^{-5}	Ramounet *et al*, 2000
	2.0×10^{-3}	100	3.0×10^{-4}	Ramounet *et al*, 2000
	2.9×10^{-4}	100	6.3×10^{-5}	Ramounet *et al*, 2000
	2.0×10^{-3}	100	1.9×10^{-4}	Ramounet *et al*, 2000

5.1×10^{-3}	100	2.7×10^{-4}	Ramounet-Le Gall *et al*, 2003
3.2×10^{-3}	100	1.6×10^{-4}	Ramounet-Le Gall *et al*, 2003
9.8×10^{-4}	100	5.1×10^{-5}	Ramounet-Le Gall *et al*, 2003
1.0×10^{-3}	7.9	1.3×10^{-4}	Rateau-Matton *et al*, 2004
2.0×10^{-3}	0.1	3.2×10^{-5}	Rateau-Matton *et al*, 2004
1.4×10^{-2}	1	1.0×10^{-3}	Rateau-Matton *et al*, 2004

The new median of the intake and dose PDFs and the MDI and MDD with a confidence level of 95 % calculated by the classical and WeLMoS methods obtained with these values of absorption are shown in Fig. 5.8 and Table 5.5. These are considered as the best estimates of the MDI and MDD for the monitoring programme of R4-T4 facilities for one monitoring period.

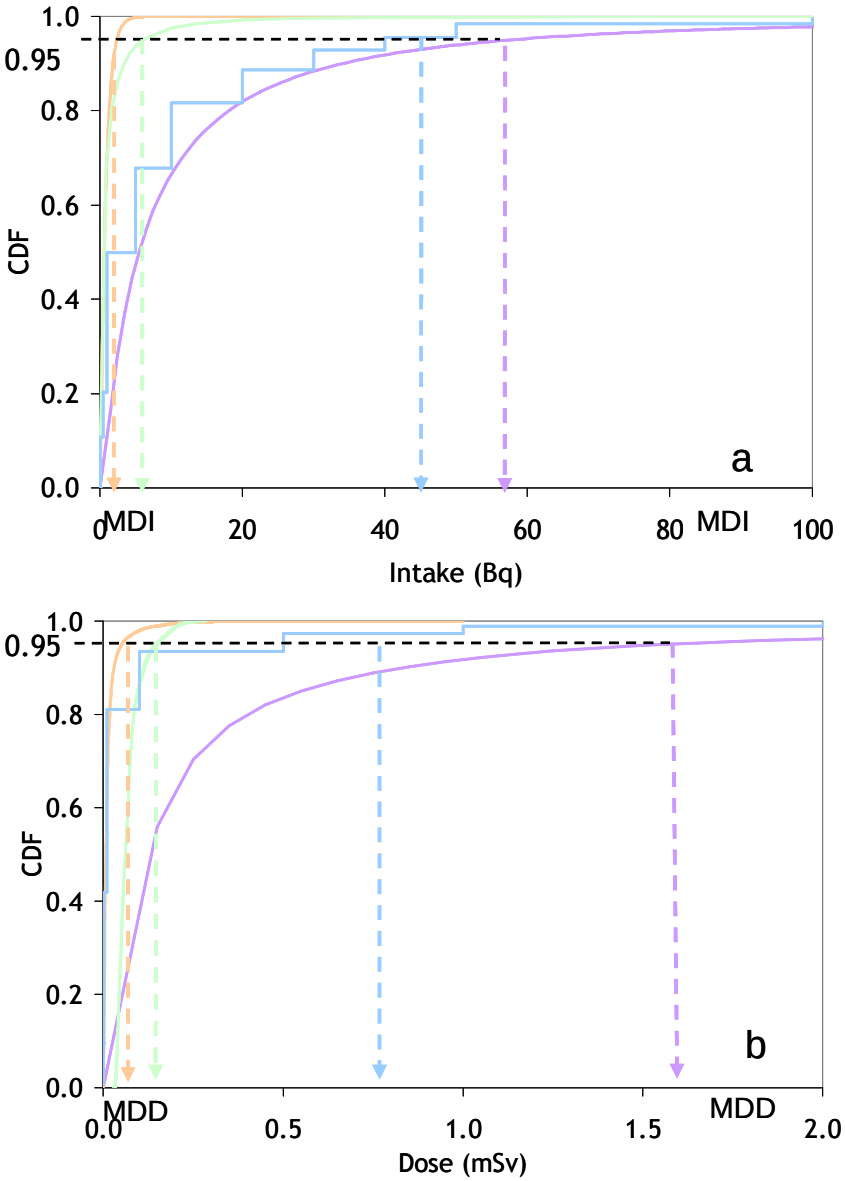

Figure 5.8: Intake (a) and dose (b) CDF obtained from the classical (green) or WeLMoS method, with uniform (purple) or exponential (orange) intake prior PDF, or from the Bayesian network with uniform intake prior PDF (blue); parameter values as described in 5.2 except for realistic values of absorption (Table 5.4); MDI (a) and MDD (b) determined with a level of confidence of 95 % (arrows).

Table 5.5: Median and 95th percentile of the intake and dose PDFs obtained from the classical or WeLMoS method with uniform or exponential intake prior PDFs or from the Bayesian network with a uniform intake prior. Parameters values as described in 5.2 except for realistic values of absorption (Table 5.4); MDI: minimum detectable intake with a level of confidence of 95 %. MDD: minimum detectable dose with a level of confidence of 95 %.

	Intake (Bq)		Dose (mSv)	
Method	Median	MDI (95th percentile)	Median	MDD (95th percentile)
Classical	0.6	6.0	6.2×10^{-2}	1.5×10^{-1}
WeLMoS, exponential *P(i)*	0.6	6.1	6.3×10^{-3}	2.7×10^{-2}
WeLMoS, uniform *P(i)*	5.5	57	1.3×10^{-1}	1.6
WeLMoS, alpha *P(i)*		$< 10^{-9}$		$< 10^{-6}$
Bayesian network, uniform *P(i)*	5 - 10	40 - 50	0.01 – 0.1	0.5 - 1

5.6 Prior adapted to historical data

5.6.1 Method

To determine which intake prior PDF is best adapted to this study, a theoretical distribution of measurement results was calculated by direct Monte-Carlo propagation of uncertainty from the intake prior by adapting the Bayesian network (Fig. 5.9). The first step is to evaluate the probability of each measurement result M_q and of each combination of discrete values i_j, L_k, t_n, and S_o:

$$P(M_q, i_j, L_k, t_n, S_o) = P(M_q|S_o) \times P(S_o|i_j, L_k, t_n) \times P(i_j) \times P(L_k) \times P(t_n) . \quad \text{Equation 5.3}$$

The probability of M_q alone is then calculated by:

$$P(M_q) = \sum_j \sum_k \sum_n \sum_o P(M_q, i_j, L_k, t_n, S_o) . \quad \text{Equation 5.4}$$

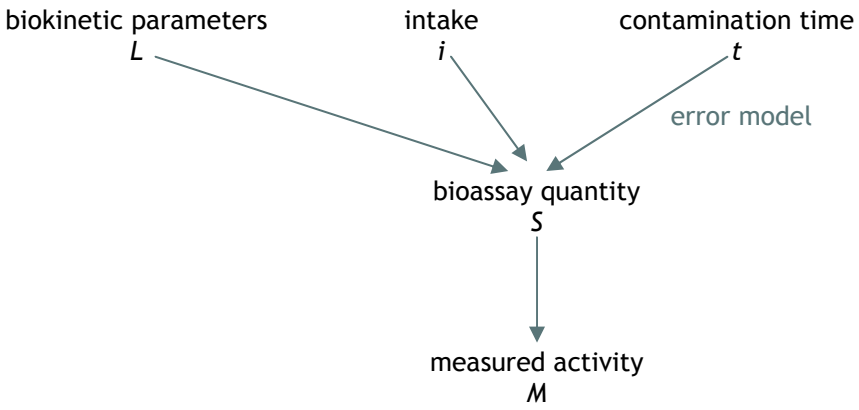

Figure 5.9: Structure of the Bayesian network used to calculate the probability of the measured activity from prior PDFs.

By assessing the percentile corresponding to the decision threshold, it is possible to predict the frequency of positive measurements according to the different intake priors (Fig. 5.10).

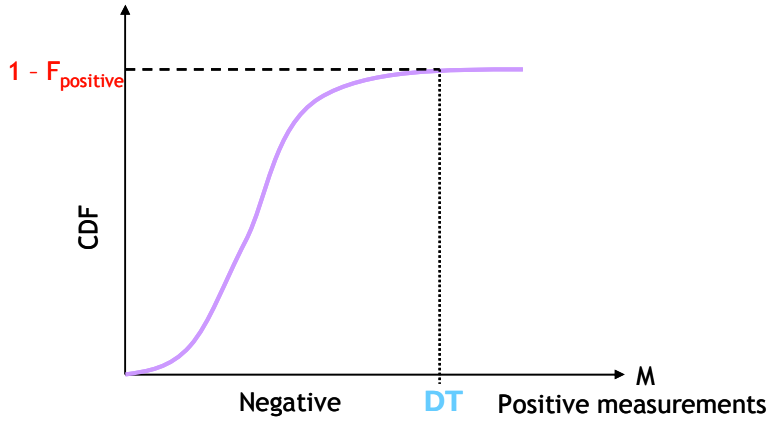

Figure 5.10: Determination of the frequency of positive measurements $F_{positive}$ from the measurement CDF

5.6.2 *Results and discussion*

The uniform prior leads to a frequency of about 0.1, the exponential prior to about 0.01 and the alpha-prior to 0.001 consistently with its definition. Compared with the observed historical frequency of 0.001, the uniform and exponential priors look too conservative while the alpha-prior seems well adapted as long as the conditions of exposure stay constant over time.

However the alpha-prior is so informative that it tends to overwhelm any source of uncertainty, yielding a posterior probability of intake very close to its prior. The strong assumption that the historical frequency of events in the past will stay *a priori* constant, is not balanced by the single data point obtained for each monitoring interval. The uniform prior is too conservative because assuming that a 10,000-Bq intake could be discovered by individual routine measurement and not by air monitoring seems unrealistic for R4-T4 facilities. Therefore, the exponential prior looks like a reasonable if subjective intermediate choice.

As no new specific information can firmly support the definitive choice of a single intake prior probability for this study, the three priors are used to model the imprecision in such choice.

5.7 Annual MDD for R4-T4 workers

The results presented above refer to the MDD of a single monitoring interval. However, a more practical estimator of the sensitivity of a monitoring programme is the yearly MDD which can be directly compared with the dose limits, constraints or annual objective fixed by the company.

In order to calculate the annual MDD, it is assumed that only one intake may occur per year. It occurs in the first monitoring interval and is followed by as many routine measurements as performed in a year. All the measurement results are assumed to be at the DT.

5.7.1 $^{239}PuO_2$

The modelling of the uncertain parameters is the same as in Section 5.2 except for the absorption which is the same as in Table 5.4. The results are gathered in Table 5.6.

Table 5.6: Median and 95th percentile of the intake and dose PDFs obtained from the WeLMoS method with uniform or exponential intake prior PDFs and from the Bayesian network with a uniform intake prior. Parameters values as described in 5.2 except for realistic values of absorption (Table 5.4)

	Intake (Bq)		Dose (mSv)	
Method	Median	MDI (95th percentile)	Median	MDD (95th percentile)
WeLMoS, exponential *P(i)*	0.7	2.5	7.2×10^{-3}	2.6×10^{-2}
WeLMoS, uniform *P(i)*	3.8	31	4.7×10^{-2}	8.4×10^{-1}
WeLMoS, alpha *P(i)*		$< 10^{-9}$		$< 10^{-6}$
Bayesian network, uniform *P(i)*	1 - 5	20 - 30	0.001 – 0.01	0.1 – 0.5

The workers of R4-T4 facilities are monitored every 6 months. Therefore, two measurements separated by 6 months are considered here. Adding a second measurement at the DT decreases the MDD largely for the uniform intake prior and little for the exponential intake prior. The exponential prior appears so informative that adding a measurement equal to the DT does not significantly change the posterior probability. The second measurement at DT even increases the dose median because it brings knowledge in contradiction with the exponential prior, which would predict a value less than DT.

5.7.2 *Different spent fuels*

For completion, it is important to calculate the MDD for the whole isotopic composition of the spent fuel (Table 4.3) rather than only for ^{239}Pu.

To take account of the isotopic composition, it is assumed that only ^{239}Pu is measured in the faecal sample. ^{239}Pu intake i_{239} is assessed from this measurement and the intakes of other isotopes are derived from the known isotopic composition. To calculate the corresponding effective dose, a dose coefficient for the mixture $e_{50,\,mix}$ is used:

$$E = i_{239} \times e_{50,\,mix}\text{, and} \qquad \text{Equation 5.5}$$

$$e_{50,\,mix} = \frac{\%_{238}}{\%_{239}} e_{50,\,238} + e_{50,\,239} + \frac{\%_{240}}{\%_{239}} e_{50,\,240} + \frac{\%_{241}}{\%_{239}} e_{50,\,241}\text{,} \qquad \text{Equation 5.6}$$

where $e_{50,\,j}$ is the dose coefficient of the Pu isotope j and $\%_j$ its relative abundance in the mixture activity.

The MDD are calculated using the same parameter as in Section 5.2 but with the complete isotopic composition and the realistic values of the absorption into blood (Table 5.4) for the uniform, exponential and alpha intake priors with the WeLMoS method and with the Bayesian network. The results are gathered in Table 5.7.

Table 5.7: Annual MDDs obtained by the WeLMoS method and by the Bayesian network with uniform, exponential or alpha intake prior probability. Application to workers of R4-T4 facilities for observed faecal measurements at the decision threshold for different spent fuels.

Intake prior	Method	Spent fuel	MDD (mSv)
Uniform *P(i)*	WeLMoS	PWR1	17
		PWR2	20
		BWR	20
		MOX	24
		MOX_RP	13
	Bayesian network	PWR1	8 < MDD < 9
		PWR2	9 < MDD < 10
		BWR	9 < MDD < 10
		MOX	10 < MDD < 15
		MOX_RP	6 < MDD < 7
Exponential *P(i)*	WeLMoS	PWR1	3.4×10^{-1}
		PWR2	3.5×10^{-1}
		BWR	3.6×10^{-1}
		MOX	4.2×10^{-1}
		MOX_RP	2.4×10^{-1}
	Bayesian network	PWR1	0.5 < MDD < 1
		PWR2	0.5 < MDD < 1
		BWR	0.5 < MDD < 1
		MOX	1 < MDD < 2
		MOX_RP	0.5 < MDD < 1
Alpha *P(i)*	WeLMoS	PWR1	$MDD < 10^{-6}$
		PWR2	$MDD < 10^{-6}$
		BWR	$MDD < 10^{-6}$
		MOX	$MDD < 10^{-6}$
		MOX_RP	$MDD < 10^{-6}$
	Bayesian network	PWR1	MDD = 0[a]
		PWR2	MDD = 0[a]
		BWR	MDD = 0[a]
		MOX	MDD = 0[a]
		MOX_RP	MDD = 0[a]

[a] The dose 0 mSv corresponds to a percentile higher than the 95th.

MDDs for the different spent fuels are close or above the annual dose limit of 20 mSv with the uniform intake prior probability. With the exponential intake prior, the MDDs are below 0.5 mSv per year for the WeLMoS method and close to 1 mSv for the Bayesian network. With the alpha prior, the MDD is below 1 nSv.

The differences between the WeLMoS method and the Bayesian network can be explained by the differences in modelling Type B uncertainty, absorption into blood and in the definition of parameter priors as continuous or discrete. Despite, these strong differences, results are very close.

The MDDs for the different spent fuels are in the same range but the spent MOX is associated with the highest doses because it has the lowest content of ^{239}Pu, inducing the highest $e_{50,\ mix}$ (Eq. 5.6).

5.8 Conclusion

In this section, the MDD was calculated for the workers of R4-T4 facilities using the classical method, the WeLMoS method and the Bayesian network applied to one monitoring period, or to the whole year. The isotopic composition was taken into account to derive the actual MDD for the current monitoring programme. The influence of the uncertain parameters on the MDD was quantified: the intake prior probability and the absorption into blood are the most important. The methods which were compared provide a general frame to estimate MDD and to assess the quality of a monitoring program by comparing MDD with dose constraints, as the monitoring program allows the detection of doses higher than the MDD with a certain confidence level.

The classical method suffers from a lack of flexibility, as it cannot integrate several measurement results so far, and from implicit hypotheses on the uncertain variables. On the other hand, to estimate the MDD with the WeLMoS method or the Bayesian network, an intake prior probability has to be chosen. Since multiple priors may often be selected, a sensitivity analysis of the MDD for different intake priors would be warranted; or an uncertainty analysis for MDD may include each possible intake prior with an associated probability weight. We have judged that in this study, the exponential prior is a reasonable but subjective choice, subject to further discussion.

CHAPTER 6

Optimisation of a monitoring programme

In the previous section, different methods to calculate the MDD for the current monitoring programme of AREVA NC R4-T4 facilities were presented along with their results. As the MDD is a measure of the sensitivity of a monitoring programme, it can be used to optimise the programme by considering the balance between the MDDs of different programmes and the corresponding cost associated with the required measurements.

6.1 Parameters of the study

In order to derive MDDs for different monitoring programmes, the parameters of exposure were considered as in Section 5.2. Firstly, it was supposed that a possible contamination of workers could occur by acute inhalation of Pu dioxide particles at an unknown time during the monitoring interval *T*. The isotopic compositions of the different dioxides are presented in Table 4.3. Secondly, it was assumed that all the observed measurements of the routine faecal or urine samples equalled 5 counts (DT). All uncertain parameters were modelled by PDFs except for absorption.

- The time of contamination was modelled by a uniform PDF between 0 and *T*.
- A uniform PDF between 1 and 10 µm was assigned to the AMAD of the aerosol.
- The uncertainty on the absorption from airways into blood was modelled by the realistic results obtained for Pu dioxide and MOX: Table 5.4 for the WeLMoS method; Type M with a probability of 0.162 and Type S with a probability of 0.838 for the Bayesian network.
- The measurement uncertainty was represented by a Poisson PDF with a mean background of 2.2 counts per 48 h.
- The measurement uncertainty introduced by Type B uncertainty was modelled by a lognormal PDF with a geometric mean of 1 and a SF of 3.

Three, uniform, exponential and alpha, prior PDFs of the intake were considered. Alpha was set to 0.001 consistently with the historically observed frequency of positive measurement results in AREVA NC facility. All priors were truncated at 10,000 Bq.

6.2 Envisaged monitoring programmes

Having determined the MDD for the current monitoring programme with the WeLMoS method and with the Bayesian network, MDDs for a set of conceivable programmes were calculated using the Bayesian network:

a) faecal measurement every 2 years,
b) faecal measurement every year,
c) faecal measurement every 6 months (current),
d) urine measurement every 6 months,
e) urine and faecal measurements alternately every 6 months,
f) faecal and urine measurements alternately every 6 months,
g) faecal and urine measurements every 6 months,
h) faecal measurement every 3 months,
i) urine measurement every 3 months.

These programmes cover a large spectrum of possible measurement frequency and techniques.

6.3 Method

The Bayesian network was used to model the actual limited knowledge on the uncertain parameters by discrete probability rather than by more informative continuous probability. Three different networks were used consistently with the yearly numbers of measurements (Fig. 2.18 for 1 measurement, Fig. 5.3 for 2 measurements, and Fig. 6.1 for 4 measurements).

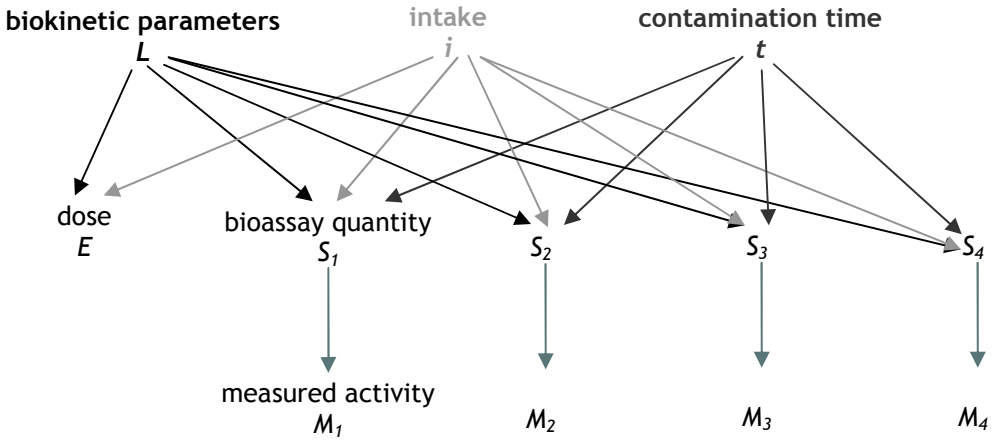

Figure 6.1: Structure of the Bayesian network used to infer the posterior probabilities of intake and dose from 4 measured activities.

The calculation of the posterior probabilities of intake and dose within the Bayesian network for 4 measurements is performed according to Eq. 6.1 to 6.6, following the same logic as for one measurement (Section 2.5.4). The first step is evaluating the joint probability of each combination of discrete values i_j, L_k, t_n, $S_{1,o}$, $S_{2,q}$, $S_{3,r}$, $S_{4,u}$ and E_p:

$$P(i_j, L_k, t_n, S_{1,o}, S_{2,q}, S_{3,r}, S_{4,u}, E_p) = P(S_{1,o}|i_j, L_k, t_n) \times P(S_{2,q}|i_j, L_k, t_n) \times P(S_{3,r}|i_j, L_k, t_n)$$
$$\times P(S_{4,u}|i_j, L_k, t_n) \times P(E_p|i_j, L_k) \times P(i_j) \times P(L_k) \times P(t_n). \quad \text{Equation 6.1}$$

The joint probabilities of i and S_1, S_2, S_3, S_4; E and S_1, S_2, S_3, S_4; S_1, S_2, S_3 and S_4 are then calculated:

$$P(i_j, S_{1,o}, S_{2,q}, S_{3,r}, S_{4,u}) = \sum_p \sum_k \sum_n P(i_j, L_k, t_n, S_{1,o}, S_{2,q}, S_{3,r}, S_{4,u}, E_p), \quad \text{Equation 6.2}$$

$$P(S_{1,o}, S_{2,q}, S_{3,r}, S_{4,u}, E_p) = \sum_j \sum_k \sum_n P(i_j, L_k, t_n, S_{1,o}, S_{2,q}, S_{3,r}, S_{4,u}, E_p), \quad \text{Equation 6.3}$$

$$P(S_{1,o}, S_{2,q}, S_{3,r}, S_{4,u}) = \sum_p \sum_j \sum_k \sum_n P(i_j, L_k, t_n, S_{1,o}, S_{2,q}, S_{3,r}, S_{4,u}, E_p). \quad \text{Equation 6.4}$$

Finally, the posterior probabilities are evaluated through Bayes' theorem:

$$P(i_j | M_1, M_2, M_3, M_4) = \frac{\sum_o \sum_q \sum_r \sum_u P(M_1|S_{1,o}) \times P(M_2|S_{2,q}) \times P(M_3|S_{3,r}) \times P(M_4|S_{4,u}) \times P(i_j, S_{1,o}, S_{2,q}, S_{3,r}, S_{4,u})}{\sum_o \sum_q \sum_r \sum_u P(M_1|S_{1,o}) \times P(M_2|S_{2,q}) \times P(M_3|S_{3,r}) \times P(M_4|S_{4,u}) \times P(S_{1,o}, S_{2,q}, S_{3,r}, S_{4,u})},$$

Equation 6.5

$$P(E_p | M_1, M_2, M_3, M_4) = \frac{\sum_o \sum_q \sum_r \sum_u P(M_1|S_{1,o}) \times P(M_2|S_{2,q}) \times P(M_3|S_{3,r}) \times P(M_4|S_{4,u}) \times P(S_{1,o}, S_{2,q}, S_{3,r}, S_{4,u}, E_p)}{\sum_o \sum_q \sum_r \sum_u P(M_1|S_{1,o}) \times P(M_2|S_{2,q}) \times P(M_3|S_{3,r}) \times P(M_4|S_{4,u}) \times P(S_{1,o}, S_{2,q}, S_{3,r}, S_{4,u})}.$$

Equation 6.6

An additional measurement M_i multiplies the number of calculations in the Bayesian network by the number of discrete values of S_i. Therefore, the discretisation of the variables was adapted to each different Bayesian network according with an affordable computation time (Table 6.1). The detailed algorithm is presented in Appendixes.

Table 6.1: Discretisation of the variables in the Bayesian network.

Number of measurements per year	Variable	Discretisation
1	Intake (Bq)	0; 10^{-4}; 5x10^{-4}; 10^{-3}; 5x10^{-3}; 10^{-2}; 5x10^{-2}; 10^{-1}; 5x10^{-1}; 1; 5; 10; 20; 30; 40; 50; 100; 150; 300; 600; 1,000
	AMAD (μm)	1; 3; 5; 10
	Absorption into blood	Type M; Type S
	Time of contamination (d)	0; 10; 20; 30; 40; 50; 60; 70; 80; 90; 100; 110; 120; 130; 140; 150; 160; 170; 180
	Bioassay quantity (Bq)	0; 10^{-7}; 10^{-6}; 5x10^{-6}; 10^{-5}; 2x10^{-5}; 3x10^{-5}; 4x10^{-5}; 5x10^{-5}; 6x10^{-5}; 7x10^{-5}; 8x10^{-5}; 9x10^{-5}; 10^{-4}; 2x10^{-4}; 3x10^{-4}; 4x10^{-4}; 5x10^{-4}; 6x10^{-4}; 7x10^{-4}; 8x10^{-4}; 9x10^{-4}; 10^{-3}; 2x10^{-3}; 3x10^{-3}; 4x10^{-3}; 5x10^{-3}; 6x10^{-3}; 7x10^{-3}; 8x10^{-3}; 9x10^{-3}; 10^{-2}; 2x10^{-2}; 3x10^{-2}; 4x10^{-2}; 5x10^{-2}; 6x10^{-2}; 7x10^{-2}; 8x10^{-2}; 9x10^{-2}; 10^{-1}; 2x10^{-1}; 3x10^{-1}; 4x10^{-1}; 5x10^{-1}; 6x10^{-1}; 7x10^{-1}; 8x10^{-1}; 9x10^{-1}; 1; 2; 3; 4; 5; 6; 7; 8; 9; 10; 20; 30; 40; 50; 60; 70; 80; 90; 100; 200; 300; 400; 500; 600; 700; 800; 900; 1,000
	Dose (mSv)	0; 10^{-3}; 10^{-2}; 10^{-1}; 5x10^{-1}; 1; 2; 3; 4; 5; 6; 7; 8; 9; 10; 15; 20; 50; 100; 500; 1,000; 10,000

2	Intake (Bq)	0; 10^{-4}; $5x10^{-4}$; 10^{-3}; $5x10^{-3}$; 10^{-2}; $5x10^{-2}$; 10^{-1}; $5x10^{-1}$; 1; 5; 10; 20; 30; 40; 50; 100; 150; 300; 600; 1,000
	AMAD (µm)	1; 3; 5; 10
	Absorption into blood	Type M; Type S
	Time of contamination (d)	0; 10; 20; 30; 40; 50; 60; 70; 80; 90; 100; 110; 120; 130; 140; 150; 160; 170; 180
	Bioassay quantity (Bq)	0; 10^{-6}; 10^{-5}; 10^{-4}; $5x10^{-4}$; 10^{-3}; $5x10^{-3}$; 10^{-2}; $5x10^{-2}$; 10^{-1}; $5x10^{-1}$; 1; 5; 10; 50; 100; 200; 500; 1,000
	Dose (mSv)	0; 10^{-3}; 10^{-2}; 10^{-1}; $5x10^{-1}$; 1; 2; 3; 4; 5; 6; 7; 8; 9; 10; 15; 20; 50; 100; 500; 1,000; 10,000.
4	Intake (Bq)	0; 10^{-4}; 10^{-3}; 10^{-2}; 10^{-1}; 1; 10; 100; 1,000
	AMAD (µm)	1; 5; 10
	Absorption into blood	Type M; Type S
	Time of contamination (d)	0; 10; 90; 180
	Bioassay quantity (Bq)	0; 10^{-6}; 10^{-5}; 10^{-4}; $5x10^{-4}$; 10^{-3}; $5x10^{-3}$; 10^{-2}; $5x10^{-2}$; 10^{-1}; $5x10^{-1}$; 1; 5; 10; 50; 100; 1,000
	Dose (mSv)	0; 10^{-3}; 10^{-1}; $5x10^{-1}$; 1; 5; 10; 20; 1,000; 10,000

6.4 Results and discussion

The MDDs obtained for the different programmes of monitoring of the internal exposure in R4-T4 facilities are gathered in Table 6.2. The monitoring programme (a) was not evaluated with a uniform intake prior probability because the MDD of programme (b) is already higher than 20 mSv which is not appropriate for routine monitoring.

The results were studied to look for the best compromise between the cost of the measurements and the sensitivity of the programme. Globally, the ranking of the different programmes according to their sensitivities is independent of the intake prior and of the isotopic composition. Regarding the sensitivity, the operator has an objective to detect any annual committed effective dose higher than 1 mSv. The discretisation was adapted to this constraint with small dose intervals around 1 mSv and larger intervals above.

Table 6.2: MDDs calculated for different monitoring programmes using the Bayesian network with parameters modelling presented in Section 6.1 and discretisations in Table 6.1

Isotopic composition	Minimum detectable dose with a confidence level of 95 % (mSv)			
	Programme	uniform *P(i)*	exponential *P(i)*	alpha *P(i)*
PWR1	a	20 < MDD	1 < MDD < 2	MDD = 0[a]
	b	20 < MDD < 50	1 < MDD < 2	MDD = 0[a]
	c	8 < MDD < 9	0.5 < MDD < 1	MDD = 0 [a]
	d	50 < MDD < 100	3 < MDD < 4	MDD = 0 [a]
	e	10 < MDD < 15	1 < MDD < 2	MDD = 0 [a]
	f	10 < MDD < 15	2 < MDD < 3	MDD = 0 [a]
	g	5 < MDD < 10	1 < MDD < 5	MDD = 0 [a]
	h	1 < MDD < 5	0.1 < MDD < 0.5	0 < MDD < 0.001
	i	20 < MDD < 1000	5 < MDD < 10	1 < MDD < 5
PWR2	a	20 < MDD	1 < MDD < 2	MDD = 0[a]
	b	20 < MDD < 50	1 < MDD < 2	MDD = 0[a]
	c	9 < MDD < 10	0.5 < MDD < 1	MDD = 0 [a]
	d	50 < MDD < 100	3 < MDD < 4	MDD = 0 [a]
	e	10 < MDD < 15	1 < MDD < 2	MDD = 0 [a]
	f	10 < MDD < 15	3 < MDD < 4	MDD = 0 [a]
	g	5 < MDD < 10	1 < MDD < 5	MDD = 0 [a]
	h	1 < MDD < 5	0.1 < MDD < 0.5	0 < MDD < 0.001
	i	20 < MDD < 1000	5 < MDD < 10	1 < MDD < 5
BWR	a	20 < MDD	1 < MDD < 2	MDD = 0[a]
	b	20 < MDD < 50	1 < MDD < 2	MDD = 0[a]
	c	8 < MDD < 9	0.5 < MDD < 1	MDD = 0 [a]
	d	50 < MDD < 100	4 < MDD < 5	MDD = 0 [a]
	e	10 < MDD < 15	1 < MDD < 2	MDD = 0 [a]
	f	10 < MDD < 15	3 < MDD < 4	MDD = 0 [a]
	g	5 < MDD < 10	1 < MDD < 5	MDD = 0 [a]
	h	1 < MDD < 5	0.1 < MDD < 0.5	0 < MDD < 0.001
	i	20 < MDD < 1000	5 < MDD < 10	1 < MDD < 5
MOX	a	20 < MDD	2 < MDD < 3	MDD = 0[a]
	b	50 < MDD < 100	2 < MDD < 3	MDD = 0[a]
	c	10 < MDD < 15	1 < MDD < 2	MDD = 0 [a]
	d	50 < MDD < 100	5 < MDD < 6	MDD = 0 [a]
	e	15 < MDD < 20	2 < MDD < 3	MDD = 0 [a]
	f	15 < MDD < 20	4 < MDD < 5	MDD = 0 [a]
	g	5 < MDD < 10	5 < MDD < 10	0 < MDD < 0.001
	h	1 < MDD < 5	0.5 < MDD < 1	0 < MDD < 0.001

	i	20 < MDD < 1000	5 < MDD < 10	1 < MDD < 5
MOX_RP	a	20 < MDD	0.5 < MDD < 1	MDD = 0[a]
	b	20 < MDD < 50	0.5 < MDD < 1	MDD = 0[a]
	c	6 < MDD < 7	0.5 < MDD < 1	MDD = 0 [a]
	d	50 < MDD < 100	2 < MDD < 3	MDD = 0 [a]
	e	8 < MDD < 9	1 < MDD < 2	MDD = 0 [a]
	f	9 < MDD < 10	1 < MDD < 2	MDD = 0 [a]
	g	1 < MDD < 5	1 < MDD < 5	MDD = 0 [a]
	h	1 < MDD < 5	0.1 < MDD < 0.5	0 < MDD < 0.001
	i	10 < MDD < 20	1 < MDD < 5	1 < MDD < 5

[a] The dose 0 mSv corresponds to a percentile higher than the 95th.

Retaining the exponential intake prior probability as a subjective reasonable choice, only two monitoring programmes ensure the detection of doses lower than 1 mSv: (c) with a MDD between 0.5 and 1 mSv for all isotopic compositions except MOX with a MDD between 1 and 2 mSv; and (h) with a MDD between 0.1 and 0.5 mSv except for MOX with a MDD between 0.5 and 1 mSv. Programme (h) is more sensitive than (c) but requires twice as many measurements. The best compromise therefore appears to be programme (c) which is currently carried out except for MOX which should be monitored by programme (h) to satisfy the constraint of 1 mSv.

Comparison with the WeLMoS method

The same study was carried out with the WeLMoS method and the modelling presented in Section 6.2 for the PWR1 isotopic composition. Only this composition was considered because the results are globally the same for all isotopic compositions. The outcome is presented in Fig. 6.2.

The MDDs calculated by the two methods are in the same range. As discussed above, the differences can be explained by the modelling of uncertainty through continuous or discrete variables. However, the ranking of the monitoring programmes is different for the two methods: with the WeLMoS method, adding measurements leads to a larger increase of the MDD than with the Bayesian network. This increase is an artefact caused by the modelling of negative measurement by a measurement equal to the DT and not between 0 and the DT.

Finally, this comparison allows validating the results of the optimisation since both methods provide similar results.

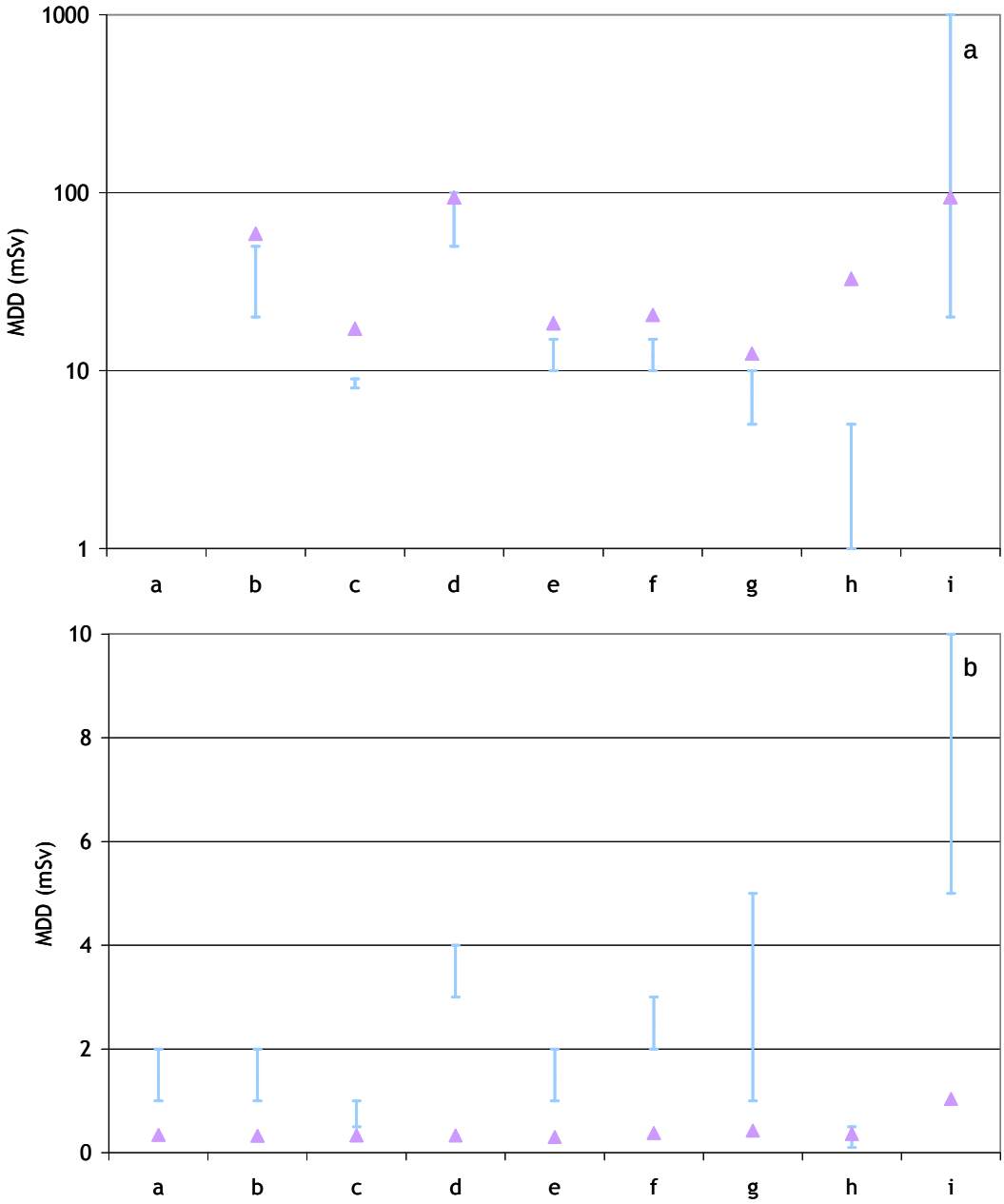

Figure 6.2: Comparison of the MDDs obtained by the WeLMoS method (▲) and by the Bayesian network (blue bars) for the PWR1 isotopic composition with the modelling presented in Section 6.2 and a uniform (a) or exponential (b) intake prior

Comparison with OMINEX project

Within the OMINEX project, Stradling *et al* (2003) provided advice on the optimisation of monitoring programmes. Intakes and doses were assessed from the excretion of workers predicted for a reference 5 µm AMAD aerosol and the Pu systemic model (ICRP, 1993), combining specific absorption parameter values with default deposition and particle transport in the respiratory tract. Stradling *et al* concluded that faecal measurement is the method of choice for the monitoring of Pu dioxide. Assuming a uniform chronic intake, quarterly or half-yearly monitoring intervals could be used to confirm that the annual doses from inhalation of Pu dioxide or MOX are unlikely to exceed 1

mSv and 6 mSv. After acute exposure, doses of 1 mSv or less can be assessed up to several weeks after exposure; and annual doses of the same magnitude after repeated intakes can be confirmed from monitoring intervals between 90 d and 1 year.

Although obtained by a deterministic approach and for a different modelling of the contamination pattern, these project conclusions and that of this work determining MDD by taking into account uncertainties in a probabilistic approach are identical especially about the choice of faecal measurements as the best measurement.

6.5 Conclusion

Estimating the MDDs for a set of possible monitoring programmes for Pu workers of R4-T4 facilities, it can be concluded, under explicit assumptions regarding the prior probabilities of uncertain parameters, that the current monitoring programme is the best compromise between the cost of the measurements and the sensitivity of the programme. This study highlights the interest of the MDD as a tool to decide which monitoring programme is the best for a situation of potential contamination considering uncertainty on exposure conditions and on measurement.

The probabilistic approach applied here as the WeLMoS method and as the Bayesian network confirms the approach performed within the OMINEX project and within the ISO standard (ISO, 2006a). However, the determination of the MDD by integrating uncertainty in exposure and in measurements is more accurate and can assure that for most exposures, the monitoring programme is satisfactory.

The choice between the use of the WeLMoS method and the Bayesian network relies on the precision in the knowledge on the different uncertain parameters. If significant knowledge is provided, continuous probability may be chosen to model the uncertainty in the uncertain parameters. Therefore, the WeLMoS method is the method of choice giving a high precision in the MDD. However, if only scarce information is gathered on uncertain parameters, it is less informative to weight large intervals by their likelihood using discrete probability than to use continuous probability leading to add unproven knowledge. Consequently, in this case, it is better to use a Bayesian network. In addition, the network can be used to discriminate quickly if a monitoring programme allows the detection of doses below 1 or 20 mSv.

The methods presented here were implemented in the OPSCI software as the first step toward an expert system to optimise monitoring programmes.

CHAPTER 7

OPSCI development and validation

7.1 Presentation

To calculate the Minimum Detectable Dose (MDD) the methods presented in the previous sections are implemented in new software developed during this study. This software named OPSCI (Optimisation des Programmes de Surveillance de la Contamination Interne) is coded in IDL® (Interactive Data Language). This language was chosen because of its use for other application in the laboratory.

OPSCI presents 4 different modules of increasing complexity:

- calculation of the dose from one measurement using ICRP reference models;
- evaluation of the dose from several measurements using ICRP reference models;
- evaluation of the MDD for one monitoring programme integrating uncertainty;
- optimisation by calculating the MDDs of different monitoring programmes, taking into account of uncertainty.

The different modules are presented in details in this section.

7.2 Module for a deterministic dose calculation from one measurement

This module calculates the intake and committed effective dose from the bioassay function and the dose coefficient calculated by DCAL software (Eckerman *et al*, 2006). The models used are the HRTM (ICRP, 1994a), the GITM (ICRP, 1979), the reference biokinetic models as well as the dosimetric models of the ICRP (ICRP, 1979, 1993, 1995a) which are implemented in DCAL. The module estimates the intake and the dose from the measurement result using Eq. 1.20 and 1.21.

7.2.1 Graphical user interface

A graphical user interface (GUI) is built for the user to define the calculation parameters and to display the results (Fig. 7.1). The parameters are:

(1) the radionuclide,
(2) the entrance route,
(3) the time since intake,
(4) the intake pattern,

(5) the type of measurement,

(6) the measured activity,

(7) the type of absorption,

(8) the AMAD.

The user can also choose to save the results in a Text file (9). To start the calculation, the button "calculation" (10) has to be pressed.

The results are then displayed as:

(11) intake in Bq,

(12) dose coefficient e_{50} in $Sv.Bq^{-1}$

(13) committed effective dose in Sv,

(14) bioassay function representing the model prediction for a unit intake as a function of time.

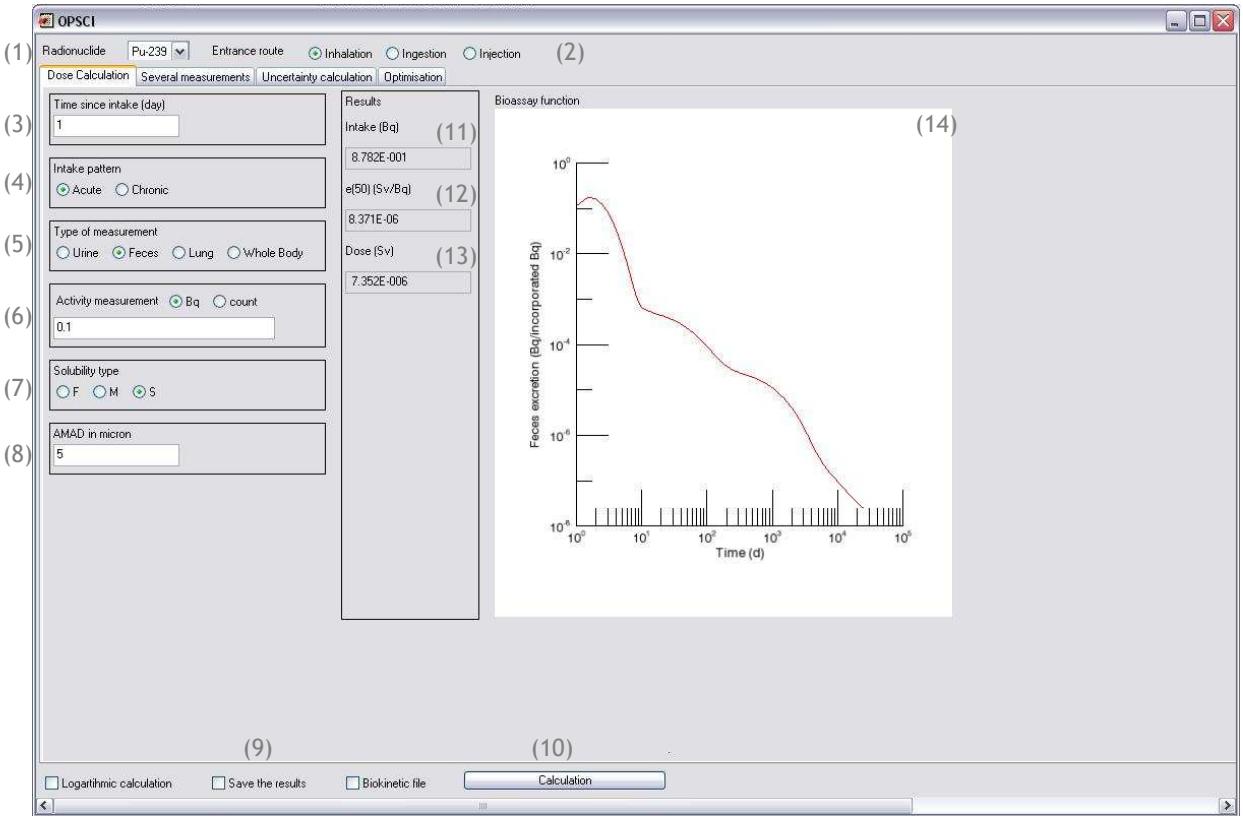

Figure 7.1: Graphical User Interface (GUI) of the module "Dose calculation for a measurement" of OPSCI

7.2.2 Description of the procedure

To calculate the dose, different steps are needed:

1) creation of an input text file for the batch mode of DCAL,

2) launch of DCAL

3) reading of the retained activity in tissues at different times by reading the .ACT file created by DCAL,
4) calculation of the bioassay function from the retained activities,
5) reading of the dose coefficient in the result file of DCAL,
6) display of the bioassay function in the GUI,
7) calculation of the bioassay function for the time since intake,
8) calculation of the intake
9) calculation of the committed effective dose
10) display of intake, dose coefficient and dose in the GUI.

7.2.3 Validation

This module was validated by comparison with the results published by Stradling *et al* (2003) for an acute or chronic contamination by inhalation of an aerosol of ^{239}Pu with an AMAD of 5 µm. The absorption into blood was modelled either by a reference Type M or Type S. The results are gathered in Table 7.1 and 7.2.

Table 7.1: Comparison between doses (mSv) obtained by OPSCI with Stradling *et al* (2003) (OMINEX) for a measurements of 3 kBq in lung, 0.1 mBq.d^{-1} in urine or 1 mBq.d^{-1} in faeces after acute contamination

Lung monitoring	Type M			Type S		
Time since intake (d)	OMINEX	OPSCI	Difference (%)	OMINEX	OPSCI	Difference (%)
1	$1.67x10^{3}$	$1.70x10^{3}$	1.56	$3.90x10^{2}$	$3.91x10^{2}$	0.26
7	$1.85x10^{3}$	$1.85x10^{3}$	1.89	$4.20x10^{2}$	$4.22x10^{2}$	0.48
30	$2.50x10^{3}$	$2.50x10^{3}$	1.84	$5.00x10^{2}$	$5.09x10^{2}$	1.80
Urine monitoring	Type M			Type S		
Time since intake (d)	OMINEX	OPSCI	Difference (%)	OMINEX	OPSCI	Difference (%)
1	$1.4x10^{-2}$	$1.4x10^{-2}$	0.00	$3.5x10^{-1}$	$3.6x10^{-1}$	2.86
7	$1.1x10^{-1}$	$1.3x10^{-1}$	18.18	2.7	2.67	-1.11
30	$3.4x10^{-1}$	$3.4x10^{-1}$	0.00	4.8	4.86	1.25
90	$4.5x10^{-1}$	$4.6x10^{-1}$	2.22	5.2	5.20	0.00
180	$6.0x10^{-1}$	$6.0x10^{-1}$	0.00	5.2	5.24	0.77
360	$8.2x10^{-1}$	$8.4x10^{-1}$	2.44	4.9	5.00	2.04
Faecal monitoring	Type M			Type S		
Time since intake (d)	OMINEX	OPSCI	Difference (%)	OMINEX	OPSCI	Difference (%)
1	$2.9x10^{-4}$	$3.0x10^{-4}$	3.45	$7.0x10^{-5}$	$7.0x10^{-5}$	0.00
7	$1.4x10^{-3}$	$1.3x10^{-2}$	828.57	$3.3x10^{-3}$	$3.2x10^{-3}$	-3.03
30	$1.2\ x10^{-1}$	$1.2\ x10^{-1}$	0.87	$2.3x10^{-2}$	$2.4x10^{-2}$	4.35
90	$4.8x10^{-1}$	$4.9x10^{-1}$	2.08	$7.7x10^{-2}$	$8.0x10^{-2}$	1.30
180	1.9	1. 8	-5.82	$2.2x10^{-1}$	$2.1x10^{-1}$	-4.91
360	5.8	5.8	1.22	$3.7x10^{-1}$	$3.7x10^{-1}$	-0.80

Table 7.2: Comparison between doses (mSv) obtained by OPSCI with Stradling *et al* (2003) (OMINEX) for a measurements of 3 kBq in lung, 0.1 mBq.d^{-1} in urine or 1 mBq.d^{-1} in faeces after chronic contamination

Lung monitoring	Type M			Type S		
Time since intake (d)	OMINEX	OPSCI	Difference (%)	OMINEX	OPSCI	Difference (%)
7	1.73×10^{3}	1.93×10^{3}	11.56	4.00×10^{2}	4.39×10^{2}	9.70
30	2.05×10^{3}	2.13×10^{3}	3.66	4.50×10^{2}	4.59×10^{2}	1.89
90	2.75×10^{3}	2.83×10^{3}	2.98	5.30×10^{2}	5.40×10^{2}	1.85
200	3.97×10^{3}	4.07×10^{3}	2.39	6.20×10^{2}	6.34×10^{2}	2.26
350	5.73×10^{3}	5.83×10^{3}	1.76	7.05×10^{2}	7.17×10^{2}	1.67
Urine monitoring	Type M			Type S		
Time since intake (d)	OMINEX	OPSCI	Difference (%)	OMINEX	OPSCI	Difference (%)
7	3.8×10^{-2}	4.0×10^{-2}	5.26	9.5×10^{-1}	9.6×10^{-1}	1.05
30	1.1×10^{-1}	1.2×10^{-1}	9.09	2.4	2.4	-0.83
90	2.1×10^{-1}	2.2×10^{-1}	4.76	3.6	3.7	2.22
200	3.2×10^{-1}	3.3×10^{-1}	3.13	4.4	4.4	0.00
350	4.2×10^{-1}	4.3×10^{-1}	2.38	4.6	4.7	1.74
Faecal monitoring	Type M			Type S		
Time since intake (d)	OMINEX	OPSCI	Difference (%)	OMINEX	OPSCI	Difference (%)
7	3.8×10^{-4}	5.5×10^{-4}	44.74	1.4×10^{-4}	1.5×10^{-4}	7.14
30	2.4×10^{-3}	2.3×10^{-3}	-3.75	5.8×10^{-4}	5.6×10^{-4}	-3.45
90	7.0×10^{-3}	6.8×10^{-3}	-3.00	1.7×10^{-3}	1.6×10^{-3}	-3.53
200	1.5×10^{-2}	1.5×10^{-2}	-0.20	3.7×10^{-2}	3.6×10^{-2}	-2.70
350	2.7×10^{-2}	2.6×10^{-2}	-3.26	6.4×10^{-3}	6.2×10^{-3}	-2.50
1000	7.6×10^{-2}	7.4×10^{-2}	-2.16	1.8×10^{-2}	1.7×10^{-2}	-3.06

For an acute contamination, the differences are small except for a urine measurement 7 days after exposure to Type M where the bioassay function used by Stradling *et al* is different from the one published by ICRP (ICRP, 1997b); and for faecal measurement 7 days after exposure to a Type M aerosol where Stradling *et al* used a dose coefficient different from ICRP.

For a chronic contamination, the differences between the doses obtained by OPSCI and by Stradling *et al* are small and can be explained by the different integration of the bioassay function used to calculate the dose.

7.3 Module for a deterministic dose calculation from several measurements

This module calculates the committed effective dose following a contamination by several radionuclides and monitored by several measurements. DCAL is used to calculate the bioassay functions and the dose coefficients for the different radionuclides.

The intake of each radionuclide is estimated as the geometric mean of the intakes determined from each measurement of this radionuclide. This mean intake is then multiplied by the corresponding dose coefficient. The total dose is the sum of the doses due to the different radionuclides.

The effect of DTPA treatment is modelled by an increase by a factor of 50 of the urinary excretion. Therefore, if DTPA is used, the urine measurements are divided by 50 (Grappin *et al*, 2007).

7.3.1 Graphical user interface

The GUI for the module "calculation of the dose for several measurements" is presented in Fig. 7.2. Firstly, the user enters:

(1) the entrance route,

(2) the use of DTPA,

(3) the intake pattern,

(4) the AMAD,

(5) the type of absorption,

(6) the measured radionuclide, time between intake and measurement, type of measurement and measured activity for each measurement.

To start the calculation, the button "calculation" (7) has to be pressed.

The results are then presented as:

(6) intake in Bq for each measurement,

(8) mean intake in Bq, dose coefficient e_{50} in Sv.Bq^{-1}, and committed effective dose in Sv for each radionuclide,

(9) total dose in Sv.

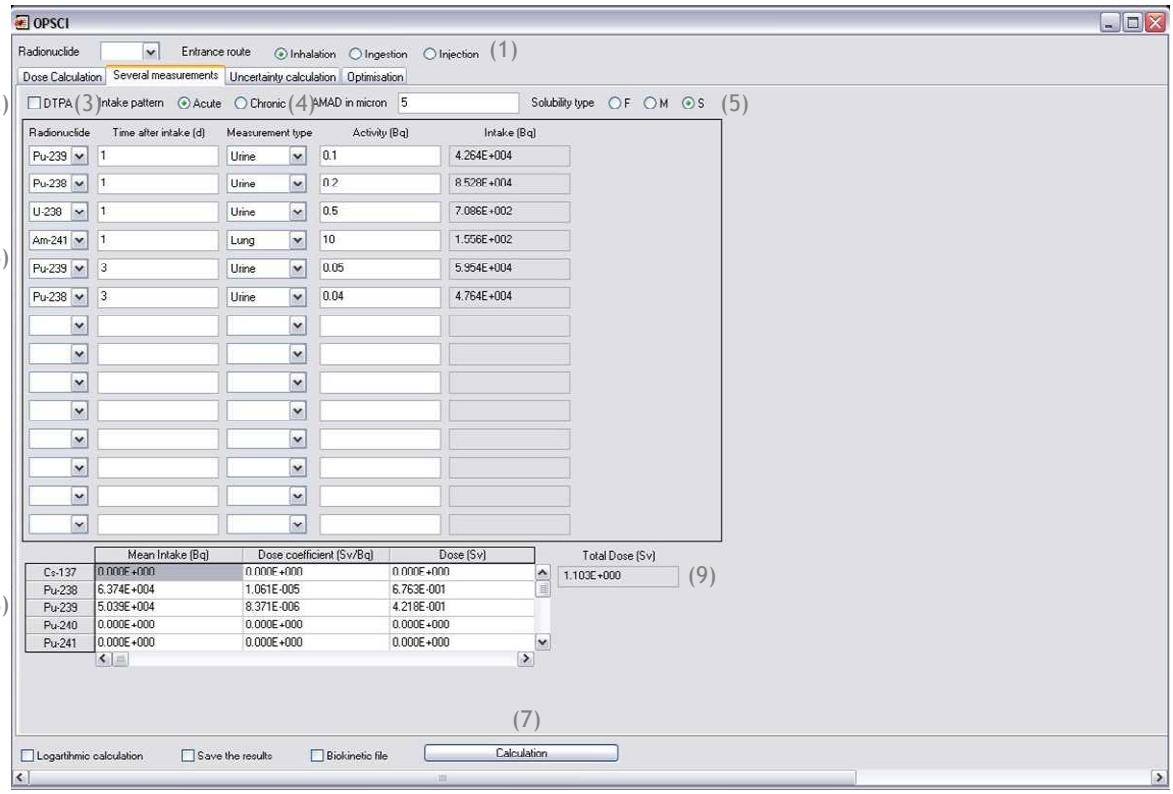

Figure 7.2: GUI of the module "Dose calculation for several measurements" of OPSCI

7.3.2 Description of the procedure

To calculate the total dose, different steps are needed, for each measurement:

1) creation of the input text file for the batch mode of DCAL,
2) launch of DCAL
3) reading of the retained activity in the tissues for different times from the .ACT file created by DCAL,
4) calculation of the bioassay function from the retained activities,
5) reading of the dose coefficient in the result file of DCAL,
6) calculation of the bioassay function of time since intake,
7) calculation of the intake
8) display of intake

Then for each radionuclide,

9) calculation of the mean intake,
10) display of the dose coefficient,
11) calculation of the dose

Finally, the total dose is calculated and displayed.

7.3.3 Validation

To validate this module, some of the measurement results from a contamination case were used. For each measurement, the intake calculated by this module is compared with the intake calculated with the same parameters by the first module. Then the intake of each radionuclide calculated as a geometric mean of the intakes calculated for each measurement fo this radionuclide and the dose estimations are compared with the results obtained with Microsoft Excel® and the intake estimated from each measurement.

The contamination occurred as an acute inhalation of a Type M aerosol with an AMAD of 5 µm. The results are gathered in Table 7.3 and 7.4. They are identical between modules 1 and 2 and between module 2 and the calculations made in Excel®., This module is therefore validated.

Table 7.3: Comparison between intakes obtained by the "dose calculation for several measurements" module of OPSCI (module 2), "dose calculation for one measurement" module of OPSCI (module 1) and Excel®.

Radionuclide	Time since intake (d)	Measurement type	activity (Bq)	Intake module 2 (Bq)	Intake module 1 (Bq)	Intake DTPA OPSCI (Bq)	Intake DTPA Excel® (Bq)
^{239}Pu	1	urine	0.68	2.94×10^{3}	2.94×10^{3}	5.87×10^{1}	5.87×10^{1}
^{241}Am	1	urine	3.9	2.19×10^{3}	2.19×10^{3}	4.39×10^{1}	4.39×10^{1}
^{239}Pu	8	urine	0.036	1.76×10^{3}	1.76×10^{3}	3.53×10^{1}	3.53×10^{1}
^{241}Am	8	urine	0.078	1.44×10^{3}	1.44×10^{3}	2.88×10^{1}	2.88×10^{1}
^{239}Pu	2	faeces	16	1.04×10^{2}	1.04×10^{2}	1.04×10^{2}	1.04×10^{2}
^{241}Am	2	faeces	34	2.21×10^{2}	2.21×10^{2}	2.21×10^{2}	2.21×10^{2}
^{239}Pu	8	faeces	27	2.17×10^{4}	2.17×10^{4}	2.17×10^{4}	2.17×10^{4}

^{241}Am	8	faeces	106	8.65×10^{4}	8.65×10^{4}	8.65×10^{4}	8.65×10^{4}
^{241}Am	1	lung	970	1.68×10^{4}	1.68×10^{4}	1.68×10^{4}	1.68×10^{4}
^{241}Am	4	lung	143	2.64×10^{3}	2.64×10^{3}	2.64×10^{3}	2.64×10^{3}
^{241}Am	8	lung	43	8.42×10^{2}	8.42×10^{2}	8.42×10^{2}	8.42×10^{2}
^{137}Cs	1	whole body	22,000	3.68×10^{4}	3.68×10^{4}	3.68×10^{4}	3.68×10^{4}
^{137}Cs	4	whole body	8,500	1.90×10^{4}	1.90×10^{4}	1.90×10^{4}	1.90×10^{4}

Table 7.4: Comparison between mean intakes and doses obtained by the "dose calculation for several measurements" module of OPSCI (module 2) and Excel®

Radionuclide	Mean intake module 2 (Bq)	Mean intake Excel® (Bq)	e_{50} module 2 (Sv.Bq^{-1})	e_{50} ICRP (Sv.Bq^{-1})	Dose module 2 (Sv)	Dose Excel® (Sv)
^{137}Cs	2.64×10^{4}	2.64×10^{4}	1.15×10^{-8}	1.15×10^{-8}	3.05×10^{-4}	3.05×10^{-4}
^{239}Pu	1.85×10^{3}	1.85×10^{3}	3.26×10^{-5}	3.20×10^{-5}	6.02×10^{-2}	6.02×10^{-2}
^{241}Am	3.02×10^{3}	3.02×10^{3}	2.71×10^{-5}	2.70×10^{-5}	8.18×10^{-2}	8.18×10^{-2}
			Total dose module 2 (Sv)		1.42×10^{-1}	
			Total dose Excel® (Sv)		1.42×10^{-1}	

7.4 Module for uncertainty dose calculation

This module calculates the MDI and MDD of a monitoring programme by integrating uncertainties on measurement and conditions of exposure. The classical and WeLMoS methods are used to derive the MDD. The Monte-Carlo sampling of the uncertain parameters is carried out by SUNSET (IRSN, France). The calculation of the bioassay function and of the dose coefficient for each sampled sets is done by DCAL.

It was shown in Section 5.3.2 that 100,000 sampled sets are needed to obtain a good convergence of the results with the WeLMoS method. However, only 61 values of absorption are used and DCAL interpolates deposition from 1, 3, 5 and 10 µm AMAD values. Therefore, the calculation of only 244 different bioassay functions and dose coefficients are required. To limit the calculation time of 100,000 sets, a text file named "biokinetic" is created to record the bioassay functions and dose coefficients corresponding to the 244 biokinetic models considered. This file can be used as an input for MDD calculation. DCAL is not used any further as the bioassay functions and dose coefficients for all the sampled sets are interpolated from this file with the same accuracy as within DCAL.

To integrate the isotopic composition (Table 5.7), a biokinetic file for this composition is created containing the bioassay functions of the reference isotope and the dose coefficient of the mixture.

7.4.1 Graphical user interface

The main GUI for the module "uncertainty dose calculation" is presented in Fig. 7.3. To calculate the MDD of a monitoring programme, the user has to define:

(1) the radionuclide,
(2) the entrance route,
(3) the numbers of sets sampled by SUNSET,
(4) whether several measurements per year are available,
(5) the modelling of measurement uncertainty,
(6) if a Poisson modelling of measurement uncertainty is used, it is applied to a measure in counts, and the counting time, the mean background and the emission yield are needed,
(7) the intake prior probability,
(8) the prior probabilities of the other parameters,
(9) optionally, the absorption into blood can be modelled by a reference Type F, M or S or read from a specified text file.

The intake pattern, the measurement type and result for one measurement per year are defined in the first module. With this GUI, the user can:

(10) create a biokinetic file for one radionuclide,
(11) asssociate the biokinetic files of several radionuclides to take into account isotopic mixture,
(12) use an existing biokinetic file,
(13) save the results in a text file,
(14) start the calculation of the MDD.

The results are displayed as CDFs (15), and as medians and 95th percentiles (16).

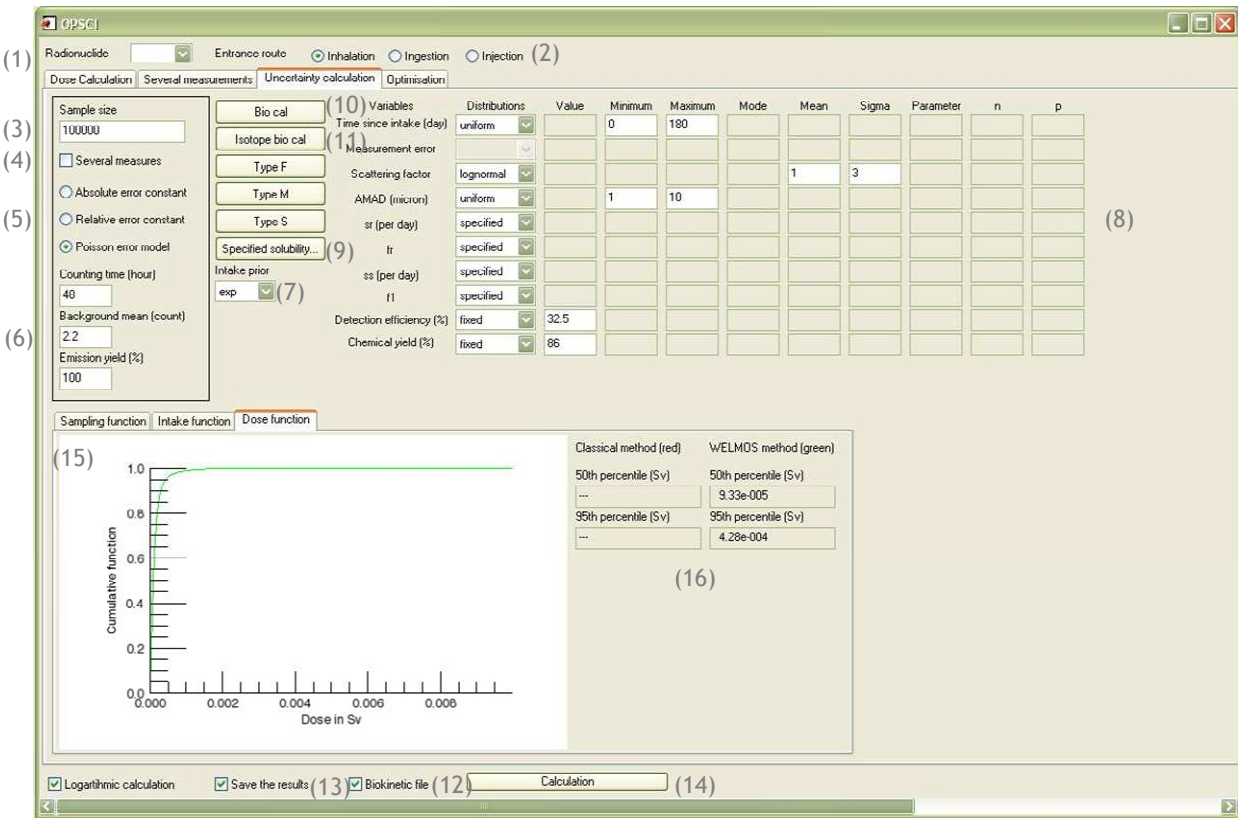

Figure 7.3: GUI of the module "Uncertainty dose calculation" of OPSCI.

To calculate annual MDD from the different routine measurements done during a year, the user, with the specific GUI presented in Fig. 7.4, can define, for each measurement:

(1) the radionuclide,
(2) the measurement type,
(3) the monitoring interval,
(4) the measurement result, which is the same for repeated measurements,
(5) the units of the result
(6) the modelling of measurement uncertainty,
(7) the counting time if the measurement result is expressed as counts,
(8) the mean background if the measurement result is expressed as counts,
(9) the emission yield if the measurement result is expressed as counts,
(10) the detection efficiency if the measurement result is expressed as counts,
(11) the chemical yield if the measurement result is expressed as counts,
(12) the mean of the normal PDF if a normal modelling of measurement uncertainty is used,
(13) the SD of the normal PDF if a normal modelling of measurement uncertainty is used,
(14) the scattering factor.

The user can add a new measurement if she needs more than the default number (15).

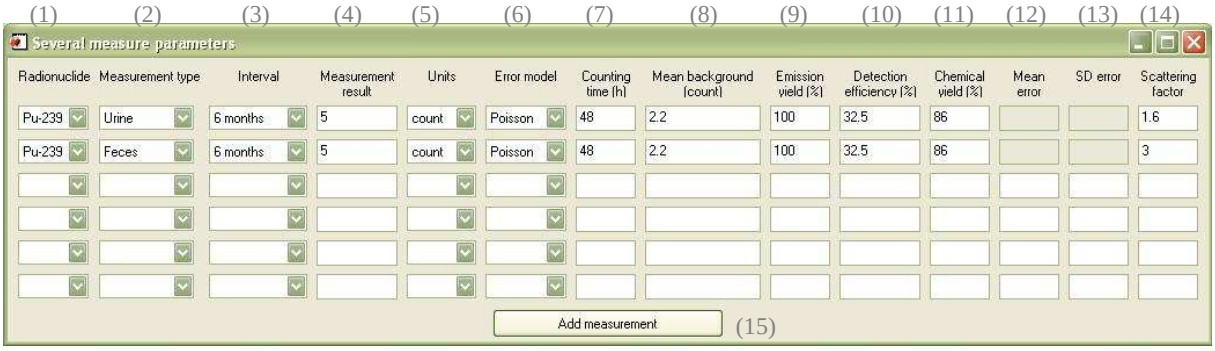

Figure 7.4: GUI to define the monitoring programme for calculation of annual MDD in the module "Uncertainty dose calculation" of OPSCI

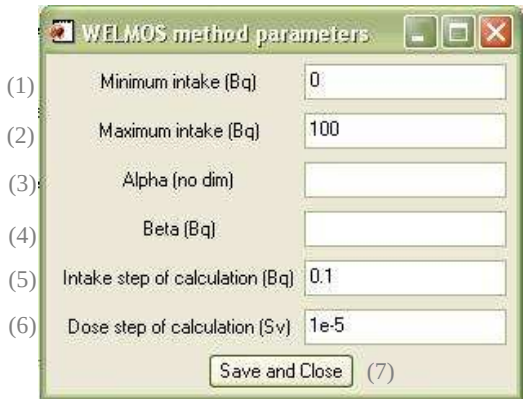

Figure 7.5: GUI to define the intake prior probability in the module "Uncertainty dose calculation" of OPSCI

By choosing in the drop-list (7) of the main GUI (Fig. 7.3), a uniform, exponential, inverse, alpha intake prior may be specified. A GUI (Fig. 7.5) is created to define its parameters:

(1) the minimum intake,
(2) the maximum intake,
(3) the alpha parameter for the alpha-prior,
(4) the beta value to add a uniform component to the alpha-prior,
(5) the interval between two intakes for the posterior probability calculation,
(6) the interval between two doses for the posterior probability calculation knowing that the number of discretised doses is equal to the number of discretised intakes.

By pressing the button (11) of the main GUI (Fig. 7.3), a new GUI is built (Fig. 7.6) to create the biokinetic file of the isotopic mixture. The user has to define:

(1) the measured radionuclide,
(2) its activity percentage in the isotopic mixture.

By pressing the button (3), the user can select its biokinetic file which name is written in (4). The same procedure is needed for all associated radionuclides (5). Another associated radionuclide can be added by pressing (6). The biokinetic file of the mixture is created by pressing (7).

Figure 7.6: GUI to create the biokinetic file of a mixture of radionuclides in the module "Uncertainty dose calculation" of OPSCI

7.4.2 Description of the procedure

To calculate the posterior probability or level of confidence of intake and dose in order to derive MDD, different steps are followed:

1) creation of the input text file of SUNSET containing the prior probabilities of the uncertain parameters,
2) launch of SUNSET,
3) reading of the result file of SUNSET containing the sampled sets of parameters,

4) calculation with the biokinetic file of the bioassay function and of the dose coefficient for each sampled set,
5) launch of the classical method if only one measurement is considered,
6) launch of the WeLMoS method
7) display of the CDFs of the dose and of the intake,
8) calculation and display of the medians and 95th percentiles of the intake and of the dose.

7.4.3 Validation

The creation of the biokinetic file for one radionuclide or for a mixture was validated by tracing each operation and comparing its results with the same operation performed in Excel®.

The classical method was validated by comparing the results obtained by OPSCI with the results obtained by Molokanov *et al* (2010) for:

- a contamination by tritiated water,
- a monitoring period of 50 days,
- a urine measurement result of 1 Bq.d^{-1},
- a uniform probability for time of contamination between 0 and 50 days,
- a Type B uncertainty modelled by a lognormal PDF with a geometric mean of 1 and a SF of 1.2,
- a measurement uncertainty modelled by a normal PDF with a mean of 1 Bq.d^{-1} and a SD of 0.3 Bq.d^{-1}.

The levels of confidence of the intake obtained by OPSCI and Molokanov *et al* are identical (Fig. 7.7). Therefore, the classical method implemented in OPSCI is validated.

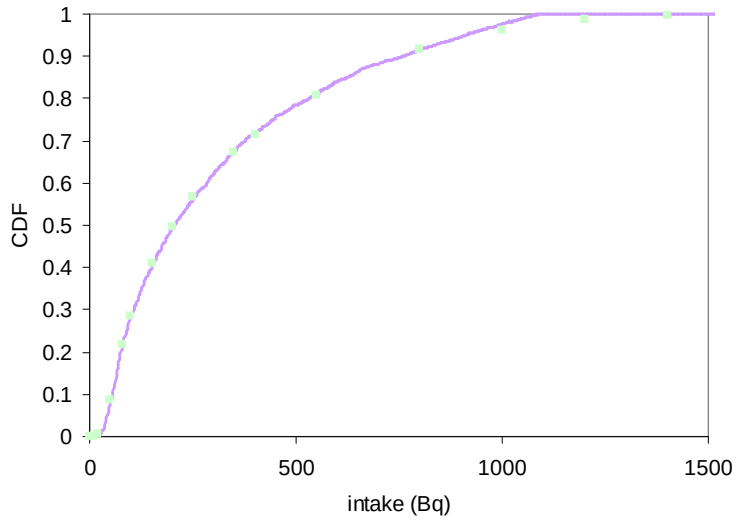

Figure 7.7: Validation of the classical method implemented in OPSCI by comparing its intake CDF (purple line) with the results obtained by Molokanov *et al* (2010) (green points)

The WeLMoS method implemented in OPSCI was validated by comparing its results with the WeLMoS method implemented in IMBA (Puncher and Birchall, 2007). The potential contamination was an acute inhalation of ^{239}Pu aerosol. As IMBA does not allow defining the variability of the absorption into blood by discrete values as done in this work, a reference Type S was assumed. The AMAD had a uniform PDF between 1 and 10 µm. The monitoring programmes were:

a) faeces every 6 months;
b) one urine measurement followed 6 months after by a faeces measurement;
c) one faeces measurement followed 6 months after by a urine measurement;
d) simultaneous urine and faeces measurements every 6 months.

The uncertainty on the time of contamination was modelled by a uniform PDF between 0 and 180 days. IMBA does not use Poisson modelling for uncertainty of measurement; a log-normal modelling was therefore used with a SF of 3 for faeces measurement or 1.6 for urine. The intake prior probability is uniform between 0.0001 and 1,000 Bq. The measurements result was set at 1.0352 x 10^{-4} Bq which was equivalent to 5 counts with the parameters of R4-T4 facilities.

The results are presented in Table 7.5. The relative differences are below 3 % for the MDI and 10 % globally for the MDD. These are explained by slight differences between the bioassay functions and dose coefficients used by OPSCI and IMBA. However, MDIs and MDDs are in the same range, the WeLMoS method implemented in OPSCI is therefore validated.

Table 7.5: Comparison of the MDI and MDD obtained by OPSCI or by IMBA with the WeLMoS method for the modelling presented above.

Monitoring programme	MDI (Bq)			MDD (Sv)		
	OPSCI	IMBA	Difference (%)	OPSCI	IMBA	Difference (%)
a	25.0	24.9	0.4	1.72×10^{-4}	1.85×10^{-4}	- 7.2
b	787	765	2.8	5.44×10^{-3}	5.46×10^{-3}	- 0.4
c	810	824	- 1.7	5.53×10^{-3}	6.17×10^{-3}	- 10.5
d	765	764	0.1	4.90×10^{-3}	5.19×10^{-3}	- 5.6

7.5 Module for optimisation

In this module, the MDI and MDD are calculated using the Bayesian networks presented in Fig. 2.18, 5.3 and 6.1. Only a measurement uncertainty modelled by a Poisson PDF and a Type B uncertainty modelled by a lognormal PDF are implemented so far. Changing the model implies changing the Bayesian network and the code.

7.5.1 Graphical user interface

The GUI of this module (Fig. 7.8) has a part dedicated to the definition of the modelling of the monitoring programme and of the exposure conditions. The parameters of the modelling are:

(1) the radionuclide,
(2) the intake pattern,
(3) the measurement type,
(4) the monitoring interval,
(5) the measurement result which is the same for repeated measurements,
(6) the counting time,
(7) the mean background,
(8) the emission yield,
(9) the detection efficiency,
(10) the chemical yield,
(11) the scattering factor.

By pressing button (12), the user copies these parameters into table (13) and selects the biokinetic file, the text file containing the absorption values and the text file containing the discretisation of the variables along with their probability. The locations of the files are written in table (13). By right-clicking, simultaneous or alternated measurements can be created (14). By pressing the calculation button (15), OPSCI calculates the MDD for each line of table (13) with the adequate Bayesian network. The MDD is then added in (16).

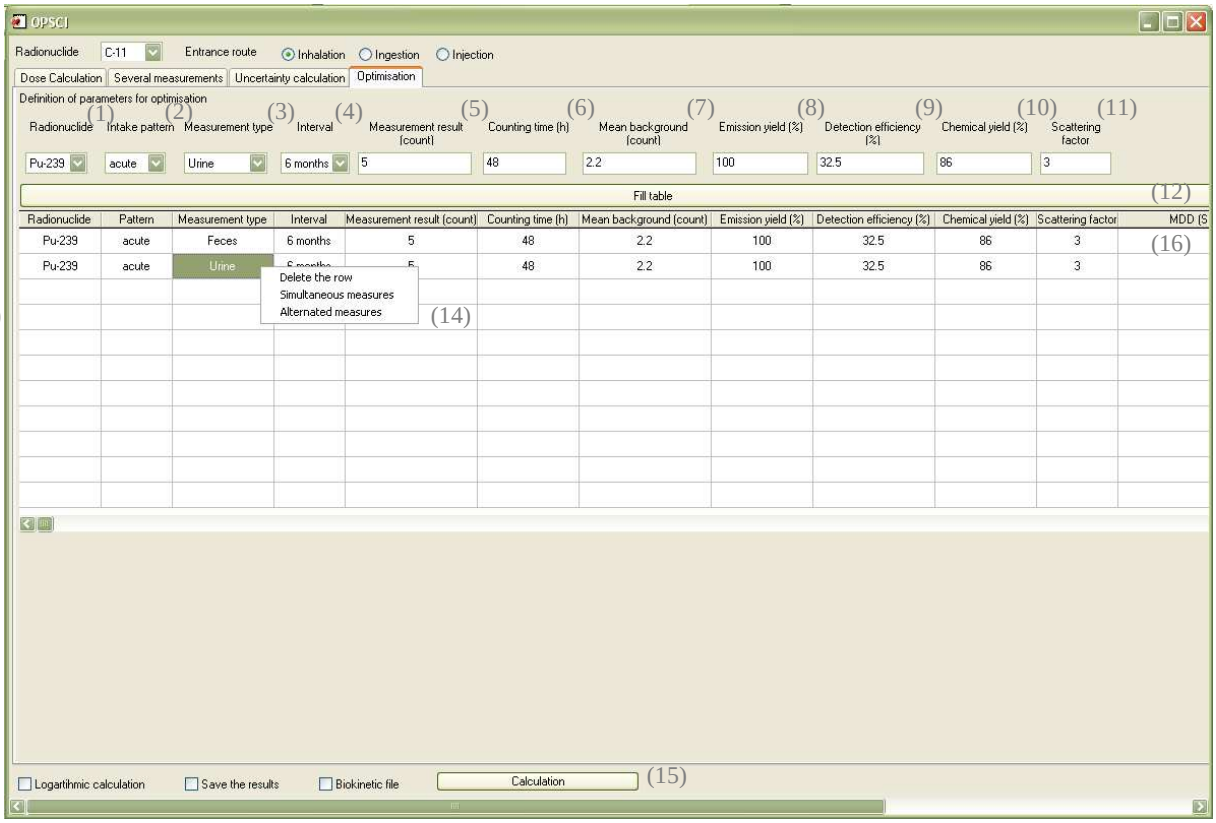

Figure 7.8: GUI of the module "Optimisation" of OPSCI

7.5.2 Description of the procedure

To calculate the MDD with the Bayesian network, the different steps are:

1) reading of the discretisation file,
2) extraction of the parameters in table (13),
3) reading from the biokinetic file of the bioassay function and of the dose coefficient,
4) launch of the Bayesian network,
5) calculation of intake and dose CDFs,
6) calculation and display of the MDD.

7.5.3 Validation

The "optimisation" module of OPSCI was validated by comparing the result of each operation in the Bayesian network of OPSCI with the same operation done in Excel® and by comparison with the WeLMoS method (Section 5.4)

7.6 Conclusion

OPSCI software presented in this section is a new tool to calculate the committed effective dose from one or several measurements using the reference models of ICRP implemented within DCAL and a deterministic approach. But its innovation lies in the evaluation of the MDD of a monitoring programme using the classical and the WeLMoS methods and furthermore in its module for the optimisation of a monitoring programme where the user can evaluate the sensitivity of several programmes and then choose the best one compromising the cost and the sensitivity. All OPSCI modules are validated by comparison with published methods or through step-by-step validation.

CHAPTER 8

Synthesis, discussions and perspectives

8.1 Synthesis

8.1.1 Direct propagation of uncertainty in prospective dosimetry

The aim of the first study was to determine the uncertainty in the prospective dose assessment from potential exposure to uranium in French nuclear facilities, and in mines and mills. Firstly, a literature review was carried out to collect information on the chemical forms of the handled compounds, on their absorption into blood from the respiratory tract and from the gut, and on the AMADs of the aerosols characterized in these facilities.

This information was then modelled by PDF when precise data were available or by possibility distributions when they were not. The RaFu method was used to propagate the uncertainty in the exposure conditions to the doses to the extra-thoracic region, to the lung and to the red bone marrow and to the effective dose from a unit intake. The results of the RaFu method were compared with results obtained by a fully probabilistic approach and by a deterministic interval approach.

For the mines and mills, the study was expanded to estimate the uncertainty in the dose received from a unit air concentration. Therefore, the uncertainty in the breathing rate of the workers was integrated along with the uncertainty in the air concentration measurement.

This work showed that the uncertainty factor evaluated by the RaFu method is intermediate between the deterministic approach where no information is provided about the likeliness of the dose; and the probabilistic approach where scarce information is modelled by informative PDF. The different approaches result in significant differences (orders of magnitudes) in the evaluated uncertainty, enforcing the importance of properly identifying the relative contribution of imprecision and variability to the overall uncertainty.

As highlighted by this study, the RaFu method can be easily used to realistically assess the prospective uncertainty in dose estimates for a characterized workplace. However, this method is presently not applicable to the inverse problem of retrospective dose calculation which is the main issue considered in the rest of this thesis.

8.1.2 Exposure to plutonium at R4-T4 facilities

The monitoring programme of workers of AREVA La Hague R4-T4 facilities was chosen as an operational application of interest to develop and evaluate methods within this study. These

workers perform the extraction and purification of plutonium nitric solution and its conversion into dioxide. In routine conditions, they could be contaminated by PuO_2 while performing maintenance operations.

The workplace and individual monitoring were studied to determine the procedures specific to the R4-T4 workers and the sensitivity of the measurement techniques in term of decision threshold.

The exposure conditions of the workers were studied in details: isotopic composition, chemical form and particle size distribution of the Pu powders. However, the complexity of the required models did not allow deriving the size distribution of an aerosol from the size distribution of the dioxide powder.

In order to obtain realistic values for the absorption parameters used in the HRTM, published experimental data from *in vitro*, *in vivo* (dog, monkey, mouse, rat) experiments and from human contamination cases were interpreted. The model predictions of Pu retention and excretion were fitted to the experimental data by varying the absorption parameters f_r, s_r, s_s. 66 sets of the three parameters were obtained for Pu dioxide as pure compound or as MOX; that were used to model the absorption variability. Absorption into blood of other Pu compounds was also derived. The correlations between the absorption parameters were considered to improve further uncertainty analyses.

8.1.3 Evaluation of a monitoring programme

The sensitivity of a routine monitoring programme can be evaluated through the minimum dose detectable (MDD) by this programme. The MDD is calculated from the detection limit of the measurement with fixed exposure conditions. However, the measurement result is subject to uncertainty as well as the conditions of exposure. Therefore, to determine accurately the sensitivity of the programme, the different sources of uncertainty should be integrated in the calculation of the MDD, accepting a reasonable (e.g. 5%) risk of missing a significant intake due to random fluctuations of the conditions of exposure and measurement: If a routine measurement is negative, the dose from intakes having occurred since the previous measurement is then less than the MDD with 95 % confidence.

To estimate MDD at a given level of confidence by taking into account the uncertainties on a monitoring programme, three methods were applied. The classical method assumes a fixed but unknown intake and provides a conservative estimation of the MDD when the biokinetic model is uncertain. The WeLMoS method and the Bayesian network are more flexible tools which considerer all uncertain parameters as random variables and calculate dose posterior probability from the combined information of bioassay measurement results and prior probabilities of intake and of all the uncertain parameters based on actual data and subjective judgment. The Bayesian network uses discrete random variables while the WeLMoS method considers continuous ones.

The MDDs obtained by the WeLMoS method and by the Bayesian network for the same uncertain parameters are similar, confirming the consistency of both methods. The sensitivity of the MDD to

the modelling of the uncertainty was studied: the intake prior probability and the absorption into blood appear to be the most influent parameters. Therefore, a set of three intake (uniform, exponential and alpha) priors was carried throughout the study to model the imprecision in the choice of this important assumption.

After having modelled the uncertainty relative to the potential exposure and monitoring programme of workers at R4-T4 facilities, the MDD was evaluated by the three methods. The sensitivity of the current monitoring programme was assessed to be below 1 mSv per year for the exponential intake prior, subjectively judged a reasonable prior probability for the intake.

8.1.4 Optimisation of a monitoring programme

The last part of this work aimed at defining the best routine monitoring programme as a compromise between its cost in terms of number and practicability of measurements; and its sensitivity evaluated by the MDD. Different possible monitoring programmes were evaluated using a Bayesian network.

The compromise between the sensitivity of the programme and the number of measurements leads to the conclusion that the current monitoring programme with a MDD below 1 mSv for the exponential intake prior is the best for R4-T4 facilities considering the potential exposure and the radiation protection objectives of the AREVA NC company.

8.1.5 OPSCI development

OPSCI was developed:

- to evaluate the committed effective dose from one or several bioassay measurements following an acute or chronic intake, with a deterministic approach using the reference models of the ICRP;
- to calculate the MDD of a routine monitoring programme with the classical and WeLMoS methods;
- to support the optimisation of monitoring by evaluating the MDDs of different possible programmes using a Bayesian network.

OPSCI was validated by comparing, for defined cases, its results with values from the literature or from well-established codes such as IMBA. It is a new tool which can be used to determine the best monitoring programme for a wide range of potential exposure situations.

8.2 Discussion and areas of improvement

8.2.1 Uncertainty modelling and propagation

To prospectively or retrospectively evaluate the uncertainty in the dose from uncertainty on measurement and exposure conditions, innovative propagation methods were applied in this study to aim at the most realistic modelling of uncertainty.

For prospective dosimetry, the Dempster-Shafer approach was used: it allows the use of probability when enough information is available to reduce uncertainty to variability and possibility when imprecision is also involved. It is therefore a good intermediate between the deterministic probabilistic approaches and appears as the method modelling the most realistically the actual knowledge on the uncertain parameters.

For retrospective dosimetry which is an inverse propagation of information from the bioassay measurement to the intake and dose, the Dempster-Shafer method cannot currently be applied. Therefore, a probabilistic approach was used to estimate the uncertainty in the dose. Three methods were used: classical, WeLMoS and Bayesian network.

The classical method makes the hypothesis that the intake is fixed but unknown and assigns prior probability to the other uncertain parameters. However, this absence of assumed knowledge on the intake makes the other hypotheses all the stronger. Moreover, this method cannot integrate several measurement results so far.

The WeLMoS method and the Bayesian network model the knowledge on the intake and on other uncertain parameters by prior (before bioassay measurement) and posterior (after bioassay measurement) probabilities. These methods have the advantage of an explicit modelling of hypotheses by the prior probabilities, which can therefore been discussed and validated by experts and/or stakeholders. On the one hand, the WeLMoS method assigns continuous probability to uncertain variables, which can be very informative and well adapted to obtain accurate results from extensive data. On the other hand, the Bayesian network assigns discrete probability to uncertain parameters, weighting intervals rather than point values. This method is consequently less informative and seems more representative of the actual knowledge of the uncertain parameters in the specific situation of routine monitoring.

Therefore, it was judged that the Bayesian network is the most adapted method for this study. However, the calculation time can be prohibitive.

Another Bayesian approach was developed by Miller *et al* (1999) in the UF code (www.lanl.gov/bayesian), using Markov Chain Monte-Carlo (Miller *et al*, 2002). Continuous probabilities are assigned to the time of contamination and to the intake while a set of different possible exposure conditions are defined by discrete values of absorption into blood and AMAD (Miller, 2008). It therefore appears as an intermediate modelling between the WeLMoS method and the Bayesian network.

In the future, it would be interesting to compare the application of the Bayesian network, WeLMoS method and UF code to the monitoring programme of R4-T4 facilities in order to more clearly identify the differences in the modelling process and their consequences in the results. From

this comparison, new methods might be developed for a better modelling of uncertainty within a reasonable calculation time.

However, the probabilistic modelling of uncertainty very still very informative because it assigns weights to every point values, while actual knowledge is often not available to fully justify such precise assignment of probability. On the other hand, possibility theory assigns weights to intervals, modelling the imprecision in the knowledge. But as seen above, no inverse propagation methods were developed using possibility. A solution for application in retrospective dosimetry could be the use of imprecise probability within a Bayesian network. An imprecise probability assigns to each point value an interval of probabilities rather than a single probability. This could be quite useful for the intake prior leading to a more conservative modelling of the information on the potential intake before any measurement takes place, which is the most influent hypothesis on the MDD assessment.

8.2.2 Prior probability

To precisely estimate the MDD with the WeLMoS method or the Bayesian network, an intake prior probability which best fits the reality should be chosen. The intake prior probability models the assumed knowledge on the intake before any bioassay measurement. It is then updated by the information brought by the measurement results into a posterior probability of intake.

The determination of the intake prior PDF is often a subjective choice of the user of the Bayesian method. Such *a priori* hypotheses are made in any statistical approach. For instance, the classical method produces implicit *a priori* knowledge on the intake through the assumptions made on the prior probabilities of the other uncertain parameters which take more weight than in the Bayesian framework. The Bayesian approaches has the strong merit of explicitly expressing all *a priori* assumptions, including on the foreseen result, thus acknowledging the subjectivity inherent to any probabilistic modelling and allowing for open discussion of these assumptions.

However, this subjectivity is not arbitrary as long as it can be supported by experimental or historical data. For Miller *et al* (1993), the intake prior probability should depend on prior knowledge of relevant events or information. This information may include the type of facility, quantities of material in use, historical records of previous bioassay results and specific incidents. In estimating the prior intake probability using historical data, Miller *et al* (1993) assume that what has happened in the past is applicable to the present. They consider that this is usually a conservative assumption for radiation safety, since the technology and methods are improving with time. However, for R4-T4 facilities, too few contaminations occurred to precisely determine a prior probability from historical data. Following this approach, Miller *et al* (2001) developed the alpha prior which varies between an inverse and a uniform PDF according to a historical frequency of positive measurements varying between 0 and 1.

Applying the alpha prior with a frequency of one positive measurement over a thousand measurements for R4-T4 facilities leads to a MDD below 1 nSv. It could be argued that if

contamination is this rare, the individual monitoring is unnecessary, workplace monitoring associated with control monitoring of a sample of workers could be sufficient.

To define realistic prior probabilities while assessing a contamination case, James *et al* (2008) derived posterior probabilities of absorption parameters for an americium compound from comprehensive bioassay data available from a contaminated worker. These posterior probabilities were then used as prior information to improve the dose assessment for a second worker contaminated with the same compound, assuming that the absorption into blood and particle transport were the same for both individuals. Still, such approach is applicable to special monitoring where comprehensive data are gathered but not to routine monitoring unless a representative and well documented case of contamination can be studied to provide generic information. Such comprehensive data is – fortunately - not available in R4-T4 to determine precise prior PDFs.

In this study, to limit the subjectivity in the choice of the intake prior probability, different extreme intake probabilities were used to quantify their influence on the intake and dose posterior probabilities. This influence is significant: the MDD varies over several orders of magnitude depending on the intake prior probability. This effect appears as a generic feature of studies where only scarce measurement results are available because the information brought by these measurements does not balance the information put in the intake prior. This is the case here when only one or two negative measurements are used to derive the magnitude of a potential intake. Similarly strong influence of the prior probability was observed during the Alpha-Risk project (European project n°516483) in the long-life dose reconstruction for uranium and plutonium workers whose bioassay data were mainly below the limit of detection (M. Puncher, personal communication). However, intake prior probabilities have almost no influence when comprehensive positive measurement data are available as in post-incidental dose calculation (James *et al,* 2008).

For R4-T4 monitoring programme, the intake prior probability uniform between 0 and 10,000 Bq seems too conservative because it implies that all the intakes between 0 and 10,000 Bq are as likely to occur and may be undetected by ambient air monitoring. The alpha prior is little influenced by the other parameters and thus seems to be too informative. Consequently, the exponential prior looks as a reasonable if subjective intermediate choice.

Since multiple priors may often be selected, a sensitivity analysis of the MDD for different intake priors would be warranted for all studies; or an uncertainty analysis for MDD should include each possible intake prior with an associated probability weight, which could be done within the frame of imprecise probability.

For R4-T4 facilities, as in the general case, an adequate intake prior probability could be derived from the ambient air monitoring. For example, the minimum activity detectable by the air monitoring could be used to determine the maximum activity inhalable by a worker while undetected by the air monitoring. Then, the maximum of the intake prior probability would rely on this data, while its shape would reflect the uncertainty on air monitoring, diffusion of aerosols and worker breathing rate. In this way, the measurement of air contamination could generally be a good basis to define a prior intake PDF. However such approach is hardly applicable to La Hague R4-T4 facilities since no ambient contamination is present on a routine basis. Nevertheless, in the general

situation, taking into account simultaneously ambient air monitoring, individual bioassay monitoring and their respective uncertainties would provide a global insight into the monitoring of workers, for both planning and control purposes. This is identified as important perspective of the present work together with its application to other nuclear or medical facilities.

8.2.3 Measurement modelling

Counts below DT

To derive the MDD of a monitoring programme, it was assumed that the routine bioassay result was equal to the decision threshold (DT) of the activity measurement technique in order to model a negative measurement in a conservative way. However, negative measurements can correspond to any value below the DT. Therefore, this method can be considered as over-conservative: the uncertainty in the raw measurement result is modelled as an interval, using the most penalizing value. It would be more realistic to apply probabilities to negative results.

Moreover, it would avoid the unrealistic increase of the MDD with the number of negative measurements observed with the exponential and alpha intake prior probabilities, which is caused by the relatively high value (DT) assigned to any negative measurement.

The MDDs for measurement results equal to 5, 4, 3, 2, 1 counts were calculated using the same modelling as in Section 5.2 but with the complete isotopic composition of PWR1 (Table 4.3) and the realistic values of the absorption into blood (Table 5.4), for the exponential intake prior with the WeLMoS method and with the Bayesian network. The results are gathered in Table 8.1.

Table 8.1: Annual MDDs obtained for the WeLMoS method and for the Bayesian network with exponential intake prior probability. Application to workers of R4-T4 facilities (see text) for an observed faecal measurement equal to 5, 4, 3, 2, or 1 counts from Pu in PWR1 spent fuel.

Method	Measurement result (counts)	MDD (mSv)
WeLMoS	5	3.4×10^{-1}
	4	2.7×10^{-1}
	3	2.2×10^{-1}
	2	1.9×10^{-1}
	1	1.7×10^{-1}
Bayesian network	5	$0.5 < MDD < 1$
	4	$0.1 < MDD < 0.5$
	3	$0.1 < MDD < 0.5$
	2	$0.1 < MDD < 0.5$
	1	$0.1 < MDD < 0.5$

Decreasing the measurement result strongly reduces the MDD. This simple calculation highlights the need for a more realistic modelling of the measurement results than the most penalizing

negative value. Therefore, to obtain a better evaluation of the MDD, a uniform probability between 0 and the DT could be assigned to the measurement results. The intervals obtained with the Bayesian network are too large to observe the decrease of the MDD. Therefore, for this study, it would have been better to use smaller intervals.

Isotopic composition

At AREVA NC La Hague bioassay laboratory, during Pu measurement, the absences of both ^{238}Pu and ^{239}Pu are tested using DTs specific to each isotope. Therefore, in a Pu negative measurement the number of counts for both ^{238}Pu and ^{239}Pu are below their respective DTs.

However, in this work, it was assumed that in a Pu negative measurement only ^{239}Pu counts were below their DT, while the quantity of ^{238}Pu and other isotopes were derived from the known isotopic composition of the radioactive material. Such modelling is over-conservative since two negative measurements (^{238}Pu and ^{239}Pu) are more informative than only one (^{239}Pu).

To determine the influence on the MDD of the negative ^{238}Pu measurement , a simple calculation was performed with the WeLMoS method using the same modelling as in Section 5.2 but with an isotopic composition of 0.36 % ^{239}Pu and 5.3 % ^{238}Pu, the realistic values of absorption into blood (Table 5.4), and the exponential intake prior. The result was taken to be either two measurements of ^{239}Pu and ^{238}Pu at their respective DTs of 5 counts; or one measurement of ^{239}Pu equal to its DT. The total intake is derived using the isotopic composition of the mixture.. The results are shown in Table 8.2.

Table 8.1: Annual MDDs obtained with the WeLMoS method and an exponential intake prior probability. Application to workers of R4-T4 facilities (see text) for faecal measurements equal of Pu with 0.36 % of ^{239}Pu and 5.3 % of ^{238}Pu

Measurement result (counts)	MDD (mSv)
1 measurement equal to DT of ^{238}Pu and 1 to DT of ^{239}Pu	2.5×10^{-2}
1 measurement equal to DT of ^{239}Pu	3.0×10^{-1}

Integrating the negative measurement of ^{238}Pu in addition to the one of ^{239}Pu decreases here the MDD by a factor of 10. This highlights the need of further work to integrate, within both the WeLMoS method and the Bayesian network, all the isotopes actually measured.

8.2.4 Conditions of exposure

The modelling of the exposure conditions used for the determination of the MDD at R4-T4 facilities could be improved in several ways:

- Instead of assuming that only one contamination may occur each year, it would be interesting to calculate MDD for an annual contamination formed of repeated acute intakes or constant chronic contamination. Such patterns of exposure seem unlikely at

R4-T4 facilities where only one bioassay measurement in a thousand is positive; however they may be most realistic in other situations (e.g. uranium process, nuclear medicine)

- The time of acute contamination is here assigned a probability uniform over the monitoring interval. However, the workers of R4-T4 are not exposed 24h a day every day but only during point maintenance operations. Therefore, the time probability should be, as far as feasible, consistent with the actual schedule of maintenance operation.
- As discussed in Section 4.4, the AMAD probability is not based on experimental data. This could valuably be improved by a workplace study to determine the aerosol size distribution in R4-T4 facilities. Moreover, such study may bring site-specific information on the absorption into blood using *in vitro* dissolution of the aerosol samples.

8.2.5 Uncertainty in the biokinetic and dosimetric models

The sources of uncertainty considered in this work are relative to the conditions of exposure and to the measurement of activity. However, the inter-individual variability is an important source of uncertainty in the assessment of intake from bioassay data which should be integrated in some way even though the effective dose coefficient is considered as fixed by the French regulation (Arreté du 1er septembre 2003).

From a given intake, the bioassay measurement is subject to the specific biokinetics of the particular worker. Still reference anatomical and physiological values (ICRP, 2002b) as well as reference biokinetic models have been applied consistently with the radiation protection purpose of this study (ICRP, 2007). This may turn out to be not protective when some intake may be underestimated due to individual deviation from reference excretion.

The inter-individual variability of plutonium faecal excretion is difficult to directly estimate for lack of suitable data. However, from the 256 faecal excretion measurement results following Pu injection referred to as “modern injection data” by Leggett (2003), a scattering factor (SF) of 2.5 can be derived. As these data correspond to several subjects, this SF quantifies simultaneously the inter- and intra-individual variabilities. Therefore, applying a SF of 3 to faecal data uncertainty (Marsh *et al*, 2008b) is likely to take into account, at least to some extend, the inter-individual variability. Moreover, the variability of Pu absorption derived from a review of the literature appears to be the main source of uncertainty beside the choice of the prior. It includes the inter-individual variability of Pu absorption as far as documented in the literature and we therefore assume that it accounts for a large part of the inter-individual variability of excretion from a given intake.

8.3 Perspectives

In this work, the uncertainty in exposure conditions and bioassay measurement were taken into consideration to quantify the uncertainty in the dose. The mathematical modelling of uncertainty and the techniques of propagation were studied to determine the most suitable approach to prospective and retrospective internal dose calculation.

Regarding retrospective dosimetry, the sensitivity of the individual monitoring programme for internal contamination at AREVA La Hague R4-T4 facilities was evaluated by the minimum detectable dose to demonstrate compliance with regulatory dose limits and for optimisation purpose. The implemented methods may be applied to any situation of exposure and monitoring programme.

8.3.1 Application to monitoring of uranium exposure

Another application of interest would be the monitoring of uranium exposure during the preparation of nuclear fuel. Such study would be different from the present one because of the alimentary intake of natural uranium which determines the detection threshold by current techniques, such as inductively coupled plasma mass spectrometry (ICP-MS), and which level depends on individual diet.

Moreover, the critical consequences of internal contamination by natural uranium are supposed to be chemical effects leading to kidney malfunctions rather than radiological injury. Therefore, it would then be interesting to quantify the results in terms of renal uranium mass concentration in addition to committed effective dose.

Exhaustive review of the exposure conditions and of the background level of alimentary uranium intake would be desirable to conduct such study. Nevertheless, consideration of potential health effects would be enabled by ongoing epidemiological (Guseva Canu *et al*, 2010) and radiobiological (Racine *et al*, 2010) studies at IRSN.

8.3.2 Application to nuclear medicine

Besides nuclear industry, radioactivity is also widely used in medicine for imaging and therapy. In nuclear medicine, short-lived radionuclides are purposely injected to patients. In France, the potential internal exposure of the medical staff is commonly monitored by half-yearly urine measurement. This monitoring can be considered as control but is not suitable for routine because of the monitoring interval, and often the measurement procedure, are much longer than the half-lives of the isotopes. However, the dose coefficients of radiopharmaceuticals are very low.

Therefore, it would be particularly interesting to apply the developed methods to occupational exposure to radiopharmaceuticals in order to propose adapted routine monitoring programmes, which could consist in workplace monitoring associated with control monitoring or individual

monitoring. Individual measurements could target urine samples, whole body or specific organs at a frequency to be determined and with different possible techniques for *in vivo* measurement (e.g. gamma camera, fixed body count unit, mobile body count unit).

In this way, the methods developed here would be an effective tool to establish a radiological protection of medical staff adapted to their exposure conditions.

8.3.3 Application to post-incidental dose assessment

The WeLMoS method and the Bayesian network could be used to evaluate the dose following an incidental contamination. In this particular case, the effective dose is calculated for regulatory purposes for the reference person of the ICRP contaminated with the same exposure conditions. However, if the contamination is significant, it is interesting to evaluate the risk of the individual quantified from an estimation of the organ absorbed dose. For risk assessment, it is acknowledged that uncertainties in biokinetic and dosimeteric models have to be considered.

Moreover, the individual organ absorbed dose can be used in epidemiological studies which quality depends on the quality of the dose assessment and its related uncertainty. However, the quantification and the modelling of inter-individual uncertainty are so far not straightforward and should be a specific research topic.

8.3.4 Application to population triage after accident

The Treatment Initiatives After Radiological Accidents project (TIARA, Ménétrier *et al*, 2007) was conducted to create a European network that may participate in facilitating the management of a crisis after accidental or malevolent dispersal of radionuclides in the environment. One objective of TIARA was to generate straightforward guidance on dose assessment.

The dispersal of radionuclides would result in a possibly large number of potentially contaminated and perhaps physically injured persons needing a treatment of mechanical or thermal trauma as well as of radioactive contamination. Such an event would require monitoring and triage to separate individuals needing immediate medical attention from those needing reassurance that doses are low and do not warrant health concern.

To facilitate triage ant treatment decisions by physicians, based on dose assessment after possible inhalation, a booklet offering practical guidance on dose assessment was written. This guidance is based on bioassay functions corresponding with a specified committed effective dose E (e.g. 1 mSv) (Hodgson *et al*, 2007): if the activity measured a given time after the event is less than this function, the corresponding dose is less than E; else the corresponding dose is more than E.

The bioassay function can be calculated for reference parameter values of ICRP. However, exposure conditions are often not known. Therefore, Hodgson *et al* (2007) calculated bioassay functions for several E, different values of AMAD and absorption types. The resulting functions allow bands to be drawn where width provide indication of the magnitude of the dose and its uncertainty.

A better modelling of uncertainty could be obtained by means of the methods developed in this work, such as the Bayesian network.

General conclusion

The potential internal contamination of workers is firstly estimated by workplace monitoring and then monitored by periodic bioassay measurements. Both are interpreted in terms of intake and committed effective dose through biokinetic and dosimetric models. Prospective dosimetry is used for planning purpose, to check if the potential exposure at a workplace conforms to the regulation and radiation protection policies.

On the other hand, retrospective dosimetry is performed from individual measurement data. After a prospective evaluation of exposure at a workplace, a suitable monitoring program can be defined by the choice of measurement techniques and frequency of measurements.

However, the actual conditions of exposure are usually not well known and the measurements are subject to errors. Major sources of uncertainty are the contamination time, the size distribution and absorption into blood of the incorporated particles, and the measurement errors. Different assumptions may be applied to model uncertain knowledge which lead to different statistical approaches.

However, while probability distributions are well adapted to model the known variability of a parameter, they may lead to an unrealistically low estimate of the uncertainty when it is due to a lack of knowledge about some input parameters. Here, an innovative mathematical method, based on the Dempster-Shafer theory, was used to deal with such imprecise knowledge. This method was applied to the prospective dosimetry of inhaled uranium dust in the nuclear fuel cycle and in mines and mills when its physico-chemical properties are not precisely known. The results show an increased estimation of the range of uncertainty as compared to the application of a probabilistic method. As showed by this work, the Dempster-Shafer method can easily be used to realistically assess the prospective uncertainty in internal dose estimates at a characterized workplace. However, this method is presently not suitable for the inverse problem of retrospective dose calculation.

When a significant exposure is expected, a routine monitoring programme is designed to verify and document that the worker's protection complies with the regulatory dose limits and dose constraints. However, the sensitivity of the monitoring programme should be evaluated by integrating uncertainty regarding the dose evaluation.

In this study, the uncertainties associated with a routine monitoring program were taken into account in order to evaluate the minimum intake and dose detectable (MDD) with a given level of confidence. Three methods were presented: the classical method supposes a fixed intake, provides

a conservative estimate of the MDD when the biokinetic model is uncertain and is not adapted so far to integrate several measurement results. The WeLMoS method and the Bayesian network, on the other hand, are more flexible and assign a prior probability to intake based on a subjective judgment.

These three methods provide a general frame to estimate MDD and to assess the quality of a monitoring program by comparing MDD with dose constraints. This methodology was applied to the monitoring program of workers in charge of plutonium purification at the AREVA NC reprocessing facility. After estimation of the MDDs corresponding to a set of possible monitoring programmes, it was concluded, under explicit assumptions regarding the prior probabilities of uncertain parameters, that the current monitoring programme is the best compromise between the cost of the measurements and the sensitivity of the programme.

This study highlights the use of the MDD as a tool to optimise monitoring programmes of potential contamination considering uncertainty on exposure conditions and on measurement. Computational techniques were implemented in the OPSCI software developed for this work and validated by comparison with the literature and with IMBA software.

To precisely estimate the MDD with the WeLMoS method and the Bayesian network, an intake prior probability distribution which best fits the reality should be chosen. Since multiple priors can often be selected, a sensitivity analysis of the MDD for different intake priors would be warranted. Moreover, probability is not always the best way to model lack of knowledge: a new method could be developed in the future mixing imprecise probability with Bayesian statistics.

Finally, the method presented here is suitable to calculate MDD for any routine monitoring program. It could be further applied to uranium and mixed oxide fuels facilities; to nuclear medicine and to population triage.

References

Arrêté du 1er septembre 2003 définissant les modalités de calcul de doses efficaces et des doses équivalentes résultant de l'exposition des personnes aux rayonnements ionisants *Journal Officiel n°262 du 13 novembre 2003* 19236

Alloul-Marmor L 2002 Reentrainement par écoulement d'air d'une contamination particulaire déposée sur une surface - Application au cas d'un "tas" de poudre. (Créteil: Université Paris XII - Val de Marne)

Andre S, Metivier H, Auget D, Lantenois G, Boyer M and Masse R 1989 Assessment of uranium tetrafluoride dissolution in the lung by in vivo and in vitro methods *Radiation protection dosimetry* **26** 75-81

Ansoborlo E, Boulaud D and B. L 1997 Distribution granulométrique d'aérosols d'uranium dans l'industrie française de fabrication du combustible *Radioprotection* **32** 319-30

Ansoborlo E, Chazel V, Henge-Napoli M H, Pihet P, Rannou A, Bailey M R and Stradling N 2002 Determination of the physical and chemical properties, biokinetics, and dose coefficients of uranium compounds handled during nuclear fuel fabrication in France *Health physics* **82** 279-89

Apostoaei A I and Miller L F 2004 Uncertainties in dose coefficients from ingestion of 131I, 137Cs, and 90Sr *Health physics* **86** 460-82

Bailey M R, Fry F A and James A C 1985a Long-term retention of particles in the human respiratory tract *J. Aerosol Sci.* **16** 295-305

Bailey M R, Hodgson A and Smith H 1985b Respiratory tract retention of relatively insoluble particles in rodents *J. Aerosol Sci.* **16** 279-93

Bailey M R, Kreyling W G, André S, Batchelor A, Collier C, Drosselmeyer E, Ferron G A, Foster P P, Haider B, Hodgson A, Masse R, Métivier H, Morgan A, Müller H-L, Patrick G, Pearman I, Pickering S, Ramsden D, Stirling C and Talbot R J 1989 An interspecies comparison of the lung clearance of inhaled monodisperse cobalt oxide particles-Part I: Objectives and summary of the results *Journal of Aerosol Science* **20** 169-88

Bailey M R, Ansoborlo E, Chazel V, Fritsch P, Hodgson A, Kreyling W G, Le Gall B, Newton D, Paquet F, Stradling N, Svartengren M, Taylor D M and Wenman-Bateson S 2004 Radionuclide biokinetics database (RBDATA-EULEP): an update *Radiation protection dosimetry* **112** 535-6

Bailey M R, Ansoborlo E, Guilmette R A and Paquet F 2007 Updating the ICRP human respiratory tract model *Radiation protection dosimetry* **127** 31-4

Bair W J and McClanahan B J 1961 Plutonium inhalation studies. II. Excretion and translocation of inhaled Pu-239-O2 dust *Archives of environmental health* **2** 648-55

Bair W J, Willard D H and Temple L A 1961 Plutonium inhalation studies. I. The retention and translocation of inhaled Pu239O2 particles in mice *Health physics* **7** 54-60

Bair W J and Willard D H 1963 Plutonium inhalation studies-III: effect of particle size and total dose on deposition, retention and translocation *Health physics* **9** 253-66

Bair W J, Métivier H and Park J F 1980 Comparison of early mortality in baboons and dogs after inhalation of 239PuO2 *Radiation research* **82** 588-610

Ballou J E, Park J F and Morrow W G 1972 On the metabolic equivalence of ingested, injected and inhaled 239Pu citrate *Health physics* **22** 857-62

Ballou J E, Dagle G E, McDonald K E and Buschbom R L 1977 Influence of inhaled Ca-DTPA on the long-term effects of inhaled Pu nitrate *Health physics* **32** 479-87

Barrett P H, Bell B M, Cobelli C, Golde H, Schumitzky A, Vicini P and Foster D M 1998 SAAM II: Simulation, Analysis, and Modeling Software for tracer and pharmacokinetic studies *Metabolism: clinical and experimental* **47** 484-92

Berkovski V, Ratia G and Bonchuk Y 2007 IMIE computer codes: 10 y in the internal dosimetry *Radiation protection dosimetry* **125** 205-8

Bess J D, Krahenbuhl M P, Miller S C, Slaughter D M, Khokhryakov V V, Khokhryakov V F, Suslova K G and Vostrotin V V 2007 Uncertainties analysis for the plutonium dosimetry model, doses-2005, using Mayak bioassay data *Health physics* **93** 207-19

Biasi L, de los Reyes A, Reeks M W and de Santi G F 2001 Use of a simple model for the interpretation of experimental data on particle resuspension in turbulent flows *Journal of aerosol science* **32** 1175-200

Birchall A, Bailey M R and James A C 1991 LUDEP. A lung dose evaluation program *Radiat Prot Dos* **38** 167-74

Birchall A and James A C 1994 A rapid method for modeling the kinetics of radioactive progeny applied to thorium in the lungs *Health physics* **67** 162-9

Birchall A, Bailey M R and Jarvis N S 1995 Application of the new ICRP respiratory tract model to inhaled plutonium nitrate using experimental biokinetic data *Proc. Int. Conf. on Radiation Dose MAnagement in the Nuclear Industry* (*Windermere, UK*) pp 216-23

Birchall A, Puncher M, Marsh J W, Davis K, Bailey M R, Jarvis N S, Peach A D, Dorrian M D and James A C 2007 IMBA Professional Plus: a flexible approach to internal dosimetry *Radiation protection dosimetry* **125** 194-7

Blanchardon E, Molokanov A, Franck D, Kochetkov O, Panfilov A and Jourdain J R 2007 Estimation of the Uncertainty in Internal Dose Calculation for Two Contamination Cases *Radiation protection dosimetry*

Bolch W E, Farfan E B, Huh C, Huston T E and Bolch W E 2001 Influences of parameter uncertainties within the ICRP 66 respiratory tract model: particle deposition *Health physics* **81** 378-94

Bolch W E, Huston T E, Farfan E B, Vernetson W G and Bolch W E 2003 Influences of parameter uncertainties within the ICRP-66 respiratory tract model: particle clearance *Health physics* **84** 421-35

Bolch W E, Eckerman K F, Sgouros G and Thomas S R 2009 MIRD pamphlet No. 21: a generalized schema for radiopharmaceutical dosimetry--standardization of nomenclature *J Nucl Med* **50** 477-84

Brooks A L, Guilmette R A, Hahn F F, Haley P J, Muggenburg B A, Mewhinney J A and McClellan R O 1992 Distribution and biological effects of inhaled 239Pu(NO3)4 in cynomolgus monkeys *Radiation research* **130** 79-87

Carbaugh E H 2003 Minimum detectable dose as a measure of bioassay programme capability *Radiation protection dosimetry* **105** 391-4

Carbaugh E H and La Bone T R 2003 Two case studies of highly insoluble plutonium inhalation with implications for bioassay *Radiation protection dosimetry* **105** 133-8

Chazel V, Houpert P, Paquet F, Ansoborlo E and Henge-Napoli M H 2000 Experimental determination of the solubility of industrial UF4 particulates *Radiation protection dosimetry* **92** 23-7

Chazel V, Houpert P, Paquet F and Ansoborlo E 2001 Effect of absorption parameters on calculation of the dose coefficient: example of classification of industrial uranium compounds *Radiation protection dosimetry* **94** 261-8

Chojnacki E, Baccou J and Destercke S 2010 Numerical accuracy and efficiency in the treatment of epistemic and random uncertainty *International Journal of General Systems* Accepted

Cochran W 1977 Sampling techniques, Third edition *John Wiley and Sons* (New-York)

Cristy M and Eckerman K F 1987 Specific absorbed fractions of energy at various ages from internal photon sources. I. Methods *Oak Ridge National Laboratory* **Report No. ORNL/TM-8381:Vol 1**

Code du Travail 2008a Code du Travail, quatrième partie - santé et sécurité au travail, livre IV - prévention de certains risques d'exposition, titre V - préventions des risques d'exposition aux rayonnements ionisants, section 2 - principe de radioprotection

Code du Travail 2008b Code du Travail, quatrième partie - santé et sécurité au travail, livre IV - prévention de certains risques d'exposition, titre V - préventions des risques d'exposition aux rayonnements ionisants, section 3 - valeurs limites d'exposition, article R4451-12

Dagle G E, Cannon W C, Stevens D L and McShane J F 1983 Comparative disposition of inhaled 238Pu and 239Pu nitrates in beagles *Health physics* **44** 275-7

Davesne E, Casanova P, Chojnacki E, Paquet F and Blanchardon E 2010 Optimisation of internal contamination monitoring programme by integration of uncertainties *Radiat Prot Dos* **submitted**

de Carlan L, Roch P, Blanchardon E and Franck D 2007 Application of voxel phantoms in whole-body counting for the validation of calibration phantoms and the assessment of uncertainties *Radiation protection dosimetry* **125** 477-82

de Finetti B 1974 *Theory of Probability, Vol. I* (New-York: J. Wiley & Sons)

Doerfel H, Andrasi A, Bailey M R, Birchall A, Castellani C M, Hurtgen C, Jarvis N S, Johansson L, Le Guen B and Tarroni G 2000 Third European intercomparison exercise on internal dose assessment (Results of a research programme in the framework of the EULEP/EURADOS Action group "Derivation of parameter values for application to the new respiratory tract for occupational exposure" 1997-1999) *Research Center Karlsruhe* (Karlsruhe) **Research report FZKA 6457, ISSN 0947-8620**

Doerfel H, Andrasi A, Bailey M R, Berkovski V, Blanchardon E, Castellani C M, Hurtgen C, Le Guen B, Malatova I, Marsh J W and Stather J 2006 General guidelines for the estimation of committed effective dose from incorporation monitoring data (Project IDEAS - EU Contract No. FIKR-CT2001-00160) *Research Center Karlsruhe* (Karlsruhe) **Research report FZKA 6457, ISSN 0947-8620**

Dorrian M D and Bailey M R 1995 Particle size distributions of radioactive aerosols measured in workplaces *Radiation protection dosimetry* **60** 119-33

Dorrian M D 1997 Particle size distributions of radioactive aerosols in the environment *Radiation protection dosimetry* **69** 117-32

Dubois D and Prade H 1988 *Possibility Theory: An Approach to Computerized Processing of Uncertainty* (New York, Plenum Press)

Dunning D E, Jr. and Schwarz G 1981 Variability of human thyroid characteristics and estimates of dose from ingested 131I *Health physics* **40** 661-75

Duport P, Robertson R, Ho K and Horvath F 1991 Flow-through dissolution of uranium-thorium ore dust, uranium concentrate, uranium dioxide, and thorium alloy in simulated lung fluid *Radiation protection dosimetry* **95** 121-33

Duport P 1994 Radiation protection in uranium mining: Two challenges *Radiation protection dosimetry* **53** 13-9

Eckerman K F, Leggett R W, Cristy M, Nelson C B, Ryman J C, Sjoreen A L and Ward R C 2006 User's Guide to the DCAL System *Oak Ridge National Laboratory, USA* **Report ORNL/TM-2001/190**

Eidson A F and Mewhinney J A 1980 In vitro solubility of yellowcake samples from four uranium mills and the implications for bioassay interpretation *Health physics* **39** 893-902

Eidson A F and Mewhinney J A 1983 In vitro dissolution of respirable aerosols of industrial uranium and plutonium mixed-oxide nuclear fuels *Health physics* **45** 1023-37

Etherington G, Stradling G N, Hodgson A and Fifield L K 2003 Anomalously high excretion of Pu in urine following inhalation of plutonium nitrate? *Radiation protection dosimetry* **105** 321-4

Etherington G, Cossonnet C, Franck D, Génicot J L, Hurtgen C, Jourdain J R, Le Guen B, Rahola T, Sovijärvi J, Stradling G N, Ansoborlo E and Bérard P 2004 Optimisation of Monitoring for Internal Exposure (OMINEX), Report NRPB-W60 *National Radiological Protection Board* (Chilton) **W60**

Etherington G, Birchall A, Puncher M, Molokanov A and Blanchardon E 2006 Uncertainties in doses from intakes of radionuclides assessed from monitoring measurements *Radiation protection dosimetry* **121** 40-51

Farfan E B, Huston T E, Bolch W E, Vernetson W G and Bolch W E 2003 Influences of parameter uncertainties within the ICRP-66 respiratory tract model: regional tissue doses for 239PuO2 and 238UO2/238U3O8 *Health physics* **84** 436-50

Farfan E B, Bolch W E, Huston T E, Rajon D A, Huh C and Bolch W E 2005 Uncertainties in electron-absorbed fractions and lung doses from inhaled beta-emitters *Health physics* **88** 37-47

Foster P P 1991 Study of a plutonium oxide fuel inhalation case *Radiation protection dosimetry* **38** 141-6

Franck D, De Carlan L, Bérard P, Dousse C, Pihet P, Razafindralambo N and Soulié R 1997 Les mesures anthroporadiamétriques dans les basses énergies : évolution technologique et bases de recherches actuelles *Radioprotection* **32** 685-96

Fritsch P 2006 Uncertainties in aerosol deposition within the respiratory tract using the ICRP 66 model: a study in workers *Health physics* **90** 114-26

Génicot J L 2003 OMINEX Work Package 3, Uncertainties on *in vivo* measurements - A survey of European laboratories, Scientific Report SCK•CEN - BLG-943 *SCK•CEN* (Mol) **BLG-943**

Grappin L, Berard P, Menetrier F, Carbone L, Courtay C, Castagnet X, Le Goff J P, Neron M O and Piechowski J 2007 Treatment of actinide exposures: a review of Ca-DTPA injections inside CEA-COGEMA plants *Radiation protection dosimetry* **127** 435-9

Guilmette R A, Diel J H, Muggenburg B A, Mewhinney J A, Boecker B B and McClellan R O 1984 Biokinetics of inhaled 239PuO2 in the beagle dog: effect of aerosol particle size *International journal of radiation biology and related studies in physics, chemistry, and medicine* **45** 563-81

Guilmette R A, Muggenburg B A, Hahn F F, Mewhinney J A, Seiler F A, Boecker B B and McClellan R O 1987 Dosimetry of 239Pu in dogs that inhaled monodisperse aerosols of 239PuO2 *Radiation research* **110** 199-218

Guilmette R A, Griffith W C and Hickman A W 1994 Intake assessment for workers who have inhaled 238Pu aerosols *Radiat Prot Dos* **53** 127-31

Guseva Canu I, Laurier D, Caër-Lorho S, Samson E, Timarche M, Auriol B, Bérard P, Collomb P, Quesne B and Blanchardon E 2010 Characterisation of protracted low-level exposure to uranium in the workplace: A comparison of two approaches *International Journal of Hygiene and Environmental Health* in press

Hamby D M and Benke R R 1999 Uncertainty of the iodine-131 ingestion dose conversion factor *Radiation protection dosimetry* **82** 245-56

Harrison J D, Khursheed A, Phipps A W, Goossens L, Kraan B and Harper F 1998 Uncertainties in biokinetic parameters and dose coefficients determined by expert judgement *Radiat Prot Dos* **79** 355-8

Harrison J D, Leggett R W, Nosske D, Paquet F, Phipps D M, Taylor D M and Metivier H 2001 Reliability of the ICRP's dose coefficients for members of the public, II. Uncertainties in the absorption of ingested radionuclides and the effect on dose estimates. *Radiation protection dosimetry* **95** 295-308

Harrison J D, Khursheed A and Lambert B E 2002 Uncertainties in dose coefficients for intakes of tritiated water and organically bound forms of tritium by members of the public *Radiation protection dosimetry* **98** 299-311

Harvey R P, Hamby D M and Benke R R 2003 Age-specific uncertainty of the 131I ingestion dose conversion factor *Health physics* **84** 334-43

Heard M J and Chamberlain A C 1984 Uptake of Pb by human skeleton and comparative metabolism of Pb and alkaline earth elements *Health physics* **47** 857-65

Hickman A W, Griffith W C, Roessler G S and Guilmette R A 1995 Application of a canine 238Pu biokinetics/dosimetry model to human bioassay data *Health physics* **68** 359-70

Hodgson A, Shutt A L, Etherington G, Hodgson S A, Rance E, Stradling G N, Youngman M J, Ziesenis A and Kreyling W G 2003 Comparison of predicted with observed biokinetics of inhaled plutonium nitrate and gadolinium oxide in humans *Radiation protection dosimetry* **105** 91-4

Hodgson A, Stradling N, Phipps A and Fell T 2007 A simple method for assessing that internal doses are below action levels *Radiation protection dosimetry* **127** 382-6

Hursh J B, Schraub A, Sattler E L and Hofmann H P 1969 Fate of 212Pb inhaled by human subjects *Health physics* **16** 257-67

Hursh J B and Spoor N L 1973 Data on man *Handbook of Experimental Pharmacology* **36** 197-239

Hurtgen C and Cossonnet C 2003 OMINEX Work Package 3, Uncertainties on bioassay measurements, Scientific Report SCK•CEN - BLG-935 *SCK•CEN* (Mol) **BLG-935**

Hurtgen C, Andrasi A, Bailey M R, Birchall A, Blanchardon E, Berkovski V, Castellani C M, Cruz-Suarez R, Davis K, Doerfel H, LeGuen B, Malatova I, Marsh J and Zeger J 2005 Intercomparison exercise on Internal Dose Assessment performed jointly by the International Atomic Energy Agency and the IDEAS project ("General Guidelines for the Evaluation of Incorporation Monitoring Data", carried out within the 5th EU Framework Programme) - Scientific report SCK•CEN-BLG-1018 *SCK•CEN* (Mol) **SCK•CEN-BLG-1018**

IAEA 1999 Assessment of occupational exposure due to intakes of radionuclides *IAEA* (Vienna) **Safety Series n° RS-G-1.2**

IAEA 2004 Quantifying uncertainty in nuclear analytical measurements *IAEA* (Vienna) **IAEA-TECDOC-1401**

International Commission on Radiological Protection 1973 Alkaline earth metabolism in adult man. ICRP Publication 20 **volume 20** (Oxford: Pergamon Press)

International Commission on Radiological Protection 1975 Report of the task group on reference man. ICRP Publication 23 **volume 23** (Oxford: Pergamon Press)

International Commission on Radiological Protection 1979 Limits for intake of radionuclides by workers. ICRP Publication 30, Part 1 *Annals of the ICRP* **2(3/4)** (Oxford: Pergamon Press)

International Commission on Radiological Protection 1993 Age-dependent doses to member of public from intake of radionuclides: Part 2 Ingestion dose coefficients. ICRP Publication 67 *Annals of the ICRP* **23(3/4)** (Oxford: Elsevier Science Ltd)

International Commission on Radiological Protection 1994a Human respiratory tract model for radiological protection. ICRP Publication 66 *Annals of the ICRP* **24(1-3)** (Oxford: Elsevier Science Ltd)

International Commission on Radiological Protection 1994b Dose coefficients for intakes of radionuclides by workers. Replacement of publication 61. ICRP Publication 68 *Annals of the ICRP* **24(4)** (Oxford: Elsevier Science Ltd)

International Commission on Radiological Protection 1995a Age-dependent doses to member of the public from intake of radionuclides: Part 3 Ingestion dose coefficients. ICRP Publication 69 *Annals of the ICRP* **25(1)** (Oxford: Elsevier Science Ltd)

International Commission on Radiological Protection 1995b Basic anatomical and physiological data: The skeleton. ICRP Publication 70 *Annals of the ICRP* **25(2)** (Oxford: Elsevier Science Ltd)

International Commission on Radiological Protection 1995c Age-dependent doses to members of the public from intake of radionuclides: Part 4 Inhalation dose coefficients. ICRP Publication 71 *Annals of the ICRP* **25(3/4)** (Oxford: Elsevier Science Ltd)

International Commission on Radiological Protection 1997a General principles for the radiation protection of workers. ICRP Publication 75 *Annals of the ICRP* **27(1)** (Oxford: Elsevier Science Ltd)

International Commission on Radiological Protection 1997b Individual monitoring for internal exposure of workers. ICRP Publication 78 *Annals of the ICRP* **27(3/4)** (Oxford: Elsevier Science Ltd)

International Commission on Radiological Protection 1998 CD-ROM Version 2.01: The ICRP database of dose coefficients: workers and members of the public: An extension of ICRP publications 68 and 72

International Commission on Radiological Protection 2002a Guide for practical application of the ICRP Human Respiratory Tract Model. Supporting guidance 3 *Annals of the ICRP* **32(1-2)** (Oxford: Elsevier Science Ltd)

International Commission on Radiological Protection 2002b Basic anatomical and physiological data for use in radiological protection: reference values. ICRP Publication 89 *Annals of the ICRP* **32(3/4)** (New York: Elsevier)

International Commission on Radiological Protection 2006 Human alimentary tract model for radiological protection. ICRP Publication 100 *Annals of the ICRP* **36(1-2)** (Oxford: Elsevier Ltd)

International Commission on Radiological Protection 2007 The 2007 Recommendations of the International Commission on Radiological Protection. ICRP Publication 103 *Annals of the ICRP* **37(2-4)** (Oxford: Elsevier)

International Commission on Radiological Protection 2008 Nuclear Decay Data for Dosimetric Calculations. ICRP Publication 107 *Annals of the ICRP* **38(3)** (Oxford: Elsevier)

International Commission on Radiological Protection 2009 Adult reference computational phantoms. ICRP Publication 110 *Annals of the ICRP* **39(2)** (Oxford: Elsevier)

International Commission on Radiation Units and Measurements 1998 Fundamental quantities and units for ionizing radiation. ICRU Report 60 (Bethesda, MD: ICRU)

IRSN 2009 La radioprotection des travailleurs - Bilan 2008 de la surveillance des travailleurs exposés aux rayonnements ionisants en France (Fontenay-aux-Roses) **Rapport DRPH/DIR/2009-16**

Ishigure N, Nakano T, Matsumoto M and Enomoto H 2003 Database of calculated values of retention and excretion for members of the public following acute intake of radionuclides *Radiation protection dosimetry* **105** 311-6

Ishigure N, Matsumoto M, Nakano T and Enomoto H 2004 Development of software for internal dose calculation from bioassay measurements *Radiation protection dosimetry* **109** 235-42

International Organization for Standardization 2000 Determination of the detection limit and decision threshold for ionizing radiation measurements -- Part 1: Fundamentals and application to counting measurements without the influence of sample treatment **ISO 11929-1:2000**

International Organization for Standardization 2001 Radiation protection - Performance criteria for radiobioassay - Part 1: General principles **ISO 12790-1:2001**

International Organization for Standardization 2006a Radiation protection - Monitoring of workers occupationally exposed to a risk of internal contamination with radioactive material **ISO 20553:2006(E)**

International Organization for Standardization 2006b Statistics - Vocabulary and symbols - Part 1: General statistical terms and terms used in probability **ISO 3534-1:2006(E)**

International Organization for Standardization 2008 Uncertainty of measurement -- Part 3: Guide to the expression of uncertainty in measurement (GUM: 1995) **ISO/IEC Guide 98-3:2008**

International Organization for Standardization 2010 Determination of the characteristic limits (decision threshold, detection limit and limits of the confidence interval) for measurements of ionizing radiation -- Fundamentals and application **ISO 11929:2010**

James A C, Filipy R E, Russell J J and McInroy J F 2003 USTUR case 0259 whole body donation: a comprehensive test of the current ICRP models for the behavior of inhaled 238PuO2 ceramic particles. U.S. Transuranium and Uranium Registries *Health physics* **84** 2-33

James A C, Sasser L B, Stuit D B, Glover S E and Carbaugh E H 2007 USTUR whole body case 0269: demonstrating effectiveness of i.v. CA-DTPA for Pu *Radiation protection dosimetry* **127** 449-55

James A C, Birchall A and Puncher M 2008 Uncertainty in internal doses: using Bayes to transfer information from one worker to another *IRPA 12* (*Buenos Aires, Argentina*)

Kanapilly G M and Diel J H 1980 Ultrafine 239PuO2 aerosol generation, characterization and short-term inhalation study in the rat *Health physics* **39** 505-19

Kanapilly G M and Boecker B B 1981 The effects of Pu-U elemental ratio on the distribution of inhaled mixed (U-Pu)O2 aerosols in rats *Inhalation Toxicology Research Institute* (Albuquerque) **LMF-91**

Khokhryakov V F, Suslova K G, Vostrotin V V, Romanov S A, Eckerman K F, Krahenbuhl M P and Miller S C 2005 Adaptation of the ICRP publication 66 respiratory tract model to data on plutonium biokinetics for Mayak workers *Health physics* **88** 125-32

Khursheed A 1998 Uncertainties in dose coefficients for systemic plutonium *Radiat Prot Dos* **78** 121-6

Krahenbuhl M P, Bess J D, Wilde J L, Vostrotin V V, Suslova K G, Khokhryakov V F, Slaughter D M and Miller S C 2005 Uncertainties analysis of doses resulting from chronic inhalation of plutonium at the Mayak production association *Health physics* **89** 33-45

Kreyling W G and Schumann G 1987 Particle transport from the lower respiratory tract *J. Aerosol Sci.* **18** 749-52

Kreyling W G, André S, Collier C G, Ferron G A, Métivier H and Schumann G 1991 Interspecies comparison of lung clearance after inhalation of monodisperse solid cobalt oxide aerosol particles *J. Aerosol Sci.* **22** 509-35

Lataillade G, Verry M, Rateau G, Métivier H and Masse R 1995 Translocation of plutonium from rat and monkey lung after inhalation of industrial plutonium oxide and mixed uranium and plutonium oxide *International journal of radiation biology* **67** 373-80

Leggett R W 2001 Reliability of the ICRP's dose coefficients for members of the public. 1. Sources of uncertainty in the biokinetic models *Radiation protection dosimetry* **95** 199-213

Leggett R W 2003 Reliability of the ICRP's dose coefficients for members of the public. III. Plutonium as a case study of uncertainties in the systemic biokinetics of radionuclides *Radiation protection dosimetry* **106** 103-20

Leggett R W, Eckerman K F, Khokhryakov V F, Suslova K G, Krahenbuhl M P and Miller S C 2005 Mayak worker study: an improved biokinetic model for reconstructing doses from internally deposited plutonium *Radiation research* **164** 111-22

Likhtarev I A, Dobroskok I A, Ilyin L A, Krasnoschekova G P, Likhtareva M, Smirnov B I, Sobolev E P, Shamov V P and Shapiro E L 1975 A study of certain characteristics of strontium metabolism in a homogeneous group of human subjects *Health physics* **28** 49-60

Lopez M A and Navarro T 2003 Sensitivity of a low energy Ge detector system for in vivo monitoring in the framework of ICRP 78 applications *Radiation protection dosimetry* **105** 477-82

Lopez M A, Etherington G, Castellani C M, Franck D, Hurtgen C, Marsh J W, Nosske D, Breustedt B, Blanchardon E, Andrasi A, Bailey M R, Balashazy I, Battisti P, Berard P, Birchall A, Broggio D, Challeton-de-Vathaire C, Cruz-Suarez R, Doerfel H, Giussani A, Hodgson A, Koukouliou V, Kramer G H, Le Guen B, Luciani A, Malatova I, Molokanov A, Moraleda M, Muikku M, Oeh U, Puncher M, Rahola T, Stradling N and Vrba T 2008 Internal dosimetry: towards harmonisation and coordination of research *Radiation protection dosimetry* **131** 28-33

Luciani A and Polig E 2000 Verification and modification of the ICRP-67 model for plutonium dose calculation *Health physics* **78** 303-10

Malarbet J L 1998 Calculations of radionuclide organ retentions from ICRP biokinetic recycling models *Radiation protection dosimetry* **79** 379-81

Maletskos C J, Keane A T, Telles N C and Evans R D 1966 The Metabolism of Intravenously Administered Radium and Thorium in Human Beings and the Relative Absorption from the Human Gastrointestinal Tract of Radium and Thorium in Simulated Radium Dial Paints *Radium and Mesothorium Poisoning Dosimetry and Instrumentation Techniques in Applied Radioactivity* 202-317

Marsh J W, Birchall A, Butterweck G, Dorrian M D, Huet C, Ortega X, Reineking A, Tymen G, Schuler C, Vargas A, Vezzu G and Wendt J 2002 Uncertainty analysis of the weighted equivalent lung dose per unit exposure to radon progeny in the home *Radiation protection dosimetry* **102** 229-48

Marsh J W, Blanchardon E, Castellani C M, Desai A D, Dorrian M D, Hurtgen C, Koukouliou V, Lopez M A, Luciani A, Puncher M, Andrasi A, Bailey M R, Berkovski V, Birchall A, Bonchug Y, Doerfel H, Malatova I, Molokanov A and Ratia H 2007 Evaluation of scattering factor values for internal dose assessment following the IDEAS guidelines: preliminary results *Radiation protection dosimetry* **127** 339-42

Marsh J W, Bessa Y, Birchall A, Blanchardon E, Hofmann W, Nosske D and Tomasek L 2008a Dosimetric models used in the Alpha-Risk project to quantify exposure of uranium miners to radon gas and its progeny *Radiation protection dosimetry* **130** 101-6

Marsh J W, Castellani C M, Hurtgen C, Lopez M A, Andrasi A, Bailey M R, Birchall A, Blanchardon E, Desai A D, Dorrian M D, Doerfel H, Koukouliou V, Luciani A, Malatova I, Molokanov A, Puncher M and Vrba T 2008b Internal dose assessments: uncertainty studies and update of ideas guidelines and databases within CONRAD project *Radiation protection dosimetry* **131** 34-9

McClellan R O 1972 Progress in studies with transuranic elements at the Lovelace Foundation *Health physics* **22** 812-22

McClellan R O, Snipes M B and Boecker B B 1984 Respiratory tract clearance of inhaled particles in laboratory animals. In: *Aerosols: Science, technology, and industrial applications of airborne particles,* ed B. Y. H. Liu, *et al.* (New-York: Elsevier) pp 1047-50

McKay M D, Beckman R J and Conover W J 1979 Comparison of three methods for selecting values of input variables in the analysis of output from a computer code *Technometrics* **21** 239-45

Menetrier F, Berard P, Joussineau S, Stradling N, Hodgson A, List V, Morcillo M A, Paile W, Holt D C and Eriksson T 2007 TIARA: treatment initiatives after radiological accidents *Radiation protection dosimetry* **127** 444-8

Mercer T T 1967 On the role of particle size in the dissolution of lung burdens *Health physics* **13** 1211-21

Métivier H, Nénot J-C, Masse R, Nolibé D and Lafuma J 1974 Etude clinique de l'épuration pulmonaire chez le singe *C. R. Acad. Sci.* **Serie D** 671-4

Métivier H, Masse R, Rateau G and Lafuma J 1980 Experimental study of respiratory contamination by a mixed oxide aerosol formed from the combustion of a plutonium magnesium alloy *Health physics* **38** 769-76

Métivier H, Masse R and Lafuma J 1983 Metabolism of plutonium introduced as Tri-N-Butylphosphate complex in the rat and removal attempts by DTPA *Health physics* **44** 623-34

Métivier H, Piechowski J, Duserre C, Rateau G, Legendre N, Menoux B and Masse R 1989 Biological behaviour of plutonium inhaled by baboons as plutonium N-tributylphosphate complex. Comparison with ICRP models *Radiation protection dosimetry* **26** 287-91

Métivier H 2006 *Radioprotection et ingénierie nucléaire* (Les Ulis: EDP Sciences)

Mewhinney J A and Diel J H 1983 Retention of inhaled 238PuO2 in beagles: a mechanistic approach to description *Health physics* **44** 623-34

Miller G, Inkret W C and Martz H 1993 Bayesian detection analysis for radiation exposure *Radiation protection dosimetry* **48** 251-6

Miller G, Inkret W C and Martz H F 1999 Internal dosimetry intake estimation using Bayesian methods *Radiation protection dosimetry* **82** 5-17

Miller G, Inkret W C, Little T T, Martz H F and Schillaci M E 2001 Bayesian prior probability distributions for internal dosimetry *Radiation protection dosimetry* **94** 347-52

Miller G, Martz H F, Little T T and Guilmette R 2002 Bayesian internal dosimetry calculations using Markov Chain Monte Carlo *Radiation protection dosimetry* **98** 191-8

Miller G 2008 Variability and uncertainty of biokinetic model parameters: the discrete empirical Bayes approximation *Radiation protection dosimetry* **131** 394-8

Molokanov A, Badjin V, Gasteva G and Antipin E 2003 Uncertainty analysis in the task of individual monitoring data *Radiation protection dosimetry* **105** 395-8

Molokanov A and Blanchardon E 2007 Dependence of the Dose Estimate on the Time Pattern of Intake by the Example of Tritiated Water Intakes *Radiation protection dosimetry* **127** 387-91

Molokanov A, Chojnacki E and Blanchardon E 2010 A simple algorithm for solving the inverse problem of interpretation of uncertain individual measurements in internal dosimetry *Health physics* **98** 12-9

Moody J C, Stradling G N, Wilson I, Pearce M J, Phipps A W, Gray S A and Hodgson A 1993 Biokinetics of plutonium in the rat after the pulmonary deposition of three nitrate bearing materials: implications for human exposure, Report NRPB-M427 *National Radiological Protection Board* (Chilton) **M427**

Morgan A, Black A, Knight D and Moores S R 1988 The effect of firing temperature on the lung retention and translocation of Pu following the inhalation of 238PuO2 and 239PuO2 by CBA/H mice *Health physics* **54** 301-10

Morin M, Nenot J C and Lafuma J 1972 Metabolic and therapeutic study following administration to rats of 238Pu-nitrate - a comparison with 239Pu *Health physics* **23** 475-80

Moss W D, Campbell E E, Schulte H F and Tietjen G L 1969 A study of the variations found in plutonium urinary data *Health physics* **17** 571-8

Motzkus C, Géhin E and Gensdarmes F 2008 Study of airborne particles produced by normal impact of millimitric droplets onto a liquid film *Experiments in Fluids* **45** 797-812

National Council on Radiation Protection and Measurements 1998 Evaluating the reliability of biokinetic and dosimetric models and parameters used to assess individual doses for risk assessment purposes. NCRP commentary No. 15 (Bethesda: NCRP)

National Council on Radiation Protection and Measurements 2006 Development of a biokinetic model for radionuclide-contaminated wounds and procedures for their assessment, dosimetry and treatment. NCRP Report No. 156 (Bethesda: NCRP)

Nénot J C, Masse R, Morin M and Lafuma J 1972 An experimental comparative study of the behaviour of 237Np, 238Pu, 239Pu, 241Am and 242Cm in bone *Health physics* **22** 657-65

Newton D, Harrison G E, Kang C and Warner A J 1991 Metabolism of injected barium in six healthy men *Health physics* **61** 191-201

Park J F, Bair W J and Busch R H 1972 Progress in beagle dogs studies with transuranium elements at Battelle-Northwest *Health physics* **22** 803-10

Patarin L 2002 *Le cycle du combustible nucléaire* (Les Ulis: EDP Sciences)

Pellow P G, Hodgson S A, Hodgson A, Rance E, Ellender M, Guilmette R A and Stradling G N 2003 Comparison of absorption after inhalation and instillation of uranium octoxide *Radiation protection dosimetry* **105** 105-8

Puncher M and Birchall A 2007 Estimating uncertainty on internal dose assessments *Radiation protection dosimetry* **127** 544-7

Puncher M, Birchall A and Marsh J W 2007 The Autocorrelation Coefficient as a Tool for Assessing Goodness of Fit between Bioassay Predictions and Measurement Data *Radiation protection dosimetry* **127** 370-3

Puncher M and Birchall A 2008 A Monte Carlo method for calculating Bayesian uncertainties in internal dosimetry *Radiation protection dosimetry* **132** 1-12

Racine R, Grandcolas L, Grison S, Stefani J, Delissen O, Gourmelon P, Veyssière G and Souidi M 2010 Cholesterol 7alpha-hydroxylase (CYP7A1) activity is modified after chronic ingestion of depleted uranium in the rat *Journal of Steroid Biochemistry and Molecular Biology* **120** 60-6

Rahola T, Etherington G, Bérard P, Le Guen B, Hurtgen C, Muikku M and Pusa S 2004 Survey of internal dose monitoring programmes for radiation workers, Report STUK-A203 *STUK* (Helsinki) **A203**

Ramounet-Le Gall B, Rateau G, Abram M C, Grillon G, Ansoborlo E, Berard P, Delforge J and Fritsch P 2003 In vivo measurement of Pu dissolution parameters of MOX aerosols and related uncertainties in the values of the dose per unit intake *Radiation protection dosimetry* **105** 153-6

Ramounet B, Matton S, Guezingar-Liebard F, Abram M C, Rateau G, Grillon G and Fritsch P 2000 Comparative biokinetics of plutonium and americium after inhalation of PuO2 and mixed oxides (U, Pu)O2 in rat *International journal of radiation biology* **76** 215-22

Ramsden D, Bains M E and Fraser D C 1970 In-vivo and bioassay results from two contrasting cases of plutonium-239 inhalation *Health physics* **19** 9-17

Rateau-Matton S, Ansoborlo E and Hodgson A 2004 Comparative absorption parameters of Pu and Am from PuO2 and mixed oxide aerosols measured after in vitro dissolution test and inhalation in rats *International journal of radiation biology* **80** 777-85

Reeks M W and Hall D 2001 Kinetic models for particle suspension in turbulent flows: theory and measurement *Journal of aerosol science* **32** 1-31

Reeve J and Hesp R 1976 A model-independent comparison of the rates of uptake and short term retention of 47Ca and 85Sr by the skeleton *Calcified tissue research* **22** 183-9

Rhoads K, Killand B W, Mahaffey J A and Sanders C L 1986 Lung clearance and translocation of 239Pu and 244Cm in rats following inhalation individually or as a mixed oxide *Health physics* **51** 633-40

Sato H, Yamada Y, Ishigure N, Nakano T, Enomoto H, Takahashi S, Kubota Y and Inaba J 1999 Retention, excretion and translocation of 239Pu in rats following inhalation of 239PuO2 calcined at 1150 and 400 degrees C *Journal of radiation research* **40** 197-204

Schwarz G and Dunning D E, Jr. 1982 Imprecision in estimates of dose from ingested 137Cs due to variability in human biological characteristics *Health physics* **43** 631-45

Shafer G 1976 *A Mathematical Theory of Evidence* (Princeton: University Press)

Smith H, Stradling G N, Loveless B W and Ham G J 1977 The in vivo solubility of plutonium-239 dioxide in the rat lung *Health physics* **33** 539-51

Snipes M B, Boecker B B and McClellan R O 1983 Retention of monodisperse or polydisperse aluminosilicate particles inhaled by dogs, rats, and mice *Toxicology and applied pharmacology* **69** 345-62

Stanley J A, Eidson A F and Mewhinney J A 1980a Deposition, retention, and dosimetry of inhaled mixed uranium-plutonium oxides (heat-treated at 1750°C) in fisher-344 rats, beagle dogs and cynomolgus monkeys *Inhalation Toxicology Research Institute* (Albuquerque) **CR-1458**

Stanley J A, Eidson A F and Mewhinney J A 1980b Deposition, retention and dosimetry of inhaled plutonium dioxide (heat-treated at 850°C) in fisher-344 rats, beagle dogs and cynomolgus monkeys *Inhalation Toxicology Research Institute* (Albuquerque) **CR-1458**

Stanley J A, Edison A F and Mewhinney J A 1982 Distribution, retention and dosimetry of plutonium and americium in the rat, dog and monkey after inhalation of an industrial-mixed uranium and plutonium oxide aerosol *Health physics* **43** 521-30

Stather J W and Howden S 1975 The effect of chemical form on the clearance of 239-plutonium from the respiratory system of the rat *Health physics* **28** 29-39

Stather J W, Howden S and Carter R F 1975 A method for investigating the metabolism of the transportable fraction of plutonium aerosols *Physics in medicine and biology* **20** 106-24

Stradling G N, Ham G J, Smith H, Cooper J and Breadmore S E 1978a Factors affecting the mobility of plutonium-238 dioxide in the rat *International journal of radiation biology and related studies in physics, chemistry, and medicine* **34** 37-47

Stradling G N, Loveless B W, Ham G J and Smith H 1978b The biological solubility in the rat of plutonium present in mixed plutonium--sodium aerosols *Health physics* **35** 229-35

Stradling G N, Stather J W, Gray S A, Moody J C, Bailey M R, Hodgson A and Collier C 1979 Factors affecting the mobility of actinide oxides and their influence on radiological protection *19th Annual Handford Life Science Symposium* pp 209-23

Stradling G N, Stather J W, Sumner S A, Moody J C and Hodgson A 1985 The metabolism and decorporation of Pu after inhalation of the tributyl phosphate complex by the rat *Health physics* **49** 499-502

Stradling G N, Stather J W, Gray S A, Moody J C, Bailey M R, Hodgson A and Collier C 1987 Studies on the metabolic behaviour of industrial actinide-bearing aerosols after deposition in the rat

lung: an experimental basis for interpreting chest monitoring data and assessing limits on intake for workers *Human toxicology* **6** 365-75

Stradling G N, Stather J W, Gray S A, Moody J C, Ellender M and Collier C 1989 Assessment of intake of an actinide-bearing dust formed from the pond storage of spent magnox fuel *Radiat Prot Dos* **26** 201-6

Stradling G N, Stather J W, Gray S A, Moody J C, Ellender M, Pearce M J and Collier C G 1992 Radiological implications of inhaled 239Pu and 241Am in dusts at the former nuclear test site in Maralinga *Health physics* **63** 641-50

Stradling G N, Hodgson S A, Hodgson A, Fell T P, Iranzo C E, Espinoza A and Aragon A 1998 Dose coefficients and assessment of intake after inhalation of contaminated dusts from Palomares *Radiation protection dosimetry* **79** 179-82

Stradling G N, Etherington G, Hodgson A, Bailey M R, Hodgson S, Pellow P, Shutt A L, Birchall A, Rance E, Newton D and Fifield L K 2002a Comparison between biokinetics of inhaled plutonium nitrate and gadolinium oxide in humans and animals *Journal of Radioanalytical and Nuclear Chemistry* **252** 315-25

Stradling G N, Hodgson A, Ansoborlo E, Bérard P and Etherington G 2002b Industrial uranium compounds: exposure limits, assessment of intake and toxicity after inhalation *National Radiological Board* **NRPB-W22 Report**

Stradling G N, Hodgson A, Fell T P, Ansoborlo E, Bérard P, Etherington G and Le Guen B 2003 Plutonium compounds: exposure limits and assessment of intake and dose after inhalation, Report NRPB-W52 *National Radiological Protection Board* (Chilton)

Toohey R, Palmer E, Anderson L, Berger C, Cohen N, Eisele G, Wachholz B and Burr W, Jr. 1991 Current status of whole-body counting as a means to detect and quantify previous exposures to radioactive materials. Whole-body Counting Working Group *Health physics* **60 Suppl 1** 7-42

Usuda K, Kono K, Dote T, Shimizu H, Tominaga M, Koizumi C, Nakase E, Toshina Y, Iwai J, Kawasaki T and Akashi M 2002 Log-normal distribution of the trace element data results from a mixture of stochastic input and deterministic internal dynamics *Biological trace element research* **86** 45-54

Zamora M L, Zielinski J M, Meyerhof D P and Tracy B L 2002 Gastrointestinal absorption of uranium in humans *Health physics* **83** 35-45

Zamora M L, Zielinski J M, Meyerhof D, Moddie G, Falcomer R and Tracy B 2003 Uranium gastrointestinal absorption: the f1 factor in humans *Radiation protection dosimetry* **105** 55-60

Appendixes

1. Literature review of the conditions of exposure to uranium compounds

1.1 AMAD

Facility	Compound	AMAD (µm)	σ_g	Reference
COGEMA Pierrelatte	UO_4	3.9	3.1	Ansoborlo *et al*, 2002
COGEMA Pierrelatte	UO_2	6.8	1.8	Ansoborlo *et al*, 2002
COGEMA Pierrelatte	U_3O_8	6.7	2	Ansoborlo *et al*, 2002
COGEMA Pierrelatte	$U_3O_8 + UO_3$	3.4	3.4	Ansoborlo *et al*, 2002
COGEMA Pierrelatte	U_3O_8 + tr UO_2F_2	5.2	2.8	Ansoborlo *et al*, 2002
COMURHEX	U_3O_8	4.4 - 5.8 - 7	1.8 - 2.2 - 2.7	Ansoborlo *et al*, 1997
COMURHEX	UF4	6.8 - 8 - 9	2.4 - 2.6 -2.9	Ansoborlo *et al*, 1997
COMURHEX	UO_3	3.1	2.6	Ansoborlo *et al*, 1997
COMURHEX	$U_2O_7(NH_4)_2$	7.8 - 7.9- 8	2	Ansoborlo *et al*, 1997
COMURHEX		5.1	2.5	Chazel *et al*, 2000
COMURHEX Malvesi	UO_2	8.5	1.8	Ansoborlo *et al*, 2002
COMURHEX Malvesi	U_3O_8	8.5	2	Ansoborlo *et al*, 2002
COMURHEX Malvesi	UF_4	5.1	2.7	Ansoborlo *et al*, 2002
COMURHEX Malvesi	UF_4	1.7	1.3	André *et al*, 1989
COMURHEX Malvesi	UO_3	6.4	1.8	Ansoborlo *et al*, 2002
COMURHEX Malvesi	UO_3 + ADU + U_3O_8	5	2	Ansoborlo *et al*, 2002
COMURHEX Malvesi	ADU	5	2.5	Ansoborlo *et al*, 2002
COMURHEX Pierrelatte	$UF_4 + UO_2F_2$	5.8	4	Ansoborlo *et al*, 2002
COMURHEX Pierrelatte	$UF_4 + UO_2F_2$	4.2	3.1	Ansoborlo *et al*, 2002
FBFC	UO_2, U_3O_8	2.9 - 4.7 - 8.2	2 - 2.7 -3.4	Ansoborlo *et al*, 1997
FBFC	UO_2, U_3O_8	1.8 - 3.9 - 5.8	2.4 - 3 -4.2	Ansoborlo *et al*, 1997
FBFC	UO_2, U_3O_8	1.3 - 5.8 - 9	1.9 - 2.4 - 2.5	Ansoborlo *et al*, 1997
FBFC Pierrelatte	UO_2	7	2.6	Ansoborlo *et al*, 2002
FBFC Pierrelatte	UO_2	2.9	1.9	Ansoborlo *et al*, 2002
FBFC Pierrelatte	U_3O_8	5.6	2.3	Ansoborlo *et al*, 2002

FBFC Romans	UO_4	1.1	1.2	Ansoborlo *et al*, 2002
FBFC Romans	UO_2 + (5-10% U_3O_8)	5.3	2.5	Ansoborlo *et al*, 2002
FBFC Romans	UO_2 + (5-10% U_3O_8)	3.1	2.1	Ansoborlo *et al*, 2002
FBFC Romans	U_3O_8	8.3	1.9	Ansoborlo *et al*, 2002
FBFC Romans	U_3O_8 + <5% UO_2	8.5	2.1	Ansoborlo *et al*, 2002
FBFC Romans	U_3O_8 + <5% UO_2	5.9	3.5	Ansoborlo *et al*, 2002
uranium mill		3 - 6		Dorrian and Bailey, 1995
uranium mill		6 - 12		Dorrian and Bailey, 1995
uranium mill		12 - 20		Dorrian and Bailey, 1995
uranium mill		12 - 20		Dorrian and Bailey, 1995
uranium mill		13	4.1	Dorrian and Bailey, 1995
uranium mill		9.1	3.2	Dorrian and Bailey, 1995
uranium mill		5.8	2.7	Dorrian and Bailey, 1995
uranium mill		14	4.1	Dorrian and Bailey, 1995
uranium mill		0.72	2.5	Dorrian and Bailey, 1995
uranium mill		4.5	2.3	Dorrian and Bailey, 1995
uranium mill		5.7	2.2	Dorrian and Bailey, 1995
uranium mill		0.5	2.8	Dorrian and Bailey, 1995
uranium mill		7		Dorrian and Bailey, 1995
uranium mill		6.8		Dorrian and Bailey, 1995
uranium mine		5		Dorrian and Bailey, 1995
uranium mine		7		Dorrian and Bailey, 1995
uranium mine		11.7		Dorrian and Bailey, 1995
uranium mine		5		Dorrian and Bailey, 1995
uranium mine		10.3	4.6	Dorrian and Bailey, 1995
uranium mine		8.3	2.7	Dorrian and Bailey, 1995
uranium mine		3		Dorrian and Bailey, 1995

1.2 s_p, s_{pt}, s_t

Compound	Facility	Measurement	s_p (d^{-1})	s_{pt} (d^{-1})	s_t (d^{-1})	Reference
UO_4	COGEMA Pierrelate	*in vitro*	1.45×10^{-1}	1.35×10^{-1}	9.90×10^{-3}	Ansoborlo *et al*, 2002
UO_4	FBFC Romans	*in vitro*	2.41×10^{-1}	1.19×10^{-1}	8.80×10^{-3}	Ansoborlo *et al*, 2002
UO_4	FBFC Romans	*in vivo*	8.12×10^{-1}	1.18×10^{-1}	2.40×10^{-2}	Ansoborlo *et al*, 2002
UO_4		*in vitro*	2.32×10^{-1}	1.08×10^{-1}	7.20×10^{-3}	Chazel *et al*, 2001
UO_4		*in vivo*	8.15×10^{-1}	1.15×10^{-1}	2.40×10^{-2}	Chazel *et al*, 2001

UO_2	COGEMA Pierrelate	*in vitro*	2.58×10^{-2}	1.23	5.90×10^{-4}	Ansoborlo *et al*, 2002
UO_2	COGEMA Pierrelate	*in vivo*	3.90×10^{-2}	1.21	1.50×10^{-3}	Ansoborlo *et al*, 2002
UO_2	COMURHEX Malvesi	*in vitro*	1.57×10^{-2}	3.74×10^{-1}	6.60×10^{-5}	Ansoborlo *et al*, 2002
UO_2	FBFC Pierrelatte	*in vitro*	1.30×10^{-4}		1.30×10^{-4}	Ansoborlo *et al*, 2002
UO_2	FBFC Pierrelatte	*in vivo*			4.90×10^{-4}	Ansoborlo *et al*, 2002
UO_2	FBFC Pierrelatte	*in vitro*	1.54×10^{-4}	1.85×10^{-3}	1.50×10^{-4}	Ansoborlo *et al*, 2002
UO_2	FBFC Pierrelatte	*in vivo*			5.80×10^{-4}	Ansoborlo *et al*, 2002
UO_2		*in vitro*	3.08×10^{-2}	1.23	6.00×10^{-4}	Chazel *et al*, 2001
UO_2		*in vivo*	5.25×10^{-2}	1.65	1.50×10^{-3}	Chazel *et al*, 2001
UO_2		*in vitro*	2.91×10^{-2}	1.11	6.00×10^{-4}	Ansoborlo *et al*, 1997
UO_2		*in vivo*	4.04×10^{-2}	4.86×10^{-2}	1.60×10^{-3}	Ansoborlo *et al*, 1997
UO_2	UK	*in vivo*	1.01×10^{-2}	9.40×10^{-1}	6.10×10^{-4}	Stradling *et al*, 2002b
UO_2	UK	*in vivo*	1.33×10^{-2}	1.29	2.60×10^{-4}	Stradling *et al*, 2002b
U_3O_8	instillation		7.26	2.87×10^{1}	5.10	Pellow *et al*, 2003
U_3O_8	inhalation		5.80	3.02×10^{1}	3.70	Pellow *et al*, 2003
U_3O_8	COGEMA Pierrelate	*in vitro*	8.22×10^{-2}	6.08×10^{-1}	7.10×10^{-3}	Ansoborlo *et al*, 2002
U_3O_8	COMURHEX Malvesi	*in vitro*	9.77×10^{-2}	3.32×10^{-1}	9.40×10^{-3}	Ansoborlo *et al*, 2002
U_3O_8	FBFC Pierrelatte	*in vitro*	8.53×10^{-2}	1.13	4.30×10^{-3}	Ansoborlo *et al*, 2002
U_3O_8	FBFC Pierrelatte	*in vivo*	1.05×10^{-1}	2.15	1.20×10^{-3}	Ansoborlo *et al*, 2002
U_3O_8	FBFC Romans	*in vitro*	2.47×10^{-2}	1.79	1.20×10^{-3}	Ansoborlo *et al*, 2002
U_3O_8	FBFC Romans	*in vivo*	6.25×10^{-2}	2.01	3.80×10^{-4}	Ansoborlo *et al*, 2002
U_3O_8		*in vitro*	2.47×10^{-2}	1.79	1.20×10^{-3}	Chazel *et al*, 2001
U_3O_8		*in vivo*	4.46×10^{-2}	2.56	3.70×10^{-4}	Chazel *et al*, 2001
U_3O_8	UK	*in vivo*	1.99×10^{-2}	4.70×10^{-1}	3.50×10^{-4}	Stradling *et al*, 2002b
UF_4	COMURHEX Malvesi	*in vitro*	9.92×10^{-2}	1.11×10^{-1}	1.00×10^{-3}	Ansoborlo *et al*, 2002
UF_4	COMURHEX Malvesi	*in vivo*	1.23×10^{-1}	8.71×10^{-2}	2.60×10^{-3}	Ansoborlo *et al*, 2002
UF_4		*in vitro*	9.88×10^{-2}	1.11×10^{-1}	1.00×10^{-3}	Chazel *et al*, 2001
UF_4		*in vivo*	1.23×10^{-1}	8.67×10^{-2}	2.60×10^{-3}	Chazel *et al*, 2001
UF_4		*in vitro*	9.92×10^{-2}	1.11×10^{-1}	1.00×10^{-3}	Chazel *et al*, 2000
UF_4		*in vitro*	4.48×10^{-1}	7.92×10^{-1}	2.70×10^{-3}	Chazel *et al*, 2000
UF_4		*in vivo*	1.23×10^{-1}	8.71×10^{-2}	2.60×10^{-3}	Chazel *et al*, 2000
UF_4	UK	*in vivo*	5.46×10^{-2}	4.54×10^{-2}	7.40×10^{-3}	Stradling *et al*, 2002b
UF_4	UK	*in vivo*	5.91×10^{-2}	5.09×10^{-2}	3.90×10^{-3}	Stradling *et al*, 2002b
UO_3	COMURHEX Malvesi	*in vitro*	7.42×10^{-2}	3.56×10^{-1}	1.30×10^{-3}	Ansoborlo *et al*, 2002
UO_3	COMURHEX Malvesi	*in vivo*	1.99×10^{-1}	8.09×10^{-2}	1.10×10^{-3}	Ansoborlo *et al*, 2002
UO_3	UK	*in vivo*	1.29	1.12×10^{-1}	3.60×10^{-3}	Stradling *et al*, 2002b
UO_3	UK	*in vivo*	1.05×10^{1}	3.50	2.00×10^{-2}	Stradling *et al*, 2002b

1.3 f_1

Parameters	f_1 min	f_1 max	f_1 median	Reference
Female	0.003	0.063	0.01	Zamora *et al*, 2003
Male	0.001	0.03	0.007	Zamora *et al*, 2003
< 25 y	0.004	0.035	0.011	Zamora *et al*, 2003
≥ 25 y	0.001	0.063	0.008	Zamora *et al*, 2003
Hi-U through food	0.003	0.063	0.009	Zamora *et al*, 2003
Lo-U through food	0.001	0.035	0.009	Zamora *et al*, 2003
			0.004	Harrison *et al*, 2001
			0.01	Harrison *et al*, 2001
			0.02	Harrison *et al*, 2001
			0.06	Harrison *et al*, 2001
			0.021	Zamora *et al*, 2002
			0.021	Zamora *et al*, 2002
			0.009	Zamora *et al*, 2002
			0.01	Zamora *et al*, 2002
			0.012	Zamora *et al*, 2002
			0.011	Zamora *et al*, 2002
			0.008	Zamora *et al*, 2002
			0.075	Zamora *et al*, 2002
			0.009	Zamora *et al*, 2002
			0.02	Zamora *et al*, 2002
			0.003	Zamora *et al*, 2002
			0.003	Zamora *et al*, 2002
			0.031	Zamora *et al*, 2002
			0.01	Zamora *et al*, 2002
			0.004	Zamora *et al*, 2002
			0.013	Zamora *et al*, 2002
			0.005	Zamora *et al*, 2002
			0.006	Zamora *et al*, 2002
			0.006	Zamora *et al*, 2002
			0.003	Zamora *et al*, 2002
			0.009	Zamora *et al*, 2002
			0.009	Zamora *et al*, 2002
			0.007	Zamora *et al*, 2002
			0.02	Zamora *et al*, 2002
			0.009	Zamora *et al*, 2002
			0.005	Zamora *et al*, 2002
			0.009	Zamora *et al*, 2002

0.034	Zamora *et al*, 2002
0.008	Zamora *et al*, 2002
0.025	Zamora *et al*, 2002
0.001	Zamora *et al*, 2002
0.004	Zamora *et al*, 2002
0.055	Zamora *et al*, 2002
0.013	Zamora *et al*, 2002
0.028	Zamora *et al*, 2002
0.039	Zamora *et al*, 2002
0.01	Zamora *et al*, 2002
0.029	Zamora *et al*, 2002
0.026	Zamora *et al*, 2002
0.084	Zamora *et al*, 2002
0.035	Zamora *et al*, 2002
0.006	Zamora *et al*, 2002
0.011	Zamora *et al*, 2002
0.03	Zamora *et al*, 2002
0.001	Zamora *et al*, 2002
0.007	Zamora *et al*, 2002
0.024	Zamora *et al*, 2002
0.025	Zamora *et al*, 2002
0.006	Zamora *et al*, 2002
0.01	Zamora *et al*, 2002
0.025	Zamora *et al*, 2002
0.005	Zamora *et al*, 2002
0.012	Zamora *et al*, 2002
0.017	Zamora *et al*, 2002
0.011	Zamora *et al*, 2002
0.005	Zamora *et al*, 2002
0.005	Zamora *et al*, 2002
0.004	Zamora *et al*, 2002
0.002	Zamora *et al*, 2002
0.007	Zamora *et al*, 2002
0.005	Zamora *et al*, 2002
0.022	Zamora *et al*, 2002
0.007	Zamora *et al*, 2002
0.012	Zamora *et al*, 2002
0.012	Zamora *et al*, 2002

		0.01	Zamora *et al*, 2002
		0.005	Zamora *et al*, 2002
		0.012	Zamora *et al*, 2002
		0.006	Zamora *et al*, 2002
		0.004	Zamora *et al*, 2002
		0.015	Zamora *et al*, 2002
		0.006	Zamora *et al*, 2002
		0.008	Zamora *et al*, 2002
		0.011	Zamora *et al*, 2002
		0.003	Zamora *et al*, 2002
		0.007	Zamora *et al*, 2002
		0.021	Zamora *et al*, 2002
		0.02	Zamora *et al*, 2002
		0.012	Zamora *et al*, 2002
		0.009	Zamora *et al*, 2002
		0.05	Zamora *et al*, 2002
		0.01	Zamora *et al*, 2002
		0.011	Zamora *et al*, 2002
		0.011	Zamora *et al*, 2002
		0.007	Zamora *et al*, 2002
		0.003	Zamora *et al*, 2002
		0.008	Zamora *et al*, 2002
		0.003	Zamora *et al*, 2002
		0.003	Zamora *et al*, 2002
		0.007	Zamora *et al*, 2002
		0.004	Zamora *et al*, 2002
		0.153	Zamora *et al*, 2002
		0.007	Zamora *et al*, 2002
		0.017	Zamora *et al*, 2002
		0.015	Zamora *et al*, 2002
		0.011	Zamora *et al*, 2002
		0.007	Zamora *et al*, 2002
		0.012	Zamora *et al*, 2002
		0.011	Zamora *et al*, 2002
		0.005	Zamora *et al*, 2002
0.005	0.05	0,015-0,02	Harrison *et al*, 2001
0.003	0.02	0,01-0,015	Zamora *et al*, 2002
0.005	0.05		Harrison *et al*, 2001
0.01	0.015		Harrison *et al*, 2001

2. Algorithm of the classical method in OPSCI

(1) Definition of the input parameters

- Probability distribution of uncertain parameters: contamination time *t*, Type B error *f*, AMAD, absorption into blood *abs*
- Determination of the counting time T_{count}, detection efficiency ε, chemical yield Y_c, emission yield *Y*, the scattering factor *SF*, mean background μ_B
- Size of the sample of each uncertain parameter drawn by Monte-Carlo method, *N*
- Modelling of the measurement uncertainty as the likelihood
- Measurement result *M*

(2) Sampling with SUNSET of N sets $\{t_k, AMAD_k, abs_k, f_k\}$ according to their PDF

(3) Calculation of the bioassay function *m* and dose coefficient e_{50} for the N sets $\{t_k, AMAD_k, abs_k, f_k\}$

(4) Calculation of the maximum intake i_{max}

$$i_{\max} = \frac{M}{T_{count} \times Y \times Y_c \times \varepsilon \times Min(f_k) \times Min(m(t_k, AMAD_k, abs_k))}$$

(5) Calculation of the levels of confidence of intake *i*

Tools:

- Function to calculate the level of confidence of the intake i_j

FUNCTION level_of_confidence i_j

FOR k = 0, N (for each sampled set)

mean = i_j x $m(t_k, AMAD_k, abs_k)$ x f_k x Y x ε x Y_c x T_{count} + μ_B

IF measurement uncertainty modelling = POISSON,
$M_{cal,\,k}$ randomly drawn in POISSON(λ =mean)

IF measurement uncertainty modelling = LOGNORMAL,
$M_{cal,\,k}$ randomly drawn in LOGNORMAL(M, μ = mean, σ = SF)

IF measurement uncertainty modelling = NORMAL,

$M_{cal,\,k}$ randomly drawn in NORMAL (M, μ = mean, σ)

$P(M_{cal,\,k} \mid i_j) = 1/N$

ENDFOR

$$F_M(i_j) = \int_0^M P(M_{cal,k} | i_j) dM_{cal,k}$$

$$P(i < i_j) = 1 - F_M(i_j)$$

Return, $P(i < i_j)$

END

- Procedure to calculate the levels of confidence of the intake by dichotomy techniques

PRO dichotomy, i_1, i_2

$i_3 = (i_1 + i_2)/2$

$P(i < i_3)_{true}$ = level_of_confidence(i_3)

$P(i < i_3)_{est}$ = linear interpolation in i_3 of (level_of_confidence(i_1), level_of_confidence(i_2))

Saving of i_3 et $P(i < i_3)_{true}$

number of dichotomy call += 1

IF $\dfrac{|P(i<i_3)_{true} - P(i<i_3)_{est}|}{level\_of\_confidence(i_1)} > 10^{-2}$ *THEN*

Dichotomy(i_1, i_3)

Dichotomy(i_3, i_2)

ELSE

BREAK

END

Algorithm

$P(i < i_{min}) = level\_of\_confidence(i_{min})$

$P(i < i_{max}) = level\_of\_confidence(i_{max})$

$Dichotomy(i_{min}, i_{max})$

WHILE number of dichotomy call < 5 DO

$Dichotomy(i_1, i_3)$

$Dichotomy(i_3, i_2)$

END

(6) Determination of MDI as $P(i< MDI) = 0.95$

(7) Determination of the CDF of dose coefficient e_{50} $P(e_{50}(AMAD_k, abs_k)) = 1/N$

(8) Determination of MDD as the 95^{th} percentile of the CDF of e_{50} multiplied by MDI

3. Algorithm of the WeLMoS method in OPSCI

(1) Definition of the input parameters

- Probability distribution of uncertain parameters: contamination time *t*, Type B error *f*, AMAD, absorption into blood *abs*
- Determination of the counting time T_{count}, detection efficiency ε, chemical yield Y_c, emission yield *Y*, the scattering factor *SF*, mean background μ_B
- Intake prior probability with its minimum i_{min}, maximum i_{max}, and its discretisation step Δi
- discretisation step of the dose ΔE
- Size of the sample of each uncertain parameter drawn by Monte-Carlo method, *N*
- Modelling of the measurement uncertainty as the likelihood
- Measurement result *M*

(2) Sampling with SUNSET of N sets $\{t_k, AMAD_k, abs_k, f_k\}$ according to their PDF

(3) Calculation of the bioassay function *m* and dose coefficient e_{50} for the N sets $\{t_k, AMAD_k, abs_k, f_k\}$

(4) Calculation of the posterior probabilities of intake *i* and dose *E*

Tools:

- Function to calculate the likelihood of M given the sampled sets $\{t_k, AMAD_k, abs_k, f_k\}$ and the intake i_j

FUNCTION likelihood, i_j, t_k, $AMAD_k$, abs_k, f_k

$mean = i_j \times m(t_k, AMAD_k, abs_k) \times f_k \times Y \times \varepsilon \times Y_c \times T_{count} + \mu_B$

IF measurement uncertainty modelling = POISSON,

$P(M \mid i_j, t_k, AMAD_k, abs_k, f_k) = POISSON(M, \lambda = mean)$

IF measurement uncertainty modelling = LOGNORMAL,

$P(M \mid i_j, t_k, AMAD_k, abs_k, f_k) = LOGNORMAL(M, \mu = mean, \sigma = SF)$

IF measurement uncertainty modelling = NORMAL,

$P(M \mid i_j, t_k, AMAD_k, abs_k, f_k) = NORMAL(M, \mu = mean, \sigma)$

Return, $P(M \mid i_j, t_k, AMAD_k, abs_k, f_k)$

END

- Procedure to calculate the likelihood of M given the sampled sets $\{t_k, AMAD_k, abs_k, f_k\}$ and the intake by dichotomy techniques

PRO dichotomy, i_1, i_2

$i_3 = (i_1 + i_2)/2$

$P(M \mid i_3, t_k, AMAD_k, abs_k, f_k)_{true}$ = likelihood($i_3, t_k, AMAD_k, abs_k, f_k$)
$P(M \mid i_3, t_k, AMAD_k, abs_k, f_k)_{est}$ = linear interpolation in i_3 of
(likelihood($i_1, t_k, AMAD_k, abs_k, f_k$), likelihood ($i_2, t_k, AMAD_k, abs_k, f_k$))

Saving of i_3 et $P(M \mid i_3, t_k, AMAD_k, abs_k, f_k)_{true}$
number of dichotomy call += 1

IF $\dfrac{\left|P(M|i_3,t_k,AMAD_k,abs_k,f_k)_{true} - P(M|i_3,t_k,AMAD_k,abs_k,f_k)_{est}\right|}{likelihood(i_1,t_k,AMAD_k,abs_k,f_k)} > 10^{-3}$ *THEN*

Dichotomy(i_1, i_3)
Dichotomy(i_3, i_2)

ELSE

BREAK

END

Algorithm

FOR k = 0, N (for each sampled set)

1) Calculation of the likelihood of M given t_k, $AMAD_k$, abs_k, f_k and i

$P(M \mid i_{min}, t_k, AMAD_k, abs_k, f_k)$ = likelihood($i_{min}, t_k, AMAD_k, abs_k, f_k$)
$P(M \mid i_{max}, t_k, AMAD_k, abs_k, f_k)$ = likelihood ($i_{max}, t_k, AMAD_k, abs_k, f_k$)

Dichotomy(i_{min}, i_{max})

WHILE number of dichotomy call < 5 DO

Dichotomy(i_1, i_3)
Dichotomy(i_3, i_2)

END

2) Calculation of the dose E_{jk} corresponding to i_j et $AMAD_k$, abs_k

FOR j = 0, j_{max} DO

$E_{jk} = i_j \times e_{50}(AMAD_k, abs_k)$

ENDFOR

3) Calculation of the sets of linearly spaced intakes

$i_m = i_{min} + m \times \Delta i$

$m_{max} = (i_{max}-i_{min})/ \Delta i$

4) Calculation of the intake posterior probabilities for the linearly spaced intakes

FOR m = 1, m_{max}

$P(M \mid i_{m-1}, t_k, AMAD_k, abs_k, f_k) = likelihood(i_{m-1}, t_k, AMAD_k, abs_k, f_k)$

$P(M \mid i_m, t_k, AMAD_k, abs_k, f_k) = likelihood(i_m, t_k, AMAD_k, abs_k, f_k)$

FOR all j with i_j between i_{m-1} et i_m

$$\int_{i_{m-1}}^{i_j} P(M|i,t_k,AMAD_k,abs_k,f_k)di = \int_{i_{m-1}}^{i_{j-1}} P(M|i,t_k,AMAD_k,abs_k,f_k)di +$$

$$(P(M|i_{j-1},t_k,AMAD_k,abs_k,f_k) + P(M|i_j,t_k,AMAD_k,abs_k,f_k)) \times (i_j - i_{j-1})/2$$

$$\int_{i_{m-1}}^{i_j} P(i)di = \int_{i_{m-1}}^{i_{j-1}} P(i)di + (P(i_{j-1}) + P(i_j)) \times (i_j - i_{j-1})/2$$

ENDFOR

$$P(i_m|M,t_k,AMAD_k,abs_k,f_k) = \int_{i_{m-1}}^{i_m} P(M|i,t_k,AMAD_k,abs_k,f_k)di \times \int_{i_{m-1}}^{i_m} P(i)di$$

$$P(i_m|M) = \sum_{l=0}^{k} P(i_m|M,t_l,AMAD_l,abs_l,f_l)$$

ENDFOR

5) Calculation of the sets of linearly spaced doses

$n_{max} = m_{max}$

$E_n = n \times \Delta E$

6) Calculation of the dose posterior probabilities for the linearly spaced doses

FOR n = 1, n_{max}

$P(M \mid i_{n-1}, t_k, AMAD_k, abs_k, f_k) = likelihood(i_{n-1}, t_k, AMAD_k, abs_k, f_k)$

$P(M \mid i_n, t_k, AMAD_k, abs_k, f_k) = likelihood(i_n, t_k, AMAD_k, abs_k, f_k)$

FOR all j with E_{jk} between E_{n-1} et E_n

$$\int_{i_{n-1}}^{i_j} P(M|i,t_k,AMAD_k,abs_k,f_k)di = \int_{i_{n-1}}^{i_{j-1}} P(M|i,t_k,AMAD_k,abs_k,f_k)di +$$

$$(P(M|i_{j-1},t_k,AMAD_k,abs_k,f_k) + P(M|i_j,t_k,AMAD_k,abs_k,f_k)) \times (i_j - i_{j-1})/2$$

$$\int_{i_{n-1}}^{i_j} P(i)di = \int_{i_{n-1}}^{i_{j-1}} P(i)di + (P(i_{j-1}) + P(i_j)) \times (i_j - i_{j-1})/2$$

ENDFOR

$$P(E_n|M,t_k,AMAD_k,abs_k,f_k) = \int_{i_{n-1}}^{i_n} P(M|i,t_k,AMAD_k,abs_k,f_k)di \times \int_{i_{n-1}}^{i_n} P(i)di$$

$$P(E_n|M) = \sum_{l=0}^{k} P(E_n|M,t_l,AMAD_l,abs_l,f_l)$$

ENDFOR

ENDFOR

(5) Normalisation and calculation of the posterior CDF of intake and doses

(6) Calculation of MDI and MDD as 95th percentiles of the intake and dose posterior probabilities

4. Algorithm of the Bayesian network for one measurement

(1) Reading of the discretisation defined by the user

$i = \{i_1, i_2, \dots i_a\}$

$L = \{L_1, L_2, \dots L_b\}$ L is used instead of AMAD and abs

$t = \{t_1, t_2, \dots t_c\}$

$E = \{E_1, E_2, \dots E_d\}$

$S = \{S_1, S_2, \dots S_{1g}\}$

(2) Initialisation of the network

1) For each $\{i_i, E_j, S_k\}$, calculation of the matrix IES of size (a x d x g) with $IES[i,j,k] = P(i_i, E_j, S_k)$

FOR i = 0 TO a (loop on i)
FOR j = 0 TO d (loop on E)
FOR k = 0 TO g (loop on S)
FOR o = 0 TO c (loop on t)
FOR p = 0, TO b (loop on L)

$$P(S_k \left| i_i, t_o, L_p \right.) = \int_{k-1}^{k} LOGNORMAL\ (S, \mu = i_i \times m(t_o, L_p), \sigma = SF)dS$$

IF $i_i x e_{50}(L_p)$ belongs to $[E_{j-1}\ ;\ E_j]$ ou $[E_j\ ;\ E_{j+1}]$ THEN

$$P(E_j \mid i_i, L_p) = \frac{E_j - i_i \times e_{50}(L_p)}{E_j - E_{j-1}} or \frac{i_i \times e_{50}(L_p) - E_{j-1}}{E_j - E_{j-1}}$$

ELSE

$P(E_j \mid i_i, L_p) = 0$

$IES[i,j,k] = P(i_i, E_j, S_k) = P(i_i, E_j, S_k) + P(S_k \mid i_i, t_o, L_p) \times P(E_j \mid i_i, L_p) \times P(i_i) \times P(t_o) \times P(L_p)$

ENDFOR
ENDFOR
ENDFOR
ENDFOR
ENDFOR
ENDFOR

2) Building of the matrix IS of size (a x g) with IS[i,k] = P(i_i, S_k)

$$IS[i,k] = P(i_i, S_k) = \sum_j P(i_i, E_j, S_k) = \sum_j IES[i, j, k]$$

3) Building of the matrix ES of size (d x g) with ES[j,k] = P(E_j, S_k)

$$ES[j,k] = P(E_j, S_k) = \sum_i P(i_i, E_j, S_k) = \sum_i IES[i, j, k]$$

4) Building of the vector S of size (g) with S[k] = P(S_k)

$$S[k] = P(S_k) = \sum_i P(i_i, S_k) = \sum_i IS[i,k]$$

(3) Update of the network

1) Building of the vector I of size a with I_i =P(i_i |M)

$$I_i = \frac{\sum_k P(M|S_k) \times P(i_i, S_k)}{\sum_k P(M|S_k) \times P(S_k)} =$$

$$I_i = \frac{\sum_k P(M|S_k) \times IS[i,k]}{\sum_k P(M|S_k) \times S[k]}$$

2) Building the vector E of size d with E_j = P(D_j |M)

$$E_j = \frac{\sum_k P(M|S_k) \times P(E_j, S_k)}{\sum_k P(M|S_k) \times P(S_k)}$$

$$E_j = \frac{\sum_k P(M|S_k) \times ES[j,k]}{\sum_k P(M|S_k) \times S[k]}$$

(4) Calculation of the CDF of i and E

(5) Determination of the interval of [i_{i-1}, i_i] which have a cumulative probability comprising 0.95

(6) Determination of the interval of [E_{j-1}, E_j] which have a cumulative probability comprising 0.95

5. Algorithm of the Bayesian network for two measurements

(1) Reading of the discretisation defined by the user

$i = \{i_1, i_2, \dots i_a\}$

$L = \{L_1, L_2, \dots L_b\}$ L is used instead of AMAD and abs

$t = \{t_1, t_2, \dots t_c\}$

$E = \{E_1, E_2, \dots E_d\}$

$S_1 = \{S_{1,1}, S_{1,2}, \dots S_{1,g}\}$

$S_2 = \{S_{2,1}, S_{2,2}, \dots S_{2,h}\}$

(2) Initialisation of the network

1) For each $\{i_i, E_j, S_{1,k}, S_{2,l}\}$, calculation of the matrix IESS of size (a x d x g x h) with $IESS[i,j,k,l] = P(i_i, E_j, S_{1,k}, S_{2,l})$

FOR i = 0 TO a (loop on i)
FOR j = 0 TO d (loop on E)
FOR k = 0 TO g (loop on S_1)
FOR l = 0 TO h (loop on S_2)
FOR o = 0 TO c (loop on t)
FOR p = 0, TO b (loop on L)

$$P(S_{1,k} \left| i_i, t_o, L_p \right.) = \int_{k-1}^{k} LOGNORMAL\ (S_1, \mu = i_i \times m(t_o, L_p), \sigma = SF) dS_1$$

$$P(S_{2,l} \left| i_i, t_o, L_p \right.) = \int_{l-1}^{l} LOGNORMAL(S_2, \mu = i_i \times m(t_o, L_p), \sigma = SF) dS_2$$

IF $i_i xe_{50}(L_p)$ belongs to $[E_{j-1}\ ;\ E_j]$ ou $[E_j\ ;\ E_{j+1}]$ THEN

$$P(E_j \mid i_i, L_p) = \frac{E_j - i_i \times e_{50}(L_p)}{E_j - E_{j-1}} or \frac{i_i \times e_{50}(L_p) - E_{j-1}}{E_j - E_{j-1}}$$

ELSE

$P(E_j \mid i_i, L_p) = 0$

$IESS[i,j,k,l] = P(i_i, E_j, S_{1,k}, S_{2,l}) = P(i_i, E_j, S_{1,k}, S_{2,l}) +$
$P(S_{1,k} \mid i_i, t_o, L_p) \times P(S_{2,l} \mid i_i, t_o, L_p) \times P(E_j \mid i_i, L_p) \times P(i_i) \times P(t_o) \times P(L_p)$

ENDFOR
ENDFOR

ENDFOR
ENDFOR
ENDFOR
ENDFOR

2) Building of the matrix ISS of size (a x g x h) with ISS[i,k,l] = $P(i_i, S_{1,k}, S_{2,l})$

$$ISS[i,k,l] = P(i_i, S_{1,k}, S_{2,l}) = \sum_j P(i_i, E_j, S_{1,k}, S_{2,l}) = \sum_j IESS[i, j, k, l]$$

3) Building of the matrix ESS of size (d x g x h) with ESS[j,k,l] = $P(E_j, S_{1,k}, S_{2,l})$

$$ESS[j,k,l] = P(E_j, S_{1,k}, S_{2,l}) = \sum_i P(i_i, E_j, S_{1,k}, S_{2,l}) = \sum_i IESS[i, j, k, l]$$

4) Building of the matrix SS of size (g x h) with SS[k,l] = $P(S_{1,k}, S_{2,l})$

$$SS[k,l] = P(S_{1,k}, S_{2,l}) = \sum_i P(i_i, S_{1,k}, S_{2,l}) = \sum_i ISS[i,k,l]$$

(3) Update of the network

1) Building of the vector I of size a with $I_i = P(i_i \mid M_1, M_2)$

$$I_i = \frac{\sum_k \sum_l P(M_1 \mid S_{1,k}) \times P(M_2 \mid S_{2,l}) \times P(i_i, S_{1,k}, S_{2,l})}{\sum_k \sum_l P(M_1 \mid S_{1,k}) \times P(M_2 \mid S_{2,l}) \times P(S_{1,k}, S_{2,l})} =$$

$$I_i = \frac{\sum_k \sum_l P(M_1 \mid S_{1,k}) \times P(M_2 \mid S_{2,l}) \times ISS[i,k,l]}{\sum_k \sum_l P(M_1 \mid S_{1,k}) \times P(M_2 \mid S_{2,l}) \times SS[k,l]}$$

2) Building the vector E of size d with $E_j = P(D_j \mid M_1, M_2)$

$$E_j = \frac{\sum_k \sum_l P(M_1 \mid S_{1,k}) \times P(M_2 \mid S_{2,l}) \times P(E_j, S_{1,k}, S_{2,l})}{\sum_k \sum_l P(M_1 \mid S_{1,k}) \times P(M_2 \mid S_{2,l}) \times P(S_{1,k}, S_{2,l})}$$

$$E_j = \frac{\sum_k \sum_l P(M_1 \mid S_{1,k}) \times P(M_2 \mid S_{2,l}) \times ESS[j,k,l]}{\sum_k \sum_l P(M_1 \mid S_{1,k}) \times P(M_2 \mid S_{2,l}) \times SS[k,l]}$$

(4) Calculation of the CDF of i and E

(5) Determination of the interval of $[i_{i-1}, i_j]$ which have a cumulative probability comprising 0.95

(6) Determination of the interval of $[E_{j-1}, E_j]$ which have a cumulative probability comprising 0.95

6. Algorithm of the Bayesian network for four measurements

(1) Reading of the discretisation defined by the user

$i = \{i_1, i_2, \dots i_a\}$

$L = \{L_1, L_2, \dots L_b\}$ L is used instead of AMAD and abs

$t = \{t_1, t_2, \dots t_c\}$

$E = \{E_1, E_2, \dots E_d\}$

$S_1 = \{S_{1,1}, S_{1,2}, \dots S_{1,g}\}$

$S_2 = \{S_{2,1}, S_{2,2}, \dots S_{2,h}\}$

$S_3 = \{S_{3,1}, S_{3,2}, \dots S_{3,e}\}$

$S_4 = \{S_{4,1}, S_{4,2}, \dots S_{4,f}\}$

(2) Initialisation of the network

1) For each $\{i_i, E_j, S_{1,k}, S_{2,l}, S_{3,m}, S_{4,n}\}$, calculation of the matrix IESSSS of size (a x d x g x h x e x f) with $IESSSS[i,j,k,l,m,n] = P(i_i, E_j, S_{1,k}, S_{2,l}, S_{3,m}, S_{4,n})$

FOR i = 0 TO a (loop on i)
FOR j = 0 TO d (loop on E)
FOR k = 0 TO g (loop on S_1)
FOR l = 0 TO h (loop on S_2)
FOR m = 0 TO e (loop on S_3)
FOR n = 0 TO f (loop on S_4)
FOR o = 0 TO c (loop on t)
FOR p = 0, TO b (loop on L)

$$P(S_{1,k}|i_i, t_o, L_p) = \int_{k-1}^{k} LOGNORMAL\ (S_1, \mu = i_i \times m(t_o, L_p), \sigma = SF)dS_1$$

$$P(S_{2,l}|i_i, t_o, L_p) = \int_{l-1}^{l} LOGNORMAL(S_2, \mu = i_i \times m(t_o, L_p), \sigma = SF)dS_2$$

$$P(S_{3,m}|i_i, t_o, L_p) = \int_{k-1}^{k} LOGNORMAL\ (S_1, \mu = i_i \times m(t_o, L_p), \sigma = SF)dS_3$$

$$P(S_{4,n}|i_i, t_o, L_p) = \int_{l-1}^{l} LOGNORMAL(S_2, \mu = i_i \times m(t_o, L_p), \sigma = SF)dS_4$$

IF $i_i x e_{50}(L_p)$ belongs to $[E_{j-1}\ ;\ E_j]$ ou $[E_j\ ;\ E_{j+1}]$ THEN

$P(E_j \mid i_i, L_p) = \frac{E_j - i_i \times e_{50}(L_p)}{E_j - E_{j-1}} or \frac{i_i \times e_{50}(L_p) - E_{j-1}}{E_j - E_{j-1}}$

ELSE

$P(E_j \mid i_i, L_p) = 0$

$IESSSS[i,j,k,l,n,m] = P(i_i, E_j, S_{1,k}, S_{2,l}, S_{3,m}, S_{4,n}) = P(i_i, E_j, S_{1,k}, S_{2,l}, S_{3,m}, S_{4,n}) +$
$P(S_{1,k} \mid i_i, t_o, L_p) \times P(S_{2,l} \mid i_i, t_o, L_p) \times P(S_{3,m} \mid i_i, t_o, L_p) \times P(S_{4,n} \mid i_i, t_o, L_p) \times$
$P(E_j \mid i_i, L_p) \times P(i_i) \times P(t_o) \times P(L_p)$

ENDFOR

ENDFOR

ENDFOR

ENDFOR

ENDFOR

ENDFOR

ENDFOR

ENDFOR

2) Building of the matrix ISSSS of size (a x g x h x e x f) with $ISSSS[i,k,l,m,n] = P(i_i, S_{1,k}, S_{2,l}, S_{3,m}, S_{4,n})$

$$ISSSS[i,k,l,m,n] = P(i_i, S_{1,k}, S_{2,l}, S_{3,m}, S_{4,n}) = \sum_j P(i_i, E_j, S_{1,k}, S_{2,l}, S_{3,m}, S_{4,n})$$
$$= \sum_j IESSSS[i, j, k, l, m, n]$$

3) Building of the matrix ESSSS of size (d x g x h x e x f) with $ESSSS[j,k,l,m,n] = P(E_j, S_{1,k}, S_{2,l}, S_{3,m}, S_{4,n})$

$$ESSSS[j,k,l,m,n] = P(E_j, S_{1,k}, S_{2,l}, S_{3,m}, S_{4,n}) = \sum_i P(i_i, E_j, S_{1,k}, S_{2,l}, S_{3,m}, S_{4,n})$$
$$= \sum_i IESSSS[i, j, k, l, m, n]$$

4) Building of the matrix SSSS of size (g x h x e x f) with $SSSS[k,l,m,n] = P(S_{1,k}, S_{2,l}, S_{3,m}, S_{4,n})$

$$SSSS[k,l,m,n] = P(S_{1,k}, S_{2,l}, S_{3,m}, S_{4,n}) = \sum_i P(i_i, S_{1,k}, S_{2,l}, S_{3,m}, S_{4,n})$$
$$= \sum_i ISSSS[i, k, l, m, n]$$

(3) Update of the network

1) Building of the vector I of size a with $I_i = P(i_i \mid M_1, M_2, M_3, M_4)$

$$I_i = \frac{\sum_k \sum_l \sum_m \sum_n P(M_1|S_{1,k}) \times P(M_2|S_{2,l}) \times P(M_3|S_{3,m}) \times P(M_4|S_{4,n}) \times P(i_i, S_{1,k}, S_{2,l}, S_{3,m}, S_{4,n})}{\sum_k \sum_l \sum_m \sum_n P(M_1|S_{1,k}) \times P(M_2|S_{2,l}) \times P(M_3|S_{3,m}) \times P(M_4|S_{4,n}) \times P(S_{1,k}, S_{2,l}, S_{3,m}, S_{4,n})}$$

=

$$I_i = \frac{\sum_k \sum_l \sum_m \sum_n P(M_1|S_{1,k}) \times P(M_2|S_{2,l}) \times P(M_3|S_{3,m}) \times P(M_4|S_{4,n}) \times ISSSS[i,k,l,m,n]}{\sum_k \sum_l \sum_m \sum_n P(M_1|S_{1,k}) \times P(M_2|S_{2,l}) \times SSSS[k,l,m,n]}$$

2) Building the vector E of size d with $E_j = P(D_j \mid M_1, M_2, M_3, M_4)$

$$E_j = \frac{\sum_k \sum_l \sum_m \sum_n P(M_1|S_{1,k}) \times P(M_2|S_{2,l}) \times P(M_3|S_{3,m}) \times P(M_4|S_{4,n}) \times P(E_j, S_{1,k}, S_{2,l}, S_{3,m}, S_{4,n})}{\sum_k \sum_l \sum_m \sum_n P(M_1|S_{1,k}) \times P(M_2|S_{2,l}) \times P(M_3|S_{3,m}) \times P(M_4|S_{4,n}) \times P(S_{1,k}, S_{2,l}, S_{3,m}, S_{4,n})}$$

$$E_j = \frac{\sum_k \sum_l \sum_m \sum_n P(M_1|S_{1,k}) \times P(M_2|S_{2,l}) \times P(M_3|S_{3,m}) \times P(M_4|S_{4,n}) \times ESSSS[j,k,l,m,n]}{\sum_k \sum_l \sum_m \sum_n \sum_m \sum_n P(M_1|S_{1,k}) \times P(M_2|S_{2,l}) \times P(M_3|S_{3,m}) \times P(M_4|S_{4,n}) \times SSSS[k,l,m,n]}$$

(4) Calculation of the CDF of i and E

(5) Determination of the interval of $[i_{i-1}, i_i]$ which have a cumulative probability comprised 0.95

(6) Determination of the interval of $[E_{j-1}, E_j]$ which have a cumulative probability comprised 0.95

7. Algorithm of the RaFu method

(1) Definition of the input parameters

- Possibility distribution of uncertain parameters: AMAD, rapidly dissolved fraction f_r, rapid dissolution rate s_r and slow dissolution rate s_s in respiratory tract
- Probability distribution of the absorbed fraction in the gut f_1

(2) Sampling of N alpha-cuts of *AMAD* according to its possibility distribution

(3) Sampling of N alpha-cuts of f_r, s_r, *and* s_s according to their possibility distribution. The same value of alpha is used or not to model total correlation or independence between these parameters

(4) Sampling of N values of f1 according to its probability distribution

(5) Creation of the sets of the uncertain parameters $\{AMAD_k, f_{r,k}, s_{r,k}, s_{s,k}, f_{1,k}\}_{inf}$ to calculate the upper CDF of the dose by concatenating the most penalizing limit of one randomly chosen alpha-cut of AMAD with the most penalizing limit of the randomly chosen alpha-cut of f_r, s_r, s_s with one randomly chosen sampled value of f_1

(6) Creation of the sets of the uncertain parameters $\{AMAD_k, f_{r,k}, s_{r,k}, s_{s,k}, f_{1,k}\}_{sup}$ to calculate the lower CDF of the dose by concatenating the less penalizing limit of one randomly chosen alpha-cut of AMAD with the less penalizing limit of the randomly chosen alpha-cut of f_r, s_r, s_s with one randomly chosen sampled value of f_1

(7) Calculation of the doses for the sets $\{AMAD_k, f_{r,k}, s_{r,k}, s_{s,k}, f_{1,k}\}_{inf}$ and $\{AMAD_k, f_{r,k}, s_{r,k}, s_{s,k}, f_{1,k}\}_{sup}$ with DCAL

(8) Sorting of the doses to construct their upper and lower CDFs

Publications and oral presentations

1. Publications

Davesne E, Chojnacki E, Paquet F, Blanchardon E, Modelling the imprecision in prospective dosimetry of internal exposure to uranium, Health Physics, 96(2), pp 144-154, 2009

Davesne E, Paquet F, Ansoborlo E, Blanchardon E, Absorption of plutonium compounds in the respiratory tract, Journal of Radiological Protection, 30, pp 5-21, 2010

Davesne E, Casanova P, Chojnacki E, Paquet F, Blanchardon E, Integration of uncertainties into internal contamination monitoring, Health Physics, 99(4), pp 517-522, 2010

Davesne E, Casanova P, Chojnacki E, Paquet F, Blanchardon E, Optimisation of internal contamination monitoring programme by integration of uncertainties, RPD, in press

2. Oral presentations

Davesne E, Casanova P, Chojnacki E, Paquet F, Blanchardon E, Integration of uncertainties into internal contamination monitoring, congrès HEIR, Santa-Fé, mai 2009

Davesne E, Casanova P, Chojnacki E, Paquet F, Blanchardon E, Prise en compte des incertitudes dans la surveillance de la contamination interne, Congrés national de la SFRP, Angers, juin 2009

Davesne E, Casanova P, Chojnacki E, Paquet F, Blanchardon E, Optimisation of internal contamination monitoring programme by integration of uncertainties, congrès Individual Monitoring à Athènes, mars 2010

Davesne E, Casanova P, Chojnacki E, Paquet F, Blanchardon E, Développement d'un système expert pour la prise en compte des incertitudes dans la surveillance de la contamination interne, journées Codes de calcul en radioprotection de la SFRP, Sochaux, avril 2010